



# UNIVERSITE PARIS-EST

Ecole Doctorale Mathématiques, Sciences et Technologies de l'Information et de la  
Communication

## THESE

Présentée pour obtenir le grade de

### DOCTEUR de l'Université Gustave-Eiffel

Spécialité: Electronique, Optronique et Systèmes (CNU 63)

Présentée par:

**Viet-Duc Pham**

---

### **Power optimized waveforms for wireless power transmission**

---

Dirigée par:

**M. Laurent Cirio**

Encadrée par:

**M. Hakim Takhedmit**

Pour une soutenance le 21 Janvier 2021 devant le jury composé de :

**Rapporteurs:**

M. Yvan Duroc Professeur - Université Lyon 1 (Ampère)

M. Robert Staraj Professeur - Université Nice-Côte-d'Azur (LEAT)

**Examinateurs:**

Mme. Odile Picon Professeur émérite - Université Gustave Eiffel (ESYCOM)

M. Fabien Ferrero Professeur - Université Nice-Côte-d'Azur (LEAT)

M. Hakim Takhedmit Maître de Conférences - Université Gustave Eiffel (ESYCOM)

M. Laurent Cirio Professeur – Université Gustave Eiffel (ESYCOM)

*“LIFE IS A JOURNEY, NOT A DESTINATION.”*

RALPH WALDO EMERSON

## *Acknowledgements*

I would like to start out by expressing my deepest gratitude to my advisors, Mr. Laurent Cirio and Mr. Hakim Takhedmit, for providing me the opportunity to work on this project and for their guidance throughout my research. They are amazing professors and advisors and it was an honor for me to work with them.

I would like to thank again Prof. Takhedmit, he spent hours aiding me with my research, simulation, measurements, and for that I am truly grateful.

I would like to thank Mr. Jean-Marc Laheurte, Mrs. Elodie Richalot, Mr. Stephane Protat, Mr. Benoit Poussot, Mr. Francois Sarrazin; I have been blessed with all of their kindly supports, especially with automated measurements.

I would like to thank Mr. Yvan Duroc and Mr. Robert Staraj to accept to be my reviewers, Mrs. Odile Picon and M. Fabien Ferrero to accept to be my examiners.

I would like to thank my amazing friends Imad, Ariston, Miyassa, Aichatou, Wafa, Houssein, Jaafar, Franchesco, Mariem, Aiman... They are really kind and helpful, they bring a smile on my face every working days. I am so lucky for having them as friends.

I would like to thank my family in Vietnam, even we are very far away, but they constantly support me and give me the motivation to continue on the way that I have chosen.

Finally, I would like to thank my beloved wife, Lan Anh, for all her unconditional love and support through the years. I must be the luckiest man to have her in my life.



# Contents

<b>Acknowledgements</b>	<b>iii</b>
<b>General introduction</b>	<b>1</b>
<b>1 Introduction to WPT systems using Power Optimized Waveforms</b>	<b>5</b>
1.1 Introduction and brief history of WPT . . . . .	5
1.2 Rectenna and rectifier . . . . .	8
1.2.1 General structure of a rectenna . . . . .	9
1.2.2 Series-mounted diode rectifier . . . . .	10
1.2.3 Shunt-mounted diode rectifier . . . . .	11
1.2.4 Voltage doubler rectifier and multistage rectifier . . . . .	12
1.2.5 Frequency behavior of rectifiers/rectennas . . . . .	13
1.3 Enhancement of RF-to-dc conversion efficiency . . . . .	16
1.3.1 RF-to-dc conversion efficiency of the rectenna and its limitation . . . . .	16
1.3.2 Influence of the constitutive elements of the rectenna: diode, DC and HF filters . . . . .	17
1.4 Waveforms optimization to improve RF-to-dc conversion efficiency . . . . .	20
1.5 Conclusion . . . . .	29
<b>2 POWs applied on traditional rectifier topologies</b>	<b>39</b>
2.1 Multi-sine signal . . . . .	39
2.1.1 Multi-sine signals with different number of sub-carriers . . . . .	40
2.1.2 Multi-sine signal with different amplitudes . . . . .	43
2.1.3 Multi-sine signal with different phases . . . . .	44
2.1.4 Multi-sine signal with different frequency spacing between the sub-carriers . . . . .	45
2.2 RF pulse signal . . . . .	46
2.2.1 RF pulse signal: duty cycle and PAPR . . . . .	46
2.2.2 Voltage ripple . . . . .	47
2.3 ADS simulation . . . . .	49
2.3.1 General introduction . . . . .	49
2.3.2 Design of traditional rectifier topologies with ADS . . . . .	52
2.4 Common setup for rectifiers measurement . . . . .	58
2.5 Measurement results of traditional rectifiers . . . . .	61
2.5.1 Impact of multi-sine and RF pulse signals on the DC output performances . . . . .	61

2.5.2 DC voltage and efficiency of RF pulse signal over load value range . . . . .	67
2.6 Conclusion . . . . .	72
<b>3 Performance improvement of broadband rectifier/rectenna by using POWs</b>	<b>77</b>
3.1 Broadband rectifier . . . . .	77
3.1.1 Measurement with multi-sine signal . . . . .	80
3.1.2 Measurement with RF pulse signal . . . . .	81
3.2 Broadband rectenna characterization inside an anechoic chamber . . . . .	87
3.2.1 Broadband rectenna description . . . . .	87
3.2.2 Experimental setup for automated measurement inside anechoic chamber . . . . .	91
3.3 RF pulse signal: Time shape and spectrum considerations . . . . .	93
3.4 Broadband rectenna's measurement results . . . . .	96
3.4.1 Measurement with multi-sine signals . . . . .	96
3.4.2 Measurement with RF pulse signals . . . . .	99
3.5 Conclusion . . . . .	107
<b>4 Rectenna arrays experiments : Application to remote supply of a temperature/acceleration wireless sensor</b>	<b>111</b>
4.1 Single rectenna and rectenna arrays description . . . . .	111
4.2 Experimental characterization . . . . .	115
4.2.1 Measurement results with multi-sine signals . . . . .	115
4.2.2 Measurement results with RF pulse signal . . . . .	119
4.3 Application to remote power supply of a temperature/acceleration wireless sensor . . . . .	125
4.4 Conclusion . . . . .	128
<b>General conclusion</b>	<b>133</b>
<b>Abstract</b>	<b>137</b>

# List of Figures

1.1	Functional block diagram of Wireless power transmission system [1]. . . . .	5
1.2	Nikola Tesla in his Colorado Springs Laboratory which was constructed to experiment with radio waves for power transmission [3]. . . . .	6
1.3	Demonstration of Grand Bassin: Overview (right) and array of 2376 rectennas (left) [5]. . . . .	7
1.4	The history of radio transmission and wireless power transfer [7, 8]. . . . .	8
1.5	Block diagram of rectenna. . . . .	9
1.6	Series-mounted diode rectifier topology. . . . .	10
1.7	Example of series-mounted diode rectifier's RF-to-dc conversion efficiency [9].	10
1.8	Shunt-mounted diode rectifier topology. . . . .	11
1.9	Example of shunt-mounted diode rectifier's RF-to-dc conversion efficiency [9].	11
1.10	Voltage doubler rectifier topology. . . . .	12
1.11	Voltage multiplier scheme [18-20]. . . . .	12
1.12	Charge pump's principle. . . . .	12
1.13	Output DC voltage of multistage rectifier. (A) versus frequency. (B) versus input RF power. [18]	13
1.14	Simulated and measured efficiencies as function of frequency [32]. . . . .	14
1.15	Simulated and measured efficiencies and output dc voltages as function of frequency [33]. . . . .	14
1.16	RF-to-dc conversion efficiency at different input power levels against frequency [35]. . . . .	15
1.17	Diode's efficiency limitations [49]. . . . .	16
1.18	a) Diode junction voltage relationship. b) Equivalent circuit of the rectifying diode and DC load resistor [50]. . . . .	17
1.19	Equivalent schematic of series-mounted diode rectifier [6]. . . . .	17
1.20	Efficiency vs diode's $C_{j0}$ value ( $R_s = 5 \Omega$ ) [6]. . . . .	18
1.21	Efficiency vs diode's $R_s$ value ( $C_{j0} = 0.18 \text{ pF}$ ) [6]. . . . .	18
1.22	Efficiency vs load's value ( $C_{DC} = 33 \text{ pF}$ ) [6]. . . . .	19
1.23	Efficiency vs capacitor's value ( $R_L = 1.05 \text{ k}\Omega$ ) [6]. . . . .	19
1.24	RF-to-dc conversion efficiency of different types of waveform [51]. . . . .	20
1.25	Instantaneous power of the different types of test signals. Dashed-white line indicates the average power that is the same for all the signals. Dashed-black line indicates the peak power value [51]. . . . .	21
1.26	Signal spectrum (a) single carrier signal (b) OFDM signal (c) white noise signal (d) chaotic signal [51]. . . . .	21

1.27 Frequency domain and time domain of 3-tone and CW signals [52]. . . . .	22
1.28 Simulation of input and output waveforms (N-POWs) of voltage doubler [52].	22
1.29 Time- and frequency-domain plots of one time period of the 4-POW, Gaussian POW, and Square POW [52]. . . . .	23
1.30 Measured DC voltage (V) as function of input power (dBm) for: 1-tone (solid blue), 2-tones (red crosses), 4-tones (green stars) and 16-tones (magenta triangles) [54]. . . . .	24
1.31 Measured power gain (dB) as function of input power (dBm) for: 2-tones (red crosses), 4-tones (green stars) and 16-tones (magenta triangles) [54]. . .	24
1.32 Chaotic signal generator and DC output (voltage and efficiency) [56]. . . . .	25
1.33 Simulated IPV of different modulated signals for different roll-off factor values [66]. . . . .	26
1.34 RF-to-dc conversion efficiency of different modulated signals [66]. . . . .	27
1.35 Square pulse modulation. . . . .	27
1.36 RF-to-dc conversion efficiency of different CW and RF pulse signals [68]. . .	28
1.37 RF-to-dc conversion efficiency of different CW and RF pulse signals [68]. . .	28
2.1 Time and frequency domain of CW signal. . . . .	40
2.2 Time, frequency domain and histogram of multi-sine signal with N = 2. . . . .	41
2.3 Time, frequency domain and histogram of multi-sine signal with N = 4. . . . .	41
2.4 Time, frequency domain and histogram of multi-sine signal with N = 8. . . . .	42
2.5 Time, frequency domain and histogram of multi-sine signal with N = 16. . . . .	42
2.6 PAPR of Multi-sine signals with different number of sub-carriers. . . . .	43
2.7 PAPRs and their PDF of 8-tone signal with random amplitudes of sub-carriers.	44
2.8 PAPRs and their PDF of 8-tone signal with random phases of sub-carriers. . .	44
2.9 PAPRs and their PDF of 8-tone signal with random frequency spacing between sub-carriers. . . . .	45
2.10 Square pulse modulation. . . . .	46
2.11 Schematic of voltage-doubler topology rectifier/rectenna. . . . .	48
2.12 Input and output voltages in time domain with RF pulse signal. . . . .	48
2.13 ADS co-simulation design [7]. . . . .	51
2.14 OFDM Co-simulation. . . . .	51
2.15 OFDM signal generator in ADS. . . . .	52
2.16 Different traditional rectifier topologies, with and without matching networks. a) Series-mounted diode; b) Shunt-mounted diode; c) voltage-doubler rectifier.	53
2.17 Series-mounted diode rectifier with matching network. . . . .	53
2.18 Layouts of the series-mounted diode rectifiers with and without matching network. . . . .	54
2.19 $S_{11}$ of series-mounted diode with (line) and without (dashed-line) matching network over the frequency range and for different input power levels. . . . .	54
2.20 Voltage output and efficiency of series-mounted diode rectifiers with (line) and without (dashed-line) matching network ( $R_L = 1 \text{ k}\Omega$ ). . . . .	55

2.21	Layouts of shunt-mounted diode rectifiers with and without matching network.	55
2.22	$S_{11}$ of shunt-mounted diode with (line) and without (dashed-line) matching network over the frequency range and for different input power levels. . . . .	56
2.23	Voltage output and efficiency of shunt-mounted diode rectifiers with (line) and without (dashed-line) matching network ( $R_L = 360\Omega$ ). . . . .	56
2.24	Layouts of voltage-doubler rectifiers with and without matching network. . . . .	57
2.25	$S_{11}$ of voltage-doubler rectifier with (line) and without (dashed-line) matching network over the frequency range and for different input power levels. . . . .	57
2.26	Voltage output and efficiency of voltage-doubler rectifiers with (line) and without (dashed-line) matching network ( $R_L = 3k\Omega$ ). . . . .	58
2.27	Schematic of the measurement setup. . . . .	58
2.28	Photo of the measurement setup. . . . .	59
2.29	Multi-sine signal measurement user interface. . . . .	59
2.30	RF pulse signal measurement user interface. . . . .	60
2.31	Rectifier prototypes with and without matching network; R1, R3, R6 are series-mounted diode, shunt-mounted diode, voltage-doubler rectifiers with matching networks; R2, R4, R5 are series-mounted diode, shunt-mounted diode, voltage-doubler rectifiers without matching networks. . . . .	61
2.32	Voltage output of multisine and RF pulse signals on series-mounted diode rectifiers at -20 dBm. ( $R_L = 1 k\Omega$ ) . . . . .	62
2.33	Voltage output of multisine and RF pulse signals on shunt-mounted diode rectifiers at -20 dBm. ( $R_L = 360 \Omega$ ) . . . . .	63
2.34	Voltage output of multisine and RF pulse signals on voltage-doubler rectifiers at -20 dBm. ( $R_L = 3 k\Omega$ ) . . . . .	64
2.35	Efficiency of multisine and RF pulse signal on series-mounted diode rectifiers at 2.25 GHz. ( $R_L = 1 k\Omega$ ) . . . . .	64
2.36	Efficiency of multisine and RF pulse signal on shunt-mounted diode rectifier at 2.25 GHz. ( $R_L = 360 \Omega$ ) . . . . .	65
2.37	Efficiency of multisine and RF pulse signal on voltage-doubler rectifier at 2.25 GHz. ( $R_L = 3 k\Omega$ ) . . . . .	66
2.38	Output voltage of series-mounted diode rectifiers versus frequency at -20 and -10 dBm ( $R_L = 1 k\Omega$ ). . . . .	67
2.39	RF-to-dc conversion efficiency of series rectifiers versus resistance load at -20 dBm and -10 dBm ( $f = 2.25$ GHz). . . . .	68
2.40	Output voltage of shunt-mounted diode rectifiers versus frequency at -20 and -10 dBm ( $R_L = 360 \Omega$ ). . . . .	69
2.41	RF-to-dc conversion efficiency of shunt rectifiers versus resistance load at -20 dBm and -10 dBm ( $f = 2.25$ GHz). . . . .	70
2.42	Output voltage of voltage-doubler rectifiers versus frequency at -20 and -10 dBm ( $R_L = 3 k\Omega$ ). . . . .	70
2.43	RF-to-dc conversion efficiency of voltage-doubler rectifiers versus resistance load at -20 dBm and -10 dBm. . . . .	71

3.1 Rectifier circuit. Generic circuit layout of the wide-band rectifier with the photograph of the prototype. The parameters are : $W_1 = 2.2$ mm, $W_2 = 9.4$ mm, $W_3 = 5.5$ mm, $W_4 = 12.8$ mm, $W_5 = 2.2$ mm, $W_6 = 11$ mm, $W_7 = 1.8$ mm, $W_8 = 8.2$ mm, $W_9 = 3.4$ mm, $L_1 = 2.6$ mm, $L_2 = 6.6$ mm, $L_3 = 21.1$ mm, $L_4 = 11.4$ mm, $L_5 = 8.2$ mm, $L_6 = 2.4$ mm, $L_7 = 20.6$ mm, $L_8 = 8.2$ mm, $C_1 = C_2 = 100$ pF, $R_L = 3$ k $\Omega$ [1]. . . . .	78
3.2 Reflection coefficient ( $S_{11}$ ) versus the frequency ( $R_L = 3$ k $\Omega$ ). . . . .	78
3.3 Simulated output voltage (Volts) of the rectifier versus frequency and input RF power for $R_L = 3$ k $\Omega$ [1]. . . . .	79
3.4 RF-to-dc conversion efficiency and output voltage of the rectifier versus frequency and input RF power for $R_L = 3$ k $\Omega$ [1]. . . . .	79
3.5 Output voltage (mV) and voltage gain (dB) of the rectifier versus frequency for different number of tones ( $R_L = 3$ k $\Omega$ , $P_{RF} = -20$ dBm). . . . .	80
3.6 Output voltage (mV) and voltage gain (dB) of the rectifier versus frequency for different number of tones ( $R_L = 3$ k $\Omega$ , $P_{RF} = -10$ dBm). . . . .	81
3.7 Output voltage (mV) of RF pulse signal as a function of duty cycle, for different values of modulation frequency ( $R_L = 3$ k $\Omega$ ). . . . .	82
3.8 Voltage output, voltage gain and duty cycle of RF pulse signal versus 1-tone signal at -15 dBm ( $R_L = 3$ k $\Omega$ , $f_m = 1$ MHz). . . . .	83
3.9 Maximum efficiency of RF pulse signal versus $Z_{load}$ and frequency at -15 dBm ( $f_m = 1$ MHz). . . . .	84
3.10 Efficiency of 1-tone signal versus $Z_{load}$ and frequency at -15 dBm. . . . .	84
3.11 Efficiency gain of RF pulse signal compared to 1-tone signal versus $Z_{load}$ and frequency at -15 dBm. . . . .	85
3.12 Efficiency gain of RF pulse signal compared to 1-tone signal versus $Z_{load}$ and frequency at -5 dBm. . . . .	85
3.13 Output DC voltage and efficiency as a function of RF input power for optimized RF pulse and CW signals ( $f = 2.2$ GHz, $R_L = 3$ k $\Omega$ ). . . . .	86
3.14 Proposed rectenna layout [1]. . . . .	87
3.15 Reflection coefficient and realized gains of the antenna. . . . .	88
3.16 Received power by one, dual and quad feed lines SGA vs polarization angle (power density = $0.27 \mu\text{W}/\text{cm}^2$ , $E_{rms} = 1$ V/m) at: A, 1.85 GHz; B, 2.15 GHz; C, 2.45 GHz; D, 2.65 GHz; E, Different antenna's feeding topologies. SGA, slotted ground antenna [1]. . . . .	88
3.17 DC interconnection scheme. . . . .	89
3.18 Photographs of the fabricated rectenna: top view (left) and bottom view (right) [1]. . . . .	90
3.19 Measured efficiency and output DC voltage of the rectenna against frequency: Efficiency (left) and output DC voltage (right) ( $R_L = 3$ k $\Omega$ ).[1] . . . . .	90
3.20 Measurement setup schematic. . . . .	91
3.21 Anechoic chamber setup with horn-antenna (left) and rectenna (right). . . . .	92
3.22 Transmitted RF pulse signal in time domain ( $\beta = 10\%$ ). . . . .	94

3.23	Transmitted RF pulse signal in frequency domain ( $\beta = 10\%$ ). . . . .	94
3.24	Received RF pulse signal in time domain ( $\beta = 10\%$ ). . . . .	95
3.25	Received RF pulse signal in frequency domain ( $\beta = 10\%$ ). . . . .	95
3.26	Transmitted RF pulse signal in time domain ( $\beta = 50\%$ ). . . . .	95
3.27	Transmitted RF pulse signal in frequency domain ( $\beta = 50\%$ ). . . . .	95
3.28	Received RF pulse signal in time domain ( $\beta = 50\%$ ). . . . .	96
3.29	Received RF pulse signal in frequency domain ( $\beta = 50\%$ ). . . . .	96
3.30	Voltage output (left) and voltage gain (right) of multisine at -20 dBm ( $R_L = 3$ k $\Omega$ ). . . . .	97
3.31	Voltage output (left) and voltage gain (right) of multisine at -25 dBm ( $R_L = 3$ k $\Omega$ ). . . . .	97
3.32	Voltage output (left) and voltage gain (right) of multisine at -30 dBm ( $R_L = 3$ k $\Omega$ ). . . . .	97
3.33	Voltage output (left) and voltage gain (right) of multisine at -20 dBm and load resistance of 100 k $\Omega$ . . . . .	98
3.34	Voltage output (left) and voltage gain (right) of multisine at -25 dBm and load resistance of 100 k $\Omega$ . . . . .	98
3.35	Voltage output (left) and voltage gain (right) of multisine at -30 dBm and load resistance of 100 k $\Omega$ . . . . .	99
3.36	DC voltage of RF pulse and CW signals versus duty cycle at - 20 dBm . . . . .	99
3.37	DC voltage of RF pulse and CW signals versus duty cycle at - 25 dBm . . . . .	100
3.38	DC voltage of RF pulse and CW signals versus duty cycle at - 30 dBm . . . . .	100
3.39	Waveform optimization algorithm . . . . .	101
3.40	Output DC voltage of RF pulse and CW signals against frequency for different RF power input ( $R_L = 3$ k $\Omega$ ). . . . .	102
3.41	Output DC voltage of RF pulse and CW signals against frequency for different RF power input ( $R_L = 100$ k $\Omega$ ). . . . .	103
3.42	Voltage/efficiency gain of RF pulse against frequency for different RF power input ( $R_L = 3$ k $\Omega$ ). . . . .	104
3.43	Voltage/efficiency gain of RF pulse against frequency for different RF power input ( $R_L = 100$ k $\Omega$ ). . . . .	104
3.44	Output DC voltage and efficiency of RF pulse and CW signals versus input power ( $R_L = 3$ k $\Omega$ and $f_c = 2.4$ GHz) . . . . .	105
3.45	Output DC voltage and efficiency of RF pulse and CW signals versus input power ( $R_L = 100$ k $\Omega$ and $f_c = 2.4$ GHz) . . . . .	105
3.46	Voltage gain of RF pulse signal for different input RF powers ( $f_c = 2.4$ GHz). . . . .	106
4.1	Configuration of the third iteration Koch fractal antenna. The antenna parameters are: $W_{sub} = 55$ mm, $L_{sub} = 50$ mm, $L_{patch} = 26.4$ mm, $W_{patch} = 26.4$ mm, $X_0 = 8.06$ mm, $Y_0 = 13.2$ mm, $h_{sub} = 1.6$ mm [1]. . . . .	112
4.2	Simulated and measured reflection coefficients of the fractal antenna, simulation (solid line), and measurement (dashed line) [1]. . . . .	112

4.3	Topology of the T-junction filter and the dual cascaded Dickson voltage multiplier. The filter parameters are: $W_1 = 3$ mm, $L_1 = 3$ mm, $W_2 = 5$ mm, $L_2 = 5.33$ mm, $W_3 = 5$ mm, $W_3 = 5.33$ mm, $W_4 = 8.66$ mm, and $L_4 = 2.55$ mm [1]. . .	113
4.4	Photograph of the fabricated rectifier. . . . .	114
4.5	Top view and bottom view of 2x2 rectenna array. . . . .	114
4.6	Top view and bottom view of 3x3 rectenna array. . . . .	114
4.7	DC interconnection schemes . . . . .	115
4.8	Measured output DC voltage of CW signal on the 1x1 rectenna versus frequency ( $C_L = 10$ nF, $R_L = 10 M\Omega$ ). . . . .	116
4.9	Measured output DC voltage and voltage gain of multi-sine signal on the 1x1 rectenna versus power density at 2.45 GHz. . . . .	116
4.10	Measured output DC voltage of CW signal on the 2x2 rectenna array versus frequency ( $C_L = 10$ nF, $R_L = 10 M\Omega$ ). . . . .	117
4.11	Measured output DC voltage and voltage gain of multi-sine signal on the 2x2 rectenna versus power density at 2.45 GHz. . . . .	118
4.12	Measured output DC voltage of CW signal on the 3x3 rectenna versus frequency ( $C_L = 10$ nF, $R_L = 10 M\Omega$ ). . . . .	118
4.13	Measured output DC voltage and voltage gain of multi-sine signal on the 3x3 rectenna versus power density at 2.45 GHz. . . . .	119
4.14	Measured output DC voltage of the 1x1 rectenna versus duty cycle at 1 $\mu W/cm^2$ (left) and 10 $\mu W/cm^2$ (right). . . . .	120
4.15	Measured gain of RF pulse signal on the single cell rectenna versus duty cycle. . . . .	120
4.16	Measured output DC voltage and voltage gain of RF pulse signal on the single cell rectenna versus power density. . . . .	121
4.17	Measured output DC voltage of the 2x2 rectenna array versus duty cycle at 1 $\mu W/cm^2$ (left) and 10 $\mu W/cm^2$ (right). . . . .	121
4.18	Measured gain of RF pulse signal on the 2x2 rectenna array versus duty cycle. . . . .	122
4.19	Measured output DC voltage and voltage gain of RF pulse signal on the 2x2 rectenna array versus power density. . . . .	122
4.20	Measured output DC voltage of the 3x3 rectenna array versus duty cycle at 1 $\mu W/cm^2$ (left) and 10 $\mu W/cm^2$ (right). . . . .	123
4.21	Measured voltage of RF pulse signal on the 3x3 rectenna array versus duty cycle. . . . .	123
4.22	Measured output DC voltage and voltage gain of RF pulse signal on the 3x3 rectenna array versus power density. . . . .	124
4.23	Measurement setup for rectenna arrays measurement with sensor. . . . .	125
4.24	Temperature/acceleration sensor and data displayed on smartphone and oscilloscope. . . . .	126
4.25	Measured voltage evolution on $C_S$ as a function of time. . . . .	126

# List of Tables

1.1	Voltage doubler simulation results [52] . . . . .	23
1.2	Ideal simulated read-range [52] . . . . .	23
1.3	The performance of output voltage using impulsive wireless power transmission with horn antennas [69]. . . . .	29
2.1	Number of sub-carriers and duty cycle of pulse signal as a function of PAPR .	47
2.2	Optimum load and corresponding efficiency for CW and RF pulse signal ( $P_{in}$ = -20 dBm and $f$ = 2.25 GHz) . . . . .	71
2.3	Optimum load and corresponding efficiency for CW and RF pulse signal ( $P_{in}$ = -10 dBm and $f$ = 2.25 GHz) . . . . .	72
3.1	RF pulse and multi-sine signal voltage/efficiency gain compared to CW and multi-sine signal ( $R_L$ = 3 k $\Omega$ ) . . . . .	86
3.2	Received power for the different antennas at 2.45 GHz (power density = 0.27 $\mu\text{W}/\text{cm}^2$ , $E_{rms}$ = 1 V/m) [1] . . . . .	89
3.3	RF pulse and multi-sine signal voltage/efficiency gain compared to CW ( $R_L$ = 3 k $\Omega$ ) . . . . .	106
3.4	RF pulse and multi-sine signal voltage/efficiency gain compared to CW ( $R_L$ = 100 k $\Omega$ ) . . . . .	106
4.1	RF pulse and multi-sine signal voltage gain (dB) compared to CW signal . . .	124
4.2	Minimum power density for different input waveforms ( $\mu\text{W}/\text{cm}^2$ ) . . . . .	127
4.3	Corresponding $T_1$ and $T_2$ (s) for minimum power density of CW, 8-tone and RF pulse waveforms. . . . .	127
4.4	Stored average power ( $\mu\text{W}$ ) in the capacitor for minimum power density of CW, 8-tone and RF pulse waveforms. . . . .	128



# List of Abbreviations

<b>BLE</b>	Bluetooth Low Energy
<b>CCDF</b>	Complementaty Cumulative Distribution Function
<b>CW</b>	Continous Sinewave
<b>DC</b>	Direct Current
<b>EHS</b>	Energy Harvesting System
<b>EH</b>	Energy Harvester
<b>EM</b>	Electromagnetic
<b>FDM</b>	Frequency Division Multiplexing
<b>GSM</b>	Global System for Mobile communications
<b>IPV</b>	Instantaneous Power Variance
<b>IoT</b>	Internet-of-Things
<b>MS</b>	Multi-Sine
<b>OFDM</b>	Orthogonal Frequency Division Multiplexing
<b>PAPR</b>	Peak-to-Average Power Ratio
<b>PDF</b>	Propability Distribution Function
<b>POW</b>	Power Optimized Waveform
<b>QAM</b>	Quadrature Amplitude Modulation
<b>RF</b>	Ratio Frequency
<b>RFID</b>	Radio-Frequency IDentification
<b>STD</b>	STandart Deviation
<b>UHF</b>	Ultra High Frequency
<b>UMTS</b>	Universal Moble Telecommunications system
<b>UWB</b>	Ultra-Wide Band
<b>WPT</b>	Wireless Power Transfer



# General introduction

Recently, the Internet of Things (IoT) has been gathering a lot of interest in research as well as manufacturing. It has a huge range of applications in all aspects of our life such as: smart home, smart city, wearable devices, industrial internet, connected car, connected health. In IoT, besides of fast connection, it is needed a huge amount of sensors and electronics devices to communicate and transfer data. From 2019, the fifth generation technology standard for broadband cellular networks (5G) is starting to be used. It has greater bandwidth and excellent data transfer speed. However, one of the biggest issue in IoT is to supply power to the sensors and electronics devices as they are not always connected to the power sources. Using a traditional method such as battery causes environmental pollution and also it wastes time and resources to recharge or replace the battery manually after a certain time. For that reason, low power level WPT (Wireless Power Transmission) is one of the best answers for this problem. With WPT, the power can be transmitted wirelessly to supply the sensors and electronic devices. In WPT, RF power is converted into DC power normally by the rectifying circuit. Therefore, the sensors and electronic devices could have an extended battery life, or ideally, a full autonomy.

However, in the process of converting RF power into DC power using rectifier, due to limitations of the diodes of rectifying circuit, at low RF power, the RF-to-dc conversion efficiency is relatively low while using a conventional CW (Continuous Wave) signal. The question of how to improve the RF-to-dc conversion efficiency at low power levels is still under consideration. Among the solutions, using signals with high PAPR instead of CW has been developed and reported in some works according to the literature. It helps the rectifying circuits to provide higher DC output, voltage and/or RF-to-dc conversion efficiency, at low power input. That seems an interesting solution as without much modification of the circuit, we can have more harvested DC power at the output of the energy harvester to supply power to the sensors and electronic devices.

The objective of this thesis is to study POWs (Power Optimized Waveforms) and apply them into the energy harvesting devices in order to improve their RF-to-dc performance compared to CW signal. The POWs proposed consist of multi-sine signal and RF pulse signal. Firstly, the study of waveforms using Matlab and ADS to demonstrate the characteristics of the waveforms will be presented. Secondly, the impact of the POWs is shown on different rectifier/rectenna topologies.

This thesis consists of four chapters. In the first chapter, we start by an introduction to

the WPT and the brief history of the WPT systems. Then, we talk about the rectenna and rectifier architectures. Different topologies of rectenna/rectifier such as: series-mounted diode, shunt-mounted diode, voltage doubler, multistage rectifiers will be presented. Also, it is possible to classify rectennas/rectifiers based on their operating frequency bandwidth, such as: narrow-band, dual-band, multi-band and broadband harvesters. The limitation of the rectifier/rectenna in term of RF-to-dc conversion efficiency at low power levels will be developed. On the other hand, we consider the influence of the constitutive elements, such as diode, the DC filter as well as the HF filter, on the performance of rectifying circuit and introduce the principle of POW to enhance the performance of the circuit. Finally, we present the state of the art of POWs on RF-to-dc conversion efficiency of the rectennas/rectifiers. In this part, some recent works on POWs with different type of waveforms such as: multi-sine, OFDM, chaotic, white noise, RF pulse are mentioned. The waveforms have different characteristics and help to improve the RF-to-dc conversion efficiency of the energy harvesters. At the end, two types of waveform will be selected to further study in our thesis.

Chapters 2 presents the characteristics of waveforms, which firstly including statistical study of multi-sine signal. This study is to understand how the PAPR of multi-sine signal can be changed while varying the parameters of the waveform such as: the number of sub-carriers, the amplitudes, the phases and the frequency spacing between sub-carriers. Secondly, we study RF Pulse signals with its characteristics and explain how the PAPR can be adjusted as a function of the duty cycle of the signal. Then, ADS simulation with simulation tools such as HB (Harmonic Balance) simulation, CE (Circuit Envelope) simulation, Transient simulation, Proteemy co-simulation, and their characteristics, advantages and disadvantages will be adopted to generate, simulate and optimize the rectifying circuits. Some types of POW also have to be created using ADS to simulate with the rectifiers. Three types of rectifiers: series-mounted diode, shunt-mounted diode and voltage-doubler rectifier, with and without matching networks are designed and optimized using ADS. The simulation results of each rectifier will be displayed as well as its improvements and limitations in details. The measurement setup developed to automatically perform the measurements in order to obtain accurate results, when the waveform and rectifier topology vary, will be presented. As the last part of this chapter, measurement results of POWs on traditional rectifier topologies will be presented. Then, multi-sine and RF pulse will be applied on the circuits without matching network to compare the performance with CW applied on the circuits with matching network.

In chapter 3, we firstly present the broadband rectifier that is designed and optimized to operate in the frequency band ranging from 1.6 to 2.8 GHz. The output DC voltages with POWs are measured and presented to compare with CW signal. Secondly, the broadband rectenna is introduced and characterized with the automated measurement setup in anechoic chamber. This rectenna contains 4 accesses to capture electromagnetic incident waves regardless of the polarization angle. Each access is connected to a voltage-doubler rectifier and well connected to a resistive load using series and parallel combinations. To make sure

that the RF pulse signal is kept the same form during transmission in free space, a simulation using Matlab software has been done. Finally, the measurement results of broadband rectenna with multi-sine and RF pulse signals are also demonstrated by highlighting the output DC voltage as well as the efficiency/voltage gain improvement compared to 1-tone signal.

Chapter 4 reports an application of POW to remotely supply a temperature/acceleration wireless sensor using rectenna arrays. We firstly characterize 1x1, 2x2, and 3x3 rectenna arrays with multi-sine and RF pulse signals at 2.45 GHz to supply high DC voltage at small RF power levels. The load is a capacitor that charging between two thresholds and then discharging and recharging to supply the wireless sensor. For the same power density, we perform the measurement of charge and recharge time of the capacitor for each type of waveform. Also, the measurements with different power densities have been done to find a minimum power density required to charge the capacitor for each type of rectennas. We show that using POWs and particularly RF pulse allows to decrease the charging and recharging times or allows to decrease the power density needed for supplying the wireless sensor.



## Chapter 1

# Introduction to WPT systems using Power Optimized Waveforms

### 1.1 Introduction and brief history of WPT

Nowadays, the development of Internet of things (IoT), smart city, smart building is leading our world to the new era. Millions of smart sensors and smart devices have to be connected together, so how to power up these sensors and devices is a big question. For now, we are using the traditional electric-chemical method, such as battery. But it is a temporary method, because the battery is not durable and causes environmental pollution when replacing it. Moreover, it does not supply the autonomy for the smart sensors and smart devices. That is the reason why wireless power transmission (WPT) is one of the most effective ways we can rely on, especially for the applications that require small power levels such as wake-up sensors or electronics devices to communicate or send the data wirelessly. In that case, the power required is only several  $\mu\text{W}$  to a few  $\text{mW}$ . Wireless power transmission demonstrates "the transmission of electrical energy without wires". The primary components of WPT system (Fig.1.1) are microwave generator, transmitting antenna and rectenna (receiving antenna + rectifying circuit) [1].

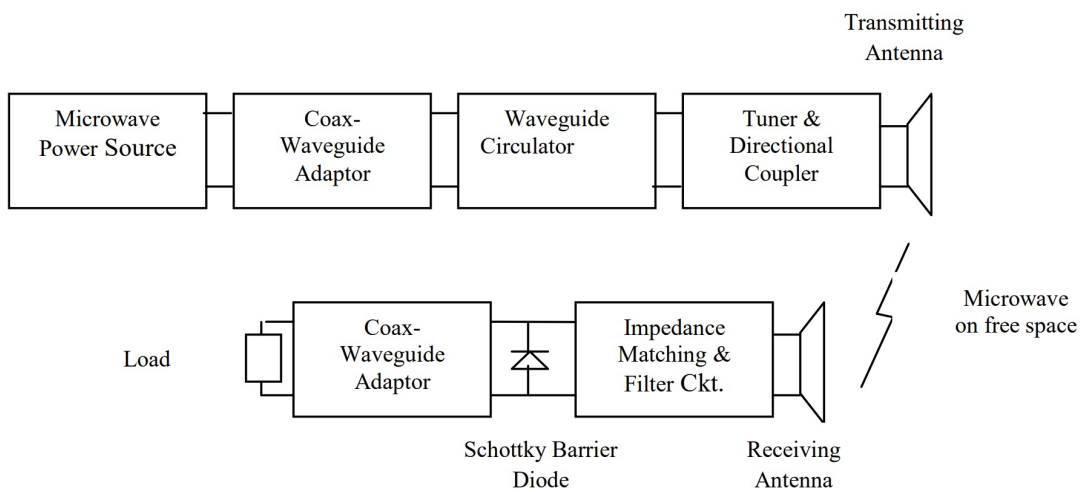


FIGURE 1.1: Functional block diagram of Wireless power transmission system [1].

High-tension power transmission in line cables, towers and sub-stations between the power-generation stations and consumers can be completely eliminated in WPT. The interconnection of electrical generation plans on global scale can be facilitated. WPT can give more freedom of choice of both receivers and transmitters, even for mobile receivers and transmitters and also reduces the cost of energy storage, energy transmission and distribution. With WPT, wireless energy can be transferred to the places that wired transmission can not reach. While WPT is functioning, the power is always available at the rectenna. The power failure due to short circuit and fault on cables would never exist in the transmission [1].

The brief history of WPT [2-8] will be presented in the next part of this section. In WPT, the RF signal is converted to DC power by the rectenna, that consists of an antenna and a rectifier. The introduction of rectenna and some of the rectifier's topologies such as series-mounted diode, shunt-mounted diode, voltage doubler, and multistage rectifier will be also presented. The rectifier/rectenna based on different operating frequency ranges such as: narrow-band, multi-band and broadband rectifier/rectenna are also introduced in this chapter. On the other hand, the problematic of WPT will be proposed to show the importance of POW (Power Optimized Waveform) in WPT as well as the RF-to-dc conversion efficiency of rectifier and rectenna. It also explained the needs of improving the RF-to-dc conversion efficiency at small RF power levels in order to supplying a required DC power to electronics sensors and devices in small power applications.

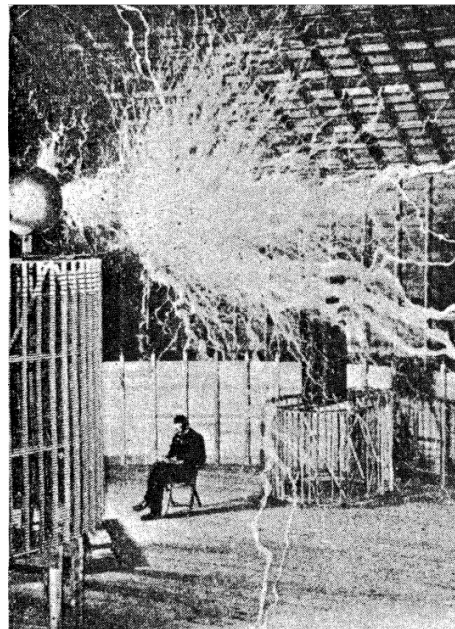


FIGURE 1.2: Nikola Tesla in his Colorado Springs Laboratory which was constructed to experiment with radio waves for power transmission [3].

The first wireless power transmission experiment was conducted by the American physicist Nikola Tesla in Colorado Springs in 1899. He took a special interest in the resonance phenomenon and tried to apply it to the WPT. He had imagined using electromagnetic waves

to deliver electricity anywhere in the world without the need for a power line (Fig.1.2) [2-4].

Tesla built a huge coil, resonating at 150 KHz and powered with a 300 kW, at the top of a tower. However, there is unfortunately no clear results on the radiated power and on the power received far from the source. Tesla's work didn't stop in Colorado Springs. At the end of the 19<sup>th</sup> century, Tesla built a transmission tower on Long Island, New York. The project was abandoned shortly before its completion due to financial problems. During the first half of the 20<sup>th</sup> century, the lack of interest in technical resources and more than that, a lack of technical capacity can explain the inadequacy of thematic WPT, especially sources that are capable of generating considerable power in high frequencies.

In 1969, Peter Glaser introduced the concept of the SPS (Solar Power System) [2]. This project could offer an alternative to the energy problems facing the planet, but also as a source of clean and environmentally friendly energy. The system resulting from this project has a satellite in geostationary orbit that captures solar energy, this solar energy is converted into microwave energy at 2.45 GHz and sent to earth. The risks at the level of the receiving antennas are significant. The power density is about  $100 \text{ W/m}^2$ .

In 1975, Raytheon's ground-based Goldstone experiment was a historic turning point in the field of WPT. It has made a considerable contribution to the validation of the concept and credibility of the SPS project. With a pilot system, 30 kW was recovered and an overall efficiency of 54% was measured and certified [2]. The distance between the transmitting and receiving antennas is 1.6 km.



FIGURE 1.3: Demonstration of Grand Bassin: Overview (right) and array of 2376 rectennas (left) [5].

Since 1994, the Electronics, Energy and Processes Laboratory of University of Reunion has been working in collaboration with the Japanese ISAS team. They've launched in a major project to study the feasibility of power transmission without wire to supply the island of Grand Bassin, a region that is very rugged and difficult to access. The transmitted power was 800 W over a distance of 40 m (Fig.1.3). In reception, a rectenna composed of 2376 dipole antennas spread over a surface area of  $11.76 \text{ m}^2$  has been used to collect and convert some of the emitted RF power. The power density at the level of the receiving antennas is estimated at about  $10 \text{ W/m}^2$  (or  $1000 \mu\text{W/cm}^2$ ). Three lamps of 9 W were switched on thanks to the developed device, the system had an overall efficiency of about 5% [5].

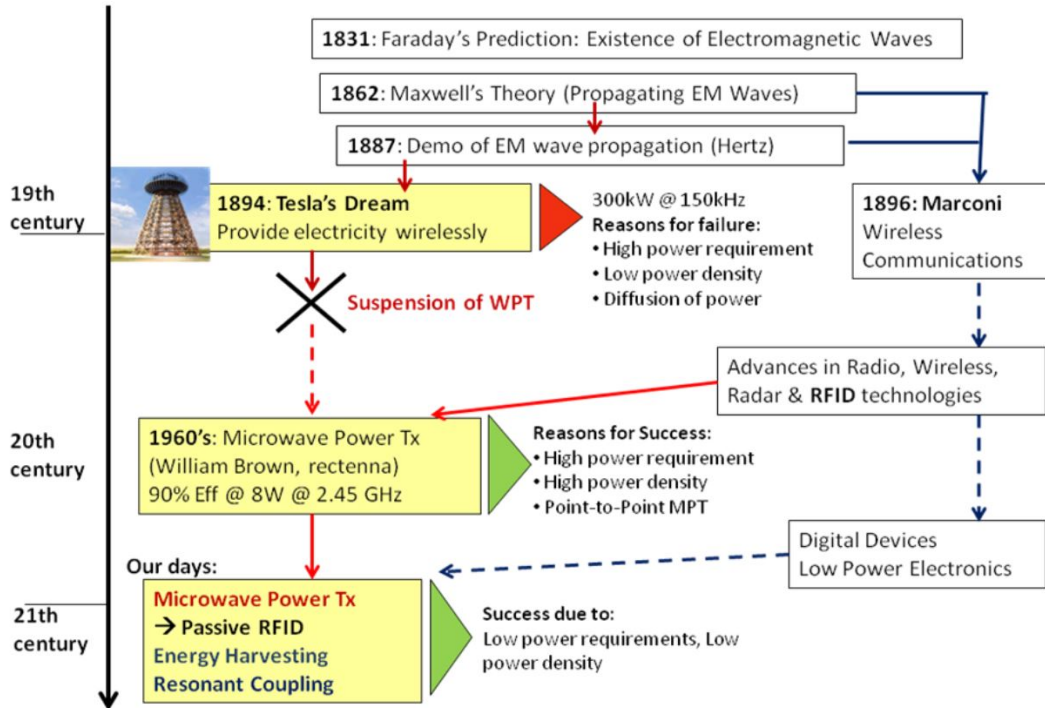


FIGURE 1.4: The history of radio transmission and wireless power transfer [7, 8].

Fig.1.4 represents the brief history schematic of WPT [7]. Base on the Faraday's prediction (1831), Maxwell's theory and demo of electromagnetic wave propagation by Hertz in the 19th century, in late 19th century, Tesla had an idea about providing electricity wirelessly as mentioned above. But it is failure to transfer 300 kW at 150 kHz due to low power density and diffusion of power. In the 60s of the 20th century, the microwave power transfer with 90 % of efficiency with a power of 8 W at the frequency of 2.45 GHz has been done by William Brown. Nowadays, micro-wave power transfer for energy harvesting is required for low power performance applications as mentioned previously in this section. For this application, rectifier, rectenna and waveform optimization are taken into account to provide the maximum RF-to-dc conversion efficiency, in order to achieve the goal that sensors and electronic devices should have the ability to harvest energy at very low power. In general, the receiving parts of WPT system play a very important role in improving the power supply to the electronics sensors and devices. For that reason, rectifying circuit and rectenna is taken into account in the next section of this chapter.

## 1.2 Rectenna and rectifier

As the main part of this thesis, rectifier or rectenna are the main parts of energy harvesters. The rectenna is a passive element consisting of antenna, rectifying circuit (rectifier) with a low pass filter between antennas and rectifying diode (or diodes). The antenna used in rectenna may be dipole, Yagi – Uda, patch or parabolic dish antenna, etc. Schottky barrier diodes (GaAs-W, Si, and GaAs) are usually used in the rectifying circuit due to the faster

transition time, much lower forward voltage drops, small threshold voltage and good RF characteristics [1].

### 1.2.1 General structure of a rectenna

To harvest the wireless energy, rectenna, which consists of a rectifier and a receiving antenna are used. The block diagram of the rectenna is shown in Fig.1.5.

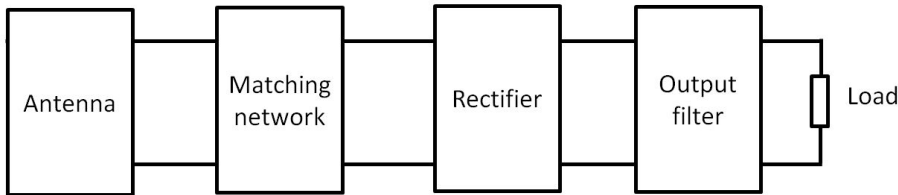


FIGURE 1.5: Block diagram of rectenna.

The Radio Frequency (RF)/microwave energy is collected by a receiving antenna and converted into DC power by a rectifying circuit (or rectifier). In order to improve the rectenna RF-to-dc conversion efficiency, two blocks can be added respectively between the antenna and the rectifier, also between the rectifier and the load resistor. In addition, it is necessary to further reduce the insertion loss and to increase the input voltage of the rectifying circuit. These blocks act both as filtering and as matching sections, they should be optimized in order to simultaneously fulfill the following functions:

- To match the antenna and the load to the rectifier
- To preserve the antenna from re-irradiating the high order harmonics generated by the rectifier.
- To preserve the load from any RF signals which are high order harmonics generated by the Schottky diode (to this end the block between the rectifier and the load should be a DC pass filter).

Moreover, the load is also needed to be optimal to get highest efficiency. Different types of rectifying circuit such as single shunt half-wave rectifier, full-wave bridge rectifier, or other hybrid rectifiers can be a rectifier part of the rectenna. The RF-to-dc conversion efficiency is mainly dependent on the circuit, especially the diode. The conversion efficiency of the rectenna with a diode also depends on the microwave input power intensity and the optimum connected load. The efficiency becomes quite small at low input power or if the circuit is not matched either between the input or the output load. The characteristic of the diode which has its own junction voltage and breakdown voltage also influence the RF-to-dc conversion efficiency. If the input voltage of the diode is lower than the junction voltage or is higher than the breakdown voltage, the diode does not show a good performance. As a result, the RF-to-dc conversion efficiency drops with a lower or higher input than the optimum [1]. Some types of rectifiers that are used in this thesis such as series-mounted diode, shunt-mounted diode, voltage doubler and multistage rectifiers will be presented in the following sections.

### 1.2.2 Series-mounted diode rectifier

The basic structure of a series mounted diode [9-13] is presented in Fig.1.6. In [9], the structure is dedicated to low power levels (considerably below 0 dBm), power handling capabilities can be traded for high sensitivity. The choice was made to use HSMS2850 zero bias Schottky diodes [14] that have low power handling capabilities, low threshold voltage (150 mV) and low junction capacitance (0.18 pF).

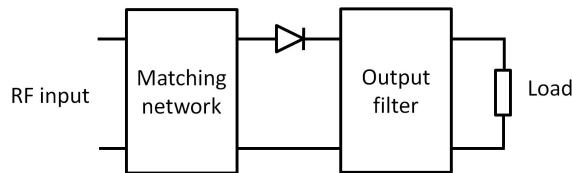


FIGURE 1.6: Series-mounted diode rectifier topology.

This rectifying circuits have a highly nonlinear behavior mostly because of the diode rectification process. It is not practical to design sub-parts independently because they highly interact with each other. The load of the input filter depends on the diode and the output filter at the diode extremity. For this reason, a global circuit optimization technique must be used for estimating the passive components of the filter elements. These optimizations were made with the software ADS (with Momentum) from Keysight Technologies.

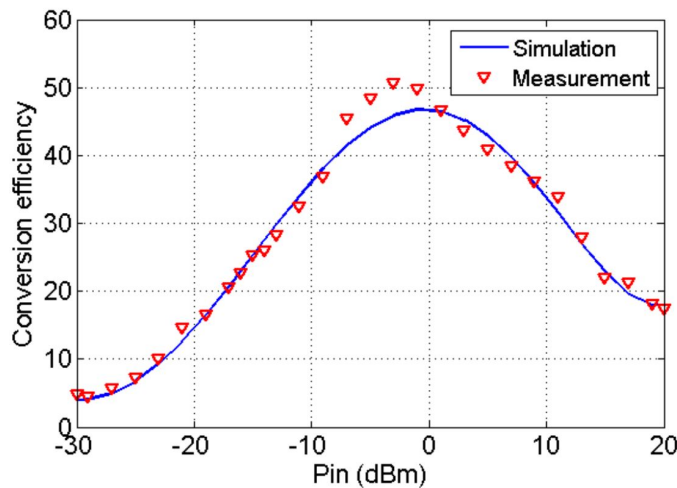


FIGURE 1.7: Example of series-mounted diode rectifier's RF-to-dc conversion efficiency [9].

Fig.1.7 traces the example of evolution of the RF-to-dc conversion efficiency as a function of the incident RF power level. The rectenna load has been tuned to obtain the maximum power point efficiency for a given input power level. Maximum conversion efficiency of roughly 50% is reached between -5 dBm and 0 dBm (1 mW) of incident power. In this case, the center frequency is 2.45 GHz and the load value is 2.4 kΩ. At lower power levels the efficiency is lower because of the threshold voltage of the diode which is comparable to the amplitude of the incident signal. For high power levels, internal diode losses become significant due to the diode series resistance. Also, the reverse breakdown voltage of the diode

limits the input power level and then the efficiency [9]. Besides, the appearance of higher order harmonics rapidly degrade the RF-to-dc conversion efficiency. Because they carry power and their levels increase N times (for the N-harmonic) faster than the fundamental frequency. Single series-mounted diode and shunt-mounted diode rectifiers can get higher efficiency in low input power [10]. In [15, 16], the RF-to-dc conversion efficiency of the series-mounted diode rectifier at 0 dBm, 2.25 GHz and  $Z_{load}$  of  $1\text{ k}\Omega$  is approximately 45 %.

### 1.2.3 Shunt-mounted diode rectifier

The shunt-mounted diode rectifier topology [9-13] is shown in Fig.1.8. Also in [9], the shunt-mounted rectifier structure has been designed for the 0 dBm to 20 dBm input power range. At these power levels, the threshold voltage has less impact on the circuit performances. The main objective is to decrease as much as possible the internal loss inherent to the rectifier diode and to increase power handling capabilities. The diode used for this structure has a threshold voltage level of 350 mV (HSMS2860 by Keysight [17]).

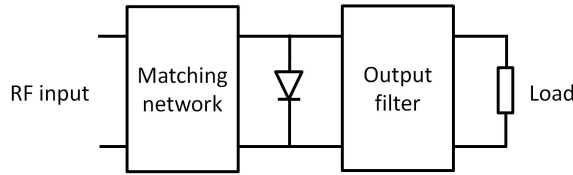


FIGURE 1.8: Shunt-mounted diode rectifier topology.

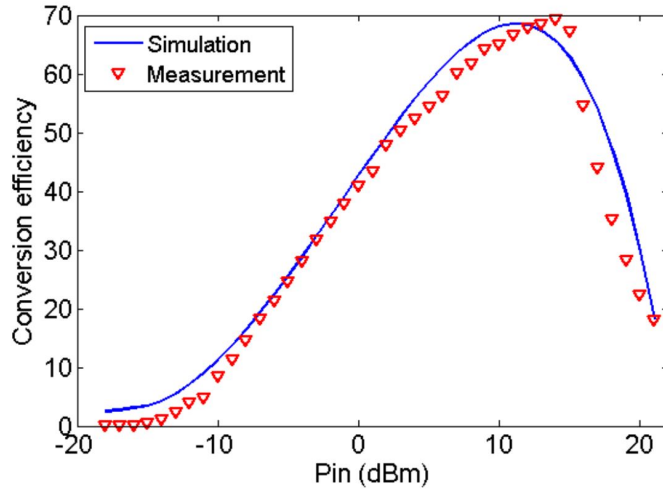


FIGURE 1.9: Example of shunt-mounted diode rectifier's RF-to-dc conversion efficiency [9].

The structure reaches maximum conversion efficiencies of 70 % for an input power of 15 dBm. The conversion efficiency has a similar dependency with respect to load impedance to that presented in Fig.1.9 with an optimal load of  $750\text{ }\Omega$  for 15 dBm input power at a frequency of 2.45 GHz [9]. Meanwhile, the efficiency of the shunt-mounted diode rectifier presented in [15, 16] at 0 dBm, 2.25 GHz and  $Z_{load}$  of  $360\text{ }\Omega$  is approximately 45 %.

### 1.2.4 Voltage doubler rectifier and multistage rectifier

The voltage doubler rectifier can be considered as the combination of the two topologies above: series-mounted diode and shunt-mounted diode. It contains two diodes: one in series and the other in parallel (as shown in Fig.1.10) which produce more voltage DC output. In [15, 16], the maximum efficiency of the voltage doubler rectifier at 0 dBm, 2.25 GHz and  $Z_{load}$  of  $3 \text{ k}\Omega$  is approximately 60 %.

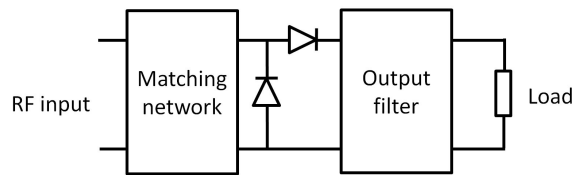


FIGURE 1.10: Voltage doubler rectifier topology.

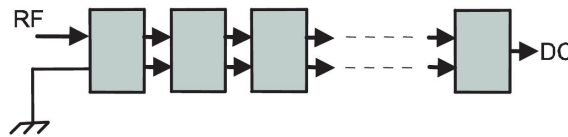


FIGURE 1.11: Voltage multiplier scheme [18-20].

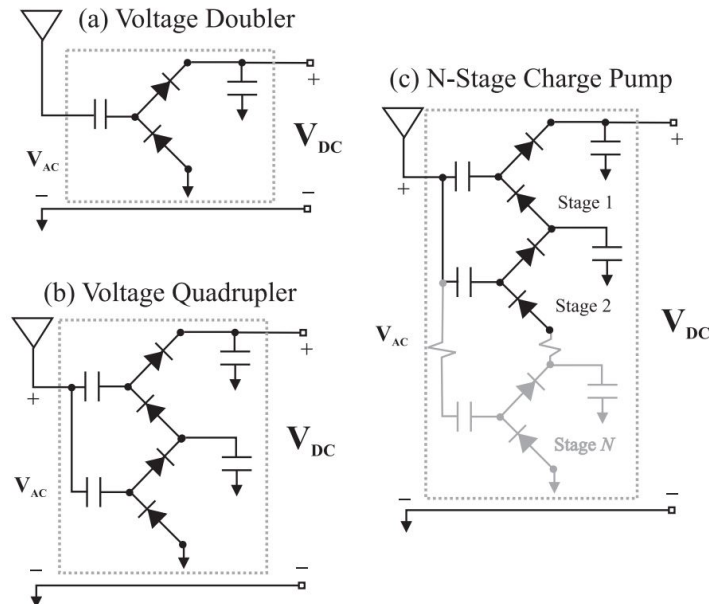


FIGURE 1.12: Charge pump's principle.

Similar to the configuration of voltage doubler rectifier, multistage rectifier is a combination of several identical cascaded stages (Fig.1.10 to Fig.1.12). Multistage rectifier can provide very high output DC voltage for several applications such as: charging the capacitor for an electrostatic vibration energy harvester [18], where the vibrations are converted into electricity by a mechanical attraction force, which depends on the voltage supplied from the rectifier to the capacitor plate.

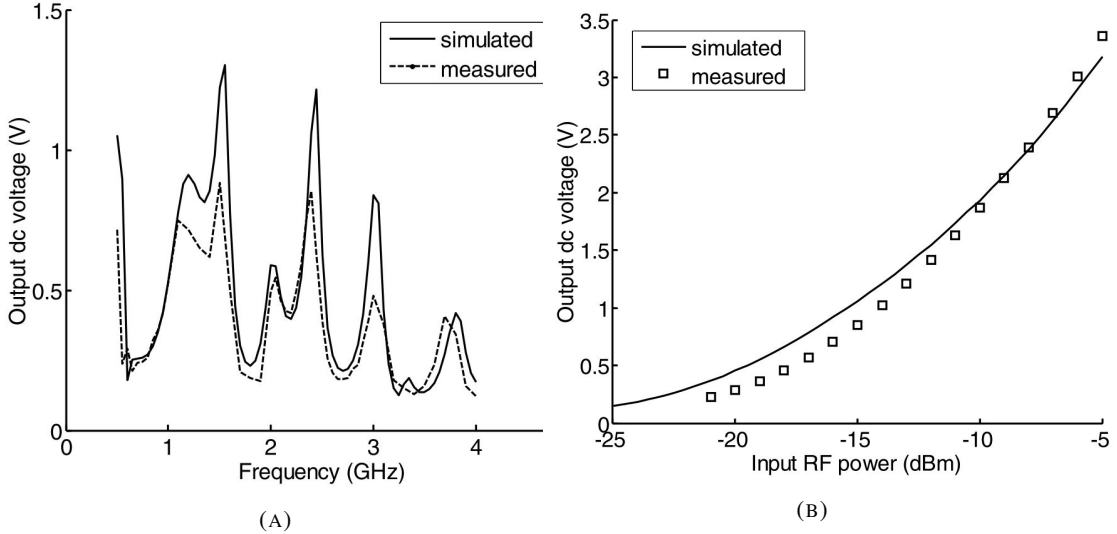


FIGURE 1.13: Output DC voltage of multistage rectifier. (A) versus frequency. (B) versus input RF power. [18]

Therefore, the output DC voltage of the rectifier is needed to be higher to reduce the charging time of the capacitor with 2.4-GHz Cockcroft–Walton multistage rectifier, which is designed and optimized to operate at low power densities and provide high voltage levels. As can be seen from Fig.1.13a and Fig.1.13b, the voltage DC output of multistage rectifier is considerably high. It reaches 3.5 V at -5 dBm. The output DC voltage get it highest value at 2.4 GHz, which is the optimum frequency of the circuit. The output DC voltage is 1.25 V at 2.4 GHz when the input power is -15 dBm. Also, in [21-23], the multistage rectifier are used in RFID applications and RF energy harvesting system using multi-band antenna arrays. For rectifier/rectenna in general, their applications in RFID and energy harvesting system can be found in [24-31].

In the next section, different types of rectifier/rectenna based on operating frequency will be presented.

### 1.2.5 Frequency behavior of rectifiers/rectennas

Power harvested wirelessly can replace completely or in part the battery in the near future, which deduct the environmental pollution significantly. Moreover, it also improves the convenience of using the smart sensors and devices without having to recharge them after certain amount of time. Ideally, the electronic devices and sensors should be able to harvest the energy from ambiance. Normally, there is different types of RF signals at different frequency ranges in the ambience. For different purposes, the rectifier/rectenna can be optimized at one frequency (narrow-band), several frequencies (multi-band), or a range of frequency (broad-band). All the rectifiers presented in section 1.2.1 to 1.2.4 are examples of narrow-band rectifier, where the circuit is optimized at a specific frequency. In this section, broadband rectifier and multi-band rectifier [32-36] will be presented. It is a promising way to help our future smart devices and sensors achieving the goal of harvesting energy wirelessly from ambience.

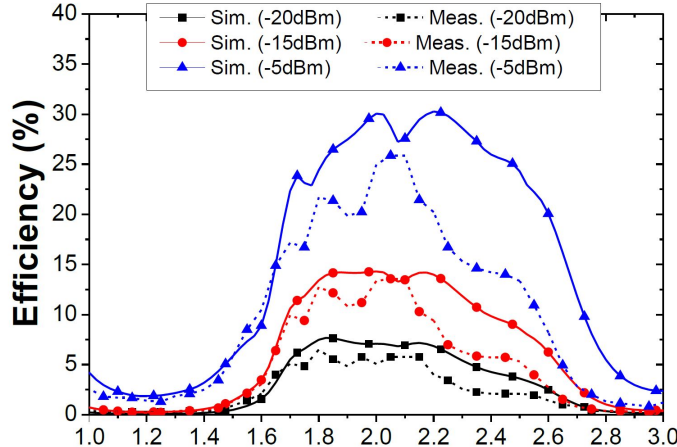


FIGURE 1.14: Simulated and measured efficiencies as function of frequency [32].

Fig.1.14 shows an example of RF-to-dc conversion efficiency of a broadband rectifier [32]. The efficiency is considerably constant at the frequency range from 1.6 to 2.8 GHz (GSM, UMTS, Wi-Fi and LTE2600/4G frequency band). For 3 levels of input powers, the behavior are the same. It demonstrates the wide-band behavior of this rectifier, different from narrow-band rectifier/rectenna that has narrow-band frequency of operation [9-31, 37]. But as can be seen, the efficiency at small power levels of -20 dBm and -15 dBm is significantly smaller than the efficiency at -5 dBm (7% at -20 dBm; 13% at -15 dBm and 30% at -5 dBm, for a frequency of 2 GHz). For that reason, improving the efficiency at low power levels is imperatively needed.

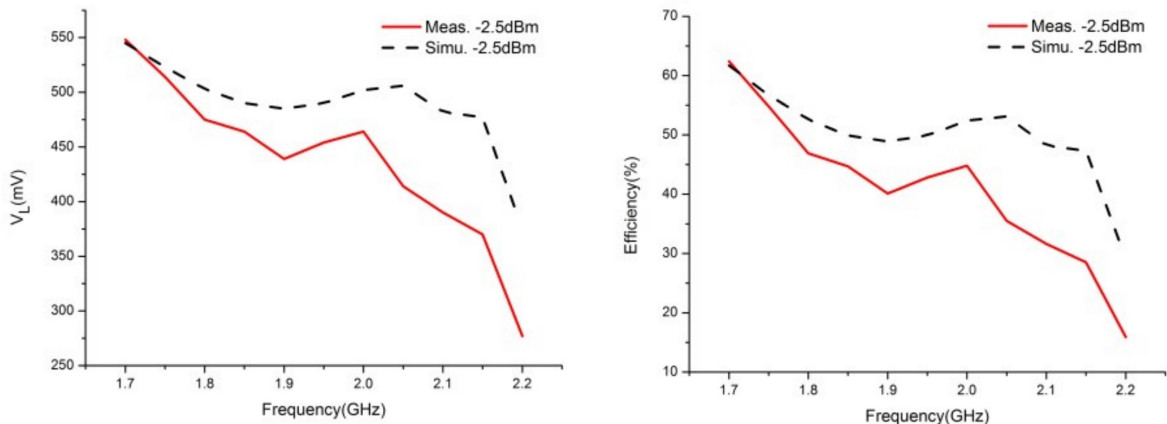


FIGURE 1.15: Simulated and measured efficiencies and output dc voltages as function of frequency [33].

Another broadband rectenna is proposed in [33]. It is aimed to harvest low-power levels (around -2.5 dBm) with a RF-to-dc conversion efficiency higher than 30 % within the frequency band ranging from 1.7 GHz to 2.1 GHz. The highest efficiency is 62.4 % at 1.7 GHz for a conventional CW (Fig.1.15).

A dual-band rectenna for ambient RF power harvesting is presented in [35]. The obtained results are shown in Fig.1.16. The rectenna is designed to harvest the ambient RF power of

GSM-1800 and UMTS-2100 bands. At -18 dBm, the highest efficiencies at 1.85 GHz and 2.15 GHz are 37.5 % and 35 %, respectively. The same behaviors are observed at other power levels from -30 to -21 dBm.

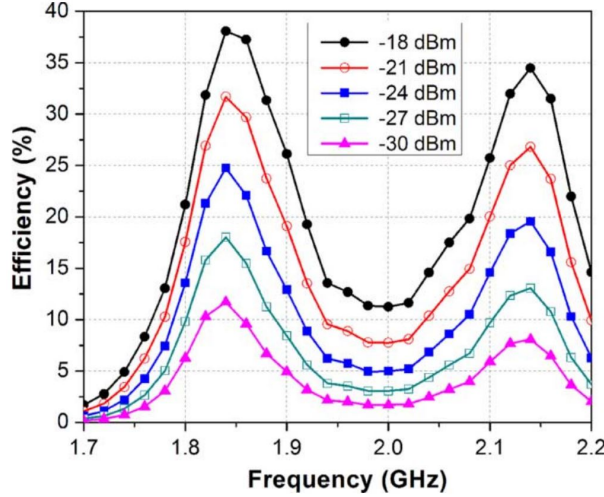


FIGURE 1.16: RF-to-dc conversion efficiency at different input power levels against frequency [35].

In [36], the authors propose a wide-band RF energy harvester for the frequency around 2.4 GHz-band ambient RF energy from wireless LAN, Wi-Fi, Bluetooth, ZigBee, etc. The rectifier was designed for low input power of -20 dBm. The measured peak efficiencies of the rectifier are 4.3 %, 24.3 %, 48.5 %, 63 % with the input power of -30, -20, -10, 0 dBm at the frequency of 2.472 GHz, respectively.

Aside from that, broadband rectifier is also presented in [38-42]. Dual-band and multi-band rectenna are demonstrated in [43-48]. They are designed and optimized for ambient energy harvesting and/or low power wireless transfer applications.

Overall, the RF-to-dc conversion efficiencies of the rectifiers and rectennas mentioned above are with a conventional CW. Except for broadband rectifier, the other structures have been previously optimized to operate at only one frequency of interest and their RF-to-dc performance decreases at other frequencies. Because for narrow-band rectifier/rectenna, the circuit is optimized to work at one frequency. Also, it obtained the highest RF-to-dc conversion efficiency at an optimum load value and RF power input. On the other hand, for multi-band rectenna, the circuit is optimized for several frequencies. Aside from that frequencies, the circuit is no more optimized and the RF-to-dc conversion efficiency decreases quickly.

The limitation of the RF-to-dc conversion efficiency is also due to the threshold voltage of the diode. Also, as the results of the non-linearity of the circuit, the DC voltage is degraded. For broadband or multi-band signal, at the same input power level, the efficiency is smaller than narrow-band rectifier. When the frequency bandwidth increases, the RF-to-dc conversion efficiency decreases. As explained, the necessity of improving the RF-to-dc conversion efficiency of rectenna and rectifier at low RF power levels is necessary and recently

attracts researchers. The state of the art and solutions for enhancing the RF-to-dc efficiency will be presented in the next section.

## 1.3 Enhancement of RF-to-dc conversion efficiency

### 1.3.1 RF-to-dc conversion efficiency of the rectenna and its limitation

Increasing the RF-to-dc conversion efficiency is one of the biggest challenges in wireless power transmission. The efficiency of the rectenna system is basically equivalent to its transfer function. It is written as the following formula:

$$\eta = 100\left(\frac{P_{out}}{P_{in}}\right) = 100\left(\frac{V_{out,DC}^2}{R_{load}}\right) \cdot \frac{1}{P_{in}} \quad (1.1)$$

where  $P_{in}$  is the input power of the system;  $P_{out}$  is the output power of the system.  $V_{out,DC}$  is the output voltage of the rectifier and  $R_{load}$  is the value of the charge.

Firstly, we can focus on rectenna, especially the diode and the DC output filter. Secondly, using power optimized waveforms (POWs) to improve the efficiency of the rectifier/rectenna is also a promising idea, which will be presented in the next sections.

As can be seen from Fig.1.17, for low input power levels, the efficiency is poor because the rectifying device is not completely switched on. As the input power increases, the efficiency increases and reaches a maximum value right before the input amplitude reaches the diode breakdown voltage ( $V_{br}$ ). After this point, the diode reverse current starts to be significant and high order harmonics start to appear, so the efficiency drops.

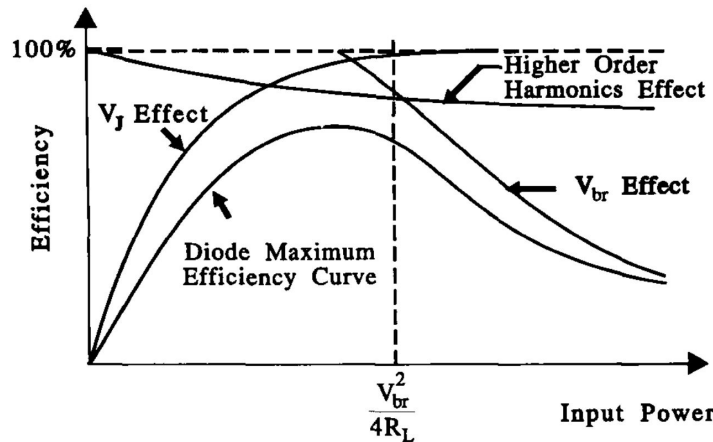


FIGURE 1.17: Diode's efficiency limitations [49].

The diode can significantly change the efficiency of the rectifier. From Fig.1.18, it can be observed that the angle  $\theta_{on}$  depends on the build-in voltage of the diode. For example, if  $V_{bi}$  (build-in voltage) is smaller,  $\theta_{on}$  will be greater. After calculation [50], the efficiency is proportional with  $\theta_{on}$ . It means with the smaller  $V_{bi}$  of the diode, we have greater efficiency. Therefore, one of the methods to improve the RF-to-dc ratio consists to fabricate new Schottky diodes with smaller  $V_{bi}$ .

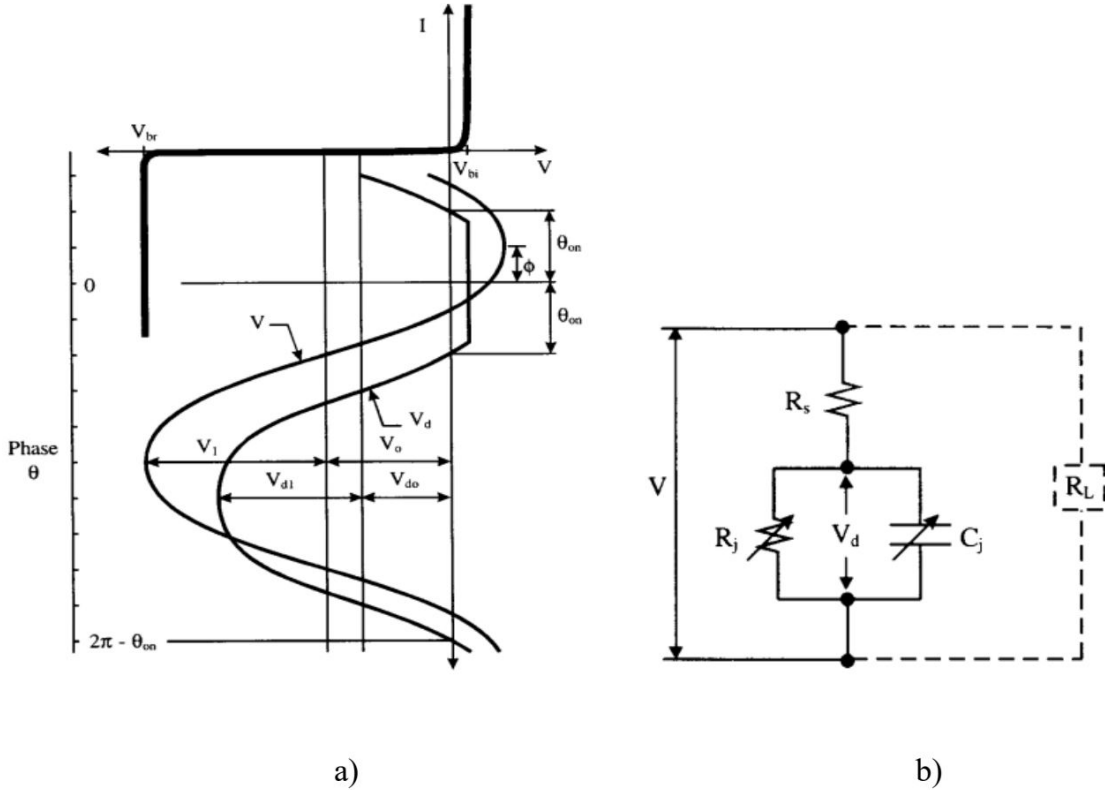


FIGURE 1.18: a) Diode junction voltage relationship. b) Equivalent circuit of the rectifying diode and DC load resistor [50].

### 1.3.2 Influence of the constitutive elements of the rectenna: diode, DC and HF filters

A solution to improve the RF-to-dc conversion efficiency is modifying the rectenna's characteristic such as the diode, the capacitance and the load resistance of the DC filter.

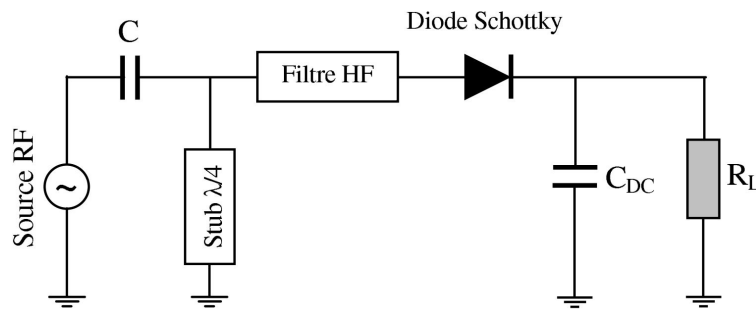


FIGURE 1.19: Equivalent schematic of series-mounted diode rectifier [6].

The impact of different parts of a rectifier (Fig. 1.19) has been developed in [6]. The author considered all the components of the rectifier thoroughly.

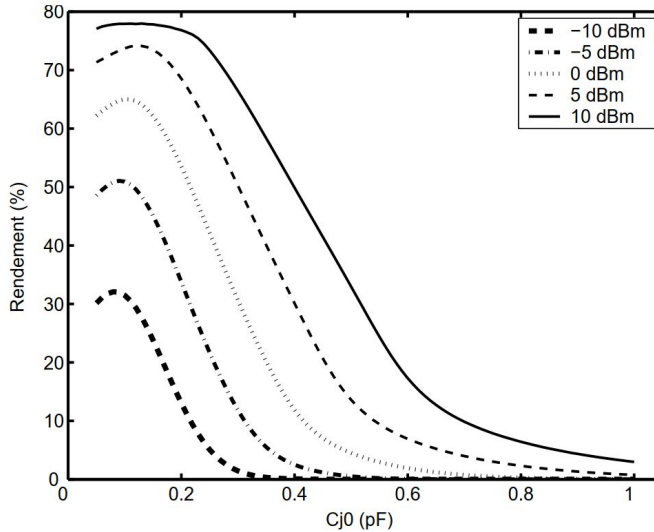


FIGURE 1.20: Efficiency vs diode's  $C_{j0}$  value ( $R_s = 5 \Omega$ ) [6].

In Fig.1.20, while varying the value of  $C_{j0}$  of the diode, the rectenna efficiency is decreased sharply when the value of  $C_{j0}$  increases. As  $C_{j0}$  is from 0 to 0.2 pF, the efficiency is quite high (up to 77 % for 10 dBm of RF input power). When  $C_{j0}$  is higher than 0.6 pF, that efficiency decreases to less than 10 %. The value  $C_{j0}$  of the diode plays an important role in RF-to-dc conversion efficiency of the rectenna.

When varying the value of  $R_s$  of the diode, as shown in Fig.1.21, the efficiency is slowly decreased as  $R_s$  increases. The variation is linear for all the input power levels.

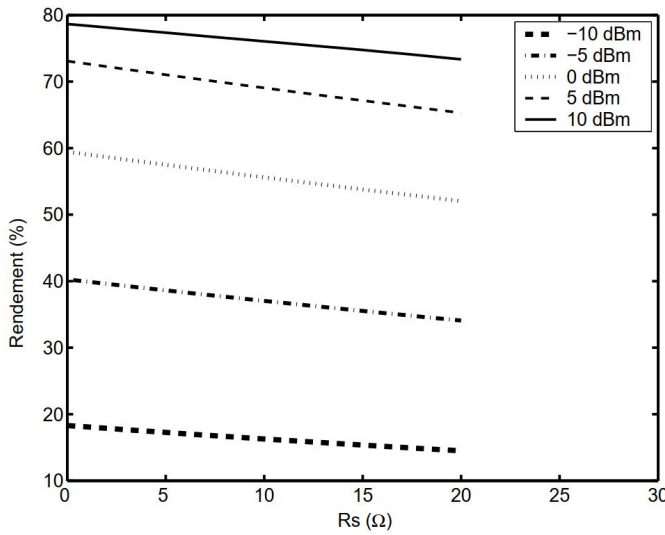
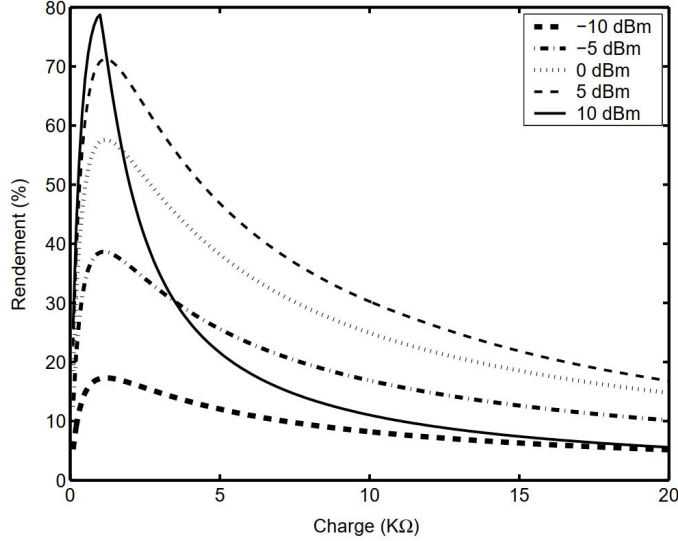
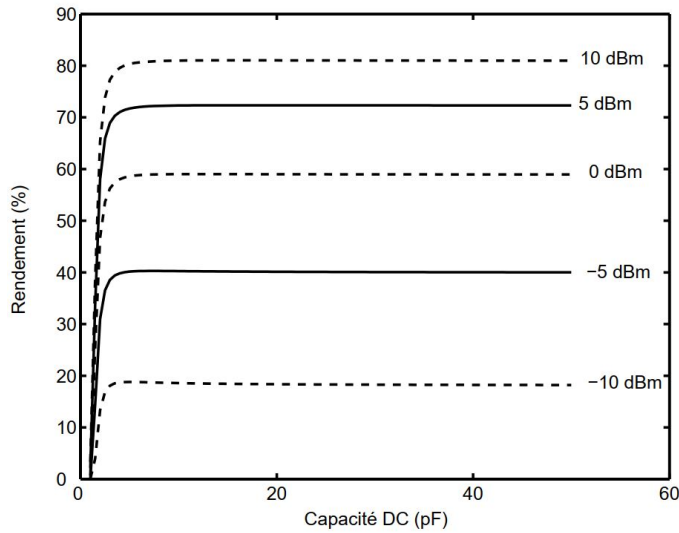


FIGURE 1.21: Efficiency vs diode's  $R_s$  value ( $C_{j0} = 0.18 \text{ pF}$ ) [6].

On the other hand, Fig1.22 shows the variation of the efficiency as a function of load for input powers, ranging from -10 to 10 dBm with considering a step of 5 dB. Load values range from  $100 \Omega$  to  $20 k\Omega$ . The results show that the efficiency is maximal around an optimal load value of  $1 k\Omega$ . For high load values, the input power reaches a critical value and the efficiency decreases

FIGURE 1.22: Efficiency vs load's value ( $C_{DC} = 33 \text{ pF}$ ) [6].

The influence of the DC filter capacitance on the conversion efficiency is exposed on Fig.1.23. The study was carried out over the power range from -10 to 10 dBm. The results show that from a certain value of the capacitance, the performance remains constant. This is because of the cutoff frequency of the low-pass filter. When this cutoff frequency is lower (or much lower) compared to the fundamental frequency, the value of the  $C_{DC}$  capacity does not matter. Overall, modifying the rectifying circuit's components values or the diode's characteristics can significantly change the performance of the energy harvesting devices.

FIGURE 1.23: Efficiency vs capacitor's value ( $R_L = 1.05 \text{ k}\Omega$ ) [6].

From this study, we can see the limitation of these types of circuits. The circuit is optimized to work around an operating point. This optimization operating point consists of a carrier frequency, an optimum load value and an input power level. For example, in this case, the optimum load value is only  $1.05 \text{ k}\Omega$ , the efficiency degrades quickly as the load value increases. At 10 dBm of power input, the efficiency is  $\approx 78 \%$  at load value of  $1.05 \text{ k}\Omega$  then

decreases to lower than 10 % at load value of  $20 \text{ k}\Omega$ . Also, the efficiency of the circuit is mainly dependent by the non-linear behavior of the diode.

So, when the circuit operates at non-optimum point, which means the frequency, the load and/or the input power level is modified, the question is how to achieve the same or better performance obtained at the optimum point. The choice for us is either to work on the diode component or to propose something else. In this thesis, without modifying the circuit, we also can achieve better RF-to-dc performance by using power optimized waveforms.

## 1.4 Waveforms optimization to improve RF-to-dc conversion efficiency

Another method of maximizing the performance of the rectenna consists of using the optimized signals with larger frequency spectrum.

As can be seen from the Fig.1.24, with different types of waveforms, such as one-tone, OFDM, chaotic and white-noise signal, applying to the same single-series-mounted diode rectifying circuit, we obtained different conversion efficiencies. The improvement at -15 dBm RF input power can be up to 43% (from 35% for CW to 50% for chaotic signal) [51]. The waveform can effect and change the efficiency of the RF-to-dc converter, so this is a very promising way to enhance the wireless power transmission with optimized-waveforms. This method is chosen in this thesis to demonstrate the advantages of POWs on RF-to-dc conversion efficiency of energy harvesting devices.

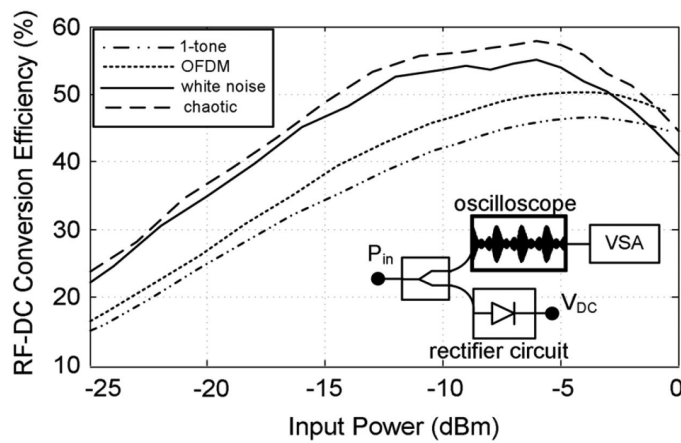


FIGURE 1.24: RF-to-dc conversion efficiency of different types of waveform [51].

By considering some types of waveform such as one-tone, OFDM, white noise and chaotic signal, the conversion efficiency can be improved with higher PAPR [51]. PAPR is calculated by this formula:

$$PAPR = 10\log_{10}\left(\frac{\text{Max}|x(t)|^2}{\langle x(t)^2 \rangle}\right) \quad (1.2)$$

Where  $x(t)$  is the time domain waveform of the signal;  $\langle x(t) \rangle$  is the average of the signal.

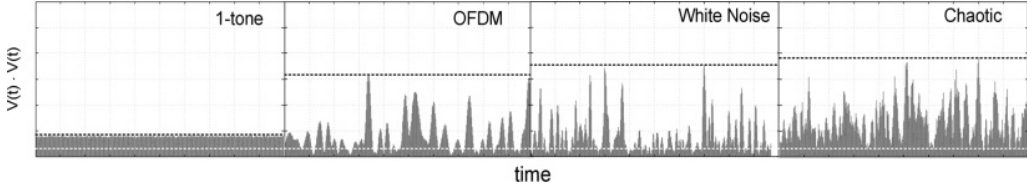


FIGURE 1.25: Instantaneous power of the different types of test signals. Dashed-white line indicates the average power that is the same for all the signals. Dashed-black line indicates the peak power value [51].

The instantaneous power of CW, OFDM, white noise and chaotic signal waveforms are presented in Fig.1.25. Meanwhile, Fig.1.26 shows the frequency spectrum of these waveforms in the frequency domain. One can clearly see that these signals has the same average power as dashed-white line but different peak power as dashed-black line. Therefore, different PAPR will be presented to give different RF-to-dc conversion efficiency as presented in Fig.1.24.

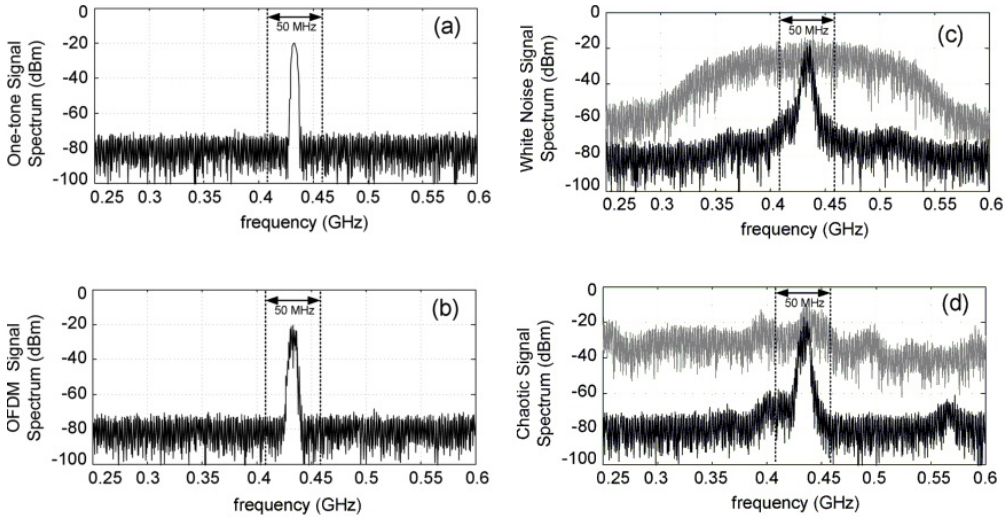


FIGURE 1.26: Signal spectrum (a) single carrier signal (b) OFDM signal (c) white noise signal (d) chaotic signal [51].

Signal with higher PAPR gives higher amplitude in a short period of time. A sufficient voltage is produced to pass the threshold voltage of the diode during that period so that the efficiency of the rectifier can be improved especially for low input power levels. Considering signal with high PAPR, multi-sine signal is generally used in WPT [15, 16, 52-65].

In [52, 53], N-POWs (N-tone multi-sine signal Power Optimized Waveforms) such as 2-POW, 4-POW and 8-POW are examined to compare the range and reliability of RFID systems for charge pump energy harvesting at 915 MHz. The read range and the DC output voltage of the RFID tags are improved with the increasing of the number of POW carriers. POW's implementation, demodulation and some types of POW like N-POW, Gaussian POW and square POW are used to measure the RFID tags sensitivity.

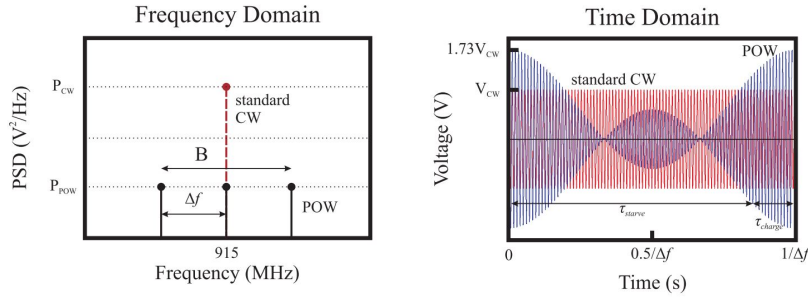


FIGURE 1.27: Frequency domain and time domain of 3-tone and CW signals [52].

The 3-tone signal (amplitude modulated signal) in frequency and time domain is proposed and explained in [52] (Fig. 1.27). In frequency domain, instead of having 1-tone signal with higher power spectral density, 3-tone signal has 3 frequencies:  $f$  (carrier frequency),  $f - \Delta f$  and  $f + \Delta f$  (where  $\Delta f$  is a frequency spacing between sub-carriers) with identical power spectral density that is equal one-third of CW. The frequency bandwidth  $B$  is  $2\Delta f$ .

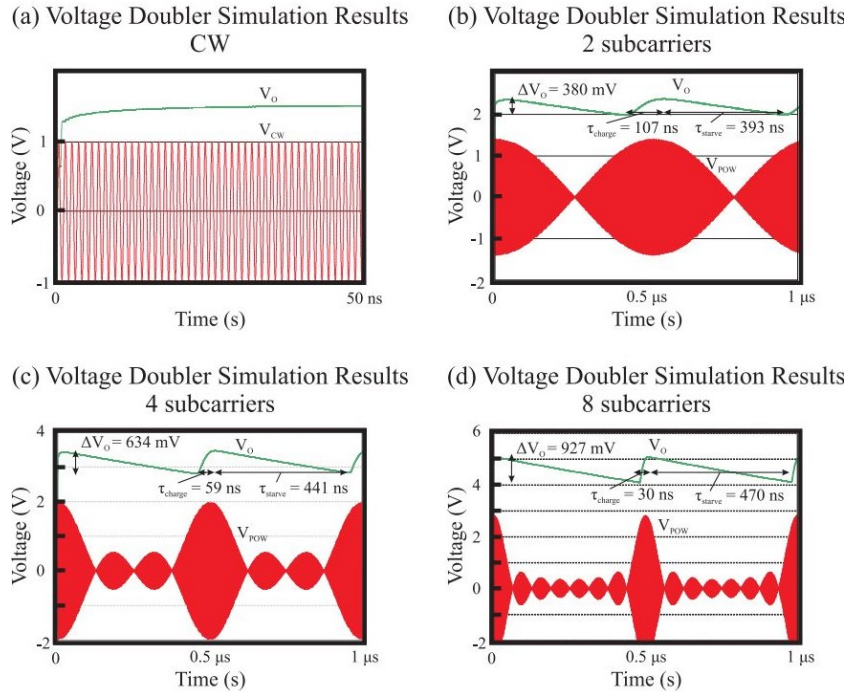


FIGURE 1.28: Simulation of input and output waveforms (N-POWs) of voltage doubler [52].

In [52], authors performed the simulation on voltage doubler rectifier with different types of input waveforms such as CW, 2-tone signal, 4-tone signal and 8-tone signal as the simulation of input and output waveforms shown in Fig. 1.28. As the number of sub-carriers doubled, we can see that the amplitude of the signal is increased by factor  $\sqrt{2}$ . It is coherence with the statement that the PAPR increases as the number of sub-carriers increases [49].

TABLE 1.1: Voltage doubler simulation results [52]

Input Type	Output Voltage	Output Ripple	Power Efficiency	Starve Time	Charge Time
915 MHz CW	1.53 V	1.25 mV	76.5 %	0.46 ns	0.08 ns
2-subcarrier POW	2.38 V	380 mV	84.1 %	107 ns	393 ns
4-subcarrier POW	3.47 V	634 mV	86.8 %	441 ns	59 ns
8-subcarrier POW	5.08 V	927 mV	89.8 %	470 ns	30 ns

The waveforms of the signal input and output are also changed. Ripple voltage appears with the multi-sine signal with the number of sub-carrier of 2 and above. The ripple voltage as well as the charge and discharge time are varied with the number of sub-carriers: as the number of sub-carriers increases, the ripple voltage is increased. For 2-tone signal,  $\Delta V_o = 380$  mV and the charging time is 107 ns. For 8-tone signal, these values are 927 mV and 30 ns, respectively. In the mean time, the discharge time is shorter. The power efficiency from Table 1.1 shows that the improvement can be up to 13.3% from 76.5% to 89.8% when replacing CW by 8-tone signal. With the PAPR increases, we obtain higher output DC voltage as demonstrated in [52-55, 59-65].

TABLE 1.2: Ideal simulated read-range [52]

Input Type	Minimum Reader Transmit Power	Read Range	Read Range Gain
915 MHz CW	7 dBm	46.4 cm	-
4-subcarrier POW	5.5 dBm	55.2 cm	+8.8 cm
8-subcarrier POW	5.1 dBm	56.8 cm	+10.4 cm

Besides, the measurement is done and the read-range of RFID is improved as presented in Table 1.2. The distance of CW is 46.4 cm, on the other hand, the distance of 4-tone signal and 8-tone signal are 55.2 cm and 56.8 cm, respectively. A POW can increase the power efficiency of charge pump based passive RF tags, which simultaneously increases read range and reliability.

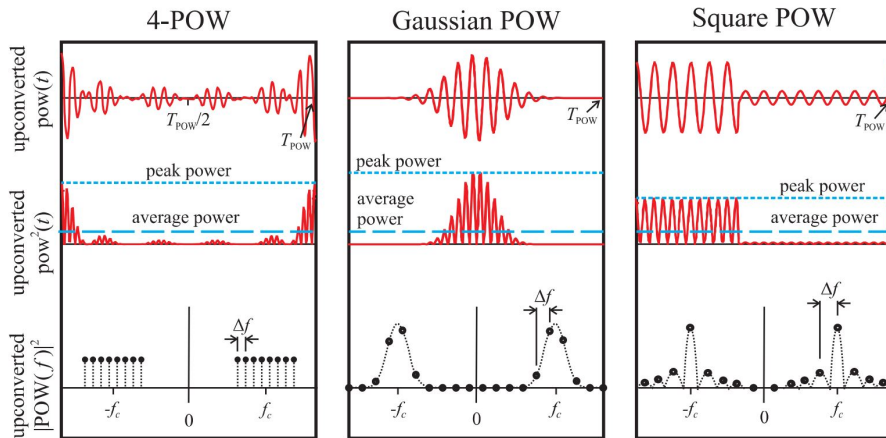


FIGURE 1.29: Time- and frequency-domain plots of one time period of the 4-POW, Gaussian POW, and Square POW [52].

Also in [52], the authors have shown that the larger peak power and more reliable envelop detection of the tag was found in Gaussian POW compared to other distribution rules such as Square POW or MS-POW (Multi-sine POW). The measurements have made to compare the performance between N-POW, Gaussian POW and Square POW with different types of tags and measure ranges. Fig.1.29 plots 3 signals in time and frequency domain all up-converted to a carrier frequency. Each plot consists of one POW period, the POW voltage waveform (top), signal power waveform (middle), and power spectral density (bottom) showing the peak power, average power, and frequency spacing.

A MS-POW can be designed and modified by its parameters such as sub carrier spacing, phase or sub carrier number. Using multi-sine excitation, the N-tone sinusoidal signals with  $0^\circ$  phase between the sub-carriers, can significantly increase the voltage DC output and also the power gain. With the same average power, the more tones applied, the more power gain achieved [54-55]. The power gain is calculated by the following equation:

$$G_p = 20\log_{10}\left(\frac{V_{outPOW}}{V_{out1-tone}}\right) \quad (1.3)$$

where  $V_{outPOW}$  is the output DC voltage of POW on the rectifier,  $V_{out1-tone}$  is the output DC voltage of CW on the rectifier.

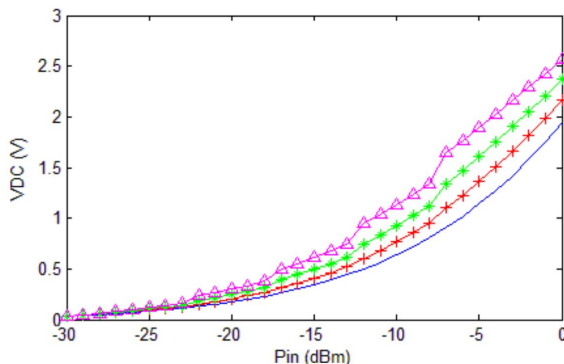


FIGURE 1.30: Measured DC voltage (V) as function of input power (dBm) for: 1-tone (solid blue), 2-tones (red crosses), 4-tones (green stars) and 16-tones (magenta triangles) [54].

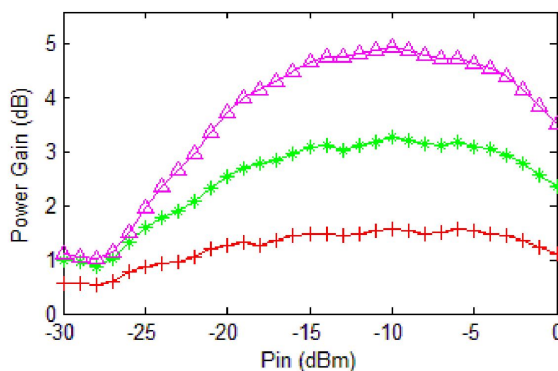


FIGURE 1.31: Measured power gain (dB) as function of input power (dBm) for: 2-tones (red crosses), 4-tones (green stars) and 16-tones (magenta triangles) [54].

In [54], the simulation and measurement on the voltage doubler rectifier have been done with 1-tone, 2-tone, 4-tone and 16-tone MS-POW, the measurement results are presented in Fig.1.30 and Fig.1.31. As can be seen, the highest gain obtained is approximately 5 dB at -15 dBm with 16-tone signal, meanwhile, with the increase of the number of sub-carriers, the power gain is improved. In term of output DC voltage, the improvement from 2V to 2.5 V is recorded at 0 dBm of input power.

Signal with high PAPR seems to be one of the most effective ways to improve the RF-to-dc conversion efficiency. That is the reason why chaotic signal with high PAPR is presented in [51, 56-58] to compare with one-tone signal.

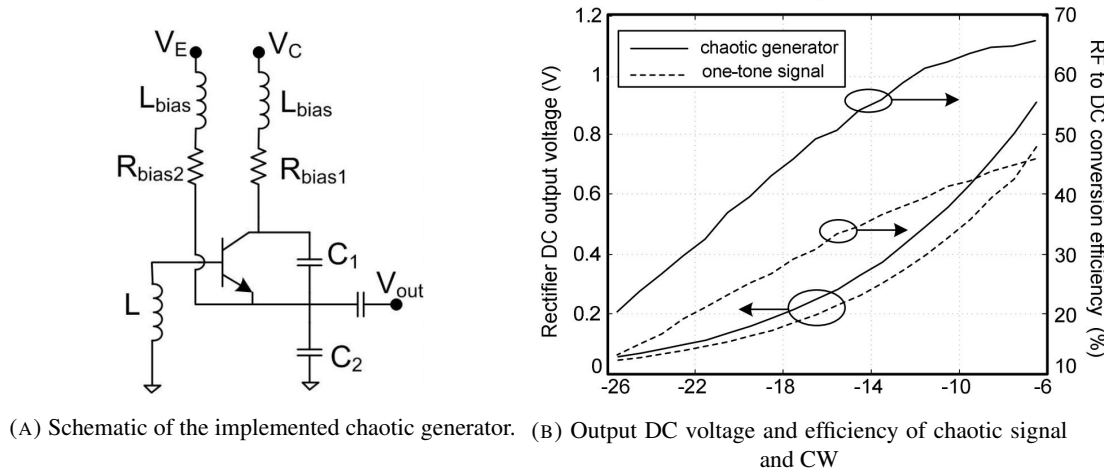


FIGURE 1.32: Chaotic signal generator and DC output (voltage and efficiency) [56].

In [56], chaotic signal is generated by an oscillator as in Fig.1.32a. The chaotic signal of 433 MHz is compared with 1-tone signal on the single series-diode rectifier. The results show that the chaotic signal with higher PAPR has the improvement in term of both output DC voltage and RF-to-dc conversion efficiency as shown in Fig.1.32b. For an input power of -6.5 dBm, the obtained DC voltage for the one-tone signal is 0.76V corresponding to a 46% RF-to-dc conversion efficiency while the chaotic signal provides a output DC voltage of 0.91 V that allows 66% of RF-to-dc conversion efficiency.

As reducing the input power level, the improvement in the RF-to-dc conversion efficiency is decreased. Despite of that, we can also obtain improvements approximately of 15% (from 22% for CW to 37% for chaotic signal) at -20 dBm RF input power. As a disadvantage, chaotic signals have a continuous and broadband spectrum, so it is necessary to filter them to avoid radiating in restricted or not allowed frequency bands. On the other hand, according to [58], synthesizing chaotic waveforms can be less complex than synthesizing other types of signals. But in our work, at the beginning of the thesis, simulating chaotic signal in time domain at the carrier frequency around 1 GHz using ADS simulation is time consuming. Moreover, the computer's configuration is not sufficient. Because it requires huge calculation and RAM (Random Access Memory) of the computer to perform the simulation. For that reason, in our thesis, the simulation of chaotic signal with rectifying circuit to compare with multi-sine signal was not completed.

Others publications also focus on signal with high PAPR to improve the performance of rectifier circuit such as [59-65]. The multi-sine signals with high PAPR are used. The measurement and the simulation also show that signals with higher PAPR have better performance in terms of RF-to-dc conversion efficiency of the rectifying circuits compared to 1-tone signal.

Not only PAPR is the factor that changes the RF-to-dc conversion efficiency of the waveforms, but instantaneous power variance (IPV), which is computed by the variation between the instant power of the signal and its average value, also plays the role on when considering the DC output. IPV is calculated as in Equation.1.4:

$$IPV = E [P - P_A]^2 \quad (1.4)$$

where  $P$  is the instantaneous power of the signal;  $P_A$  is the average power of the signal, and  $E$  denote the expectation [66].

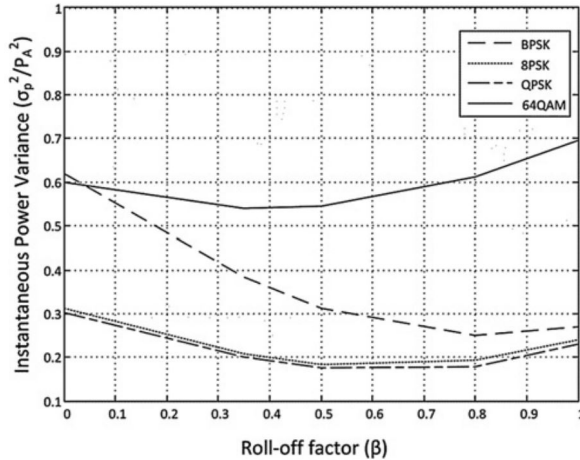


FIGURE 1.33: Simulated IPV of different modulated signals for different roll-off factor values [66].

In [66], while changing the value of roll-off factor  $\beta$ , the modulated signals such as BPSK (Binary Phase Shift Keying), 8-PSK, QPSK (Quadrature Phase Shift Keying) and 64 QAM (Quadrature Amplitude Modulation) give different IPVs. Note that roll-off factor  $\beta$  is the measure of the excess bandwidth of the filter that varies from 0 to 1. As shown in Fig.1.33, the IPV of BPSK varied the most notable as the highest value of 0.6 at  $\beta = 0$  and drops to 0.3 as  $\beta = 1$ , on the other hand, IPV of the other 3 signals are considerably constant regardless of  $\beta$ .

From Fig.1.34, at a input power of -20 dBm and 0 dBm, the RF-to-dc conversion efficiency of these signals have the same behavior versus the load value. The efficiency is higher with small load value and decreases sharply while the load value increases. The input signals have the same average power but different RF-to-dc conversion efficiency due to the difference in terms of IPV. IPV of 4-tone signal and OFDM signal is also presented in [20] to show the difference in term of output DC voltage of the 2 signals on the multi-stage rectifier.

Overall, the gap between OFDM and 1-tone signal is not significant, and OFDM signal is comparable with 4-tone signal [20].

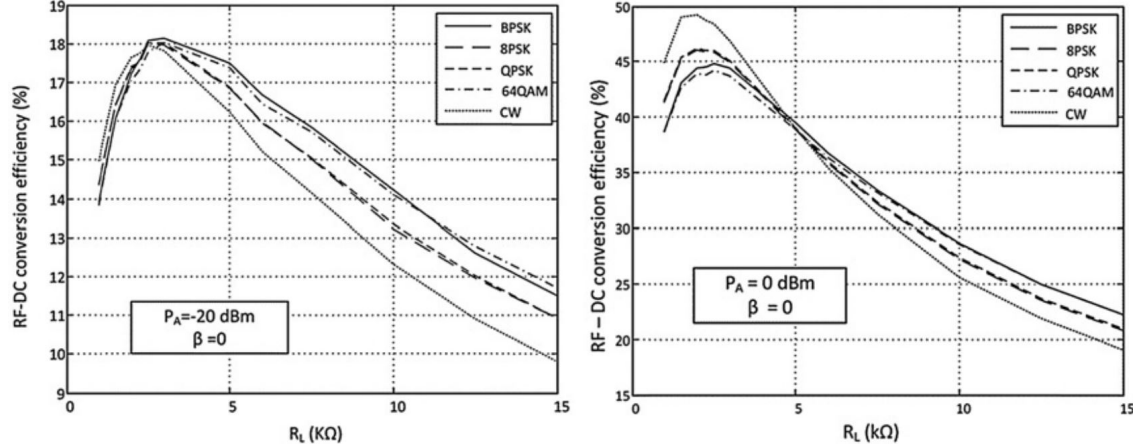


FIGURE 1.34: RF-to-dc conversion efficiency of different modulated signals [66].

Compared to these signals mentioned above (multi-sine, OFDM, chaotic, QAM, BSK, etc), RF pulse signal can reach a significantly higher PAPR [15, 16]. RF pulse signal is generated by modulation method as displayed in Fig.1.35. A square pulse with frequency  $f_m$  ( $f_c \gg f_m$ ) is used to modulate CW with frequency  $f_c$ . The shape of RF pulse depends on the shape of the periodic square signal.

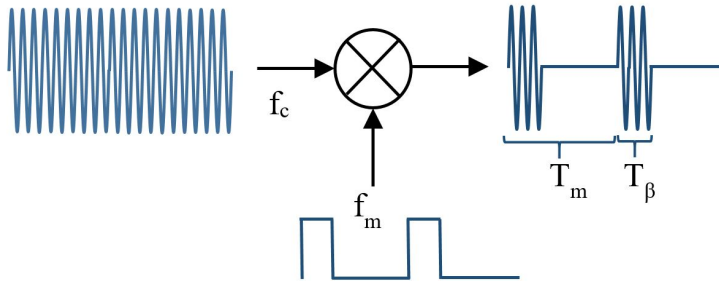


FIGURE 1.35: Square pulse modulation.

Duty cycle of RF pulse signal is calculated by this formula:

$$\beta(\%) = 100 \frac{T_\beta}{T_m} \quad (1.5)$$

While varying the duty cycle of the pulse wave, the shape of RF pulse signal changes. For duty cycle of 1.57 %, the PAPR is 21 dB, which is equivalent to 64 sub-carriers multi-sine signal [16]. It also shows the increase of output DC voltage of the shunt-mounted diode and voltage doubler rectifier while varying the duty cycle as well as the output capacitance and load's impedance [67-70]. The process of designing a proper rectenna that has optimum performance with RF pulse signal is presented in [68]. The authors test RF pulse signal with a single shunt-mounted-diode rectifier and the results are shown in Fig.1.36. CW has the

highest efficiency at the load impedance smaller than  $1 \text{ k}\Omega$ . On the other hand, RF pulse signals with different duty cycles show the improvement at higher load impedance from  $1 \text{ k}\Omega$  to  $100 \text{ k}\Omega$ . RF pulse signal with 10% of duty cycle has the best efficiency (over 70 %) at  $10 \text{ k}\Omega$ . At each level of load resistance, we can find an optimum duty cycle to have maximum performance of the circuit.

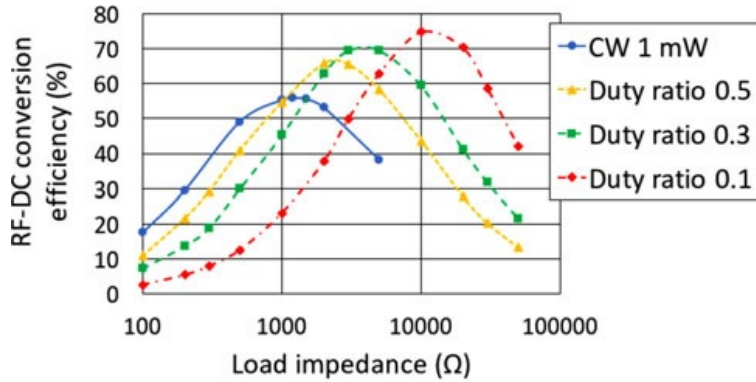


FIGURE 1.36: RF-to-dc conversion efficiency of different CW and RF pulse signals [68].

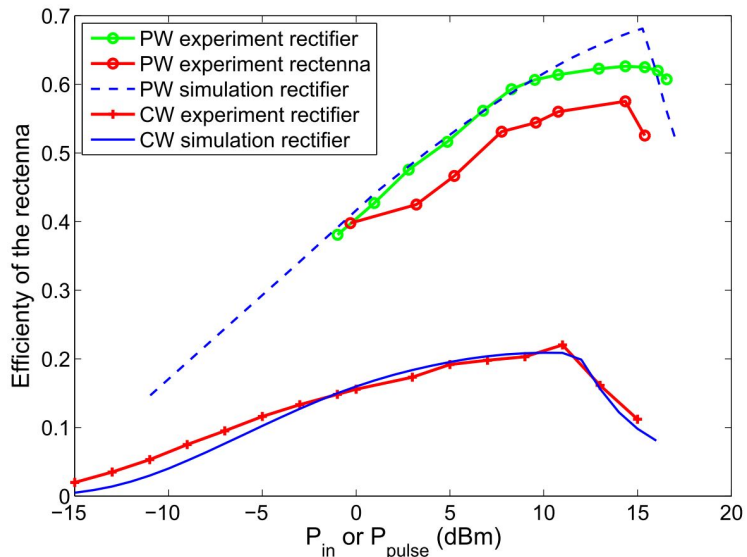


FIGURE 1.37: RF-to-dc conversion efficiency of different CW and RF pulse signals [68].

From Fig.1.37, the rectifier efficiency is increased from 20 % (1-tone) to approximately 55 % (RF pulse) at 10 dBm, which is a considerably high RF input power. RF pulse signal has the unique characteristic, which will be presented in the next chapter of this thesis for lower RF input power levels and for a wide frequency bandwidth.

In [69], using voltage-doubler rectenna, the authors show the input power advantage of using RF pulse signal over CW. To obtain a level of output DC voltage, RF pulse signal needs lower input power at the rectenna. For example to have 0.7 V, it requires RF pulse to have only -11 dBm input power, while for CW, that value is -8.9 dBm, which is 2.1 dBm higher. The same behaviors are found for other output DC voltage levels (Table.1.3).

TABLE 1.3: The performance of output voltage using impulsive wireless power transmission with horn antennas [69].

<b>To Obtain Same <math>V_{out}</math> (V)</b>	<b>Input Power Needed by</b>		<b>Saved Input Power (dBm)</b>
	<b>Using Impulse (dBm)</b>	<b>Using CW (dBm)</b>	
0.700	-11.0	-8.9	2.1
1.207	-7.3	-5.5	1.8
1.601	-5.1	-3.4	1.7
1.900	-3.7	-2.1	1.6

Overall, different type of waveforms have been studied in such as: multi-sine signal, OFDM, chaotic, RF pulse signal. OFDM has slight improvement compared to 1 tone signal and comparable with 4-tone signal. Meanwhile, chaotic signal works based on the unbalanced oscillator, has an improvement compared to CW as demonstrated in [51, 56]. Among these signals, multi-sine and RF pulse signal present adjustable PAPR by changing the number of tone for multi-sine and duty cycle for RF pulse signal. Aside of PAPR, other parameters such as carrier frequency, frequency bandwidth of the signal can be adjusted to improve the output voltage of the rectifying circuit. The improvement in terms of output DC voltage as well as RF-to-dc conversion efficiency is noticeable. For that reason, RF pulse signal and multi-sine signal will be used in this thesis. The studies of multi-sine and RF pulse with different type of rectenna, rectifiers will be demonstrated in the next chapters.

## 1.5 Conclusion

In this chapter, a general introduction to WPT system as well as the brief history of WPT have been presented. Then, the rectenna and rectifier's topologies such as series-mounted diode, shunt-mounted diode, voltage doubler and multi-stage rectifiers are demonstrated. Moreover, the rectifier classified by operating frequency such as narrow-band, multi-band and broadband are also presented. The RF-to-dc conversion efficiency of the rectennas and their limitations due to the characteristic of the diodes and other components such as capacitor and resistor of the filter are mentioned. To overcome that limitations, POWs such as multi-sine, RF pulse, OFDM, chaotic signals are proposed. The researches show that with POWs, the RF-to-dc conversion efficiency of the rectifying circuit is improved compared to CW at certain input power levels and output loads.

After considering, multi-sine signal and RF pulse signal, which show the best performance on the rectifiers are chosen for further study. The simulation and measurement of those signals on different rectifier and rectenna topologies will be found in the next chapters of this thesis.

In chapter 2, beside multi-sine and RF pulse signals, the simulation using ADS is also presented. After that, we perform the measurement on basic rectifier topologies to show the advantages of using POWs over conventional CW signal.



# Bibliography

- [1] Mohammed, S. Sheik, K. Ramasamy, and T. Shanmuganantham. *Wireless power transmission—a next generation power transmission system*, International Journal of Computer Applications 1.13 (2010): 100-103
- [2] W. C. Brown *The history of power transmission by radio waves*, IEEE Trans. Microwave Theory Tech., vol. MTT-32, pp. 1230–1242, 1984.
- [3] L. Deschamps *Transmission d'énergie sans fil - Etat de l'art et perspectives*, Technologies futures pour le transport d'électricité, REE no. 9, Octobre 2004, pp 75-81.
- [4] N. Tesla, *The Transmission of Electric Energy Without Wires (The Thirteenth Anniversary Number of the Electrical World and Engineer)*, New York: McGraw-Hill, Mar. 5, 1904.
- [5] A. Celeste, P. Jeanty and G. Pignolet, *Case Study in Reunion Island*, Sciences Directes, Acta Astronautica 54, 2004, pp 253-258.
- [6] Hakim Takhedmit *Modélisation et Conception de Circuits de Réception Complexes pour la Transmission d'Énergie Sans Fil à 2.45 GHz.*, PhD Thesis 2010.
- [7] Naoki Shinohara *Power without wires*, IEEE Microwave Magazine, Vol. 12, Issue 7, pp.S64-S73,
- [8] Alírio de Jesus Soares Boaventura *Efficient Wireless Power Transfer and Radio Frequency Identification Systems*, PhD Thesis 2016.
- [9] Marian, V., Vollaire, C., Verdier, J., and Allard, B. *Rectenna circuit topologies for contactless energy transfer*, IEEE Microwave and Wireless Components Letters, 24(5), 354-356.
- [10] F. Hoadley, S. Kennedy and G. Skibinski, *Comparison of AC to DC rectifier topologies operating on various power distribution networks*, 2008 55th IEEE Petroleum and Chemical Industry Technical Conference, Cincinnati, OH, 2008, pp. 1-9, doi: 10.1109/P-CICON.2008.4663981.
- [11] Marian, Vlad, Christian Vollaire, Bruno Allard, and Jacques Verdier. *Low power rectenna topologies for medium range wireless energy transfer*. In Proceedings of the 2011 14th European Conference on Power Electronics and Applications, pp. 1-10. IEEE, 2011.

- [12] Marian, Vlad, Salah Eddine Adami, Christian Vollaire, Bruno Allard, and Jacques Verdier. *Wireless energy transfer using zero bias Schottky diodes rectenna structures*. In Advanced Materials Research, vol. 324, pp. 449-452. Trans Tech Publications Ltd, 2011.
- [13] V. Marian, C. Menudier, M. Thevenot, C. Vollaire, J. Verdier and B. Allard, *Efficient design of rectifying antennas for low power detection*, 2011 IEEE MTT-S International Microwave Symposium, Baltimore, MD, 2011, pp. 1-4, doi: 10.1109/MWSYM.2011.5972862.
- [14] <https://datasheetspdf.com/datasheet/HSMS-2850.html>
- [15] Viet-Duc Pham, Hakim Takhedmit, Laurent Cirio. *Impact of Multisine and RF Pulse Signals on the Efficiency of Different Rectifier Topologies for WPT* March 2020, Conference: 14th European Conference on Antennas and Propagation (EuCAP), Copenhagen, Denmark
- [16] Viet-Duc Pham, Hakim Takhedmit, Laurent Cirio. *Waveform Optimization for Efficiency Improvement of Traditional RF-to-dc Rectifiers Without Input Matching Network* March 2020, Conference: 14th European Conference on Antennas and Propagation (EuCAP), Copenhagen, Denmark
- [17] <https://datasheetspdf.com/datasheet/HSMS-2860.html>
- [18] Takhedmit, H., Saddi, Z., Karami, A., Bassat, P., and Cirio, L. *Electrostatic vibration energy harvester with 2.4-GHz Cockcroft–Walton rectenna start-up*, Comptes Rendus Physique, 18(2), 98-106.
- [19] Takhedmit, H., Kilani, H., Cirio, L., Bassat, P., and Picon, O. *Design and experiments of a 2.4-GHz voltage multiplier for RF energy harvesting*, Proc. Power MEMS, 448-451.
- [20] Pham, Viet-Duc, Hakim Takhedmit, and Laurent Cirio. *Performance Improvement of a 2.4-GHz Multi-stage Rectifier Using Power Optimized Waveforms* In 2018 25th IEEE International Conference on Electronics, Circuits and Systems (ICECS), pp. 293-296. IEEE, 2018.
- [21] Barnett, Ray, Steve Lazar, and Jin Liu. *Design of multistage rectifiers with low-cost impedance matching for passive RFID tags* In IEEE Radio Frequency Integrated Circuits (RFIC) Symposium, 2006, pp. 4-pp. IEEE, 2006.
- [22] Barcak, J. Michael, and Hakan P. Partal. *Efficient RF energy harvesting by using multi-band microstrip antenna arrays with multistage rectifiers*. In 2012 IEEE Subthreshold Microelectronics Conference (SubVT), pp. 1-3. IEEE, 2012.
- [23] Seemann, K., G. Hofer, F. Cilek, and R. Weigel. *Single-ended ultra-low-power multi-stage rectifiers for passive RFID tags at UHF and microwave frequencies*. In 2006 IEEE Radio and Wireless Symposium, pp. 479-482. IEEE, 2006.

- [24] Kotani, Koji, Atsushi Sasaki, and Takashi Ito. *High-efficiency differential-drive CMOS rectifier for UHF RFIDs*. IEEE Journal of Solid-State Circuits 44, no. 11 (2009): 3011-3018.
- [25] Olgun, Ugur, C-C. Chen, and John L. Volakis. *Design of an efficient ambient WiFi energy harvesting system*. IET Microwaves, Antennas Propagation 6, no. 11 (2012): 1200-1206.
- [26] Popovic, Zoya. *Cut the cord: Low-power far-field wireless powering*. IEEE Microwave Magazine 14, no. 2 (2013): 55-62.
- [27] S. S. B. Hong, R. Ibrahim, M. H. M. Khir, H. Daud and M. A. Zakariya, *Rectenna architecture based energy harvester for low power RFID application*, 2012 4th International Conference on Intelligent and Advanced Systems (ICIAS2012), Kuala Lumpur, 2012, pp. 382-387, doi: 10.1109/ICIAS.2012.6306223.
- [28] S. D. Assimonis, S. Daskalakis and A. Bletsas, *Efficient RF harvesting for low-power input with low-cost lossy substrate rectenna grid*, 2014 IEEE RFID Technology and Applications Conference (RFID-TA), Tampere, 2014, pp. 1-6, doi: 10.1109/RFID-TA.2014.6934190.
- [29] Young-Soo Na, Jin-Sub Kim, Yong-Chul Kang, Sang-Gi Byeon and Kuk-Hwan Rha, *Design of a 2.45 GHz passive transponder using printed dipole rectenna for RFID application*, 2004 IEEE Region 10 Conference TENCON 2004., Chiang Mai, 2004, pp. 547-549 Vol. 3, doi: 10.1109/TENCON.2004.1414829.
- [30] Ghadimi, N., Ojaroudi, M. *A Novel Design of Low Power Rectenna for Wireless Sensor and RFID Applications*. Wireless Pers Commun 78, 1177–1186 (2014).
- [31] Y. Tikhov, I. Song and Y. Min, *Rectenna Design for Passive RFID Transponders*, 2007 European Conference on Wireless Technologies, Munich, 2007, pp. 237-240, doi: 10.1109/ECWT.2007.4403990.
- [32] H. Mahfoud, M. Tellache, and H. Takhedmit *A Wideband Rectifier Array on Dual-Polarized Differential-feed Fractal Slotted Ground Antenna for RF Energy Harvesting*, International Journal of RF and Microwave Computer-Aided Engineering 29, no. 8 (2019): e21775.
- [33] H. Ye and Q. Chu, *A broadband rectenna for harvesting low-power RF energy* 2016 International Symposium on Antennas and Propagation (ISAP), Okinawa, 2016, pp. 46-47.
- [34] S. Song, M. Su, Y. Liu, S. Li and B. Tang, *A novel broadband rectenna for energy harvesting*, 2016 International Symposium on Antennas and Propagation (ISAP), Okinawa, 2016, pp. 1082-1083.

- [35] H. Sun, Y. Guo, M. He and Z. Zhong, *A Dual-Band Rectenna Using Broadband Yagi Antenna Array for Ambient RF Power Harvesting*, in IEEE Antennas and Wireless Propagation Letters, vol. 12, pp. 918-921, 2013, doi: 10.1109/LAWP.2013.2272873.
- [36] Yong Huang, N. Shinohara and H. Toromura, *A wideband rectenna for 2.4 GHz-band RF energy harvesting*, 2016 IEEE Wireless Power Transfer Conference (WPTC), Aveiro, 2016, pp. 1-3, doi: 10.1109/WPT.2016.7498816.
- [37] Sampe JA, Zulkifli FF, Semsudin NA, Islam MS, Majlis BY. *Ultra low power hybrid micro energy harvester using RF, thermal and vibration for biomedical devices*. International Journal of Pharmacy and Pharmaceutical Sciences. 2016;8(2):18-21.
- [38] Song, Chaoyun, Yi Huang, Jiafeng Zhou, Jingwei Zhang, Sheng Yuan, and Paul Carter. *A high-efficiency broadband rectenna for ambient wireless energy harvesting*. IEEE Transactions on Antennas and Propagation 63, no. 8 (2015): 3486-3495.
- [39] Nie, Mei-Juan, Xue-Xia Yang, Guan-Nan Tan, and Bing Han. *A compact 2.45-GHz broadband rectenna using grounded coplanar waveguide*. IEEE antennas and wireless propagation letters 14 (2015): 986-989.
- [40] Shi, Yanyan, Jianwei Jing, Yue Fan, Lan Yang, Yan Li, and Meng Wang. *A novel compact broadband rectenna for ambient RF energy harvesting*. AEU-International Journal of Electronics and Communications 95 (2018): 264-270.
- [41] Agrawal, Sachin, Manoj Singh Parihar, and P. N. Kondekar. *Broadband rectenna for radio frequency energy harvesting application*. IETE Journal of Research 64, no. 3 (2018): 347-353.
- [42] Arrawatia, Mahima, Maryam Shojaei Baghini, and Girish Kumar. *Broadband rectenna array for RF energy harvesting*. In 2016 IEEE International Symposium on Antennas and Propagation (APSURSI), pp. 1869-1870. IEEE, 2016.
- [43] Palazzi, Valentina, Jimmy Hester, Jo Bito, Federico Alimenti, Christos Kalialakis, Ana Collado, Paolo Mezzanotte, Apostolos Georgiadis, Luca Roselli, and Manos M. Tentzeris. *A novel ultra-lightweight multiband rectenna on paper for RF energy harvesting in the next generation LTE bands*. IEEE Transactions on Microwave Theory and Techniques 66, no. 1 (2017): 366-379.
- [44] Kuhn, Veronique, Cyril Lahuec, Fabrice Seguin, and Christian Person. *A multi-band stacked RF energy harvester with RF-to-DC efficiency up to 84%*. IEEE transactions on microwave theory and techniques 63, no. 5 (2015): 1768-1778.
- [45] Okba, Abderrahim, Alexandru Takacs, Hervé Aubert, Samuel Charlot, and Pierre-François Calmon. *Multiband rectenna for microwave applications*. Comptes Rendus Physique 18, no. 2 (2017): 107-117.
- [46] Ho, Dinh-Khanh, Ines Kharrat, Van-Duc Ngo, Tan-Phu Vuong, Quoc-Cuong Nguyen, and Minh-Thuy Le. *Dual-band rectenna for ambient RF energy harvesting at GSM 900*

- MHz and 1800 MHz.* In 2016 IEEE International Conference on Sustainable Energy Technologies (ICSET), pp. 306-310. IEEE, 2016.
- [47] Adam, Ismahayati, M. Najib M. Yasin, Hasliza A. Rahim, Ping J. Soh, and M. Fareq Abdulmalek. *A compact dual-band rectenna for ambient RF energy harvesting.* Microwave and Optical Technology Letters 60, no. 11 (2018): 2740-2748.
- [48] Chandravanshi, Sandhya, Sanchari Sen Sarma, and Mohammad Jaleel Akhtar. *Design of triple band differential rectenna for RF energy harvesting.* IEEE Transactions on Antennas and Propagation 66, no. 6 (2018): 2716-2726.
- [49] T. Yoo and K. Chang, *Theoretical and experimental development of 10 and 35 GHz rectennas,* in *IEEE Transactions on Microwave Theory and Techniques*, vol. 40, no. 6, pp. 1259-1266, June 1992, doi: 10.1109/22.141359.
- [50] J. O. McSpadden, Lu Fan and Kai Chang *Design and experiments of a high-conversion-efficiency 5.8-GHz rectenna,* in *IEEE Transactions on Microwave Theory and Techniques*, vol. 46, no. 12, pp. 2053-2060, Dec. 1998, doi: 10.1109/22.739282.
- [51] Collado, A., and Georgiadis, A. *Optimal waveforms for efficient wireless power transmission,* IEEE Microwave and Wireless Components Letters, 24(5), 354-356.
- [52] Trotter, M. S., Griffin, J. D., and Durgin, G. D. *Power-optimized waveforms for improving the range and reliability of RFID systems,* In *RFID, 2009 IEEE International Conference on*(pp. 80-87). IEEE.
- [53] Trotter and Durgin, G. D. *Survey of range improvement of commercial RFID tags with power optimized waveforms,* In *RFID, 2010 IEEE International Conference on*(pp. 195-202). IEEE.
- [54] Boaventura, A. S., and Carvalho, N. B. *Maximizing DC power in energy harvesting circuits using multisine excitation,* In *Microwave Symposium Digest (MTT), 2011 IEEE MTT-S International* (pp. 1-4). IEEE.
- [55] Valenta, C. R., and Durgin, G. D. *Rectenna performance under power-optimized waveform excitation,* In *RFID (RFID), 2013 IEEE International Conference on* (pp. 237-244). IEEE.
- [56] Collado, A., and Georgiadis, A. *Improving wireless power transmission efficiency using chaotic waveforms,* In *Microwave Symposium Digest (MTT), 2012 IEEE MTT-S International* (pp. 1-3). IEEE.
- [57] Oppenheim, A. V., and Cuomo, K. M. *Chaotic signals and signal processing,* The Digital Signal Processing Handbook, CRC Press, Boca Raton, FL.
- [58] Boaventura, A., Belo, D., Fernandes, R., Collado, A., Georgiadis, A., and Carvalho, N. B. *Boosting the efficiency: Unconventional waveform design for efficient wireless power transfer,* IEEE Microwave Magazine, 16(3), 87-96.

- [59] Litvinenko, Anna, Janis Eidaks, and Arturs Aboltins. *Usage of Signals with a High PAPR Level for Efficient Wireless Power Transfer.*, In 2018 IEEE 6th Workshop on Advances in Information, Electronic and Electrical Engineering (AIEEE), pp. 1-5. IEEE, 2018.
- [60] Boaventura, Alírio J. Soares, Ana Collado, Apostolos Georgiadis, and Nuno Borges Carvalho. *Spatial power combining of multi-sine signals for wireless power transmission applications.*, IEEE Transactions on Microwave Theory and Techniques 62, no. 4 (2014): 1022-1030.
- [61] Valenta, Christopher R., Marcin M. Morys, and Gregory D. Durgin. *Theoretical energy-conversion efficiency for energy-harvesting circuits under power-optimized waveform excitation.*, IEEE Transactions on Microwave Theory and Techniques 63, no. 5 (2015): 1758-1767.
- [62] Pan, Ning, Daniel Belo, Mohammad Rajabi, Dominique Schreurs, Nuno Borges Carvalho, and Sofie Pollin. *Bandwidth analysis of RF-DC converters under multisine excitation.*, IEEE Transactions on Microwave Theory and Techniques 66, no. 2 (2017): 791-802.
- [63] Pan, Ning, Alirio Soares Boaventura, Mohammad Rajabi, Dominique Schreurs, Nuno Borges Carvalho, and Sofie Pollin. *Amplitude and frequency analysis of multi-sine wireless power transfer.*, In 2015 Integrated Nonlinear Microwave and Millimetre-wave Circuits Workshop (INMMiC), pp. 1-3. IEEE, 2015.
- [64] Del Prete, Massimo, Alessandra Costanzo, Diego Masotti, Tommaso Polonelli, Michele Magno, and Luca Benini. *Experimental analysis of power optimized waveforms for enhancing wake-up radio sensitivity.*, In 2016 IEEE MTT-S International Microwave Symposium (IMS), pp. 1-4. IEEE, 2016.
- [65] Del Prete, Massimo, Alessandra Costanzo, Michele Magno, Diego Masotti, and Luca Benini. *Optimum excitations for a dual-band microwatt wake-up radio.*, IEEE Transactions on Microwave Theory and Techniques 64, no. 12 (2016): 4731-4739.
- [66] Blanco, J., Bolos, F., and Georgiadis, A. *Instantaneous power variance and radio frequency to dc conversion efficiency of wireless power transfer systems*, IET Microwaves, Antennas and Propagation, 10(10), 1065-1070
- [67] T. Hirakawa, C. Wang and N. Shinohara *RF-DC conversion efficiency improvement for microwave transmission with pulse modulation* Wireless Power Transfer, page 1 of 10. Cambridge University Press, 2019.
- [68] Ibrahim, Rony, Damien Voyer, Mohamad El ZFoghb, Julien Huillery, Arnaud Bréard, Christian Vollaire, Bruno Allard, and Youssef Zaatar. *Novel design for a rectenna to collect pulse waves at 2.4 GHz* IEEE Transactions on Microwave Theory and Techniques 66, no. 1 (2017): 357-365.

- [69] Lo, Chun-Chih, Yu-Lin Yang, Chi-Lin Tsai, Chieh-Sen Lee, and Chin-Lung Yang. *Novel wireless impulsive power transmission to enhance the conversion efficiency for low input power* In 2011 IEEE MTT-S International Microwave Workshop Series on Innovative Wireless Power Transmission: Technologies, Systems, and Applications, pp. 55-58. IEEE, 2011.
- [70] C. Yang, Y. Yang and C. Yang, *Adaptive pulse waveform modulation to enhance wireless power efficiency for biomedical applications*. 2013 IEEE MTT-S International Microwave Symposium Digest (MTT), Seattle, WA, 2013, pp. 1-3.



## Chapter 2

# POWs applied on traditional rectifier topologies

In this chapter, multi-sine signal, RF pulse signal, and their characteristics will be considered by simulations using Matlab and ADS. We study the impacts of multi-sine signal's parameters such as: number of sub-carriers, phases, amplitudes and sub-carriers spacing. Modifying one of these parameters changes the waveforms and also the PAPR of multi-sine signal. Moreover, generating RF pulse signal and the variation of PAPR due to the duty cycle characteristics will be investigated as an important part in this chapter. The freedom of choice of its PAPR is one of the most interesting characteristic that makes this type of waveform suitable for improving the RF-to-dc efficiency.

ADS simulation is also an important part in my thesis. This chapter introduces ADS simulation as well as the designing process of some traditional rectifier topologies such as: series-mounted diode, shunt-mounted diode and voltage-doubler rectifiers. The first measurement results on these types of rectifier will be presented, with and without matching networks and in the wide range of resistance load values.

### 2.1 Multi-sine signal

Multi-sine signal is the most popular waveform that be used in wireless power transmission. The continuous waveform (CW or one-tone signal) will be compared with the N-tone signal. Formula of multi-sine signal (N-tone signal) used here is:

$$v(t) = \sum_{k=1}^N A_k \sin \left( [\omega - \frac{\Delta\omega}{2}(N-1) + \Delta\omega(k-1)]t + \phi_k \right) \quad (2.1)$$

where  $A_k$  is the amplitude of  $k^{th}$  sub-carrier

$\phi_k$  is the phase of  $k^{th}$  sub-carrier

N is the number of the sub-carriers

$\omega = 2\pi f$  with f is the center frequency

$\Delta\omega = 2\pi\Delta f$  with  $\Delta f$  is the frequency spacing between the sub-carriers.

Each parameter plays an importance role in the creation of the multi-sine signal. By varying those, the form of the signal will be changed as well as their amplitudes. Therefore,

the PAPR of the signal will be changed. These parameters will be varied to show their effects on the PAPR of the signal in the next sections by statistical study.

### 2.1.1 Multi-sine signals with different number of sub-carriers

In this section, we will plot the frequency and time domains of the N-tone signal with the parameters:  $f = 1 \text{ GHz}$ ,  $\Delta f = 10 \text{ MHz}$ ,  $\Phi_k = 0^0$ , as well as its histogram. The amplitudes  $A_k$  are the same between sub-carriers. Notice that a histogram is a graphical representation of the distribution of numerical data. It represents an estimation of the probability distribution of a continuous variable (quantitative variable).

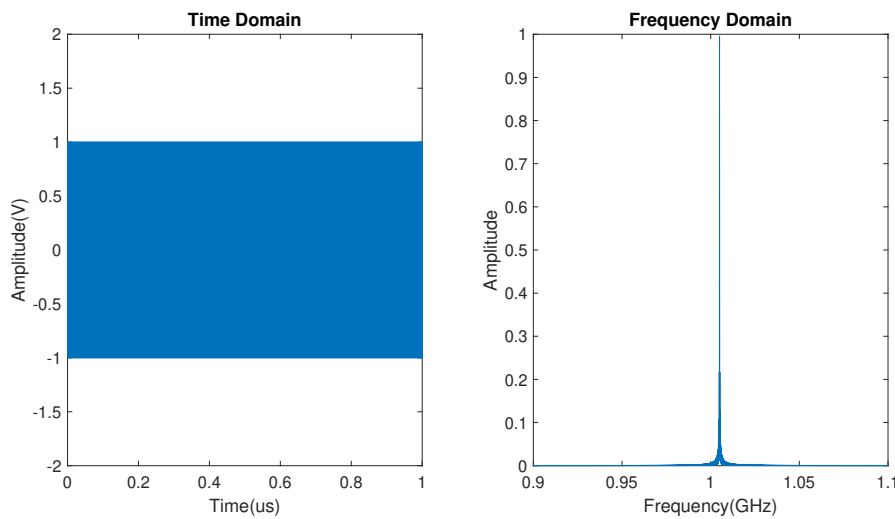


FIGURE 2.1: Time and frequency domain of CW signal.

Fig.2.1 displays time and frequency domain of CW signal. This signal has the amplitude of 1 V, the carrier frequency is 1 GHz.

In Fig.2.2, we can see the 2-tone signal also in time and frequency domain. In time domain, the shape of the signal is changed with the maximum amplitude is equal 1.4142 V. The average power of the signal is unchanged but the peak value of the amplitude is changed (by the factor of  $\sqrt{2}$ ). In frequency domain, the sub-carrier frequencies are at 0.995 GHz and 1.005 GHz. The frequency bandwidth is also the frequency spacing, which is 10 MHz. The histogram illustrates that the amplitude gets the highest proportion distribution of 7.96 % at the value of 0. On the other hand, the maximum amplitude (1.4142 V) has the lowest proportion of about 2.5 %. Overall, higher amplitude of the signal gets smaller proportion. It shows that the highest amplitude happens in a shorter period of time compared to other values of amplitude of the signal.

As can be seen in Fig.2.3, the sub-carriers frequencies are at 0.985 GHz, 0.995 GHz, 1.005 GHz and 1.015 GHz with the maximum amplitude of 2 V. The histogram illustrates that the amplitude gets the highest proportion distribution of 15.3 % at the value of 0. while the highest amplitude is at the lowest proportion, less than 1 %, at the value of 2 V. The highest amplitude of 4-tone signal happens in a shorter period of time with an amplitude greater than 2-tone signal, which presents a higher PAPR for the signal.

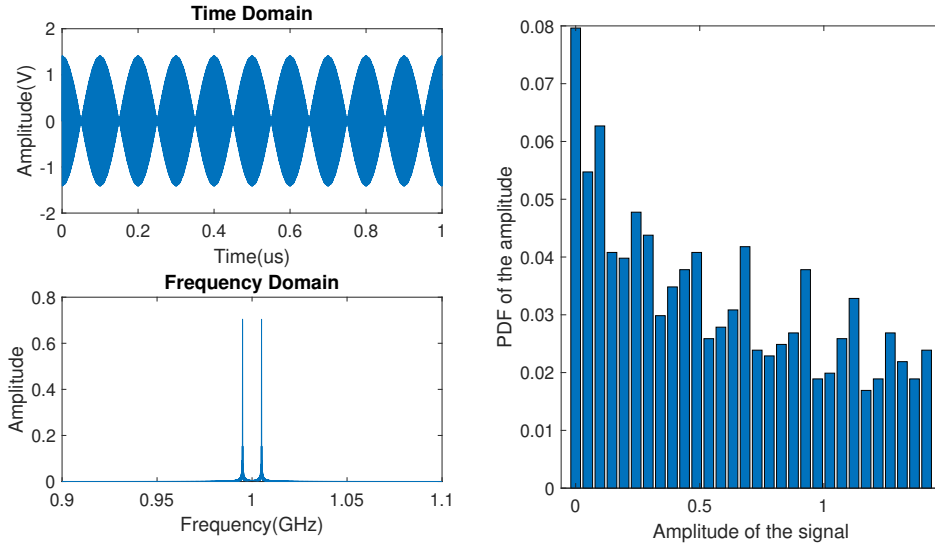


FIGURE 2.2: Time, frequency domain and histogram of multi-sine signal with  $N = 2$ .

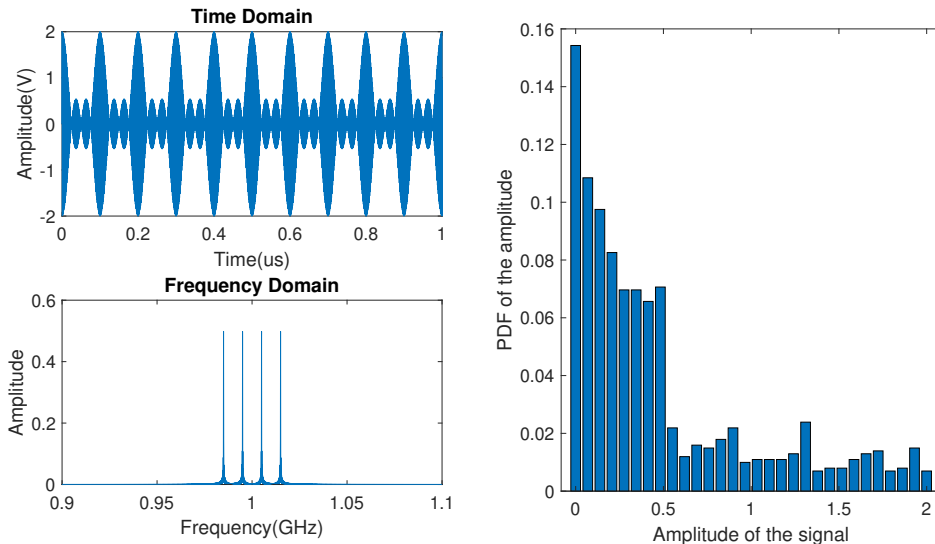


FIGURE 2.3: Time, frequency domain and histogram of multi-sine signal with  $N = 4$ .

In the Fig.2.4 and Fig.2.5, we can observe the histogram when  $N = 8$  and  $N = 16$ , corresponding to 8-tone and 16-tone multi-sine signals. When  $N$  increases, the amplitude of the signal also increases. Also, the maximum amplitude of the signal happens in a smaller duration of time. The maximum amplitudes are 2.83 V and 4 V, respectively, for 8-tone and 16-tone signal. Also, their proportion is smaller than 0.5 %.

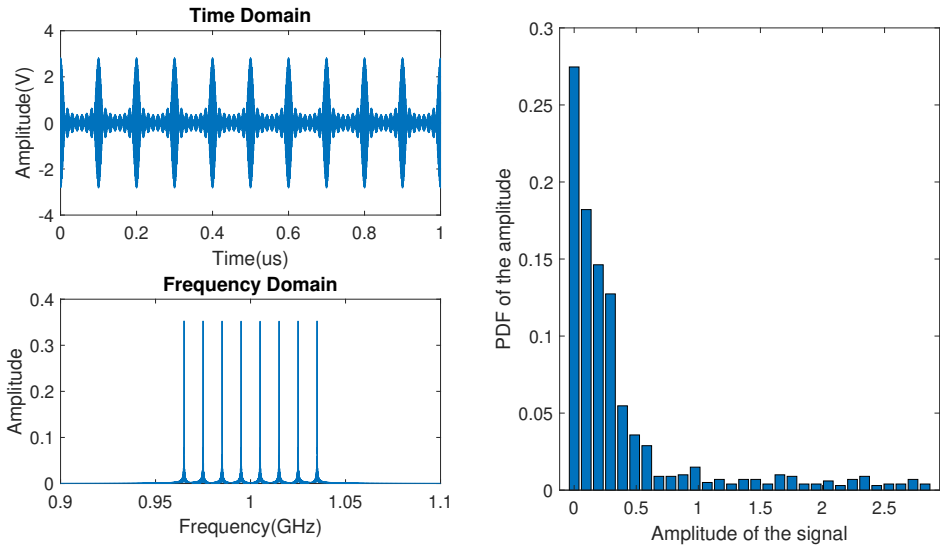


FIGURE 2.4: Time, frequency domain and histogram of multi-sine signal with  $N = 8$ .

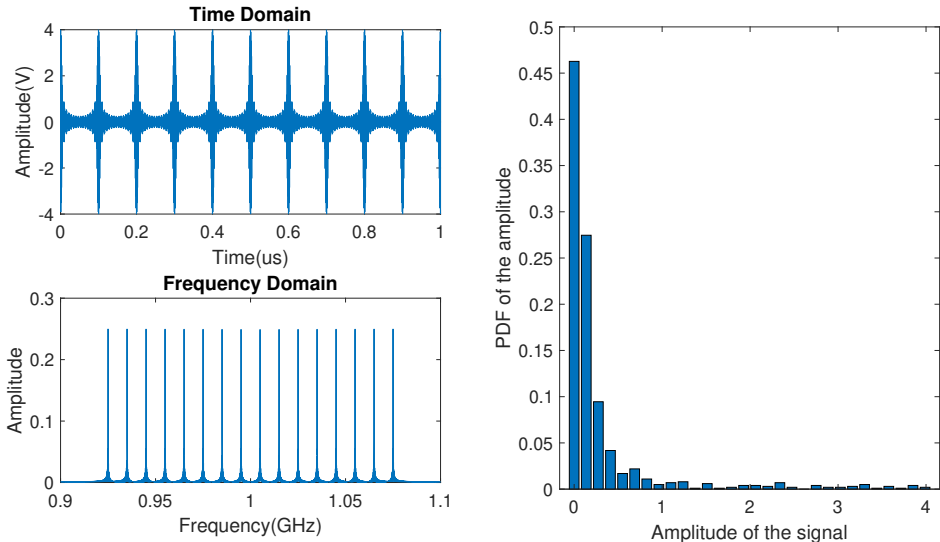


FIGURE 2.5: Time, frequency domain and histogram of multi-sine signal with  $N = 16$ .

Fig.2.6 shows the comparison of the PAPR of these multi-sine signals mentioned above, which can lead to the conclusion that if all the parameters are the same for all the sub-carriers (amplitude,  $\Delta f$ ,  $\Phi$ ), when we increase the number of sub-carriers, the PAPR also increases. When the number of sub-carriers gets doubled, the PAPR is increased by 3dB.

In the next parts, statistical studies will show the variation of PAPR when varying some parameters of multi-sine signal to show which is the best case to have the highest PAPR. Indeed, at the beginning of the thesis, we had some references have shown that as the PAPR increases, the DC output generally increases (but not all the time) [1-4]. That is the reason why we tried to find the maximum PAPR for multi-tone signals and to see how the PAPR

varies according to the different parameters of these signals (amplitudes, frequency spacing and phases).

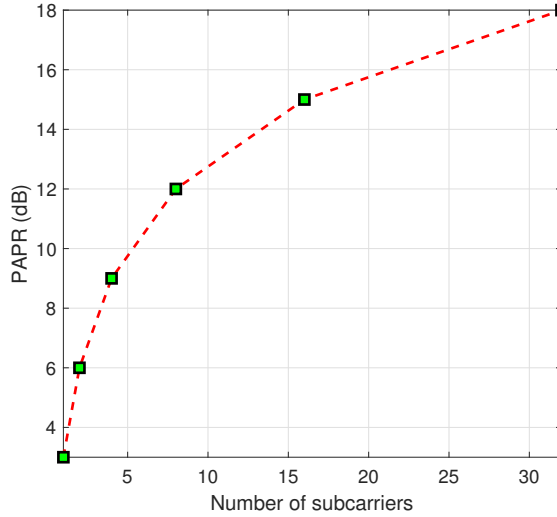


FIGURE 2.6: PAPR of Multi-sine signals with different number of subcarriers.

### 2.1.2 Multi-sine signal with different amplitudes

In this case, all the parameters are the same as the previous section. We consider the number of sub-carrier  $N = 8$  and the amplitude  $A_k$  of each sub-carrier takes random values from  $A_{min}$  to  $A_{max}$ . In Matlab program, with setup of  $A_{min} = 0$  and  $A_{max} = 10$ . We create 10000 multi-sine waveforms (or "samples") with different value of  $A_k$ . The results can be observed in Fig.2.7. The average power is kept the same between samples. From the statistic information, we have the maximum PAPR of 12.03 dB, the minimum PAPR of 7.3 dB and the average value of  $\approx 11$  dB for 10000 samples. The PAPR of 8-tone signal when the amplitudes are identical between the sub-carriers is 12 dB.

Other parameter that we need to consider here is the STD (Standard deviation) [5]. The STD is defined with the following relation:

$$s = \left( \frac{1}{n} \sum_{i=1}^n (x_i - \langle x \rangle)^2 \right)^{\frac{1}{2}} \quad (2.2)$$

where

$$\langle x \rangle = \frac{1}{n} \sum_{i=1}^n x_i \quad (2.3)$$

Matlab function `std(PAPR)` returns the standard deviation of a vector PAPR. It indicates the instantaneous variation of the PAPR compared with its average value. The STD of all the PAPR here is 0.638 which is relatively small compared to the average value of the PAPR of 11 dB.

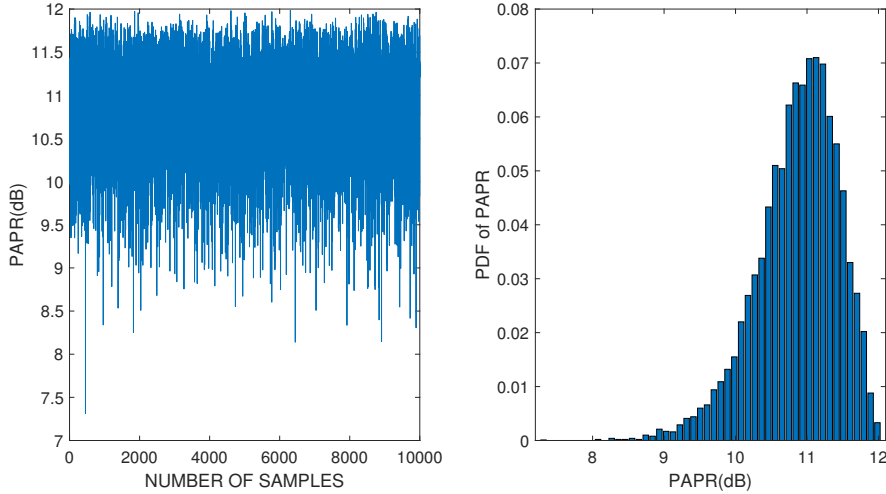


FIGURE 2.7: PAPRs and their PDF of 8-tone signal with random amplitudes of sub-carriers.

We can conclude that when we choose different amplitudes to the sub-carriers of multi-sine signal, the PAPR decreases. The best case, in terms of PAPR, is obtained when all sub-carriers have the same amplitude. Also, with small value of STD, statistically, when  $A_k$  varies randomly, there is a high possibility that the PAPR of 8-tone signal is in the range from 10 to 12 dB.

### 2.1.3 Multi-sine signal with different phases

In this section, the multi-sine signal with different phases between the sub-carriers will be examined.

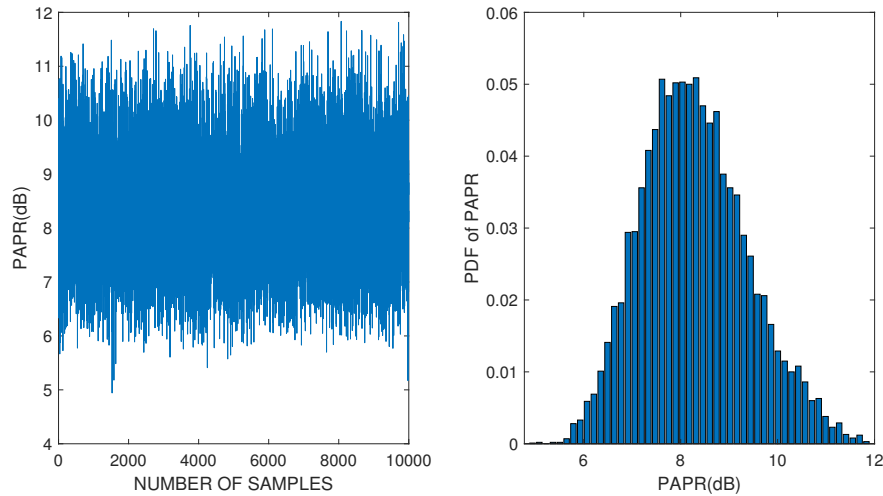


FIGURE 2.8: PAPRs and their PDF of 8-tone signal with random phases of sub-carriers.

In equation 2.1, consider that  $f = 1$  GHz;  $\Delta f = 10$  MHz;  $A_k = 1$ ;  $N = 8$  and the only changed value between the sub-carriers is  $\phi_k$ . It is chosen randomly from  $0^\circ$  to  $90^\circ$ . We

use Matlab software to create 10000 multi-sine signals (or samples) and calculate the PAPRs (Fig.2.8). The PAPR values are concentrated from 7.5 to 8.5 dB as can see from the histogram. The average value calculated by Matlab is 8.3 dB.

On the other hand, the STD is equal to 1.07, so the difference between the average value and instantaneous PAPR is higher than the previous result while varying amplitudes. Overall, the PAPR in this case get the maximum value of 11.95 dB  $\approx$  12 dB, which is comparable to the PAPR of 8-tone signal with the same phases for all sub-carriers (12 dB). So we can conclude that, statistically, the PAPR of multi-sine signal decreases when we put different phases for different sub-carriers. The possibility that the PAPR of each sample reaches the maximum value of 8.29 dB is lower in comparison with multi-sine and random amplitudes.

#### 2.1.4 Multi-sine signal with different frequency spacing between the sub-carriers

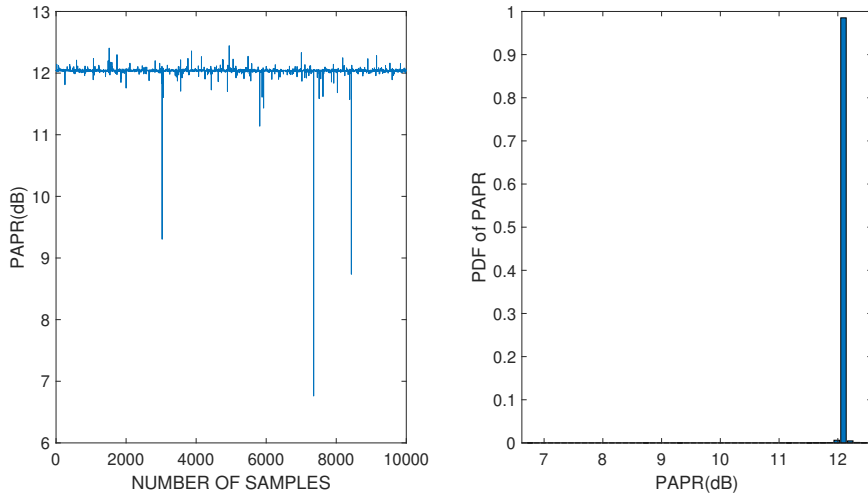


FIGURE 2.9: PAPRs and their PDF of 8-tone signal with random frequency spacing between sub-carriers.

When the frequency spacing  $\Delta f$  between the sub-carriers is randomly modified, the range of frequency is changed. Now, we will see the impact of this parameter to the PAPR of the signal.

Consider that  $f = 1$  GHz,  $A_k = 1$ ,  $N = 8$  and  $\phi_k = 0^\circ$ . Consider  $\Delta f$  randomly varying from 1 kHz to 100 MHz, the PAPR of the multi-sine signals is shown in Fig.2.9. PAPR values are mostly concentrated at the average value of 12.06 dB. We have some exceptional values of 3 dB when all the frequency spacing is equal 0 which makes 8-tone signal becomes 1-tone signal. The STD is equal is 0.07, which is considerably small because all the PAPR values are concentrated at  $\approx$  12 dB.

In general, this study allows to identify the law of variation of the PAPR as a function of the amplitude, phase and frequency spacing distributions. In most cases, when the parameters are the same between sub-carriers, the highest PAPR of multi-sine signal is achieved.

In the next sections, the study of RF pulse signal, its characteristic and behavior of its PAPR will be presented.

## 2.2 RF pulse signal

### 2.2.1 RF pulse signal: duty cycle and PAPR

RF pulse signal is the modulated square pulse. The modulation process is displayed in Fig.2.10. Continuous sine wave with frequency  $f_c$  is modulated by the square pulse with frequency  $f_m$  ( $f_c \gg f_m$ ) to generate the RF pulse at the output. The shape of RF pulse depends on the shape of the periodic square signal. Within one period, the time at high level of square signal is defined as  $T_\beta$ .

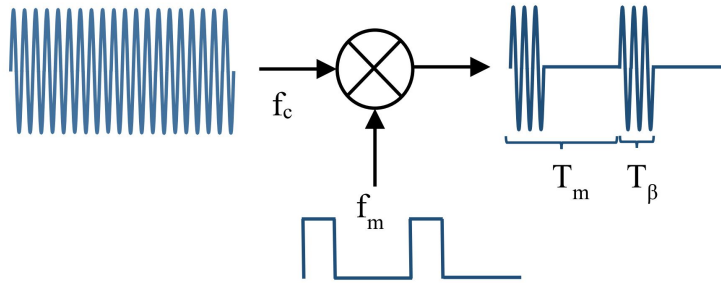


FIGURE 2.10: Square pulse modulation.

Duty cycle of RF pulse signal is calculated by this formula:

$$\beta(\%) = 100 \frac{T_\beta}{T_m} \quad (2.4)$$

where  $T_m = \frac{1}{f_m}$ . The PAPR of a signal is calculated as:

$$PAPR = 10 \log_{10} \left( \frac{\max(x(t)^2)}{\langle x(t)^2 \rangle} \right) \quad (2.5)$$

where  $x(t)$  is the time domain waveform of the signal and  $\langle x(t) \rangle$  is the average value of  $x(t)$ . With RF pulse signal, the maximum power is calculated by the following equation:

$$\max(x(t)^2) = 100 \frac{\langle x(t)^2 \rangle}{\beta} \quad (2.6)$$

As the PAPR of continuous sine wave is 3 dB, we have that:

$$PAPR(\beta) = 3 + 10 \log_{10} \left( \frac{100}{\beta} \right) \quad (2.7)$$

$$PAPR(\beta) = 23 + 10 \log_{10} \left( \frac{1}{\beta} \right) \quad (2.8)$$

Consider that  $\beta \geq 1 \%$ , so the maximum PAPR obtained can be 23 dB as  $\beta = 1 \%$  and decreased to 3 dB as  $\beta$  increased to 100 %. The relation between  $\beta$  and PAPR can be seen from Table.2.1. The duty cycle of RF pulse signal and the equivalent number of tones of multisine signal are given for different values of PAPR. The number of sub-carriers has to be significantly high to obtain the same PAPR of RF pulse signal as the duty cycle is smaller

than 10 %. For example, for a PAPR of 21 dB, multi-sine signal needs 64 sub-carriers, when RF pulse's duty cycle is 1.57 %.

TABLE 2.1: Number of sub-carriers and duty cycle of pulse signal as a function of PAPR

PAPR (dB)	Number of tones (multi-sine)	Duty cycle (%) of RF pulse signal
3	1-tone signal	100
6	2-tone signal	50
9	4-tone signal	25
12	8-tone signal	12.5
15	16-tone signal	6.25
18	32-tone signal	3.13
21	64-tone signal	1.57

As mentioned above, when varying the duty cycle of RF pulse signal, the ratio  $T_\beta/T_m$  is varied. The time that the signal is at high level is changed with duty cycle  $\beta$ . To have high PAPR, the duty cycle of RF signal need to be small (equation 2.8). On the other hand, concentrating the energy on a small time interval makes the discharge time much longer compared to that in CW. Therefore, it would increase the ripple voltage.

### 2.2.2 Voltage ripple

The ripple of the output DC voltage is one of the issues of traditional rectifiers when dealing with RF pulse signals.

For a conventional CW signal of frequency  $f_c$ , to reduce the ripple of the output voltage, the time constant of the low-pass filter must be much significantly greater than the period of the input RF signal.

$$\tau = R_L C_2 \gg T_c = \frac{1}{f_c} \quad (2.9)$$

For RF pulse signal, the design of filter requires more attention. The carrier frequency targeted in this work is a few GHz while the modulation frequency is a few MHz. In order to illustrate these aspects, we have chosen a voltage-doubler topology rectifier as shown in Fig.2.11. The conversion circuit contains an HF input filter which also serves as an impedance matching network, a DC output filter consisting of the capacitor  $C_2$  and the resistor  $R_L$ , an input capacitor  $C_1$  and two Schottky diodes  $D_1$  and  $D_2$ . The "receiving antenna + input matching network" can be modeled by a voltage source ( $V_S$ ) provided with its internal resistance ( $R_S$ ). The role of the output filter is to eliminate the fundamental frequency and the harmonics, it transmits the DC component without ripple.

Fig.2.12 shows the waveforms of the input and output voltages. During the first operating phase, in the time interval  $[0 T_\beta]$ , the capacitors  $C_1$  and  $C_2$  are gradually charged through the internal resistance  $R_S$  of the equivalent generator. During the second operating phase, in the

time interval  $[T_\beta \ T_m]$ , the capacitor  $C_2$  discharges through the load resistor  $R_L$ . This discharge period could be longer or shorter depending on the value of the duty cycle. The output load  $R_L$  is often much greater than the resistance  $R_S$ .

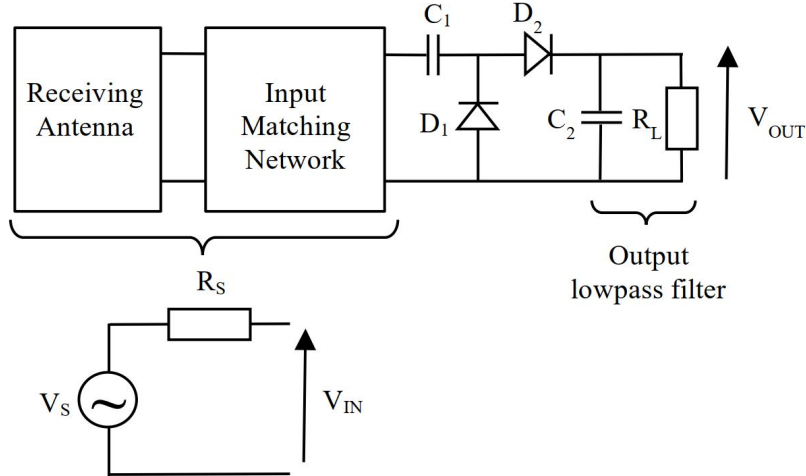


FIGURE 2.11: Schematic of voltage-doubler topology rectifier/rectenna.

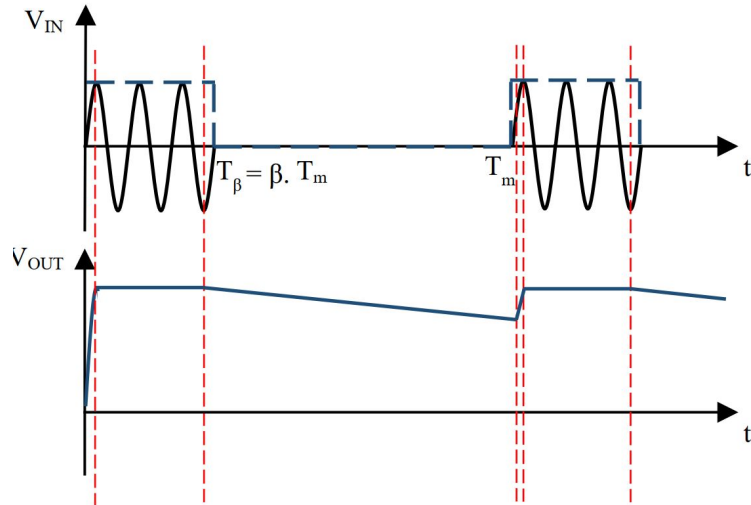


FIGURE 2.12: Input and output voltages in time domain with RF pulse signal.

In order to reduce the ripple of the output voltage  $V_{OUT}$  during the discharge phase, the capacitor  $C_2$  must be increased to obtain a greater time constant. The discharge time constant must verify the following relation:

$$R_L \cdot C_2 \gg T_{off} = \left(1 - \frac{\beta}{100}\right) \cdot T_m = \left(1 - \frac{\beta}{100}\right) / f_m \quad (2.10)$$

Indeed, the load  $R_L$  represents the input impedance of the device to be supplied, it cannot be modified easily. The ripple of the output voltage depends particularly on the modulation frequency, the duty cycle, the capacitor  $C_2$  and the load  $R_L$ .

From the equation (2.10), at a constant RF input power, the input voltage applied to the diodes during the period of time where the RF pulse is turned on increases when the duty cycle decreases. The output DC voltage will continue to increase as the duty cycle decreases. This is true when considering the time period between 0 and  $T_\beta$  as sufficient to completely charge the capacitor  $C_2$ . In this case, the maximum output voltage will be obtained for the smallest duty cycle value. However, if the duty cycle becomes too small, the output capacitor  $C_2$  will not be able to charge at its maximum voltage. Consequently, there is an optimum duty cycle value which allows to maximize the output DC voltage. This optimum depends on the output low pass filter components ( $R_L$  and  $C_2$ ), the carrier frequency, the modulation frequency, the input power level and the other components of the rectifier (lumped and distributed elements).

In the next parts of this chapter, some ADS simulation types will be presented as well as their characteristics. The explication of choosing ADS simulation methods and rectifiers are also enlightened. Normally with RF signal simulation, we can choose between Harmonic Balance, Circuit Envelope or Transient simulations. For some simulations, it requires the ADS to perform the combination of analog and digital simulations. For that reason, ADS co-simulation is desired to fulfill the requirement. There are two types of ADS co-simulation which will be presented and the best we will be selected to perform the simulation.

## 2.3 ADS simulation

### 2.3.1 General introduction

Advanced Design System (ADS) is an electronic design automation software system produced by Keysight Technologies to design RF electronic products. There are some types of simulations in ADS which are suitable for our research and their properties. It includes Transient Simulation, Circuit Envelope Simulation, Harmonic Balance Simulation [6]. It also allows co-simulations. Each type of simulation has their advantages as following.

Transient simulation:

- Analysis performed in the Time Domain
- Use any sources.
- Time Domain data can be transformed in frequency domain.
- Integrates with System simulation and Agilent Ptolemy

Circuit Envelope (CE) simulation:

- Time samples the modulation envelope
- Compute the spectrum at each time sample
- Use equations on the data

- Faster than Harmonic Balance (HB) or Spice in many cases.
- Integrates with System simulation and Agilent Ptolemy

Harmonic balance is a frequency-domain analysis technique for simulating nonlinear circuits and systems. It is well-suited for simulating analog RF and microwave circuits, since these are most naturally handled in the frequency domain. Circuits that are best analyzed using HB under large signal conditions are listed below:

- power amplifiers, frequency multipliers, mixers, oscillators, modulators.
- Harmonic Balance Simulation calculates the magnitude and phase of voltages or currents in a potentially nonlinear circuit.
- Compute quantities such as third-order intercept (TOI) points, total harmonic distortion (THD), and inter-modulation distortion components
- Perform power amplifier load-pull contour analyses
- Perform nonlinear noise analysis. Simulate oscillator harmonics, phase noise, and amplitude limits

For multi-sine signal, conventional simulation such as HB and CE is useful and sufficient. For modulated signal such as RF pulse signal, ADS co-simulation [7] is needed to simulate the signal. There are two types of ADS co-simulation that are suitable for our work that supported by ADS and adapt for our problem: Data Flow/ Circuit Envelope co-simulation and Data Flow/Transient co-simulation, which are identified with the following characteristics:

#### Data Flow/Circuit Envelope (DF/CE):

- Suitable for an RF simulation
- The output of the Circuit Envelope simulator is a collection of time waveforms, each at a different fundamental frequency. It is needed to select the waveform by specifying this fundamental frequency.

#### Data Flow/Transient :

- Suitable for a base-band simulation.
- Time-sink is used to collect complex data or base-band signal.

The ADS co-simulation have been used at the beginning of my thesis when we created and simulated the OFDM signal. Top level of design systems has two parts: Digital Signal Processing (DSP) network and Analog/RF (A/RF) network (Fig.2.13). DSP network consists of blocks: mod\_ofdm, QAM\_Mod, TimedSink and SpectrumAnalyzer. The A/RF network consists of OFDM\_series\_rectifier block (Fig.2.14). The second layer of the system consist of the OFDM signal generator, which is packed in the mod\_ofdm block and a single series-mounted diode, which is packed in the OFDM\_series\_rectifier block.

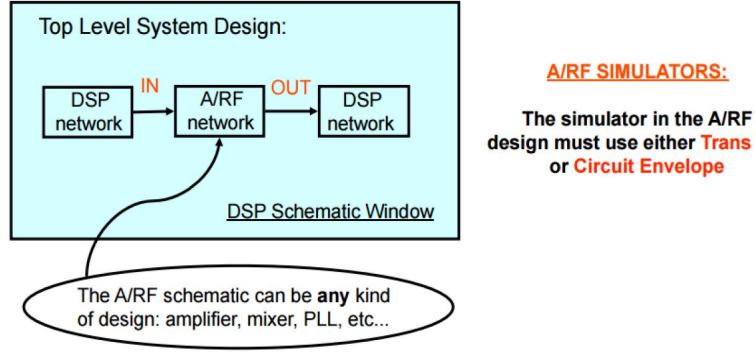


FIGURE 2.13: ADS co-simulation design [7].

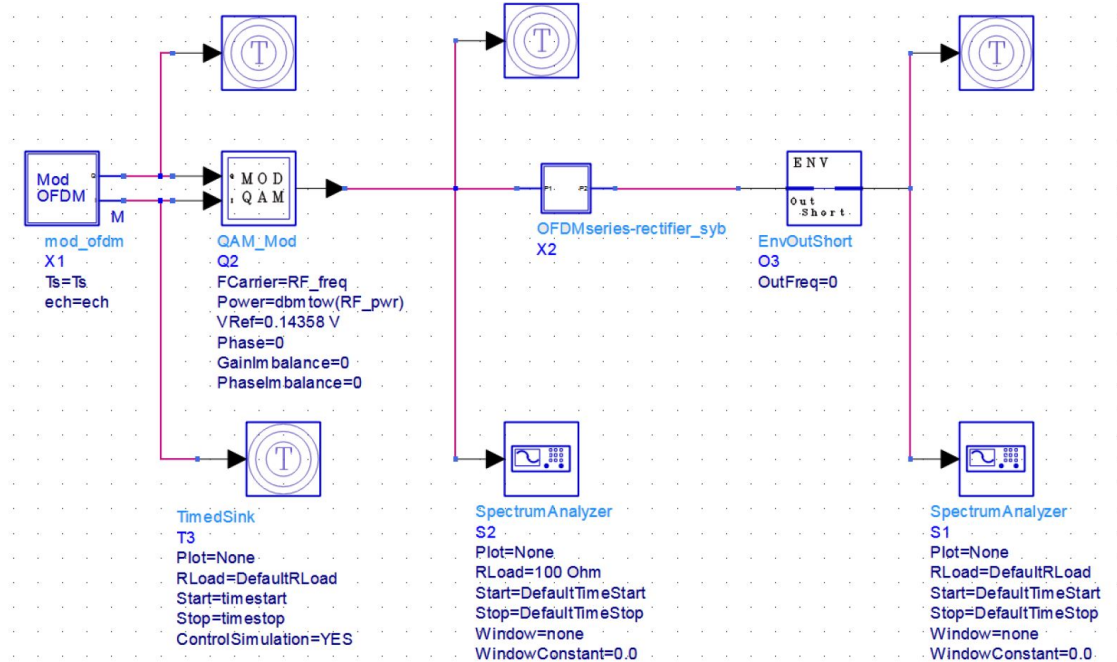


FIGURE 2.14: OFDM Co-simulation.

The OFDM signal generator is shown in Fig.2.15. Bits generator block generate random binary data with proportion of zeros is 0.5 before entering the modulation QAM64 block, which can be replaced with several modulation options such as BQSP, 4-QAM, 16-QAM. Modulated signal will be transformed by FFT block before being filtered by Raised-cosine filter, which is used for pulse shaping with different roll-off factors  $\beta$ . The complex output of Raised-cosine filter will be separated into real part and imaginary part by CxtoRect block. Port P1 and P2 will be entered the Quadrature amplitude modulator with internal oscillator to obtain the OFDM signal.

The OFDM signal pass the Rectifier block, which consist of the rectifier designed as we want. The signal output of the rectifier has to go to the EnvOutShort block that allows the specific frequency pass through. To have voltage DC output, the OutFreq is set to 0. The simulation results show that OFDM signal has a output voltage/efficiency comparable with 4-tone signal [8]. For that reason, we have stopped considering OFDM because it is more complicate to generate and only give the same performance as 4-tone signal.

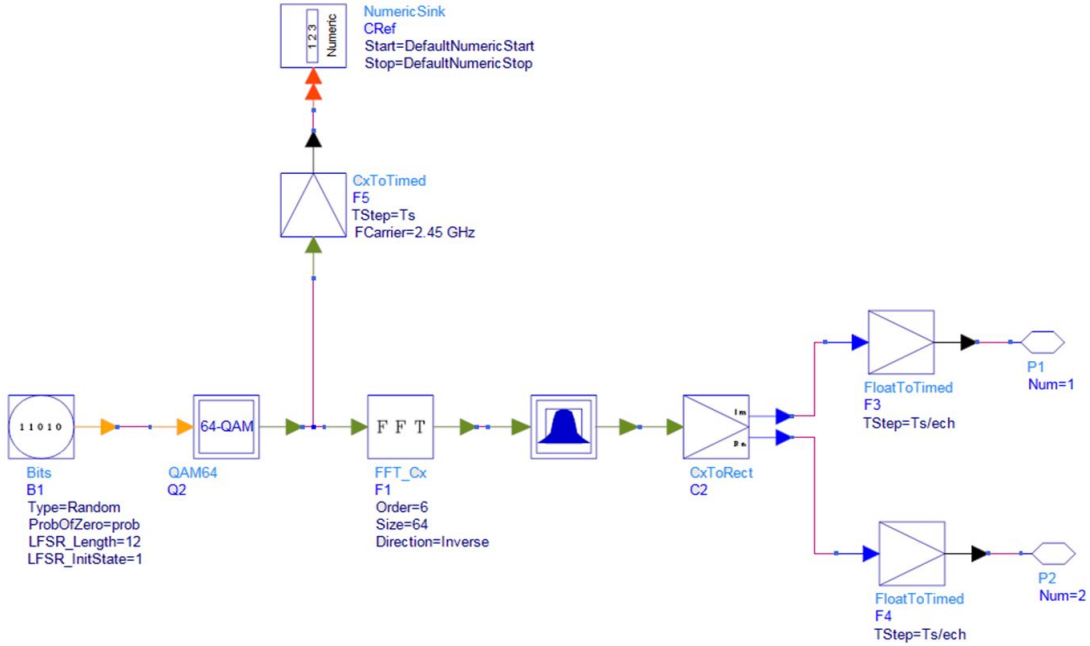


FIGURE 2.15: OFDM signal generator in ADS.

Also, in our study, DF/CE co-simulation is the most suitable method to simulate the RF pulse signal. It reduces the simulation time notably and it also can trace the output data in a longer period in frequency and time domain. However, the co-simulation of RF pulse signal with the rectifier circuit requires a huge amount of RAM and very time consuming. So, in my work, ADS allows to simulate and observe the characteristic of RF pulse signal. The combination between RF pulse and rectifier circuits will be performed experimentally.

### 2.3.2 Design of traditional rectifier topologies with ADS

With ADS, we design different rectifier topologies: series-mounted diode, shunt-mounted diode and voltage-doubler, with and without the input impedance matching network. Simulation by ADS have been conducted on these three structures and results, in terms of output voltage and efficiency, are presented and compared to those of optimized structure which are supplied by CW.

Three classic topologies of rectifiers are shown in Fig.2.16, with and without matching network. About matching network, normally, RF-to-dc rectifiers need an input HF filter which provides impedance matching between the RF source (receiving antenna) and the diode (or diodes) and prevents high order harmonics rejection. Depending on whether a narrow-band or wide-band conversion circuit is designed, the constraints on the input filter change. However, this input filter often made in transmission-line sections takes up a lot of space in the rectifier. This represents a strong constraint for miniaturization. Also, the design and optimization of such circuits are time consuming and expensive in terms of the use of CAD tools.

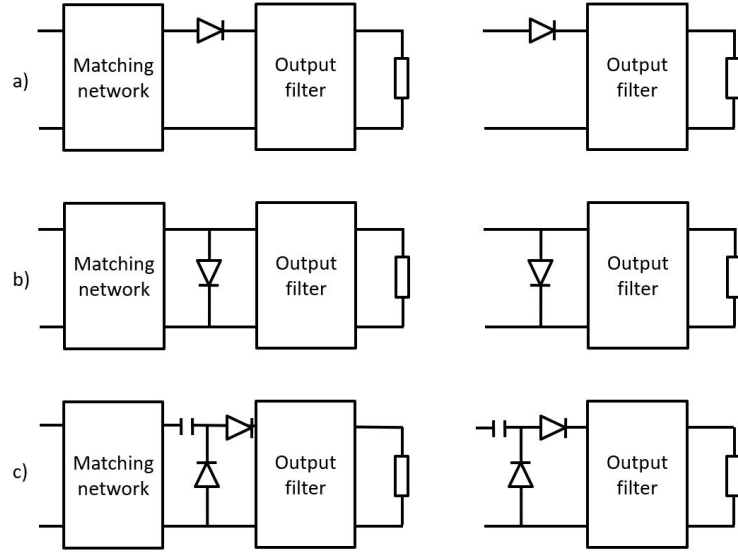


FIGURE 2.16: Different traditional rectifier topologies, with and without matching networks. a) Series-mounted diode; b) Shunt-mounted diode; c) voltage-doubler rectifier.

While designing the rectifier, input matching network is one of the most important part as it matches the impedance of the RF source with the rectifier input. It needs to be optimized so that maximum power will be transferred from the RF source to the diode (or diodes). The process of designing the impedance matching network in ADS consists to determine the lengths and widths of the micro-strip lines. Fig. 2.16 displays a schematic of series-mounted diode rectifier with matching network. We use HB simulation to design the rectifiers with a CW signal. In designing process of such rectifiers, finding the most favorable dimension of matching network takes the most substantial time.

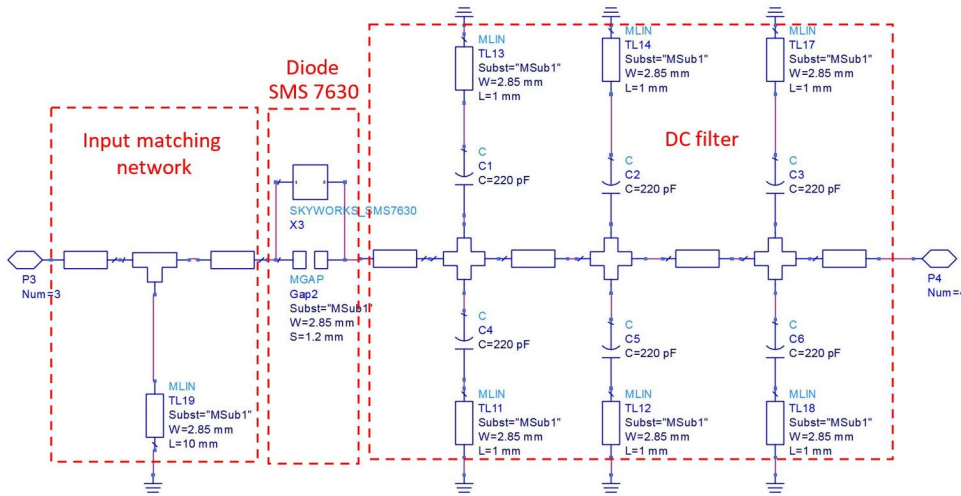


FIGURE 2.17: Series-mounted diode rectifier with matching network.

In this part, we will answer the question of whether POWs allow a non-optimized conversion circuit without an adaptation circuit to achieve the same performances of a circuit

which is itself optimized. In other words, we want to know if it is possible to transfer the circuit design effort to the POW part.

In Fig.2.17, the schematic of the series-mounted diode rectifier is proposed. This simulation first is done with the ADS schematic to find the dimension of micro-strip line for input matching network as well as the filter. Then, the co-simulation Harmonic Balance-Momentum will be done to obtain the final circuit. The Schottky diode used here is a sky-works SMS-7630 and the output is filtered by 6 identical capacitors of 220 pF. The load resistance is optimized at 1 k $\Omega$ , 360  $\Omega$ , and 3 k $\Omega$  for series-mounted diode, shunt mounted diode, and voltage-doubler, respectively. From the designing optimization process using ADS, it can be observed that the dimension of rectifiers without matching network are considerably smaller than that of rectifiers containing input matching network. The surface is reduced from 14.87 to 8.648 cm<sup>2</sup>, which is 41.8 % of reduction in term of circuit area (Fig.2.18).

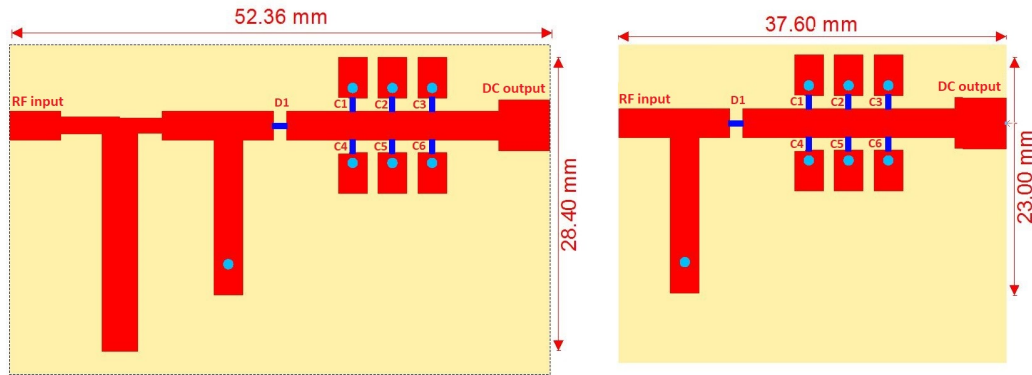


FIGURE 2.18: Layouts of the series-mounted diode rectifiers with and without matching network.

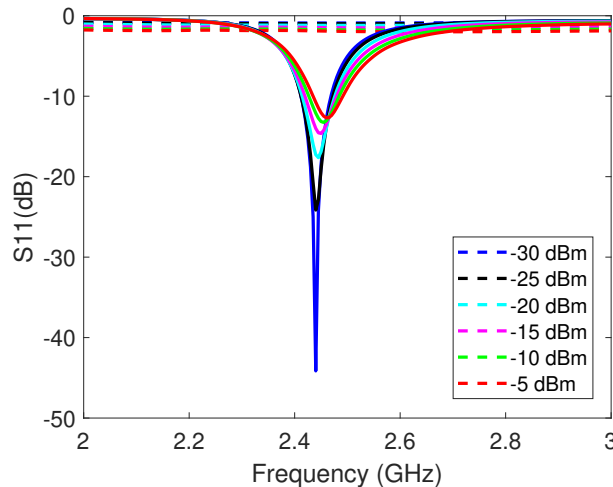


FIGURE 2.19:  $S_{11}$  of series-mounted diode with (line) and without (dashed-line) matching network over the frequency range and for different input power levels.

The  $S_{11}$ -parameter simulation is shown in Fig.2.19. As the circuit is optimized at 2.45 GHz, the  $S_{11}$  parameter of matching network is perfectly matched at that frequency. There

are 6 curves found in the figure because the simulation is operated under 6 input power from -30 to -5 dBm with a step of 5 dBm. In contrast,  $S_{11}$  parameters of circuit without matching network (dashed-line) are close to 0 dB over the simulated frequency range (from 2 to 3 GHz).

After having the  $S_{11}$  parameter to ensure the circuit is well optimized at specific frequency, we apply 1-tone signal at the input of the two rectifiers, with and without input matching network. The output DC voltage is plotted in Fig.2.20a at 6 levels of input power from -25 to -5 dBm at the frequency range from 2 GHz to 3 GHz. As can be seen, for the rectifier with matching network, the output DC voltage has its highest value at or close to 2.45 GHz at all the power levels. For example, at -5 dBm, the DC voltage increases from nearly 0 V at 2 GHz and surge to 0.63 V and then drops slowly to 0.25 V at 3 GHz. The same behavior can be found at others input power levels. In contrast, the voltage DC output of rectifier without matching network shows a nearly constant level at all the frequency range. Obviously, without matching network, the DC's value is smaller than that of rectifier with matching network at the optimum frequency of 2.45 GHz.

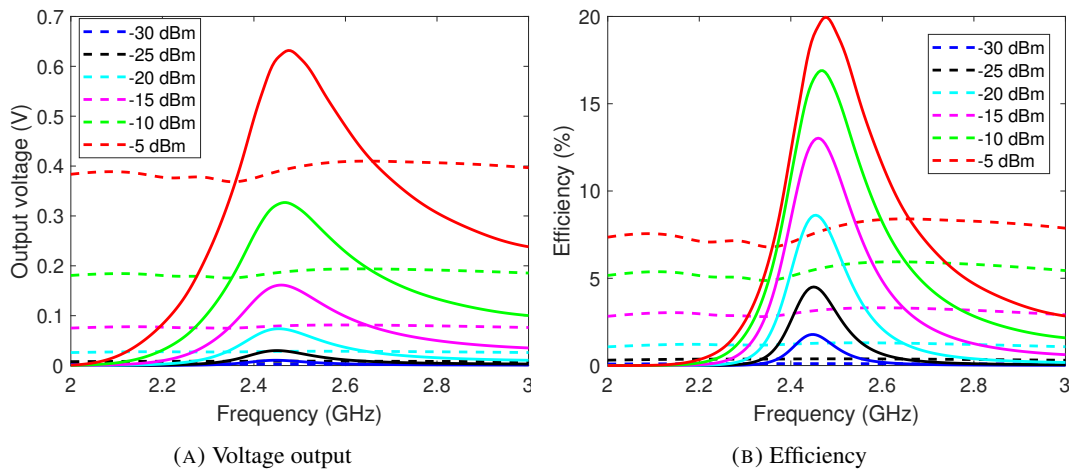


FIGURE 2.20: Voltage output and efficiency of series-mounted diode rectifiers with (line) and without (dashed-line) matching network ( $R_L = 1 \text{ k}\Omega$ ).

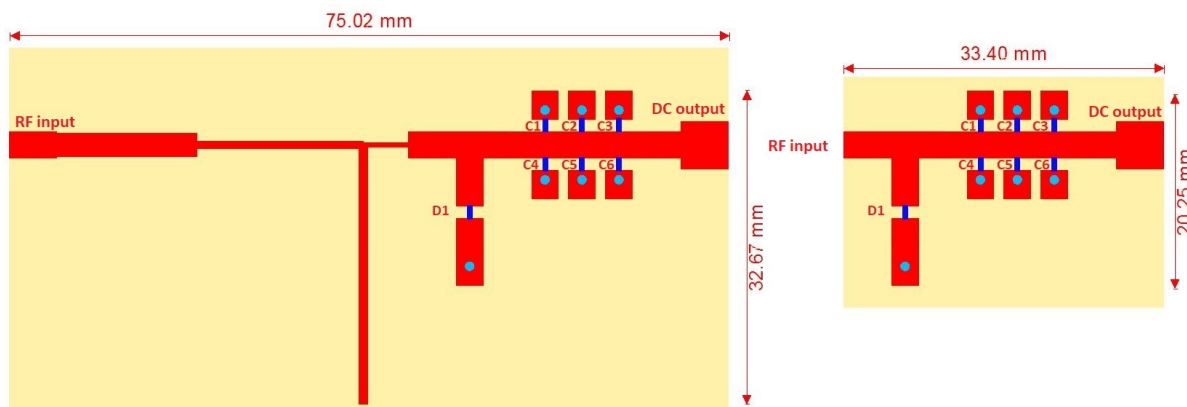


FIGURE 2.21: Layouts of shunt-mounted diode rectifiers with and without matching network.

As the load's resistance is optimized at  $1\text{ k}\Omega$ , the efficiency of the rectifier is calculated and plotted in Fig.2.20b. While the highest efficiency obtained by rectifier with matching network at -5 dBm is approximately 20%, the efficiency of rectifier without matching network is only 8%, which is significantly smaller. The same performance can be found at others input power levels.

We have done the same process of optimizing and designing for shunt-mounted diode rectifier and voltage-doubler. The layout with and without matching network of shunt-mounted diode rectifiers are presented in Fig.2.21. The surface area of the shunt-mounted rectifier is reduced from  $24.50\text{ cm}^2$  to  $6.70\text{ cm}^2$ , which represents 72.7 % of area reduction. The  $S_{11}$  of the circuit is shown in Fig.2.22.

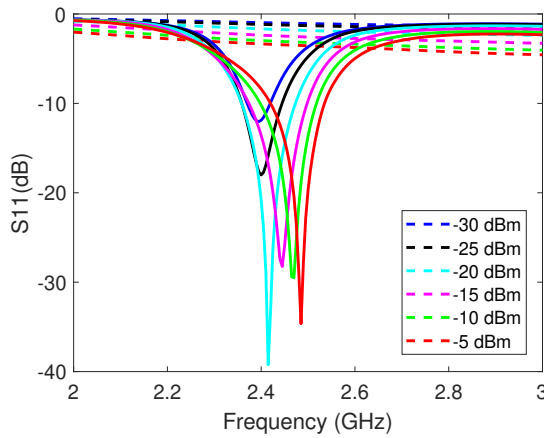


FIGURE 2.22:  $S_{11}$  of shunt-mounted diode with (line) and without (dashed-line) matching network over the frequency range and for different input power levels.

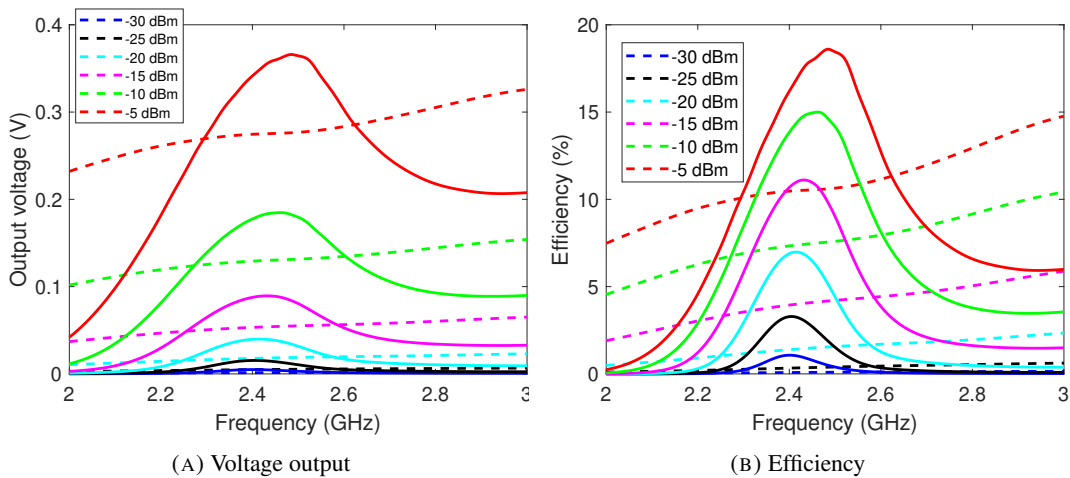


FIGURE 2.23: Voltage output and efficiency of shunt-mounted diode rectifiers with (line) and without (dashed-line) matching network ( $R_L = 360\Omega$ ).

As can be seen from Fig.2.23a and Fig.2.23b, the behavior of the output voltage and efficiency of CW on the shunt-mounted diode rectifier are similar to those of series-mounted diode rectifier. The maximum output voltage is found at the optimized frequency or close

to it (2.45 GHz) and degrades at other frequencies for circuit with matching network. At -5 dBm, the highest DC voltage and efficiency are 0.36 V and 18.5 %, respectively. For non-optimized rectifier, the nearly constant (slowly increased) values of voltage and efficiency can be seen over the considered frequency band.

The layout with and without matching network of voltage-doubler rectifiers are presented in Fig.2.24. The  $S_{11}$  of those circuits are shown in Fig.2.25. Also, the area of the PCB is reduced significantly from  $9.15 \text{ cm}^2$  to  $4.03 \text{ cm}^2$ , which corresponds to about 56 % of area reduction. We have the output voltage and efficiency, obtained with CW, presented in Fig.2.26a and Fig.2.26b. As expected, the highest output voltage and efficiency of 1.2 V at -5 dBm is found at 2.45 GHz for optimized voltage-doubler rectifier. The output voltage of that circuit is higher than series and shunt-mounted diode rectifiers. For non-optimized voltage-doubler circuit, wide-band behavior are also obtained in the considered frequency band, ranging from 2 to 3 GHz.

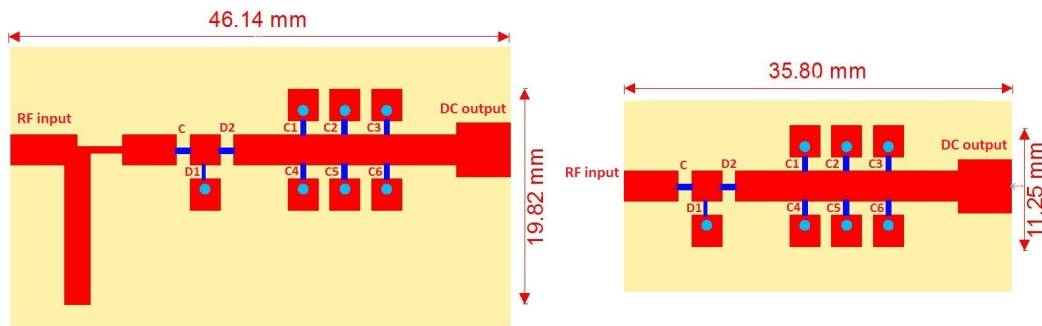


FIGURE 2.24: Layouts of voltage-doubler rectifiers with and without matching network.

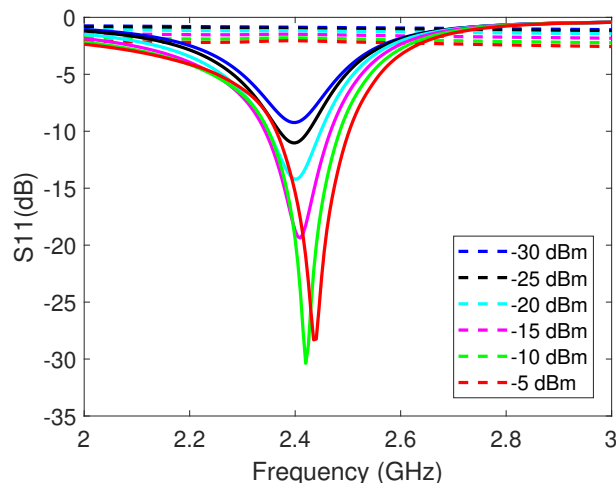


FIGURE 2.25:  $S_{11}$  of voltage-doubler rectifier with (line) and without (dashed-line) matching network over the frequency range and for different input power levels.

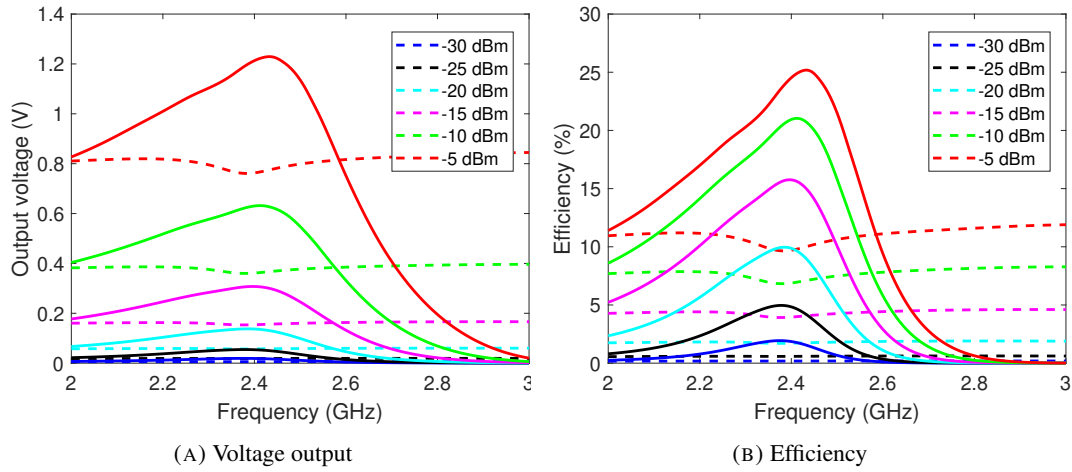


FIGURE 2.26: Voltage output and efficiency of voltage-doubler rectifiers with (line) and without (dashed-line) matching network ( $R_L = 3k\Omega$ ).

With the non-optimized and more compact rectifier, we will show that it can have a better performance than the optimized rectifier by using the power optimized waveforms such as multi-sine and RF pulse signal. Details will be presented in the next sections.

## 2.4 Common setup for rectifiers measurement

To automatically characterize the rectifiers, we have developed an automated measurement setup shown in Fig.2.27 and Fig.2.28. In this setup, the computer controls the system with Matlab program. The signal generator (Keysight N5182A) receives the command from PC and compares the power output with the power measured by the power meter (Keysight E4419A) to calibrate and then set the correct value of input power to the rectifier.

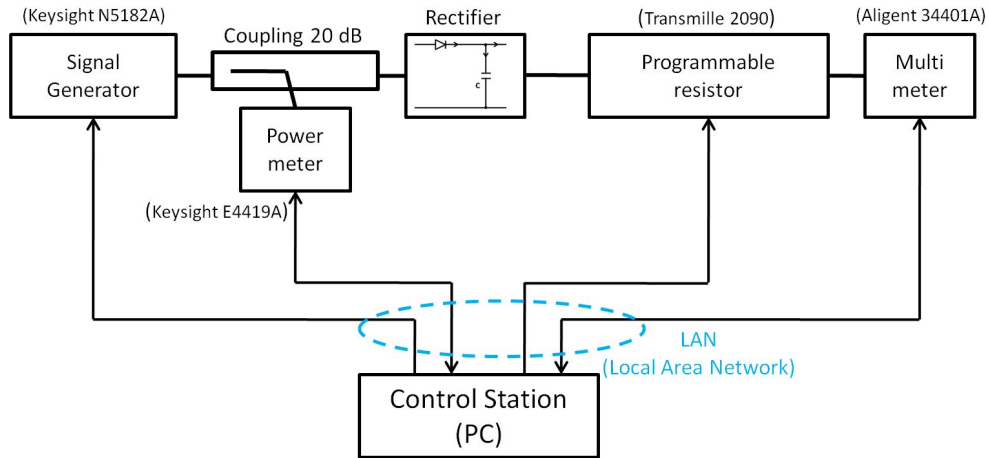


FIGURE 2.27: Schematic of the measurement setup.

After setting the value of resistance load by the programmable resistor (Transmille 2090), the multi-meter (Agilent 34401A) will send the data to the computer after each measurement. With control program, multisine signals with different number of sub-carriers  $N = 1, 2, 4$ ,

8-tone are created. Also, for multi-sine signal, the frequency spacing, the amplitudes, the phases are kept the same between sub-carriers. We generate the signals with the same average power for different number of sub-carriers. For the pulse signal, duty cycle varies from 1 to 99% and modulation frequency is 1 MHz. The same here, for a certain RF power, while varying the duty cycle, the average power is kept the same between the RF pulse signals.

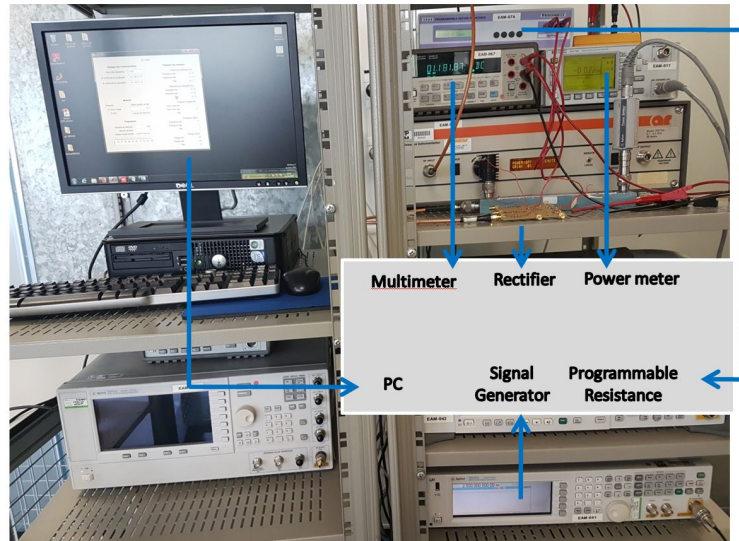


FIGURE 2.28: Photo of the measurement setup.

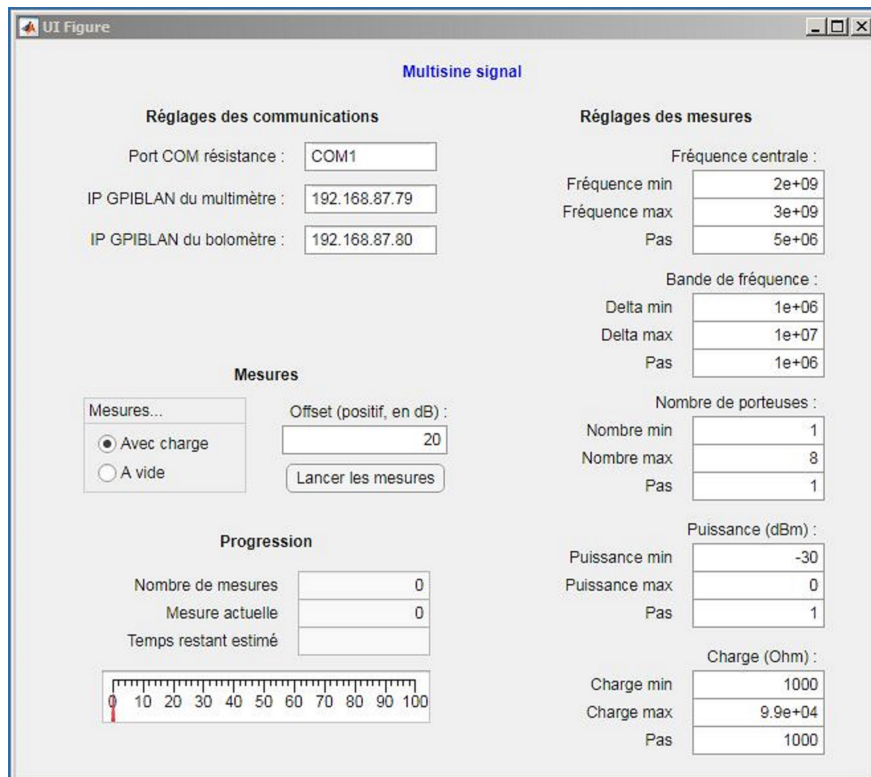


FIGURE 2.29: Multi-sine signal measurement user interface.

Fig.2.29 shows the user interface of Matlab program controller for multi-sine signal measurement. On the interface, there are the options to firstly select the central frequency at three values: frequency min, frequency max and frequency step. This block allows the signal generator to generate the center frequency of the signal on the desired frequency range. The frequency band-width tab also has 3 parameters:  $\Delta f_{min}$ ;  $\Delta f_{max}$ , and  $\Delta f_{step}$  to create multisine signal with varied frequency band-width. The same options are available to adjust the number of sub-carriers, the power level and the load's value. Due to the limitation of the programmable resistor (Transmille 2090), the maximum value of load's resistance is  $100\text{ k}\Omega$ .

Offset value is defined in order to compensate the power loss on the systems before transmitting to the rectifier. Thanks to this offset value, the power meter can display the correct value of power levels. The progression section is to estimate the measurement time and display also the progress of the measurement in percentage.

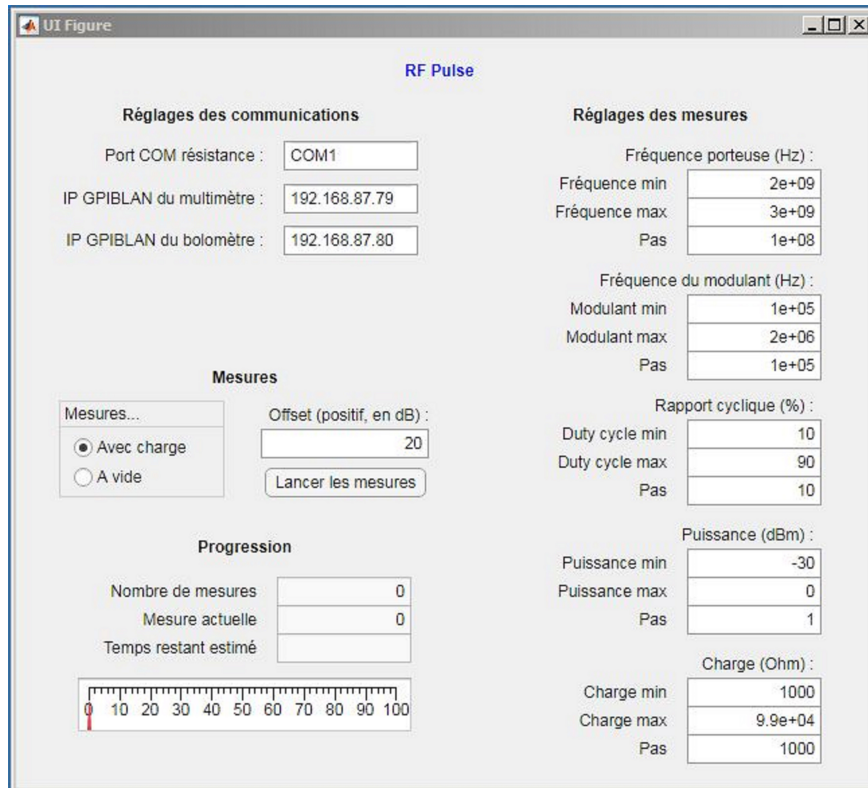


FIGURE 2.30: RF pulse signal measurement user interface.

For the RF pulse case, a duty cycle block is added on the user interface (Fig.2.30). This duty cycle can be adjusted between 1 and 99 % with a minimum step of 1 %. Also, the modulated frequency block is also included. The modulation frequency can be adjusted from 1 to 6 MHz due to the limitation of the signal generator. Also, a capacitor of 10 nF is added at the output of the rectifier to eliminate the voltage ripple. The minimum time constant of the rectifier  $R_L \cdot C$  is  $3.6\text{ }\mu\text{s}$  (as  $R_L = 360\text{ }\Omega$  for shunt-mounted diode rectifier). On the other hand, the maximum ripple is obtained for the minimum value of  $f_m$  and  $\beta$  (1 MHz and 1 %, respectively), which corresponds to a maximum value of  $T_{off}$  of  $0.99\text{ }\mu\text{s}$ . For that reason, the equation (2.10) is always satisfied.

## 2.5 Measurement results of traditional rectifiers

### 2.5.1 Impact of multi-sine and RF pulse signals on the DC output performances

This section presents the measurement results of the conventional topologies of rectifier that are designed and optimized in section 2.4. The circuit is shown in Fig.2.31. In the first place, the CW signal is applied to the rectifier with matching network, that voltage output is used as the voltage DC reference to compare with other voltages DC output. Then, the multi-sine signals with the number of sub-carriers of 1, 2, 4, and 8-tones. The center frequency ranges from 2 to 2.5 GHz and the frequency spacing of 10 MHz are created.

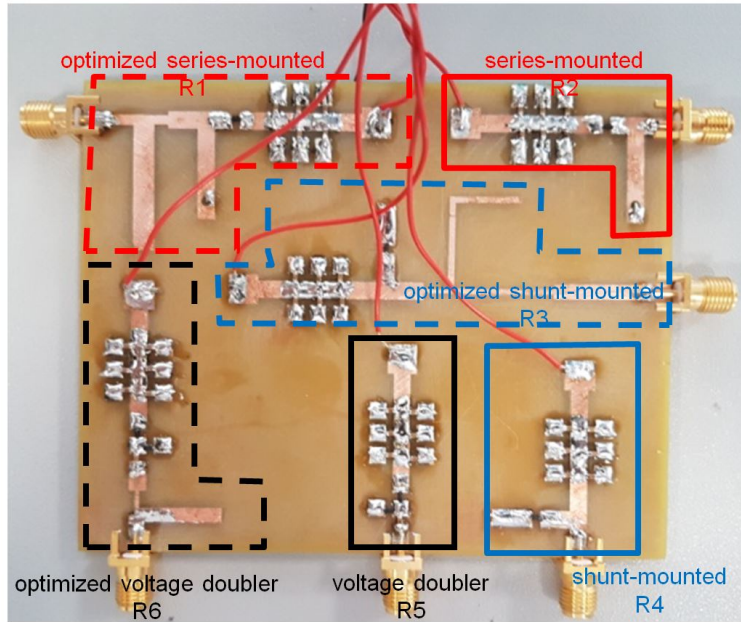


FIGURE 2.31: Rectifier prototypes with and without matching network; R1, R3, R6 are series-mounted diode, shunt-mounted diode, voltage-doubler rectifiers with matching networks; R2, R4, R5 are series-mounted diode, shunt-mounted diode, voltage-doubler rectifiers without matching networks.

We use the RF pulse signals with varied duty cycle from 1 to 99 % and modulation frequency of 1 MHz. Then, for one operating point (valid for a specific frequency and load value), the optimum duty cycle that gives the highest DC voltage will be selected. The 2 signals will be tested with the rectifiers without matching network and the results will be compared to the reference DC voltage provided by optimized rectifiers.

The circuits are printed on FR4 substrate ( $\epsilon_r = 4.4$ ) with the thickness of 1.6 mm and the dimension of 80mm x 100mm. The diode used is Schottky SMS-7630 and the output voltage is filtered by 6 identical capacitors of 220 pF. The load resistance is optimized at 1  $k\Omega$ , 360  $\Omega$ , and 3  $k\Omega$  for series-mounted diode, shunt mounted diode, and voltage-doubler, respectively, as previously mentioned for the simulations.

The measurement results of series-mounted diode rectifier at -20 dBm of input power and frequency range from 2 to 2.5 GHz are depicted in Fig.2.32. In the case of optimized rectifier,

CW (1-tone) signal gives a high selective output DC voltage at the optimum frequency of 2.25 GHz. The maximum voltage reaches 35 mV with the optimum charge of  $1 \text{ k}\Omega$ . On the other hand, series-mounted diode rectifier without matching network is frequency wide-band. As it is not optimized, the voltage output of 1-tone signal (dashed-red curve) is significantly lower when comparing to that of the optimized rectifier. By increasing the number of sub-carriers of multisine signal, the output DC voltage constantly increases simultaneously over the frequency range of interest. The 8-tone signal gives the voltage output as relatively twice as the voltage output of 1-tone signal. For example, at 2.25 GHz, DC voltage of 8-tone signal is 25 mV, that value for 1-tone signal is only 13.5 mV. The DC output of 8-tone signal approaches the optimum rectifier's DC output using CW signal. For all the measurements, multi-sine signal has the same average power with CW signal. Multi-tone signal helps the rectifier without matching network increase the output DC voltage in all the frequency range.

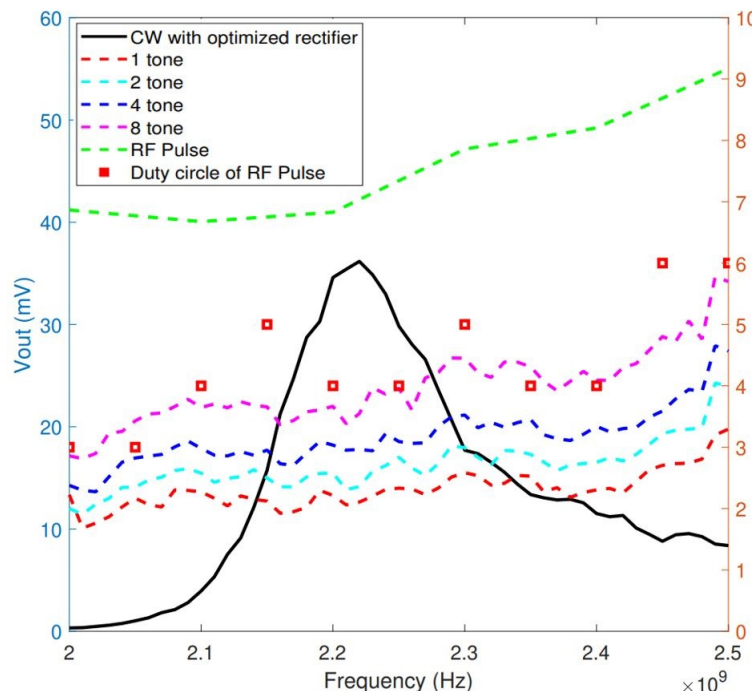


FIGURE 2.32: Voltage output of multisine and RF pulse signals on series-mounted diode rectifiers at -20 dBm. ( $R_L = 1 \text{ k}\Omega$ )

Also from Fig.2.32, RF pulse signal's DC output, in color green, outperforms other types of waveform even compared with the optimized rectifier's voltage output at its optimum frequency. At each frequency, the duty cycle of RF pulse signal varies from 1 to 99 %. Then, the duty cycle that give the highest output DC voltage is chosen as optimum duty cycle for that frequency. For example, at 2 GHz, the RF pulse signal with duty cycle of 3 % gives the highest output DC voltage (41 mV). Over the frequency range, the optimum duty cycle of RF pulse signal varied from 3 to 6%. Besides, the PAPR of RF pulse signal (when duty cycles vary from 3 to 6 %) varies from 15 to 18 dB. The output voltage of RF pulse signal is two times higher than that of 8-tone signal. Meanwhile, the PAPR of multi-sine signals are varied from 3 to 12 dB (1-tone to 8-tone signal).

Fig.2.33 shows the measurement results of shunt-mounted diode rectifier. The behavior of voltage output of each signals are quite similar to the series-mounted diode rectifier. CW reaches its highest output DC voltage of approximately 17 mV at the frequency of 2.25 GHz and an optimum load of  $360 \Omega$ . Shunt-mounted diode rectifier without matching network has its output DC voltage increased by the number of sub-carriers of multisine signals in all the frequency range. The 8-tone signal gives the output DC voltage approximately 40 to 50 % higher than that of 1-tone signal on non-optimized circuit. For example, at 2.25 GHz, output DC voltage of 8-tone signal is 12.5 mV while that value of 1-tone signal is 8.5 mV.

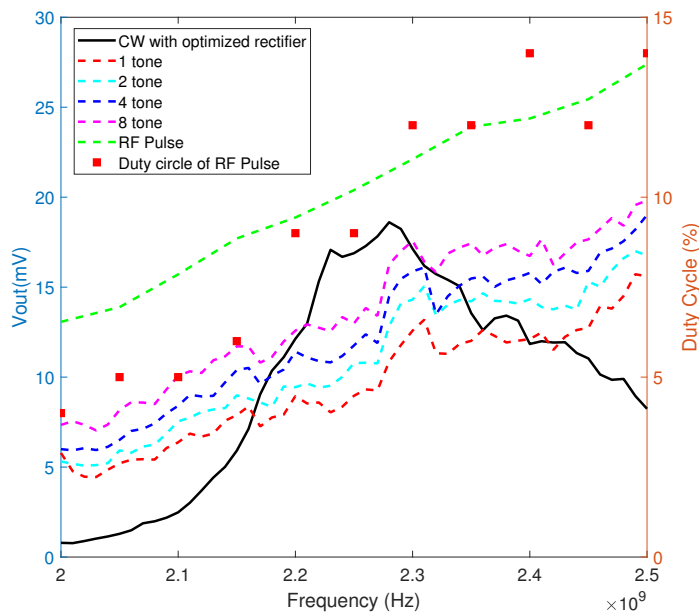


FIGURE 2.33: Voltage output of multisine and RF pulse signals on shunt-mounted diode rectifiers at -20 dBm. ( $R_L = 360 \Omega$ )

Besides, RF pulse signal's voltage output provides highest value for the duty cycle varied from 4 to 14%. With that optimized values, the PAPR of RF pulse signal varies from 20 dB to 31 dB. Over the frequency band, RF pulse has the highest output voltage even compared with 1-tone signal on optimum circuit. Also, RF pulse signal gives the output voltage higher than 40 % compared to 8-tone signal on non-optimized circuit. At 2.25 GHz, the DC voltage for RF pulse and 8-tone signal is 20.5 mV and 12.5 mV, respectively, which means 60 % higher for RF pulse signal.

Optimized voltage-doubler rectifier allows much higher voltage output using CW compared to series-mounted diode and shunt-mounted diode rectifiers as it obtains approximately 60 mV at -20 dBm and 2.2 GHz (Fig.2.34). The gap between optimized and non-optimized rectifiers is noticeable in this case. However, 8-tone signal's voltage output still exceeds the performance of 1-tone signal's on the voltage-doubler without matching network. Furthermore, RF pulse has the same behavior as the case of series-mounted diode rectifiers when it reaches highest DC output when the duty cycle alternates between 2% to 4%. The duty cycle of RF pulse signal are smaller in this case compared to shunt-mounted diode rectifier. The

PAPRs in this case vary from 17 to 20 dB.

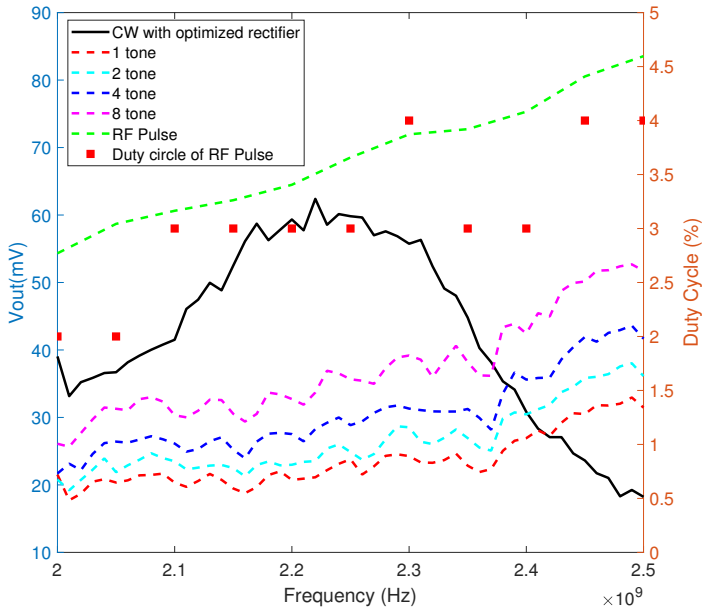


FIGURE 2.34: Voltage output of multisine and RF pulse signals on voltage-doubler rectifiers at -20 dBm. ( $R_L = 3 \text{ k}\Omega$ )

In all cases, the choice is made between the duty cycle and the modulation frequency. Both parameters are played at the same time in order to control the times when the pulse is on/off. The whole trade-off lies in choosing the smallest possible duty cycle while ensuring that the discharge time is not large compared to the time constant of the low-pass filter. However, as fixing the modulated frequency of 1 MHz, we can change only duty cycle to have the maximum performance.

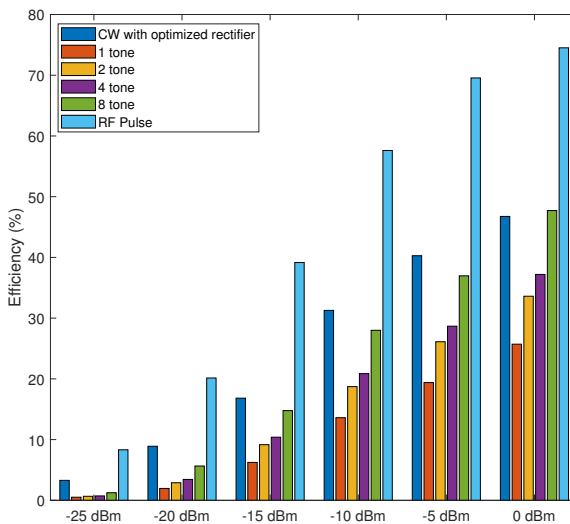


FIGURE 2.35: Efficiency of multisine and RF pulse signal on series-mounted diode rectifiers at 2.25 GHz. ( $R_L = 1 \text{ k}\Omega$ )

To observe the performance over the input power range, we plot the measurement results as bar graphs. Fig.2.35, Fig.2.36, and Fig.2.37 present the RF-to-dc conversion efficiency of RF pulse, multi-sine and CW signal over the input power range from -25 to 0 dBm, with a step of 5 dBm at the middle of the frequency band (2.25 GHz).

For series-mounted diode, as look at the bar chart (Fig.2.35), the efficiency of RF pulse is approximately 60% to 250% higher than the performance of CW on optimum circuit as it increases from 3.3% to 8.3% at -25 dBm and from 46% to 74.5% at 0 dBm. Also, the efficiency of non-optimized circuit with multisine signal matches the efficiency of CW signal on matched rectifier when the RF power increases and particularly at 0 dBm. Meanwhile, RF pulse signals perform a significantly higher efficiency at all the input power levels.

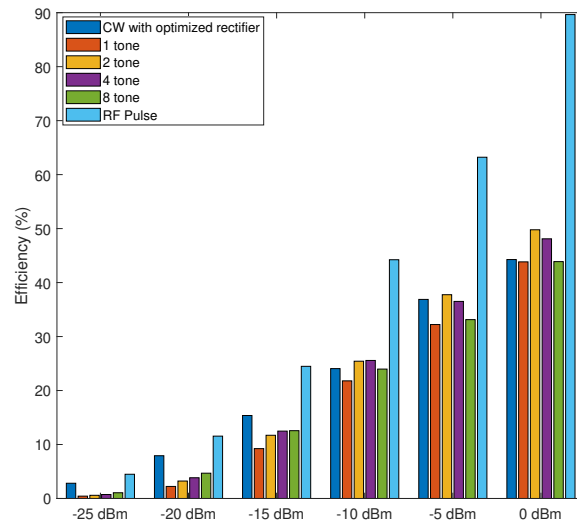


FIGURE 2.36: Efficiency of multisine and RF pulse signal on shunt-mounted diode rectifier at 2.25 GHz. ( $R_L = 360 \Omega$ )

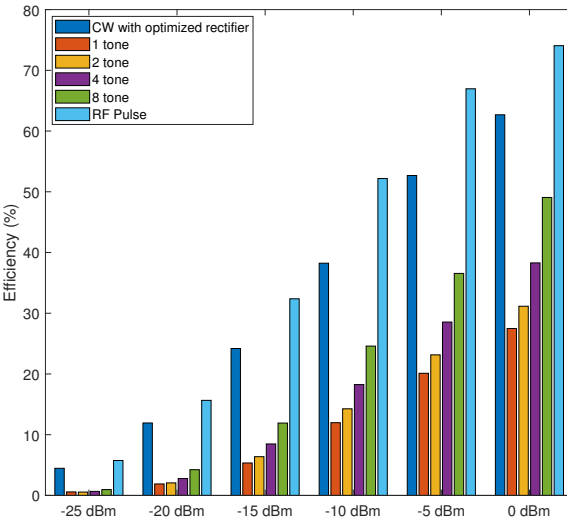


FIGURE 2.37: Efficiency of multisine and RF pulse signal on voltage-doubler rectifier at 2.25 GHz. ( $R_L = 3 \text{ k}\Omega$ )

A similar performance can be found on shunt-mounted diode (Fig.2.36), when the efficiency is improved from 2.8% to 4.5% at -25 dBm and from 44% to 89% at 0 dBm for the CW on optimized rectifier and RF pulse on non-optimized rectifier, respectively.

For voltage-doubler rectifier, the performance of RF pulse signal on non-optimized circuit is better than that of CW signal on optimized circuit. However, this enhancement is smaller than those of series and shunt-mounted diode rectifier. At -25 dBm, the efficiency grows from 4.5% to 5.7% while at 0 dBm, it increases from 62 to 74% (Fig.2.37).

The results show the impact of optimized waveforms, multisine and RF pulse signals, on three basic types of rectifiers. Without making efforts on designing matching network of the rectifiers, optimized waveforms can compensate the RF-to-dc conversion performance and enhance the bandwidth of the non-optimized rectifiers. The 8-tone multisine signal has the voltage output comparable to 1-tone signal applied on optimized rectifier for series and shunt-mounted diode rectifier. Meanwhile, RF pulse signal surpasses it even at the optimized frequency for rectifier with matching network. The duty cycle of RF pulse is recorded at low value from 2% to 4% (PAPR = 17 to 20 dB) for series-mounted diode and voltage-doubler rectifiers, and 4 to 14% (PAPR = 11.5 to 17 dB) for shunt-mounted diode rectifier.

The RF pulse-modulated signal outperforms the performances of 1-tone signal over power range values, with an efficiency improvement from 46% to 74.5% for series-mounted diode and 44% to 89% for shunt-mounted diode at 0 dBm input power.

Also from the results, at the optimized load resistance of each rectifying circuit, RF pulse signal shows a better performance overall compared to multi-sine signal over the frequency band of interest regardless of the input power. For that reason, in the next section of this chapter, the performance of only RF pulse signals with different duty cycles will be taken into account on those circuits, under the variation of load values from  $300 \Omega$  to  $100 \text{ k}\Omega$ . The load value varies from the optimum value of the circuit supplied by CW to a few hundreds

$k\Omega$ . In reality, some sensors have an input impedance which varies in time (measure, sleep or data transfer mode). This study allows to evaluate the performance of the rectifier when the load impedance can vary in time. Also, the sensor's impedance is often far or even too far from the optimum load impedance as previously considered. At high load impedance, for example, of  $100 k\Omega$ , the efficiency of the circuit is close to 0 %. By using RF pulse signal, we want to bring the maximum of the DC output to the load value of the sensor.

### 2.5.2 DC voltage and efficiency of RF pulse signal over load value range

Similar to the previous measurement, in the first place, the CW is applied to the rectifier with matching network. This output voltage is used as the voltage DC reference to compare with RF pulse signal's output DC voltage. The load value is changed from  $300 \Omega$  to  $100 k\Omega$ . Instead of varying and finding the optimum duty cycle for each center frequency and input power as in previous section, the duty cycles of RF pulse signal are constant at 2, 10, 35 and 85 %, which corresponds to the PAPR of 20, 13, 7.5 and 3.7 dB, respectively.

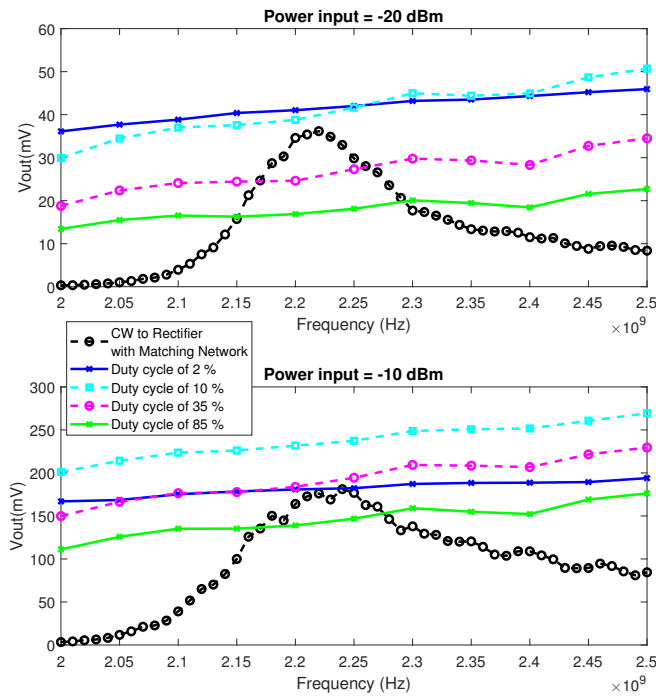


FIGURE 2.38: Output voltage of series-mounted diode rectifiers versus frequency at -20 and -10 dBm ( $R_L = 1 k\Omega$ ).

We firstly display on Fig.2.38 the output DC voltage of different RF pulse signals on the non-optimized rectifier and the DC output of CW on matched rectifying circuit at the input power of -20 dBm, -10 dBm and the frequency ranging from 2 GHz to 2.5 GHz. The load value is fixed at  $1 k\Omega$  (optimum value). The measurements have been done with the input power levels from -25 to 0 dBm but we choose 2 levels of input power (-20 and -10 dBm) in this section. It shows different behaviors.

As can be seen, CW has its highest output DC voltage of 35 mV at -20 dBm and 180 mV at -10 dBm at optimum frequency of 2.25 GHz. On the other hand, RF pulse signals with different duty cycles show the variation of output DC voltages. At -20 dBm and 2.25 GHz, maximum output DC voltage of RF pulse signal is 44 mV at the duty cycle of 2%, which is 25.8% higher in term of voltage and 58% higher in term of DC power compared to 1-tone signal on optimized rectifier. Similar results are obtained at input power of -10 dBm. With other frequencies, the voltage gain and power gain are even significantly higher because the performance of the optimized rectifier is degraded on both side of the center frequency.

To conclude, at the frequency range of interest, RF pulse signal presents a relatively constant voltage output at small duty cycle at 2 levels of input power, -20 and -10 dBm. Outside of the optimum frequency where DC output of CW signal is considerably decreased, RF pulse allows to increase output DC voltage over the entire frequency band.

At higher value of input power, the RF pulse signal has different behavior. At -20 dBm, the RF pulse signal with 2 % duty cycle has a comparable output voltage to RF pulse signal with 10 % duty cycle. While at -10 dBm, RF pulse signal with 10 % of duty cycle has a better performance over the frequency band. The PAPR is relatively high of 13 dB or 20 dB for duty cycle of 10 % and 2 %, respectively. For higher value of duty cycle (35 % and 85 %), the output voltage of RF pulse signal on non-optimized circuit is smaller than that of CW on optimized circuit, except outside the center frequency. With higher duty cycle, the PAPR is significantly decreased. The PAPR is only 3.7 dB for RF pulse signal with duty cycle of 85 % (compared to 3 dB of 1-tone signal). The best performance overall obtained at small duty cycle, which gives high PAPR values.

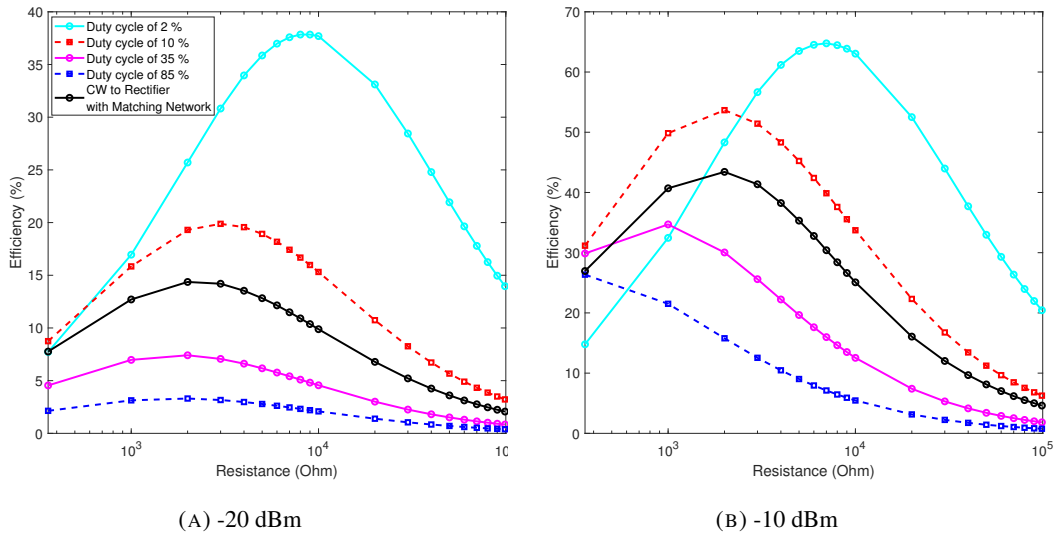


FIGURE 2.39: RF-to-dc conversion efficiency of series rectifiers versus resistance load at -20 dBm and -10 dBm ( $f = 2.25$  GHz).

Keeping the input power of -20 dBm and -10 dBm and the frequency of 2.25 GHz, when varying the load values from  $300\ \Omega$  to  $100\ k\Omega$ , we have the experimental results in Fig.2.39a and Fig.2.39b.

While varying the load value, the efficiency is plotted instead of the voltage output to compare the performance of the rectifier. At -20 dBm, the efficiency of CW on optimized rectifier obtains its maximum value of 14% when the load resistance is around  $1\text{ k}\Omega$  to  $3\text{ k}\Omega$ . RF pulse presents a considerably higher efficiency on non-optimized rectifying circuit. The maximum RF-to-dc conversion efficiency is 37.5%, when the duty cycle is 2% and a load of  $10\text{ k}\Omega$ , which is about 3 times higher than the efficiency of 1-tone signal on optimized rectifier.

At -10 dBm, these values are 42% and 65%, respectively. At different load resistances, we can easily find an appropriate RF pulse signal with the optimum duty cycle to provide the RF-to-dc conversion efficiency equal or higher than the performance of optimum rectifying circuit with 1-tone signal.

The similar results of shunt-mounted diode and voltage-doubler rectifiers can be found in Fig.2.40 to Fig.2.43 with some minor differences. For shunt-mounted diode rectifier, as shown in Fig.2.40, at -20 dBm and 2.25 GHz, the maximum output DC voltage of 1-tone signal on rectifier with matching network is 17 mV. RF pulse signal DC output reaches the maximum value of 20 mV with a duty cycle of 9%. We have a voltage gain of 17.6% and the power gain of 38% at 2.25 GHz. At -10 dBm, the voltage increases from 96 mV to 127 mV with RF pulse signal at 35% of duty cycle. In all the frequency range and mainly outside of the center frequency, the DC output provided by RF pulse signal is considerably much higher than that of the 1-tone signal.

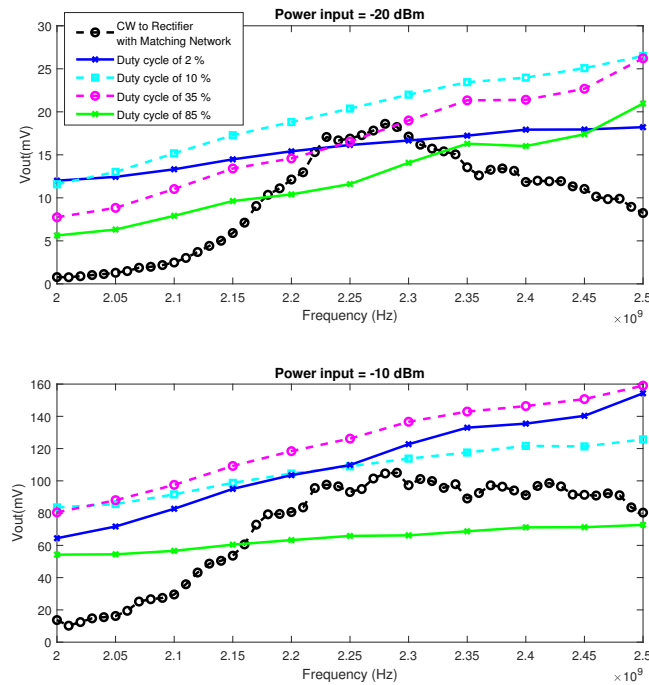


FIGURE 2.40: Output voltage of shunt-mounted diode rectifiers versus frequency at -20 and -10 dBm ( $R_L = 360\ \Omega$ ).

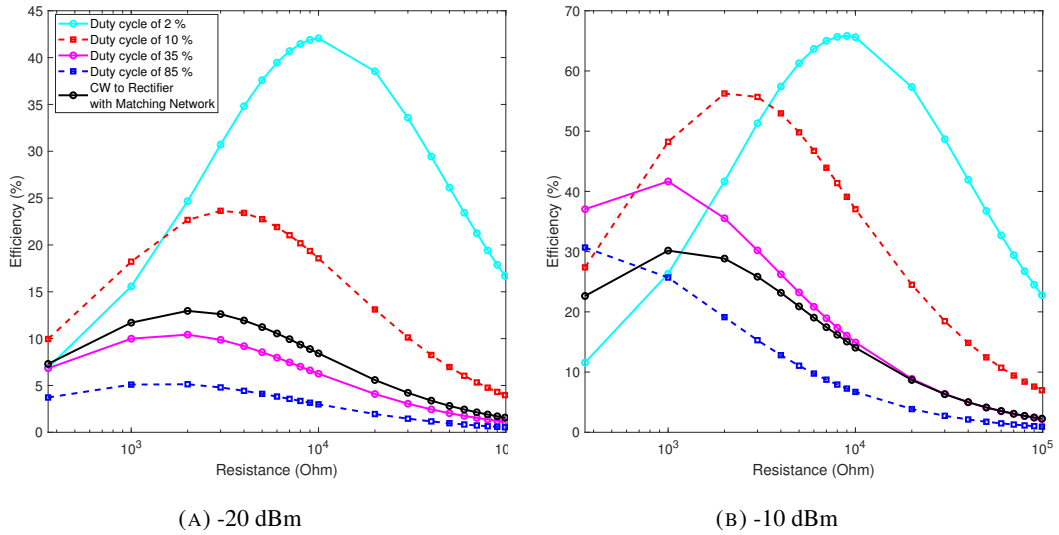


FIGURE 2.41: RF-to-dc conversion efficiency of shunt rectifiers versus resistance load at -20 dBm and -10 dBm ( $f = 2.25 \text{ GHz}$ ).

When varying the load resistance (Fig. 2.41), at -20 dBm, RF pulse signal efficiency with small duty cycle again outperforms the optimum rectifier efficiency with the performance of 10% and 7.29% at optimum load, and 42% to 8% at  $10 \text{ k}\Omega$ , respectively. Meanwhile, at -10 dBm of input power, RF pulse efficiency is significantly higher than that of 1-tone and we can also find an optimum duty cycle which maximize the efficiency when the load varies.

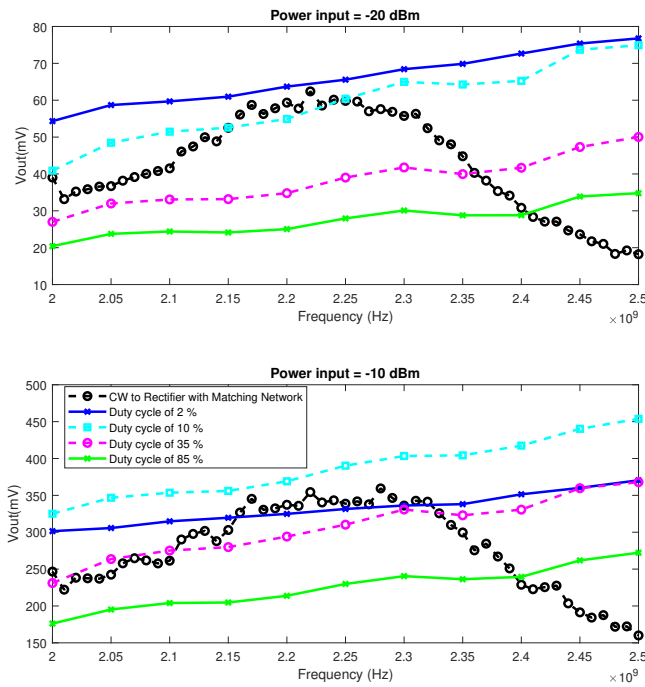


FIGURE 2.42: Output voltage of voltage-doubler rectifiers versus frequency at -20 and -10 dBm ( $R_L = 3 \text{ k}\Omega$ ).

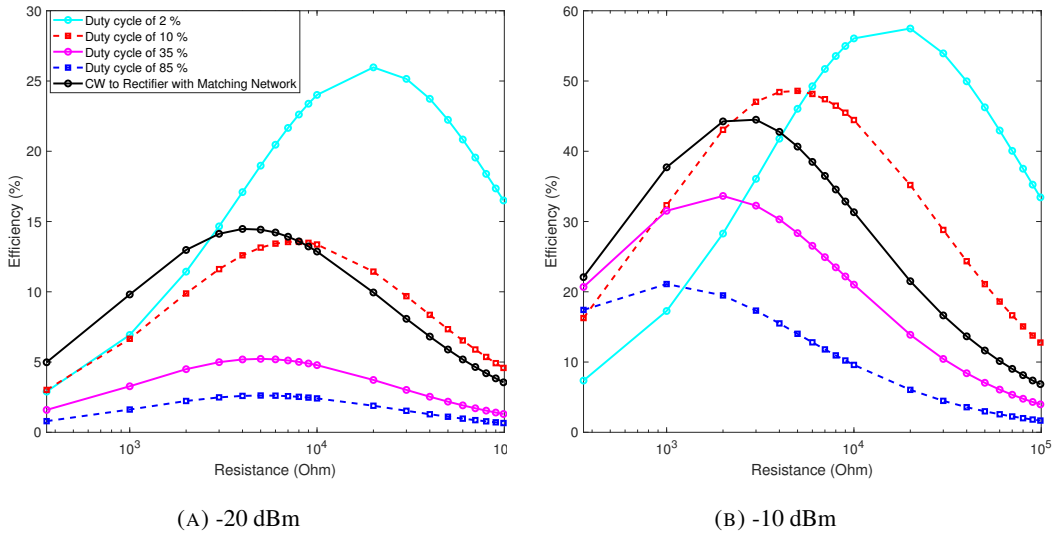


FIGURE 2.43: RF-to-dc conversion efficiency of voltage-doubler rectifiers versus resistance load at -20 dBm and -10 dBm.

For voltage-doubler rectifier, as presented in Fig.2.42 to Fig.2.43, the output DC voltage of 1-tone signal on optimized rectifier is significantly higher in comparison with series-mounted and shunt-mounted diode rectifiers. For that reason, the improvement between RF-pulse voltage and 1-tone signal voltage is smaller at optimum frequency. However, RF pulse signal still providing better performances. At -20 dBm and 2.25 GHz, the voltage gain calculated is of 8.7 % and the power gain is 18 %.

In the resistance load range from  $360\ \Omega$  to  $2\ k\Omega$ , the 1-tone signal efficiency is higher than RF pulse at all the duty cycles. From  $3\ k\Omega$  to  $100\ k\Omega$ , only the RF pulse signal with duty cycle smaller than 10 % can give better performance than 1-tone signal. The best improvement recorded at  $20\ k\Omega$ , when the RF pulse gives 25 % and the 1-tone signal give only 10 % in term of RF-to-dc conversion efficiency.

Tables 2.2 and 2.3 summarize the main previous results at the center frequency of 2.25 GHz (where  $R_o$  is the optimum load value for each signal):

Signal	Series		Shunt		Voltage-doubler	
	$R_o$ (kΩ)	$\eta$ (%)	$R_o$ (kΩ)	$\eta$ (%)	$R_o$ (kΩ)	$\eta$ (%)
CW	2	13.7	2	12.5	4	14
RF Pulse 2 %	10	37.5	10	42	20	26
RF Pulse 10 %	3	20	3	24	8	13
RF Pulse 35 %	2	7	2	10	5	5
RF Pulse 85 %	2	2.7	1	5	5	2.5

TABLE 2.2: Optimum load and corresponding efficiency for CW and RF pulse signal ( $P_{in} = -20$  dBm and  $f = 2.25$  GHz)

Signal	Series		Shunt		Voltage-doubler	
	$R_o$ (kΩ)	$\eta$ (%)	$R_o$ (kΩ)	$\eta$ (%)	$R_o$ (kΩ)	$\eta$ (%)
CW	2	43	1	30	3	43
RF Pulse 2 %	7	64	9	66	20	57
RF Pulse 10 %	2	53	2	57	5	48.5
RF Pulse 35 %	1	32	4	42	2	33
RF Pulse 85 %	0.36	27	0.36	30.5	1	21

TABLE 2.3: Optimum load and corresponding efficiency for CW and RF pulse signal ( $P_{in} = -10$  dBm and  $f = 2.25$  GHz)

In general, RF pulse signal with smaller duty cycle gives better performance. At -20 dBm and 2.25 GHz, only RF pulse signals with duty cycle of 2 % and 10 % show a higher RF-to-dc compared to CW signal.

Similar results can be found at -10 dBm of input power. For each duty cycle value, the maximum of efficiency is obtained for a certain value of resistance load. The highest efficiency obtained by RF pulse signal is 57 %, when the duty cycle is 2 % and the load resistance is 20 kΩ. Whereas, the reference efficiency of 1-tone and optimized rectifier is only about 15 %. These results show that optimizing the duty cycle makes it possible to maximize the efficiency when load resistance varies in a large range.

Overall, the results show, by using three traditional RF-to-dc rectifiers, that optimized RF pulse signal provides better performances compared to 1-tone signal, even when applied on optimized and well matched rectifiers. The optimization of the pulse waveform, instead of the conversion circuit, makes it possible to deliver equal or even better performances. It also allows more flexibility in terms of operating frequency and output load. This solution allows RF-to-dc conversion circuits maintaining optimal operation for different frequencies and different load values. At -20 dBm input power and 2.25 GHz, efficiency gains of 58%, 38% and 18% are obtained by series, shunt and voltage-doubler rectifiers, respectively. Similar results are obtained at other power levels. This work shows that the optimized RF pulse signals can transform non-optimized rectifiers into wide band rectifiers in term of frequency and load resistance. Performances are superior in comparison with rectifiers with input matching networks, which present an optimum operation under a narrow frequency band.

## 2.6 Conclusion

In this chapter, the complete study of multi-sine signal and RF pulse signal are presented in every aspects. Then, the introduction of ADS simulation is presented with different simulation methods. After that, the designing procedure of 3 traditional rectifier topologies are mentioned in order to test with the POW. To do so, we have developed an automated measurement setup. Finally, the measurement results with POWs on the rectifiers are presented.

The statistical study shows that multisine signal has highest PAPR while all the parameters are identical between sub-carriers. After that, RF pulse signal characteristics have been presented.

The simulation results on basic topologies of rectifiers on ADS schematic as well as ADS layout show that signal with higher PAPR has better performance than 1-tone signal. Finally, the measurement on 3 types of rectifier has been done with multi-sine and RF pulse signals. Optimized waveforms can compensate the RF-to-dc conversion performance on the non-optimized rectifiers. For the non-optimized series-mounted and shunt-mounted diode rectifier, 8-tone multisine signal has the output voltage comparable to 1-tone signal applied on optimized rectifier. RF pulse signal surpasses it even at the operating frequency of narrow-band and optimized rectifier on the entire frequency bandwidth. Measurement results also show that the optimization of the pulse waveform, instead of the conversion circuit, makes it possible to deliver equal or even better performances in terms of DC voltage/efficiency and frequency bandwidth. The duty cycle of RF pulse should be at low values which means that the PAPR must be significantly high to achieve good performance, especially for low input power levels. We have shown that when the load varies, the duty cycle can be adjusted to maximize the performance of the rectifier.

The results of chapter 2 show a broadband aspect of the circuits. In the next chapter, the measurement results of broadband rectifier and broadband rectenna will be presented to demonstrate the RF-to-dc conversion improvement by using multi-sine and RF pulse signals. The two waveforms not only improve the performance of basic rectifier topologies but also increase the RF-to-dc conversion efficiency of broadband energy harvesting devices.



# Bibliography

- [1] Collado, A., and Georgiadis, A. *Optimal waveforms for efficient wireless power transmission*, IEEE Microwave and Wireless Components Letters, 24(5), 354-356.
- [2] Valenta, C. R., and Durgin, G. D. *Rectenna performance under power-optimized waveform excitation*, In RFID (RFID), 2013 IEEE International Conference on (pp. 237-244). IEEE.
- [3] Boaventura, A. S., and Carvalho, N. B. *Maximizing DC power in energy harvesting circuits using multisine excitation*, In Microwave Symposium Digest (MTT), 2011 IEEE MTT-S International (pp. 1-4). IEEE.
- [4] Collado, A., and Georgiadis, A. *Improving wireless power transmission efficiency using chaotic waveforms*, In Microwave Symposium Digest (MTT), 2012 IEEE MTT-S International (pp. 1-3). IEEE.
- [5] <https://www.mathworks.com/help/matlab/ref/std.html>
- [6] <http://edownload.software.keysight.com/eedl/ads/2011/pdf/adstour.pdf>
- [7] [http://edownload.software.keysight.com/eedl/ads/2011\\_01/pdf/ptolemy.pdf](http://edownload.software.keysight.com/eedl/ads/2011_01/pdf/ptolemy.pdf)
- [8] Pham, Viet-Duc, Hakim Takhedmit, and Laurent Cirio. *Performance Improvement of a 2.4-GHz Multi-stage Rectifier Using Power Optimized Waveforms* In 2018 25th IEEE International Conference on Electronics, Circuits and Systems (ICECS), pp. 293-296. IEEE, 2018
- .



## Chapter 3

# Performance improvement of broadband rectifier/rectenna by using POWs

### 3.1 Broadband rectifier

In previous chapter, we have shown that the RF-to-dc conversion efficiency and output DC voltage can be optimized on the broad-band non-optimized rectifiers. Wide-band aspects (frequency and output load) offer many possibilities in terms of the choice of the operating frequency for the power transfer. Wide-band rectifier/rectenna also gives a flexibility to better adapt to the input impedance of the sensors and electronics devices, which is normally far from the optimum load of the narrow-band rectifier/rectenna.

In this chapter, we firstly propose a broadband and optimized rectifier and then present the measurements of the DC output by using multi-sine signal and pulse signal. Secondly, the automated measurement setup in the anechoic chamber will be developed to perform the measurement with broadband rectenna. We will show the improvement of the DC output of the broadband rectifier/rectenna by using multi-sine and RF pulse signals.

The broadband rectifier/rectenna used in this study has been previously designed and optimized to operate at the frequency range from 1.6 to 2.8 GHz (GSM, UMTS, Wi-Fi and LTE2600/4G frequency band) [1]. It contains an input filter, a DC low pass filter, an output load, and 2 Schottky diodes. It is configured as a voltage doubler to produce higher output DC voltage compared to single-mounted diode rectifier. Due to the demand of harvesting RF energy at a wide-band of frequency, the input impedance matching network of the rectifier is designed as a micro-strip non-uniform transmission lines (NUTL). To get a compact rectenna, S-shaped filter geometry is used as the input impedance matching network. We choose the Schottky diode SMS7630-079LF from Skyworks as its low biasing voltage requirement for a small power input.

Fig.3.1 shows the layout and the prototype of the rectifier. It is designed and optimized using Harmonic Balance and Momentum simulation of Keysight ADS with its dimensions in details. The optimum load's resistance of the rectifier is  $3 \text{ k}\Omega$ . The prototype is printed on a 1.6 mm thick FR-4 substrate ( $\epsilon_r = 4.3$ ).

Fig.3.2 shows the measured reflection coefficient ( $S_{11}$ ) of the rectifier over the frequency band ranging from 1 to 3 GHz, for different input power levels from -25 to -5 dBm with reference of  $50\ \Omega$ . The output resistance load is fixed to  $3\ k\Omega$ . The results are obtained for a CW input signal. For -25 dBm,  $S_{11}$  is smaller than -1.8 dB in the frequency range from 1.6 to 2.6 GHz. The  $S_{11}$  is improved when the input RF power level increases.

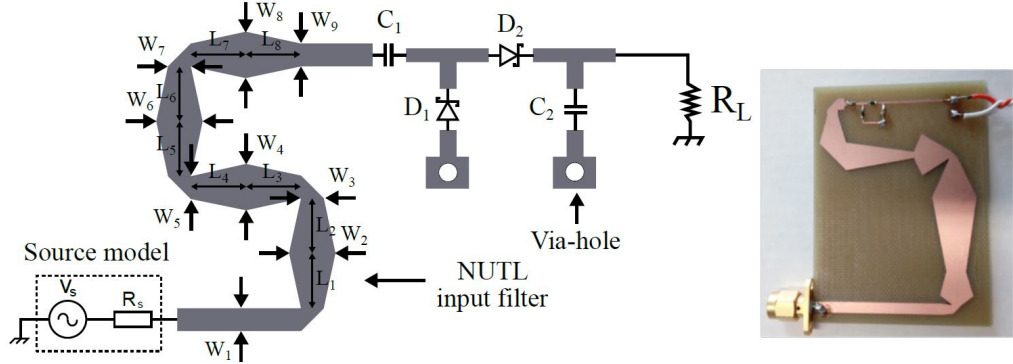


FIGURE 3.1: Rectifier circuit. Generic circuit layout of the wide-band rectifier with the photograph of the prototype. The parameters are :  $W_1 = 2.2$  mm,  $W_2 = 9.4$  mm,  $W_3 = 5.5$  mm,  $W_4 = 12.8$  mm,  $W_5 = 2.2$  mm,  $W_6 = 11$  mm,  $W_7 = 1.8$  mm,  $W_8 = 8.2$  mm,  $W_9 = 3.4$  mm,  $L_1 = 2.6$  mm,  $L_2 = 6.6$  mm,  $L_3 = 21.1$  mm,  $L_4 = 11.4$  mm,  $L_5 = 8.2$  mm,  $L_6 = 2.4$  mm,  $L_7 = 20.6$  mm,  $L_8 = 8.2$  mm,  $C_1 = C_2 = 100\ pF$ ,  $R_L = 3\ k\Omega$  [1].

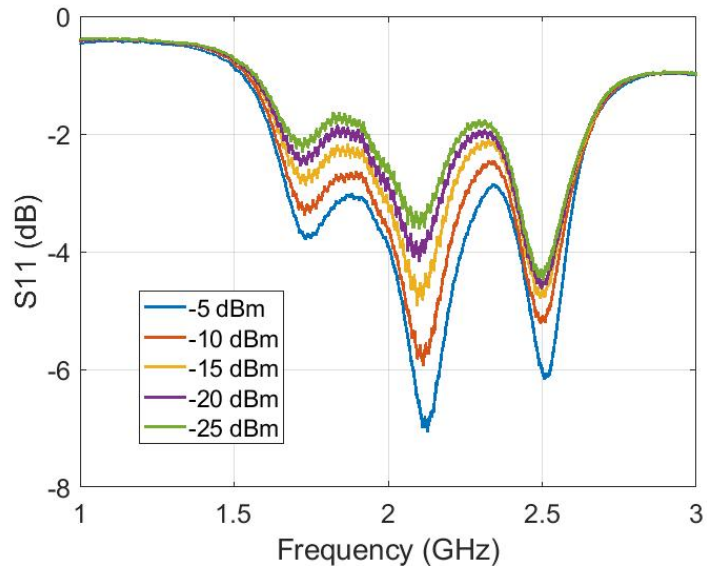


FIGURE 3.2: Reflection coefficient ( $S_{11}$ ) versus the frequency ( $R_L = 3\ k\Omega$ ).

Applying CW at the input, the output DC voltage of the rectifier versus frequency and input RF power is presented in Fig.3.3. The frequency range is from 1 to 3 GHz and the input power levels are from -40 dBm to -0.2 dBm. As can be seen, the output DC voltage gets the maximum value in the frequency range from 1.6 to 2.8 GHz, while the input power is from -6 to 0 dBm. The maximum output DC voltage is 1.1 V at 2.2 GHz and input power of -0.2

dBm. The results are coherent with the  $S_{11}$  parameter measured and displayed in Fig.3.2 with lowest  $S_{11}$  founded in the frequency range from 1.6 to 2.8 GHz.

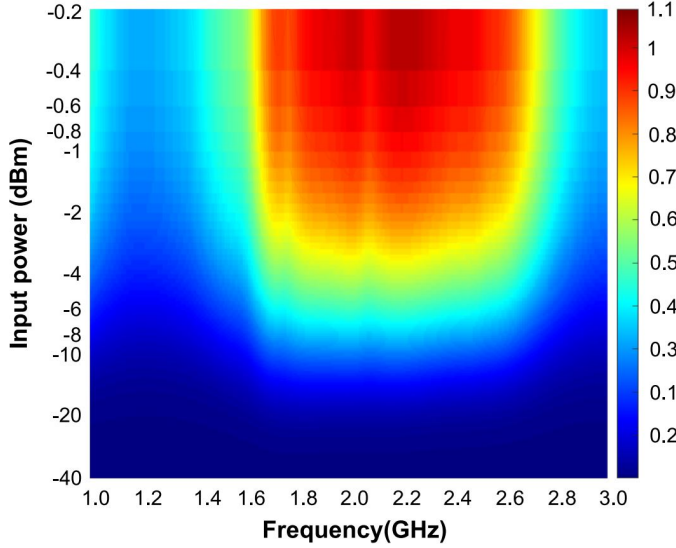


FIGURE 3.3: Simulated output voltage (Volts) of the rectifier versus frequency and input RF power for  $R_L = 3 \text{ k}\Omega$  [1].

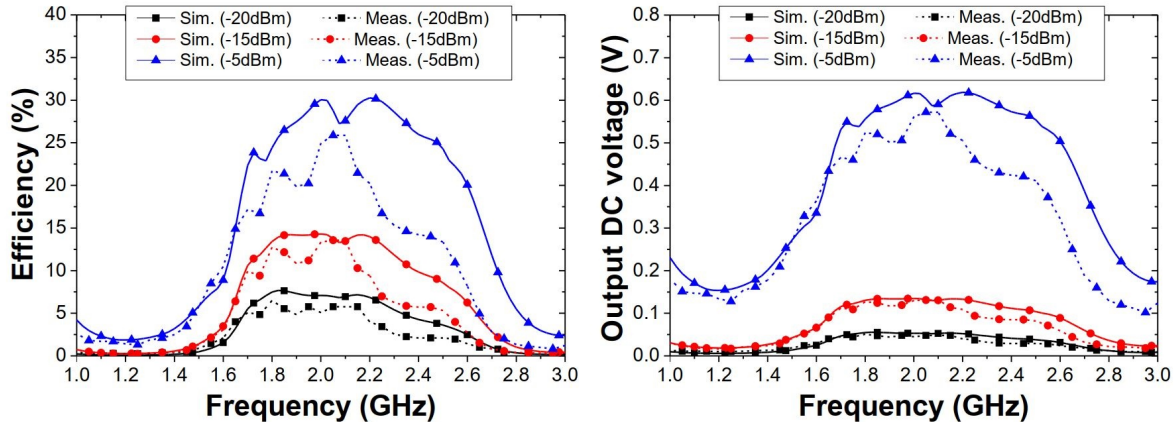


FIGURE 3.4: RF-to-dc conversion efficiency and output voltage of the rectifier versus frequency and input RF power for  $R_L = 3 \text{ k}\Omega$  [1].

Fig.3.4 presents the simulated and measured RF-to-dc conversion efficiency and output DC voltage of broadband rectifier with CW signal input. The frequency range is also from 1 to 3 GHz. As can be seen, the broadband behavior of the circuit is clearly shown in this figure. For example, at -5 dBm, the efficiency is higher than 15 % in the frequency range from 1.6 to 2.8 GHz. At other frequencies, the efficiency as well as output DC voltage drops sharply to lower than 5 %.

The efficiency of the broadband rectifying circuit is considerably low at small input power. At -20 dBm, highest efficiency is only 7 % at 1.8 GHz and much more smaller at other frequencies. Improving the RF-to-dc conversion efficiency for such a circuit at small power input is a great challenge. In the next sections, we test and compare multi-sine signal and RF pulse signal applied to this circuit to enhance the RF-to-dc conversion efficiency.

### 3.1.1 Measurement with multi-sine signal

Measurements with multisine signal have been done with a number of sub-carriers (N) up to 16 and power input of -20 and -10 dBm. The similar results have been found in others power input such as -25; -15 and -5 dBm. While varying the center frequency, the frequency bandwidth (BW) is fixed at 10 MHz for all multi-sine signals. So, as the number of sub-carriers varies, we have the relation between frequency spacing ( $\Delta f$ ) between sub-carriers and the frequency bandwidth as below:

$$\Delta f = \frac{BW}{N-1} \quad (3.1)$$

Fig.3.5 and Fig.3.6 display the output DC voltage (left) and the voltage gain (right) of multi-sine signals on the broadband rectifier at -20 dBm and -10 dBm, respectively. The voltage gain is calculated using the following equation:

$$G_p = 20\log_{10}\left(\frac{V_{outPOW}}{V_{out1-tone}}\right) \quad (3.2)$$

where  $V_{outPOW}$  is the output DC voltage of POW on the rectifier,  $V_{out1-tone}$  is the output DC voltage of CW on the rectifier.

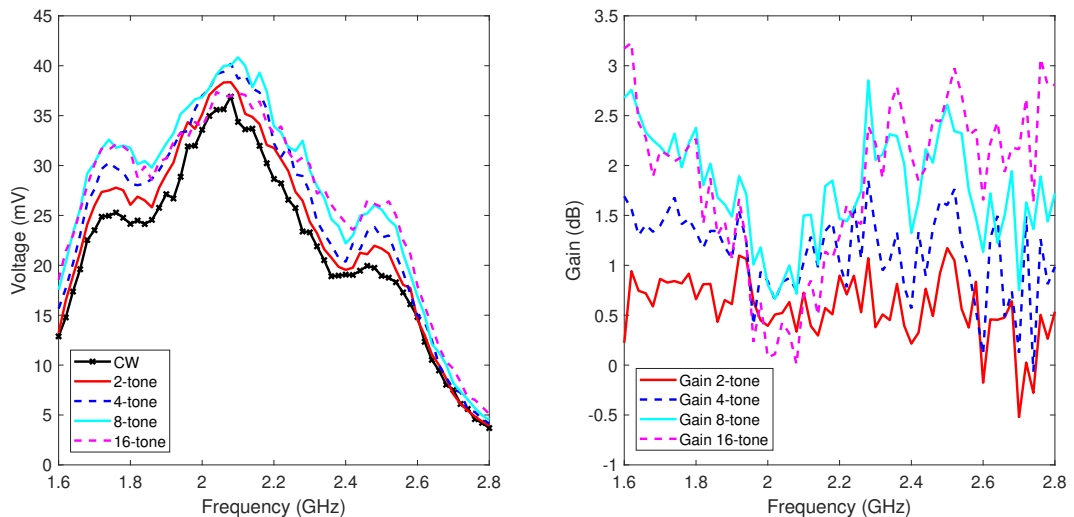


FIGURE 3.5: Output voltage (mV) and voltage gain (dB) of the rectifier versus frequency for different number of tones ( $R_L = 3 \text{ k}\Omega$ ,  $P_{RF} = -20 \text{ dBm}$ ).

At -20 dBm, the voltage gain is mostly over 0 dB at all frequency range as well as number of tones, which means that multi-sine signals often give better performance than 1-tone signal. In the order of increment of number of sub-carriers, the PAPR of the multi-sine signal increases. Also, the voltage output and the voltage gain are more or less increased over the frequency range of interest. The highest gain obtained is 3 dB at 1.6 GHz for 16-tone signal. Meanwhile, the lowest gain recorded at the center of frequency band from 2 to 2.2 GHz, where the circuit has the highest voltage output of approximately 40 mV for 1-tone signal. With that value, the highest RF-to-dc conversion efficiency recorded is 5.3 %.

The rectifier has a better performance as the reflection coefficient has the lowest value at the center frequency bandwidth (Fig.3.2). Therefore, there are a smaller margin for improvement compared to other frequencies.

Similar results are found at -10 dBm, except for the 16-tone signal which gives a smaller output DC voltage and a small voltage gain despite a relatively high PAPR value. The lowest gain recorded is -2 dB. The explanation could be at higher power input, the non-linearity is more important, so the losses of the rectifier with signals with high PAPR is more significant. Besides, for 8-tone signal, the highest gains are 3.5 dB at 2.8 GHz and 2 dB at 1.6 GHz. The highest gains happen at the limits of the frequency band. At the frequencies where the circuit is not fully optimized, there is more margin to improve the performance using power optimized waveforms.

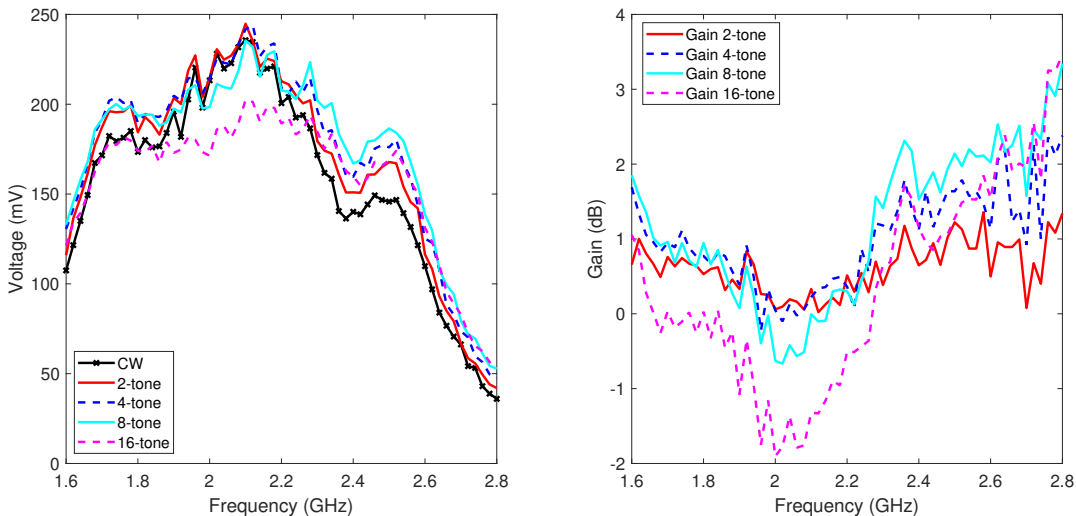


FIGURE 3.6: Output voltage (mV) and voltage gain (dB) of the rectifier versus frequency for different number of tones ( $R_L = 3 \text{ k}\Omega$ ,  $P_{RF} = -10 \text{ dBm}$ ).

### 3.1.2 Measurement with RF pulse signal

For RF pulse signal, there are 2 main parameters: modulation frequency ( $f_m$ ) and duty cycle ( $\beta$ ). As the part of optimization process, measurement with different value of  $f_m$  have been done. Due to characteristic of our signal generator N5182 Keysight Technology, the maximum value of modulation frequency is 125 MHz, we choose the maximum value of  $f_m$  of 6 MHz to have a sufficient number of the sampling points. The modulation frequency takes three values : 1, 3 and 6 MHz while the RF input power ranges from -20 to -10 dBm by 5 dB step.

In measurements with RF pulse signal, the capacitor of 10 nF is connected at the output of the rectenna to eliminate the voltage ripple. According to the equation (2.10), the maximum ripple is obtained for the minimum value of  $f_m$  and  $\beta$  (1 MHz and 1 %, respectively), which corresponds to a maximum value of  $T_{off}$  of 0.99  $\mu\text{s}$ . The minimum time constant  $R_L.C$  is 30  $\mu\text{s}$  (as  $R_L = 3 \text{ k}\Omega$ ). The equation (2.10) is then satisfied for all measurements.

We show in Fig.3.7 an example of the optimization steps when the carrier frequency equal to 2 GHz. In the measurement, we keep the load resistance of  $3\text{ k}\Omega$ . We can see that while varying  $f_m$ , the maximum output DC voltages obtained at different input power levels are not the same and depend on the duty cycle. For example, at -20 dBm, the maximum DC voltage of 60 mV is obtained with  $f_m$  equal to 1 MHz and duty cycle of 17%. On the other hand, at -15 dBm, the maximum DC output of 150 mV is obtained with  $f_m = 6$  MHz and duty cycle of 30 %. The difference between the measurement results of the three modulation frequencies are not noticeable. It is also true for other carrier frequencies. Overall, the modulated frequency (from 1 to 6 MHz) does not have a high impact on the voltage DC output as well as the efficiency of the RF pulse signal on broadband rectifier.

In the next sections of this chapter, to facilitate the measurement procedure, we choose the modulated frequency  $f_m = 1$  MHz in all the following measurements. The value of duty cycle  $\beta$  will be varied to find the optimum RF pulse signal for each carrier frequencies.

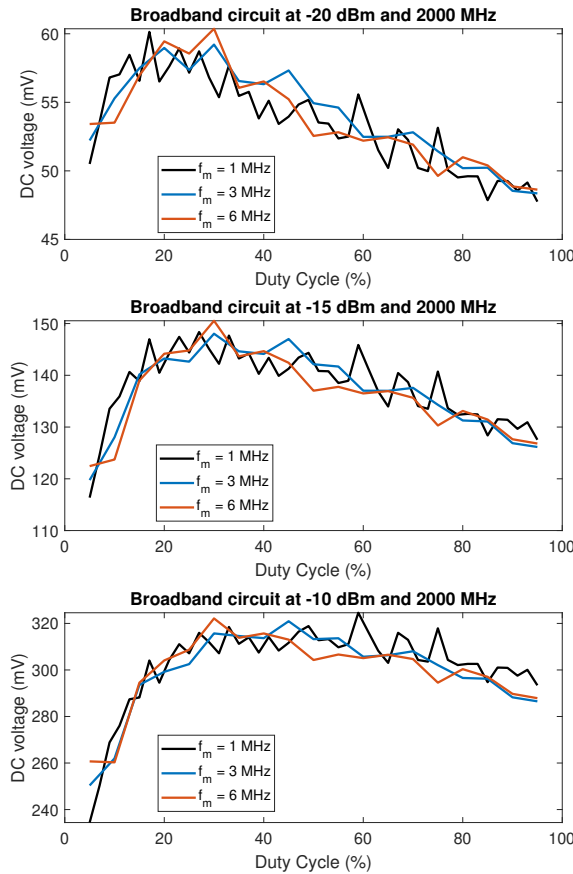


FIGURE 3.7: Output voltage (mV) of RF pulse signal as a function of duty cycle, for different values of modulation frequency ( $R_L = 3\text{k}\Omega$ ).

Fig.3.8a gives the highest output DC voltage of RF pulse signal at -15 dBm RF input power and the corresponding optimal duty cycles when the carrier frequency varies between 1.6 to 2.8 GHz. The output DC voltage for 1-tone signal is also given as a reference and for

comparison. At 1.6 GHz, the output DC voltage increases from 42 mV for 1-tone signal to 83 mV for RF pulse signal with 8 % duty-cycle, which corresponds to a voltage gain of 5.2 dB.

Fig.3.8b presents the voltage/efficiency gain of RF pulse signal over 1-tone signal. The gain obtained at the central frequencies from 2 to 2.2 GHz is approximately 2.9 dB, the duty cycle is above 20 % ( $\text{PAPR} \approx 10 \text{ dB}$ ). From 2.5 to 2.8 GHz, the gain increases and reaches 8 dB, with the duty cycle of 5 % ( $\text{PAPR} \approx 16 \text{ dB}$ ). Overall, the voltage gain of RF pulse signal is higher than 2.9 dB over the frequency range of interest, especially at two ends of the frequency range, while the duty cycle  $\beta$  is lower than 15 % ( $\text{PAPR}$  higher than 11.2 dB). It can be explained that for 1-tone signal and at the center of the considered frequency range, the rectifying circuit has higher output DC voltage than at the edged frequencies, which allows better margin of improvement with RF pulse signal.

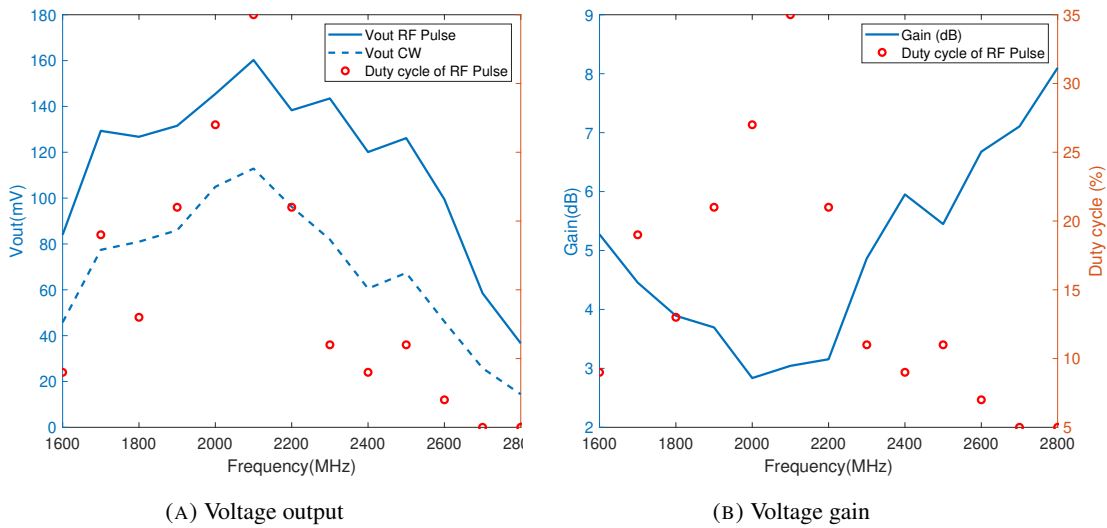


FIGURE 3.8: Voltage output, voltage gain and duty cycle of RF pulse signal versus 1-tone signal at -15 dBm ( $R_L = 3 \text{ k}\Omega$ ,  $f_m = 1 \text{ MHz}$ ).

Optimum duty cycles are obtained in the range from 5 to 35 % (Fig.3.8). As the duty cycle decreases, the RF input voltage increases in the shorter period of time ( $T_\beta = \beta \cdot T_m$ ), which may sometimes insufficient to charge the capacitor of the output filter. The optimum duty cycle should balance the charging time and the amplitude of the RF input voltage. The optimum duty cycle is considerably high ( $\beta \geq 20 \%$ ) in the center of the frequency band, where the voltage gain is low and the output DC voltage of 1-tone signal is sufficiently high compared to that at the edged frequencies. In contrast, the optimum duty cycle is lower ( $\beta < 15 \%$ ) in the frequency band where the output DC voltage of 1-tone signal is decreased.

Figures 3.9 and 3.10 display the distributions of the maximum efficiency of RF pulse signal and 1-tone signal as a function of resistance load and frequency. The RF power is fixed at -15 dBm. The results show that the maximum efficiency of RF pulse signal that can be reached is 50.32 % while that value of 1-tone signal is only 27.7 %. At the frequencies closer to 2.2 GHz, the efficiency of RF pulse signal is significantly higher than the two edges

of the frequency band at 1.6 and 2.8 GHz. Similar behavior can be observed with 1- tone signal (Fig. 3.10).

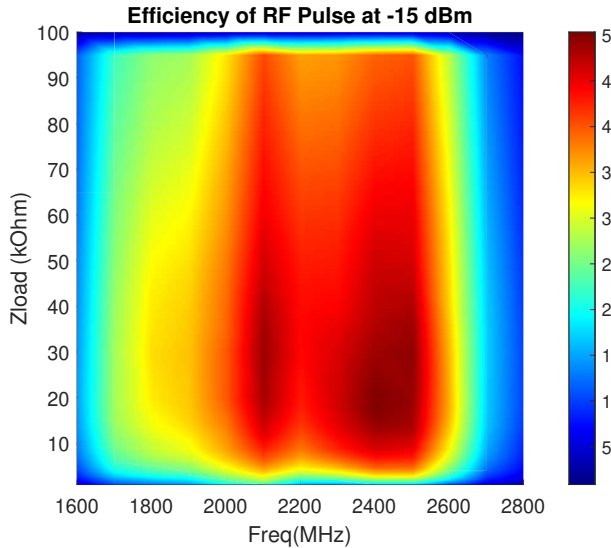


FIGURE 3.9: Maximum efficiency of RF pulse signal versus  $Z_{load}$  and frequency at -15 dBm ( $f_m = 1$  MHz).

With RF pulse signal, the efficiency is considerably improved over the frequency band of interest in the wide range of resistive loads.

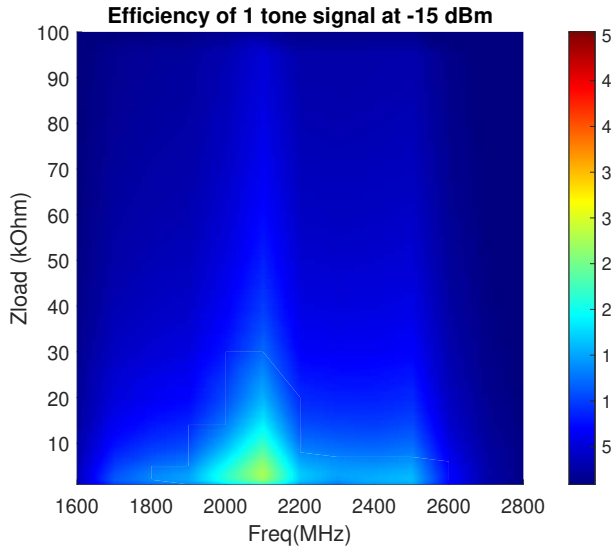


FIGURE 3.10: Efficiency of 1-tone signal versus  $Z_{load}$  and frequency at -15 dBm.

In Fig.3.11, at -15 dBm, the efficiency gain shows the contrast with the efficiency's distribution. At optimum frequency range from 1.8 GHz to 2.5 GHz (see Fig.3.9), the gain is considerably small especially when load values are smaller than  $10\text{ k}\Omega$ . Besides, once the load's values are higher, the gain is constantly improved for all the frequency range of interest. Highest gain obtained is 14.25 dB at 1.6 GHz and 2.8 GHz and load resistance of  $40\text{ k}\Omega$  and  $90\text{ k}\Omega$ , respectively.

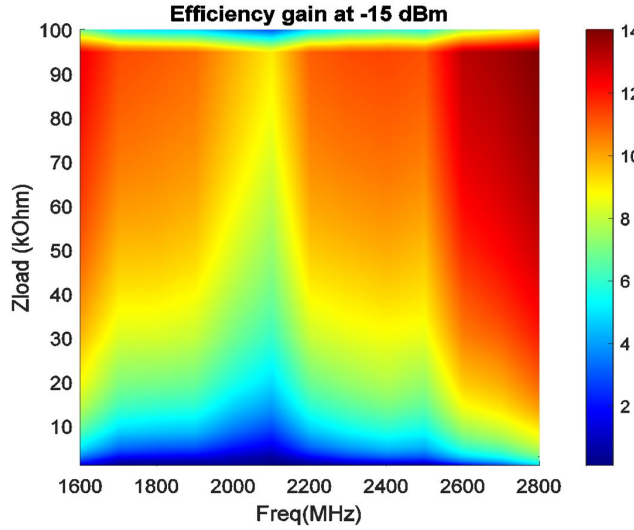


FIGURE 3.11: Efficiency gain of RF pulse signal compared to 1-tone signal versus  $Z_{load}$  and frequency at -15 dBm.

Meanwhile, at -5 dBm, a similar behavior can be found in Fig.3.12. The gain is improved in central frequency range from 1.8 GHz to 2.6 GHz but with higher load's values of  $30\text{ k}\Omega$  to  $90\text{ k}\Omega$ . The highest efficiency gain is 12.95 dB at the limit of the frequency band.

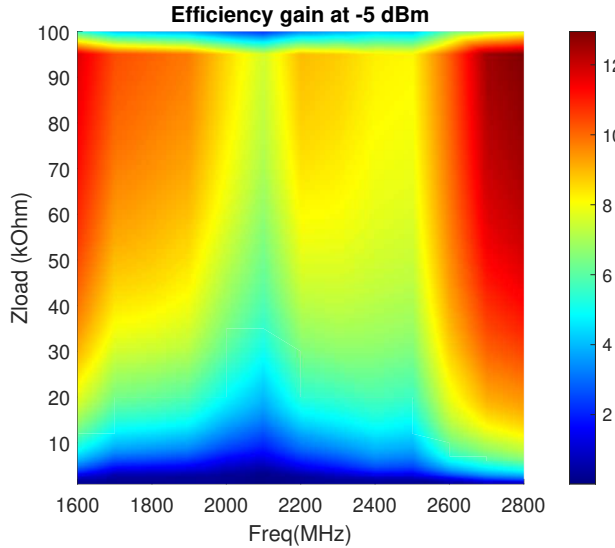


FIGURE 3.12: Efficiency gain of RF pulse signal compared to 1-tone signal versus  $Z_{load}$  and frequency at -5 dBm.

On the other hand, by setting the frequency to 2.2 GHz and the load value to  $3\text{ k}\Omega$ , efficiencies and output DC voltages of RF pulse and CW signals versus the RF power input dBm are shown in Fig.3.13. For RF pulse signal, as the input power increases, the output DC voltage and the efficiency increase. The maximum output DC voltage is 0.71 V and the efficiency is 40 % at -5 dBm. Meanwhile, for CW, the values are 0.52 V and 21.9 %, respectively. The efficiency of RF pulse has been almost doubled in comparison with CW through the input power range.

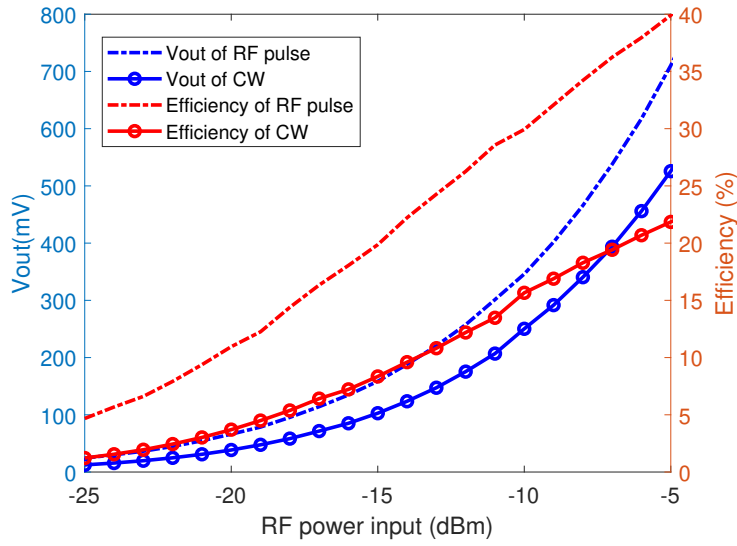


FIGURE 3.13: Output DC voltage and efficiency as a function of RF input power for optimized RF pulse and CW signals ( $f = 2.2$  GHz,  $R_L = 3\text{ k}\Omega$ ).

To summarize, the table 3.1 gives a comparison between the performances of 1-tone signal, multi-tone signal and RF pulse signal at 3 frequency values (1.6, 2.2 and 2.8 GHz), for 2 input power levels: -20 and -10 dBm. RF pulse signal clearly shows much better performance in terms of voltage gain compared to CW and multi-sine signals over the frequency range and for different input powers.

Waveform	$G_p$ at 1.6 GHz		$G_p$ at 2.2 GHz		$G_p$ at 2.8 GHz	
	-10 dBm	-20 dBm	-10 dBm	-20 dBm	-10 dBm	-20 dBm
CW	1	1	1	1	1	1
2-tone	0.65	0.22	0.51	0.89	1.34	0.53
4-tone	1.69	1.69	0.86	1.02	2.38	0.99
8-tone	1.85	2.67	0.44	1.29	3.34	1.72
16-tone	1.05	3.17	-0.50	1.47	3.46	2.81
RF pulse	6.23	4.40	2.53	4.04	7.92	7.57

TABLE 3.1: RF pulse and multi-sine signal voltage/efficiency gain compared to CW and multi-sine signal ( $R_L = 3\text{ k}\Omega$ )

In this section, RF pulse signal is proposed for WPT with broadband operating frequency. The measurements on broadband rectifier show the performance improvement of RF pulse compared to 1-tone signal. Overall, the voltage output is improved over the frequency range of interest despite the variation of load resistance. At optimum load resistance of  $3\text{ k}\Omega$ , the highest gain recorded is 8 dB at 2.8 GHz with a duty cycle of 5% and a PAPR value of 16 dB. While varying the load value, the gain is significantly higher at 14.25 dB and 12.95 dB at -15 dBm and -5 dBm respectively for the frequency of 2.8 GHz. That maximum values are obtained with the load value of  $90\text{ k}\Omega$ . The output DC voltage enhancement also depends on how the rectifying circuit is optimized. At central frequencies and smaller load's resistance,

the voltage gain is smaller than that achieved at the two ends frequencies. For example, from Table 3.1, at 2.2 GHz, the voltage gain of RF pulse signal is only 2.53 dB at -10 dBm. That values for 1.6 Ghz and 2.8 GHz are 6.23 dB and 7.92 dB, respectively. Indeed, the rectifying circuit is less optimized at these frequencies (1.6 and 2.8 GHz), where the output DC voltage for 1-tone signal is considerably small. RF pulse signal outperforms multi-sine signal over the frequency bandwidth.

## 3.2 Broadband rectenna characterization inside an anechoic chamber

In this section, a broadband rectenna which is designed and optimized to operate from 1.6 to 2.8 GHz will be characterized with multi-sine and optimized RF pulse signal. The experiments will be performed inside an anechoic chamber using automated measurement setup.

### 3.2.1 Broadband rectenna description

The proposed antenna (Fig.3.14) is a wideband fractal-shaped slotted ground antenna (SGA). All accesses are well matched, the reflection coefficient is less than -10 dB over the frequency band of interest (Fig.3.15).

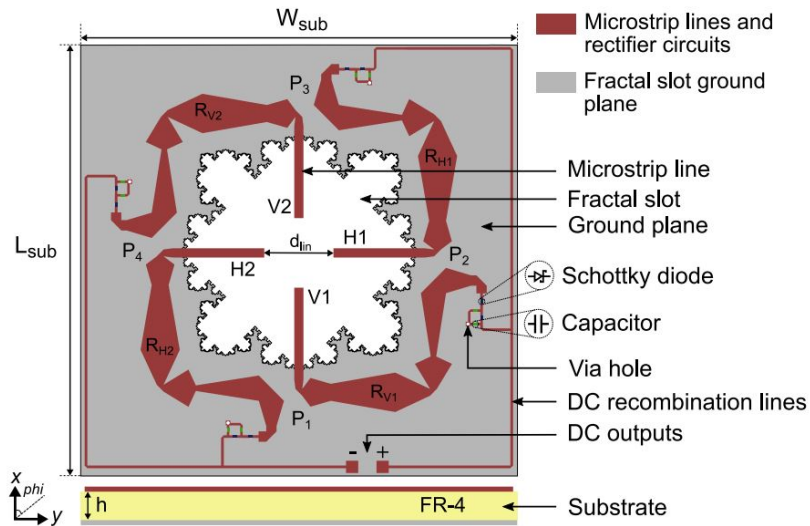


FIGURE 3.14: Proposed rectenna layout [1].

By using a differential-feed topology, the receiving power amount is increased. The fractal SGA is fed by a DP-DF (Dual-Polarized and Differential-feed) lines composed of four 50-Ohms microstrip transmission lines etched on the bottom along x and y axes and denoted  $H_1$ ,  $H_2$ ,  $V_1$  and  $V_2$ , for linear horizontal and vertical polarizations [1]. Fig.3.15 shows the measured and simulated gains of the antenna in the frequency range from 1 to 3 GHz. Due to the fabrication and measurement tolerances, there are differences between the simulated and measured curves.

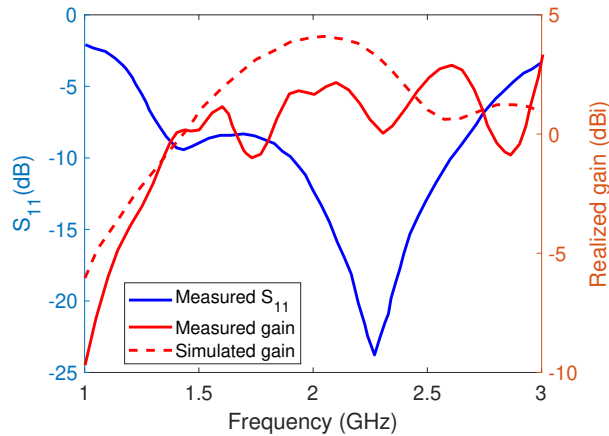


FIGURE 3.15: Reflection coefficient and realized gains of the antenna.

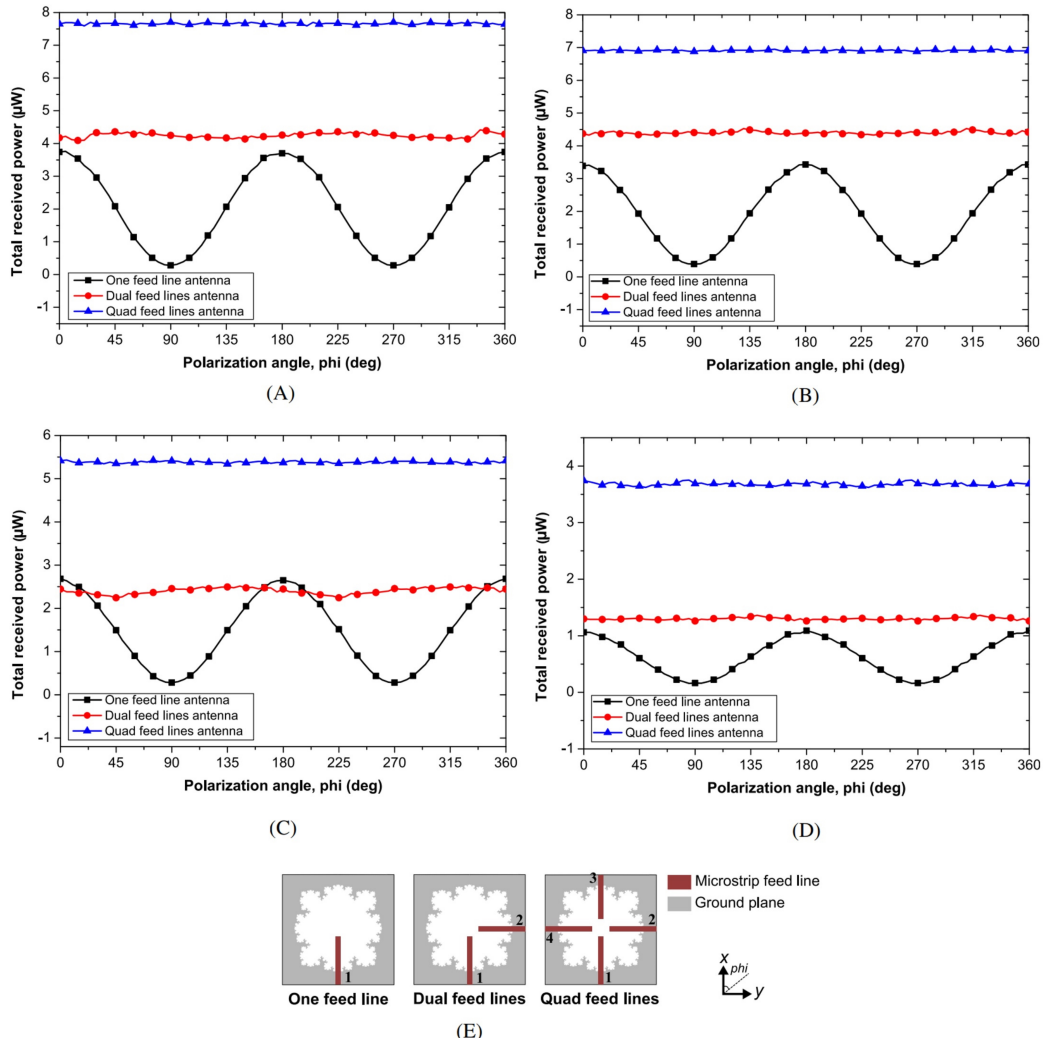
FIGURE 3.16: Received power by one, dual and quad feed lines SGA vs polarization angle (power density =  $0.27 \mu\text{W}/\text{cm}^2$ ,  $E_{rms} = 1 \text{ V/m}$ ) at: A, 1.85 GHz; B, 2.15 GHz; C, 2.45 GHz; D, 2.65 GHz; E, Different antenna's feeding topologies. SGA, slotted ground antenna [1].

Fig.3.16 shows the comparison between the incident power received by one, dual, and

quad-feed lines SGA with different polarization angles. The simulation is performed by ANSYS HFSS software. As can be seen, regardless of the polarization angle and the operating frequency, for dual and quad feed lines SGA, the received power is almost constant. It is not true for one feed line SGA, where the received power varies with the variation of polarization angle. For some cases, the power received by the quad-feed lines can be doubled the dual-feed lines.

On the other hand, table 3.2 shows the received power for the different antennas at 2.45 GHz with power density of  $0.27 \mu\text{W}/\text{cm}^2$  and  $E_{rms} = 1 \text{ V/m}$ . From the results, for both LHCP and RHCP polarization, the received power of quad-feed lines is always two time higher than that of dual-feed lines. Also, that power is doubled in comparison with the power received by linear polarization.

TABLE 3.2: Received power for the different antennas at 2.45 GHz (power density =  $0.27 \mu\text{W}/\text{cm}^2$ ,  $E_{rms} = 1 \text{ V/m}$ ) [1]

Polarization	One feed line (P1), $\mu\text{W}$	Dual feed lines (P1 + P2), $\mu\text{W}$	Quad feed lines (P1 + P2 + P3 + P4), $\mu\text{W}$
Linear (phi = 0°)	2.68	2.53	5.42
LHCP	1.91	5.2	10.92
RHCP	2.07	5.22	10.9

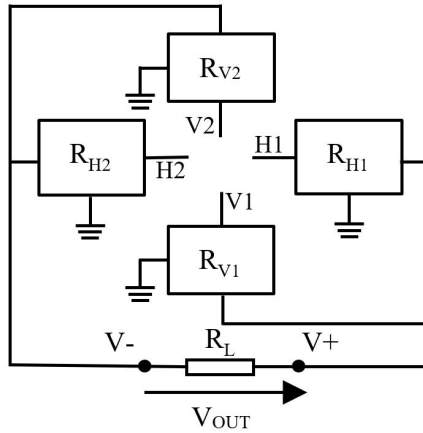


FIGURE 3.17: DC interconnection scheme.

The rectifying part contains 4 identical rectifiers denoted as  $R_{H1}$ ,  $R_{V1}$ ,  $R_{H2}$  and  $R_{V2}$ . Each rectifier contains an input filter, a DC low-pass filter and 2 Schottky diodes configured as a voltage doubler. It provides higher output DC voltage compared to single-mounted diode rectifiers. Due to the demand of harvesting RF energy over a wide frequency band, the input impedance matching network of the rectifier is designed as a microstrip non-uniform transmission lines (NUTL), which can provide broadband impedance matching.

The Schottky diode SMS7630-079LF from Skyworks is chosen. Its low biasing voltage property fill the requirement for a small power operation. Rectifier  $R_{H1}$ ,  $R_{V1}$  are connected

in parallel as well as  $R_{H2}$ ,  $R_{V2}$ . This interconnection topology is more robust with respect to the power imbalances that there may be between the horizontal and vertical accesses. These 2 sub-arrays are then connected in series to enhance the output DC voltage. They are power balanced. The DC interconnection of the different rectifiers is depicted in Fig.3.17.

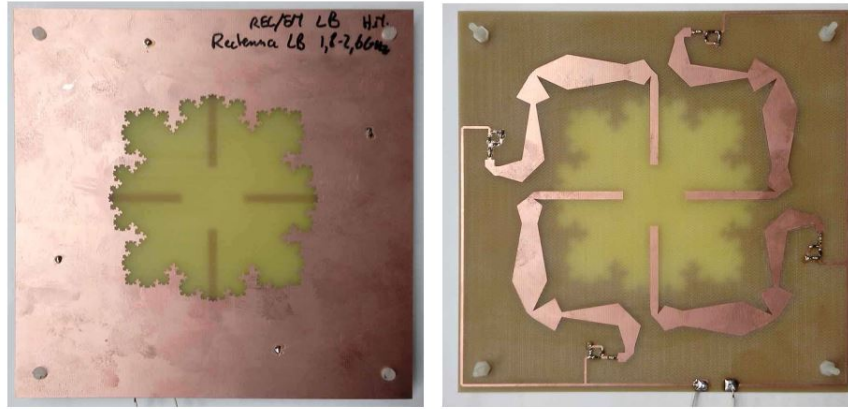


FIGURE 3.18: Photographs of the fabricated rectenna: top view (left) and bottom view (right) [1].

The rectenna is printed on a FR4 substrate with the thickness of 1.6 mm. The top view (fractal SGA) and bottom view (microstrip lines and rectifier array) of the rectenna prototype are displayed in Fig.3.18. The dimensions of the rectenna is 140 x 140 mm.

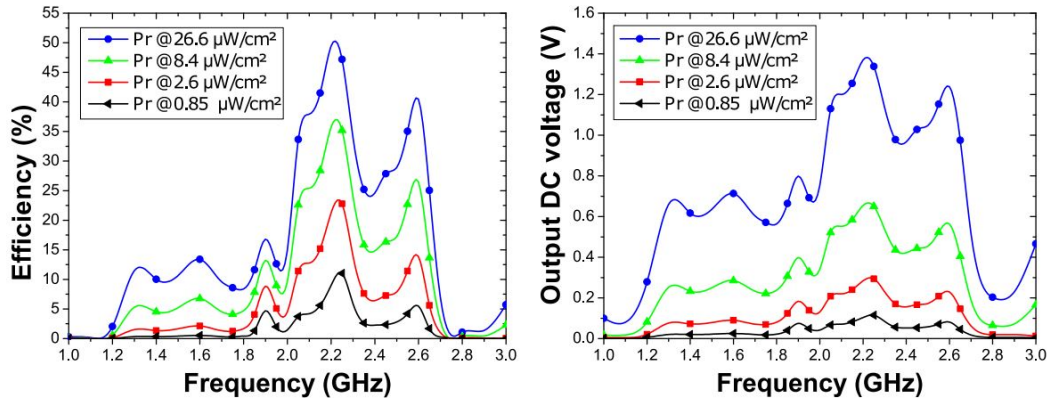


FIGURE 3.19: Measured efficiency and output DC voltage of the rectenna against frequency: Efficiency (left) and output DC voltage (right) ( $R_L = 3k\Omega$ ).[1]

Fig.3.19 shows the measured efficiency and output DC voltage of the rectenna against frequency from 1 to 3 GHz in the case of 1-tone signal. There are 4 levels of power density for this measurement: 0.85  $\mu\text{W}/\text{cm}^2$ , 2.6  $\mu\text{W}/\text{cm}^2$ , 8.4  $\mu\text{W}/\text{cm}^2$  and 26.6  $\mu\text{W}/\text{cm}^2$ , which correspond to the following power input levels: -20 dBm, -15 dBm, -10 dBm and -5 dBm for the center frequency of 2 GHz [1].

As the purpose of this rectenna is to operate in the frequency range from 1.6 to 2.8 GHz, we can see that the output DC voltage and the efficiency decrease at the edged frequencies around 1 and 3 GHz. With the increase of power density (or power input), the efficiency and

the voltage output of the rectenna increase. A maximum efficiency of 50% is achieved at 2.2 GHz for a power density of  $26.6 \mu\text{W/cm}^2$ . The same behavior and the same pattern have been found at all power density levels. However, at small power density of  $0.85 \mu\text{W/cm}^2$  (or -20 dBm), the efficiency is low. The highest value obtained at that power density is 10 % at 2.2 GHz.

### 3.2.2 Experimental setup for automated measurement inside anechoic chamber

We have shown in Fig.3.20 the schematic of the measurement setup, in which the computer controls the system with Matlab program automatically. The setup outside of the anechoic chamber is the same with the measurement setup presented in chapter 2 except the power amplifier and the motor-controller are added. The motor-controller rotates the horn antenna at different angles to vary the emitter's angle. With control program, we can generate multisine signals with different center frequency, frequency bandwidth and number of sub-carriers ( $N = 1, 2, 4, 8$ , etc...). Also, it allows to generate RF pulse with varied center frequency, modulation frequency and the duty cycle  $\beta$  (from 1 to 99%). The generated signals are applied to the input of the horn antenna.

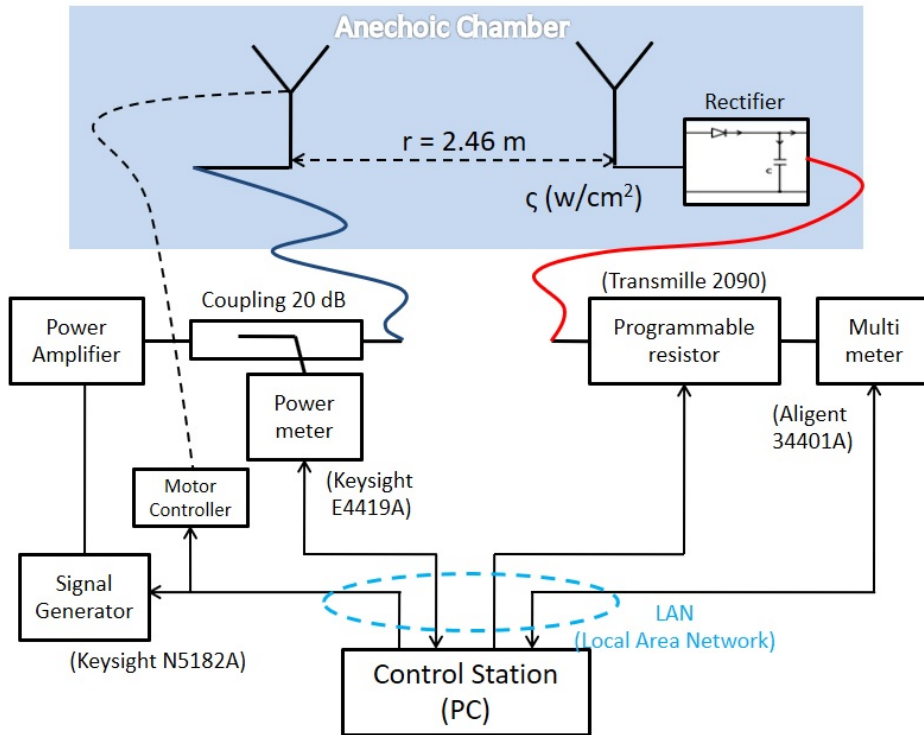


FIGURE 3.20: Measurement setup schematic.

The horn antenna then transmits the signal automatically to the rectenna. The output voltage of the rectenna is measured by using the multi-meter and the results are saved and

used during the post-processing. Inside the anechoic chamber, the horn-antenna and rectenna are positioned as in Fig.3.21.

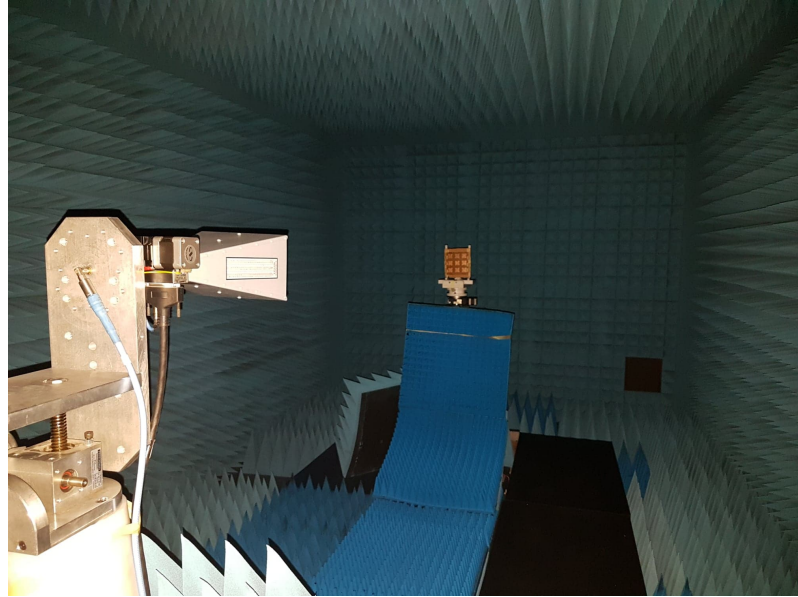


FIGURE 3.21: Anechoic chamber setup with horn-antenna (left) and rectenna (right).

The distance R is adjusted as desired and to satisfy the far-field condition. The main purpose of this distance R is to obtain a specific power density at the input of the rectenna. The power density ( $W/m^2$ ) at the rectenna depends on the transmitted power, the transmitted gain, the distance between the horn transmitter antenna and the rectenna by the following equations:

$$\rho = \frac{P_t G_t}{4\pi R^2} \quad (3.3)$$

where  $\rho$  is the power density,  $P_t$  is the power transmitted by the horn antenna,  $G_t$  is the gain of the horn antenna. To calculate the power received at the rectenna, the effective aperture given by  $A_{ER}$  is calculated as follows:

$$A_{ER} = \frac{\lambda^2}{4\pi} G_r \quad (3.4)$$

$$P_r = A_{ER} \cdot \rho \quad (3.5)$$

where  $P_r$  is the power received by the rectenna,  $G_r$  is the gain of the rectenna.

To control RF power level received by the rectenna, Matlab program handles the calculation using Friis transmission formula and sets the appropriate values of the power amplifier (AR 20S1G4) gain and also the generator output power. The power meter (Agilent E4419A) measures the transmitted power to the horn antenna and compares it to the pre-calculated value. Several measurements are required to get the targeted power level. Once the transmitted power value is set, the RF signal is transmitted to the rectenna. Then, programmable

resistor (Transmille 2090) sets the resistor load value. The multi-meter (Agilent 34401A) measures the output DC voltage and sends it to the main program. These loops are repeated until all the measurements are done.

The same with measurement setup for rectifier, when performing the measurement with rectenna using RF pulse signal, the capacitor of 10 nF is also added at the output of the circuit to satisfy the equation (2.10).

The efficiency is calculated by the equation below:

$$\eta (\%) = 100 \frac{P_{out}}{P_r} = 100 \frac{V_{out}^2}{R_L} \frac{1}{P_r} \quad (3.6)$$

where  $V_{out}$  is the output DC voltage,  $R_L$  is the load resistance. On the other hand, the efficiency gain of RF pulse to 1-tone signal is computed by this formula:

$$G_p = 20 \log_{10} \left( \frac{V_{out,POW}}{V_{out,1-tone}} \right) \quad (3.7)$$

The user interface used for automated measurement in anechoic chamber is the same with the automated measurement presented in chapter 2. The only difference is that, in this case, we have 2 options of measurement. The first option allows to have the same power density ( $\mu\text{W}/\text{cm}^2$ ) at the rectenna despite of varying the frequency. The second option allows to have the same input power level (dBm) at the rectenna when the frequency varies. The choice of measurement type depends on the type of rectenna used in the measurement.

### 3.3 RF pulse signal: Time shape and spectrum considerations

To make sure that the time shape and/or the spectrum of the signal received at the input of our antenna when propagating is maintained, simulations by Matlab software have been done. The idea is to create a pulse signal for different values of duty cycle, to calculate its spectrum at the transmitter side and then to determine the time and frequency domains distortion of the pulse signal at the receiver (rectenna) at a fixed distance from the transmitter. The RF pulse signal will be normalized and plotted in time and frequency domains using DFT (Discrete Fourier Transform). After calculating the path loss, the signal received at the input of the rectenna will be plotted in time and frequency domains in order to compare with the original transmitted signal. The study makes sure that the RF pulse signal is kept at the input of the rectenna despite of the distance R between the horn antenna and the rectenna. The calculation of RF pulse signal  $X(f)$  in frequency domain is based on the following equation:

$$X(f) = \frac{1}{N} \sum_{n=1}^N x(n\Delta t) e^{j \cdot 2\pi f n \Delta t} \quad (3.8)$$

or

$$X(f) = \frac{1}{N} \sum_{n=1}^N x(n\Delta t) (\cos(2\pi f n \Delta t) + j \sin(2\pi f n \Delta t)) \quad (3.9)$$

when  $\Delta t$  is the time sampling interval and N is the number of sampling points with the relation:  $t = N \cdot \Delta t$ .

The path loss (PL) is calculated as below:

$$PL(f) = \left(\frac{4\pi R}{\lambda_0}\right)^2 = \left(\frac{4\pi R f}{c}\right)^2 \quad (3.10)$$

and the phase difference between the transmitter and the receiver is calculated as:

$$\phi(f) = (2\pi R)/\lambda_0 = 2\pi R \cdot \frac{f}{c} \quad (3.11)$$

where  $R$  is the distance between the transmitter and the receiver.  $\lambda_0$  is the free-space wavelength, and  $c$  is the speed of light.

From that, we have the received signal in frequency domain:

$$Y(f) = X(f) \cdot PL(f) \cdot e^{(j\phi(f))} \quad (3.12)$$

The reverse DFT is performed to obtain received signal in time domain and then compare it to the transmitted one:

$$y(t) = \frac{1}{M} \sum_{m=1}^M Y(m\Delta f) \cdot (\cos(2\pi m\Delta f t) - j \sin(2\pi m\Delta f t)) \quad (3.13)$$

where  $X(f)$  and  $Y(f)$  are the transmitted and received signals in frequency domain, and  $x(t)$ ,  $y(t)$  are the transmitted and received signals in time domain, respectively.  $M$  is the number of frequency sampling points,  $\Delta f$  is the frequency spacing between two consecutive sampling frequencies.

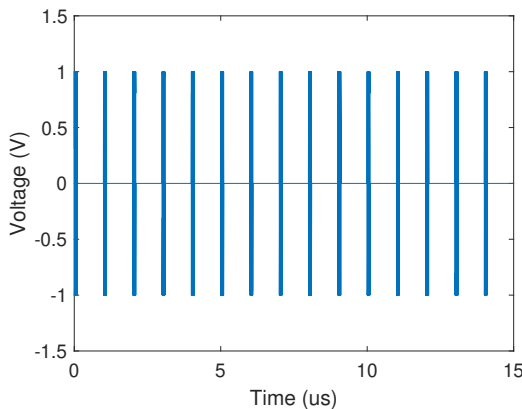


FIGURE 3.22: Transmitted RF pulse signal in time domain ( $\beta = 10\%$ ).

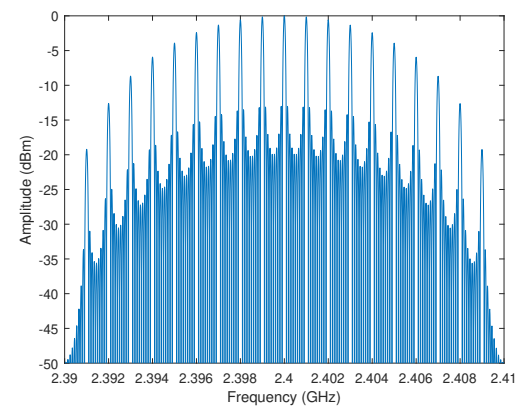


FIGURE 3.23: Transmitted RF pulse signal in frequency domain ( $\beta = 10\%$ ).

All the signals are normalized before plotting. Fig.3.22 and Fig.3.23 show the original transmitted RF pulse signal at the duty cycle of 10 % in time and frequency domains. The frequency range is defined from 2.39 to 2.41 GHz, the number of periods is 15 with  $f_m = 1$  MHz and  $f_c = 2.4$  GHz. Where  $f_m$  is the modulated frequency and  $f_c$  is the carrier frequency of RF pulse signal. We can see that with  $R = 2$  m and  $\beta = 10\%$ , the transmitted and received

signals are identical in frequency domain. Meanwhile in time domain, receiving signal with  $\beta = 10\%$  has a small difference with original signal. (Fig.3.24 and Fig.3.25). The maximum difference calculated by Matlab is 0.26 % in term of amplitude between transmitted and received RF pulse signal.

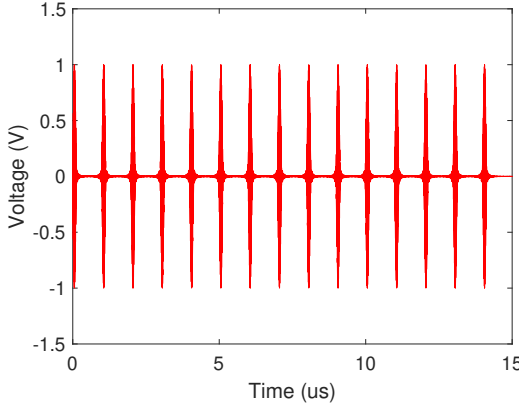


FIGURE 3.24: Received RF pulse signal in time domain ( $\beta = 10\%$ ).

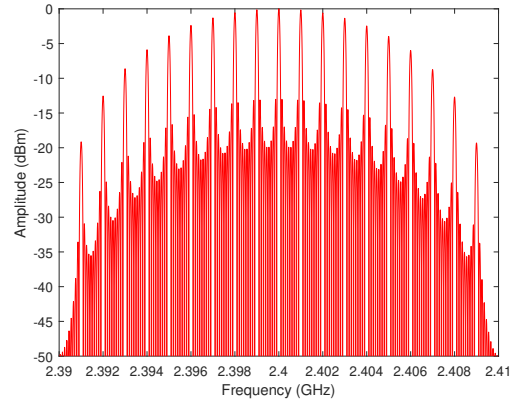


FIGURE 3.25: Received RF pulse signal in frequency domain ( $\beta = 10\%$ ).

For  $\beta = 50\%$  (Fig.3.26 to Fig.3.29), the 2 signals in time and frequency domains are almost identical with the difference of only 0.053 % in term of amplitude between transmitted and received signals. Similar results are found in other values of duty cycle.

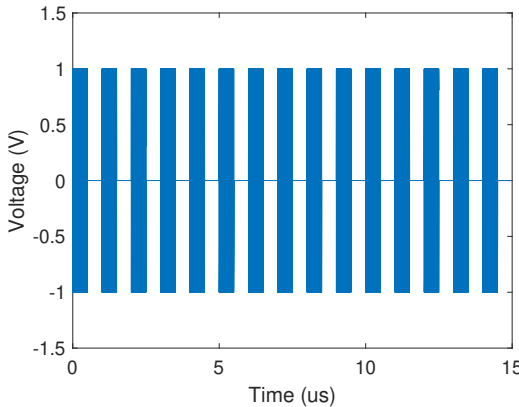


FIGURE 3.26: Transmitted RF pulse signal in time domain ( $\beta = 50\%$ ).

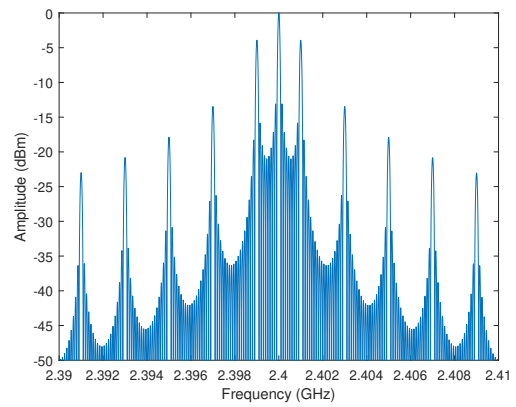


FIGURE 3.27: Transmitted RF pulse signal in frequency domain ( $\beta = 50\%$ ).

After this simulation, we consider that the distance  $R = 2\text{m}$  is suitable for the maintaining the signal's waveforms at the input of the rectenna in anechoic chamber. Other simulations for the distance  $R$  varying from 0.5 to 10 m have been done. Similar behaviors are found for different values of  $R$ . The propagation does not modify too much the frequency spectrum in comparison with the transmitted one.

From all the simulations, we can conclude that the transmitted RF pulse waveform received at the rectenna keeping almost the same shape in time domain and spectrum in frequency domain. The RF pulse signal created by signal generator can be controlled by the spectrum analyzer before emitting by the horn antenna. In contrast, it is difficult to show or obtain the waveform received by the rectenna. For this reason, the simulations are importance to confirm the waveform received by the rectenna and to perform the measurements in anechoic chamber with RF pulse signal, which will be presented in the next section of this chapter.

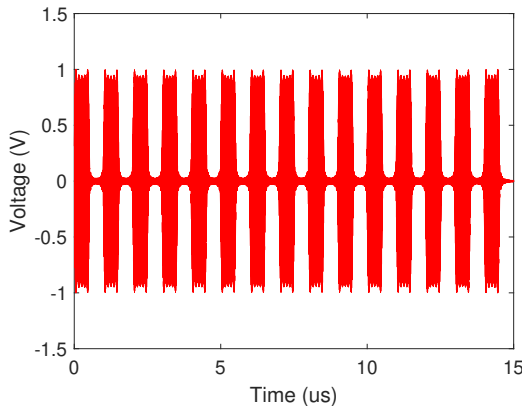


FIGURE 3.28: Received RF pulse signal in time domain ( $\beta = 50 \%$ ).

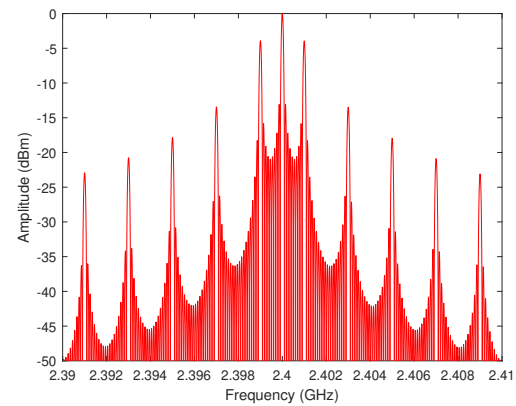


FIGURE 3.29: Received RF pulse signal in frequency domain ( $\beta = 50 \%$ ).

## 3.4 Broadband rectenna's measurement results

Improving the efficiency of the rectenna at small power input using multi-sine signal and RF pulse signal will be presented in this section with measurement results.

### 3.4.1 Measurement with multi-sine signals

Measurement with multi-sine signals has been done using the measurement setup presented in section 4.1. The frequency range is 1.6 to 2.8 GHz. Here, we consider four input multi-sine waveforms: 1-tone, 2-tone, 4-tone and 8-tone signals.

Figures 3.30, 3.31 and 3.32 show the output DC voltages and the voltage gains of multi-sine signal on the frequency range and for a load values of  $3 \text{ k}\Omega$ . The transmitted power is calculated in order to have the power levels of -30, -25 and -20 dBm at the input of the rectenna.

At -20 dBm, the DC voltages of multi-sine signals are slightly improved in general, but decreased at some frequencies compared to 1-tone signal. For example, at 2.2 GHz, where the DC voltage has the highest value with CW, the gain of 8-tone signal is -0.5 dB. While at 1.6 GHz, the voltage gain is 1 dB. Less variation is found at smaller power input levels. For -25 dBm, the voltage gains vary from -0.5 to 0.9 dB and for -30 dBm, it is from -0.2 to 0.6 dB.

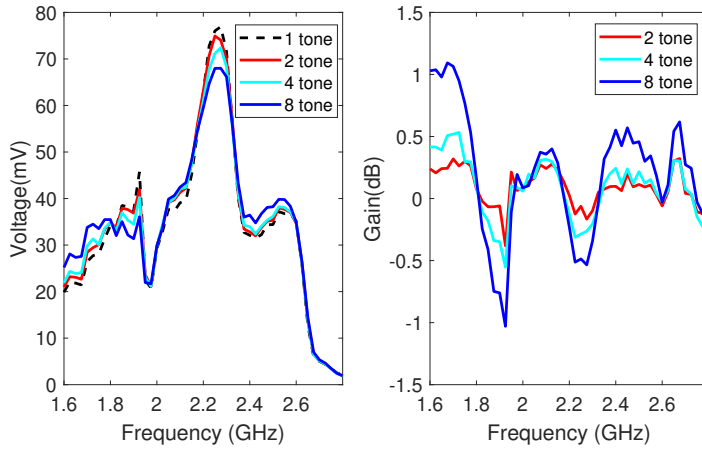


FIGURE 3.30: Voltage output (left) and voltage gain (right) of multisine at -20 dBm ( $R_L = 3 \text{ k}\Omega$ ).

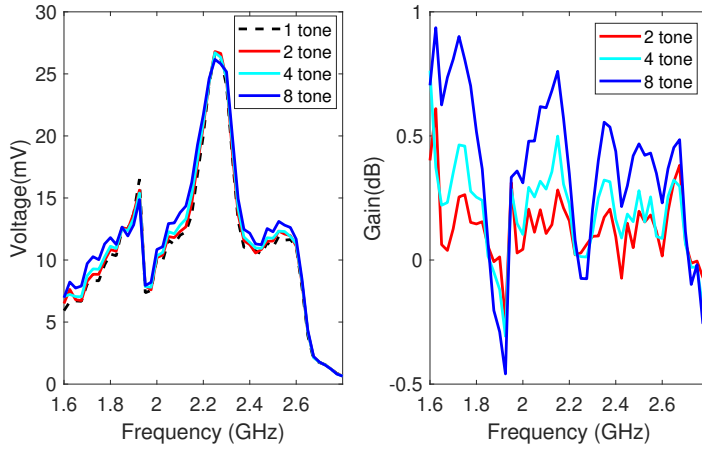


FIGURE 3.31: Voltage output (left) and voltage gain (right) of multisine at -25 dBm ( $R_L = 3 \text{ k}\Omega$ ).

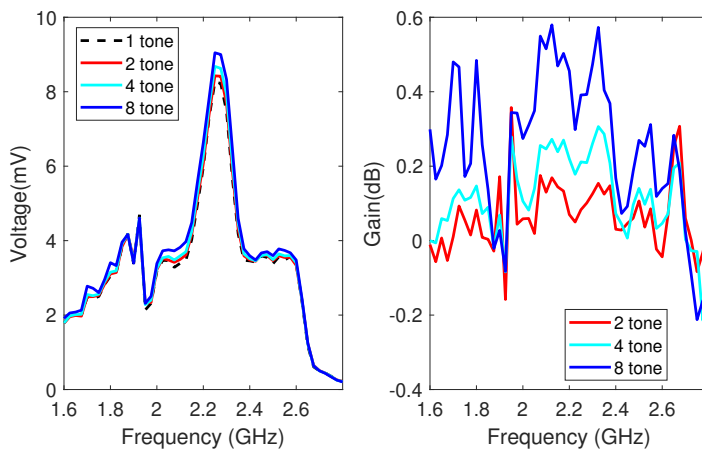


FIGURE 3.32: Voltage output (left) and voltage gain (right) of multisine at -30 dBm ( $R_L = 3 \text{ k}\Omega$ ).

Overall, the gain increases with number of sub-carriers and the PAPR. However, when the output DC voltage obtained with CW on the rectenna is considerable high (at 1.9, 2.2 and 2.6 GHz), the gain becomes close to 0 dB or even smaller than 0 dB.

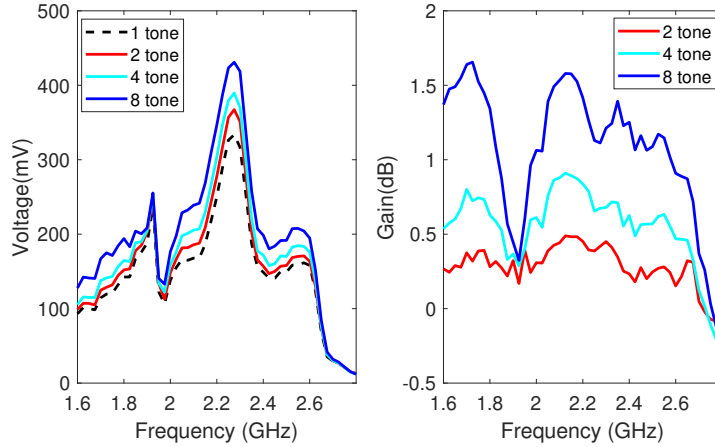


FIGURE 3.33: Voltage output (left) and voltage gain (right) of multisine at -20 dBm and load resistance of 100 k $\Omega$ .

To test the circuit under non-optimized condition, we modify the resistance value to 100 k $\Omega$ . The results are shown in Figures 3.33, 3.34 and 3.35. As can be seen, with a load of 100 k $\Omega$ , the improvements in terms of voltage gain are better in comparison when the load value is 3 k $\Omega$ . The clearer improvement can be seen from those figures. With the increase of number of sub-carriers, multi-sine signals have better voltage gain compared to 1-tone signal.

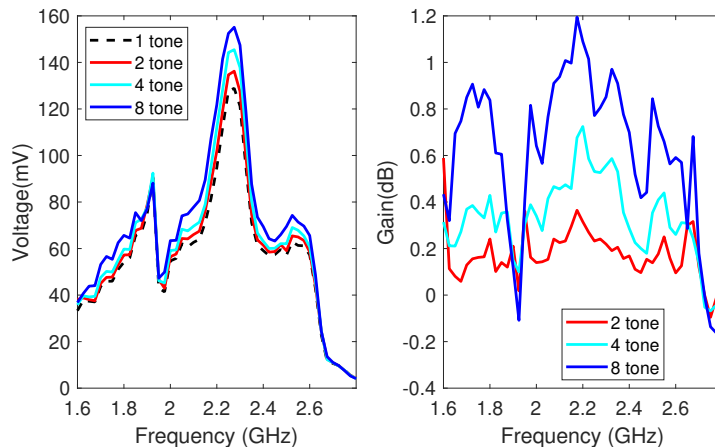


FIGURE 3.34: Voltage output (left) and voltage gain (right) of multisine at -25 dBm and load resistance of 100 k $\Omega$ .

At -20 dBm, the highest gain is 1.6 dB at 1.7 GHz and 2.2 GHz. For -25 dBm, similar results are obtained with the highest gain of 1.2 dB. That value for -30 dBm is 0.9 dB. Overall, the gains are higher than 0 in the frequency range except for 1.9 GHz and frequencies higher than 2.7 GHz. It corresponds to the  $S_{11}$  curve displayed in Fig.3.2 where the  $S_{11}$  value at 1.9 GHz and over 2.7 GHz are higher in comparison with other frequencies.

For broadband rectenna, with variation of load value in the frequency band of 1.6 to 2.8 GHz, multi-sine signals show a small improvement. But these improvements depend on the frequency and are non-uniform in the bandwidth because of the non-linearity of the circuit. Moreover, it is also because the DC voltage with CW is not constant. At certain frequencies, we can find a negative gains at both  $3\text{ k}\Omega$  and  $100\text{ k}\Omega$ .

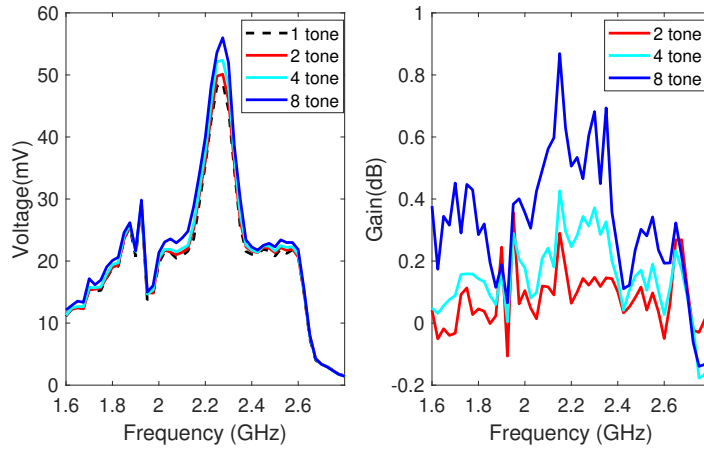


FIGURE 3.35: Voltage output (left) and voltage gain (right) of multisine at -30 dBm and load resistance of  $100\text{ k}\Omega$ .

In the next section, we consider RF pulse signal. The measurement with RF pulse signal will be taken into account to show the greater improvement compared with CW and multi-sine signals.

### 3.4.2 Measurement with RF pulse signals

Measurement with RF Pulse signal has been done using the measurement setup presented in section 3.2.

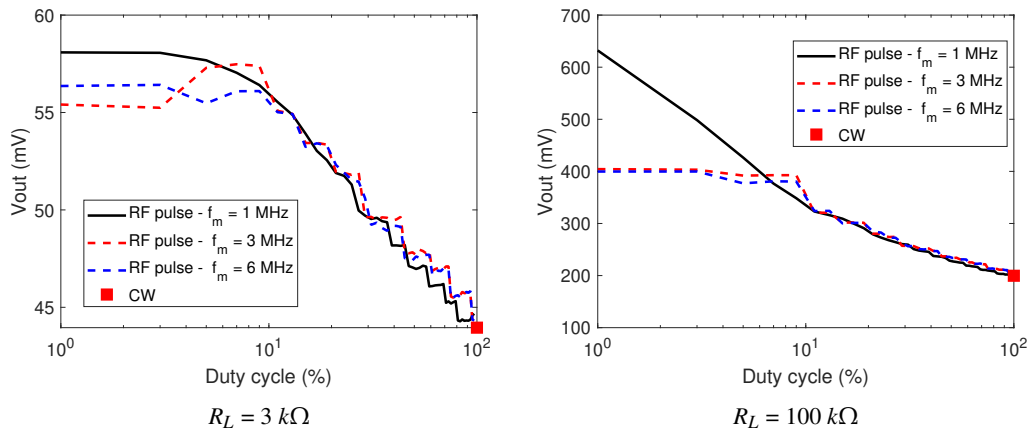


FIGURE 3.36: DC voltage of RF pulse and CW signals versus duty cycle at -20 dBm

Figures 3.36, 3.37 and 3.38 show the output DC voltage as a function of the duty cycle, from 1 to 99%, for different values of modulation frequency (1, 3 and 6 MHz). Three input

power levels (-20, -25 and -30 dBm) and two load values (3 and 100 kΩ) were considered. The carrier frequency of 2.4 GHz is chosen as an example to demonstrate the DC voltage behavior of the rectifier. Also, the results obtained for a 1-tone signal are given as a reference and for comparison.

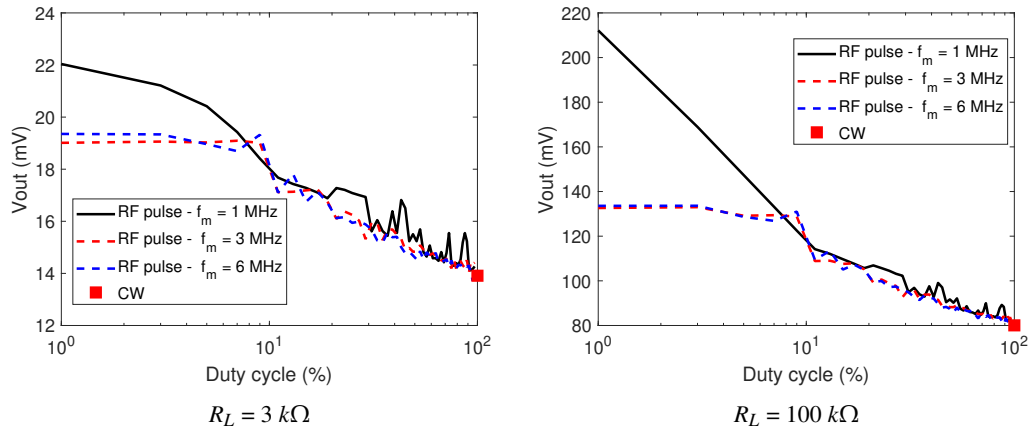


FIGURE 3.37: DC voltage of RF pulse and CW signals versus duty cycle at - 25 dBm

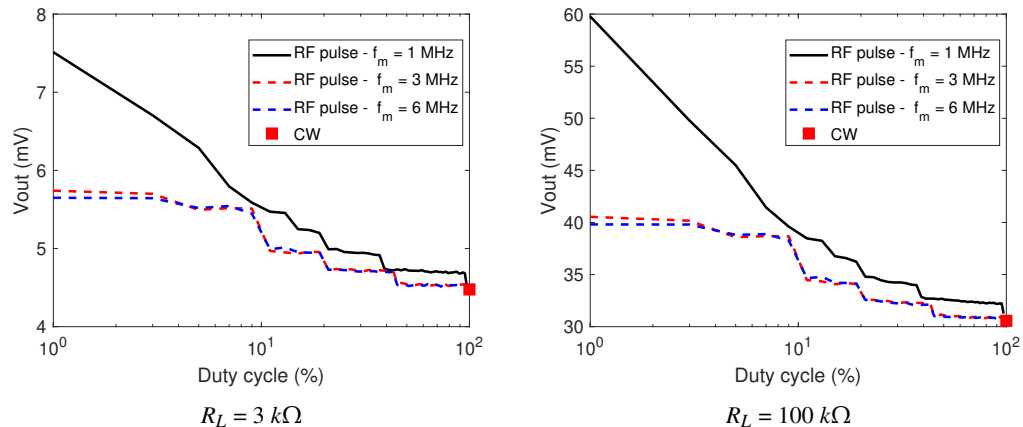


FIGURE 3.38: DC voltage of RF pulse and CW signals versus duty cycle at - 30 dBm

As can be seen, as the duty cycle increases the output DC voltage of RF pulse signal decreases to reach the value of voltage obtained using 1-tone signal. For a duty cycle of 99%, all the curves reach the voltage value obtained with CW. As the duty cycle increases, the PAPR and also the maximum input voltage decreases (Table 2.1). This explains the decrease in voltage as a function of the duty cycle. Furthermore, it can be noted that the voltage curves obtained for 3 and 6 MHz of modulation frequency and for low values of duty cycle are lower compared to those obtained for 1 MHz. This is mainly due to the decrease in the duration when the RF pulse is turned on and which becomes insufficient to fully charge the output capacitor (DC filter). It is also because the spectral occupancy of the input signal considerably increases for small values of the duty cycle when the modulation frequency increases, which degrades the DC output.

Indeed, when the duty cycle decreases and the modulation frequency increases, the period of time during which the pulse is turned on is not sufficiently large to charge the output capacitor to its maximum voltage. The different curves meet for higher duty cycle values, from around 10%. This behavior is found for all three power levels (-30, -25 and -20 dBm) and both load values (3 and 100 kΩ).

At -20 dBm and for a load of 3 kΩ, the maximum voltage of 58 mV is obtained at 1 MHz of modulation frequency and 1% of duty cycle. The voltage obtained for 1-tone signal is 44 mV. The improvement in the DC output due to the optimized waveform corresponds to a gain of 2.4 dB. For a load of 100 kΩ and a RF power of -25 dBm, a maximum voltage of 210 mV is obtained for a modulation frequency of 1 MHz and a duty cycle of 1%. The reference voltage obtained for a CW signal is only 80 mV. A gain of 8.4 dB is thus obtained under these conditions. On the other hand, the maximum voltage obtained for 3 and 6 MHz is only 135 mV. The improvement is noticeable for the input power of -30 dBm also. For the load of 3 kΩ, RF pulse allows 7.5 mV ( $\beta = 1\%$ ) while CW allows only 4.5 mV of output DC voltage. For the load of 100 kΩ, RF pulse gives the DC voltage which is double as CW signal (60 mV and 30 mV, respectively).

At 2.4 GHz, and for -30, -25 and -20 dBm of input power levels, the pulse signal with  $f_m = 1$  MHz always shows better DC output with small duty cycle values. The maximum output DC voltage is achieved at 1% of duty cycle.

```

Algorithm of finding optimized waveform:
for  $P_{RF} = -30$  to  $0$  dBm; {varying the input power}
    for  $R_L = 1$  to  $100$  kΩ; {varying the output load}
        for  $f = 1.6$  to  $2.8$  GHz; {varying the frequency}
            Initialize  $V_{out\_max}(P_{RF}, R_L, f) = 0$ ;
            for  $f_m = 1$  to  $6$  MHz {varying modulation frequency}
                for  $\beta = 1$  to  $99\%$  {varying duty cycle}
                    Signal_generation( $\beta$ );
                    {generate RF pulse signal with duty cycle  $\beta$ }
                    if  $V_{out\_max}(P_{RF}, R_L, f) < V_{out\_measurement}(\beta)$ ;
                         $V_{out\_max}(P_{RF}, R_L, f) = V_{out\_measurement}(\beta)$ ;
                        {update  $V_{out\_max}$ }
                    end if
                end for
            end for
        end for
    end for
end for

```

FIGURE 3.39: Waveform optimization algorithm

We have performed the simulations of the RF pulse signal in frequency domain with three modulated frequencies: 1 MHz, 3 MHz and 6 MHz and the carrier frequency of 2.4 GHz using Matlab software. The simulation results show that when the modulation frequency increases and/or the duty cycle decreases, the pulse width decreases. In the meantime, the

spectrum occupancy is increased, which means that the power concentration around the carrier frequency is smaller. This is the case with modulated frequency of 3 MHz and 6 MHz, compared to 1 MHz. For that reason, with small values of duty cycle, the DC output voltages at 3 MHz and 6 MHz are lower than that at 1 MHz. When the duty cycle becomes higher, the difference in frequency domain between RF pulse signals with the different modulated frequency values becomes smaller. Therefore, from 10 % of duty cycle, the DC outputs are nearly the same for the different values of the modulation frequency

This optimization follows the algorithm shown in Fig 3.39. The parameters are chosen based on the characteristics of the input waveforms and the rectenna. For RF pulse signal, there is only 2 parameters: duty cycle and modulated frequency. The duty cycle is varied from 1 to 99 %. Due to characteristic of our signal generator N5182 Keysight Technology, the maximum value of modulation frequency is 125 MHz, we choose the maximum value of  $f_m$  is 6 MHz to have a sufficient number of sampling points. The minimum of  $f_m$  is set to 1 MHz to satisfy the equation (2.10) for all measurements with variation of the parameters. Therefore, the modulation frequency takes three values: 1, 3 and 6 MHz. The load impedance is chosen as 3 k $\Omega$  and 100 k $\Omega$ . The choice is made because the optimized resistance of the rectifying circuit for CW signal is 3 k $\Omega$ . We have also tested the rectenna with a load sufficiently far from the optimized load resistance. Besides, the carrier frequency is chosen based on the operating frequency of the rectenna from 1.6 to 2.8 GHz. The RF power levels are taken from -30 to 0 dBm. One of the objectives of this work is to improve output voltage and the RF-to-dc conversion efficiency of the rectenna under pulse wave excitation and at low and medium RF power levels. Depending on the different input parameters, the carrier frequency, the input RF power level and the output load, the duty cycle value which allows maximizing the output voltage varies between 1 and 20%. The modulation frequency is kept at 1 MHz.

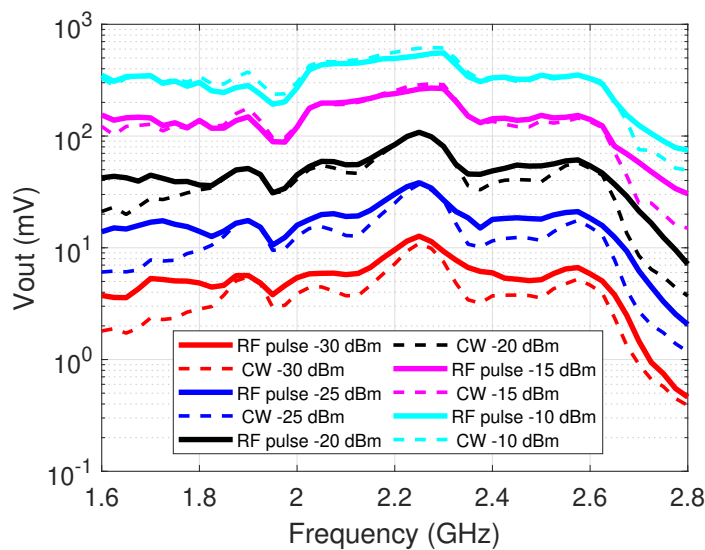


FIGURE 3.40: Output DC voltage of RF pulse and CW signals against frequency for different RF power input ( $R_L = 3 \text{ k}\Omega$ ).

The optimization procedure of the pulse-waveform is applied to characterize the rectenna

at different frequencies, different input power levels and different load values. The relevant results are presented in this part and discussed. Figure 3.40 displays the output DC voltage of the rectenna as a function of the frequency from 1.6 to 2.8 GHz. Measurements were made for a  $3\text{ k}\Omega$  load and for power levels ranging from -30 to -10 dBm with a step of 5 dB. The voltage curves obtained with the optimized pulse waveform are systematically compared to those obtained by using the 1-tone signal.

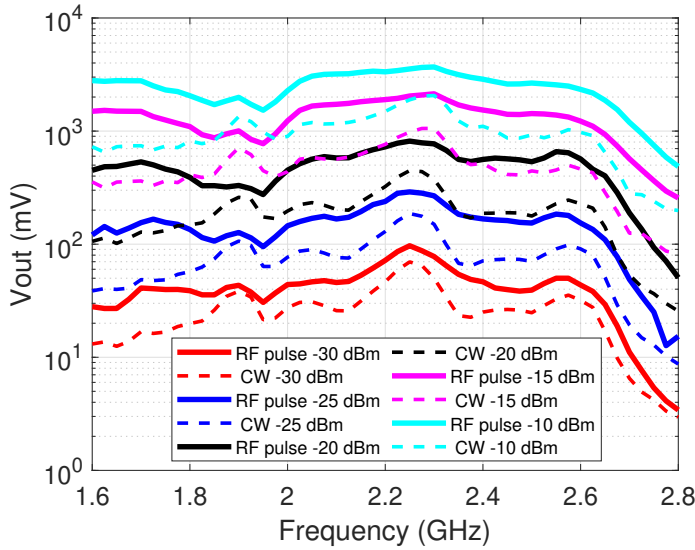


FIGURE 3.41: Output DC voltage of RF pulse and CW signals against frequency for different RF power input ( $R_L = 100\text{ k}\Omega$ ).

Similar measurements were made using a load of  $100\text{ k}\Omega$ . The results are presented in Fig.3.41. This allows observing the voltage improvement behavior at low and high load resistances.

The output voltage curves for 1-tone signal decrease slightly for frequencies below 1.8 GHz and above 2.6 GHz. For a load of  $3\text{ k}\Omega$  and for low input powers down to -20 dBm, the DC voltage is improved on the frequency band of interest. This improvement is greater at frequencies below 1.8 GHz and above 2.6 GHz. For powers of -15 and -10 dBm, the improvement is smaller except for frequencies below 1.8 GHz and above 2.6 GHz. For a load of  $100\text{ k}\Omega$ , the voltage is improved for all power levels and over the entier frequency band of interest. Indeed, at center of the frequency band (2.2 GHz), DC voltage obtained with RF pulse signal is significantly higher than that of 1-tone signal as it increases from 447 mV to 815 mV at -20 dBm. In the meantime, the efficiency is improved from 5.05% to 16.78%.

The duty cycle of RF pulse signal required to reach the maximum output DC voltage varies between 1 % and 20 % within the frequency range, regardless the resistance load value. For example, at load value of  $3\text{ k}\Omega$ , the optimum duty cycles are 10% and 20 % for the frequency of 1.85 and 1.95 GHz, respectively. For load value of  $100\text{ k}\Omega$ , we can find the maximum optimum duty cycle of 15 % for the frequency of 2.15 GHz.

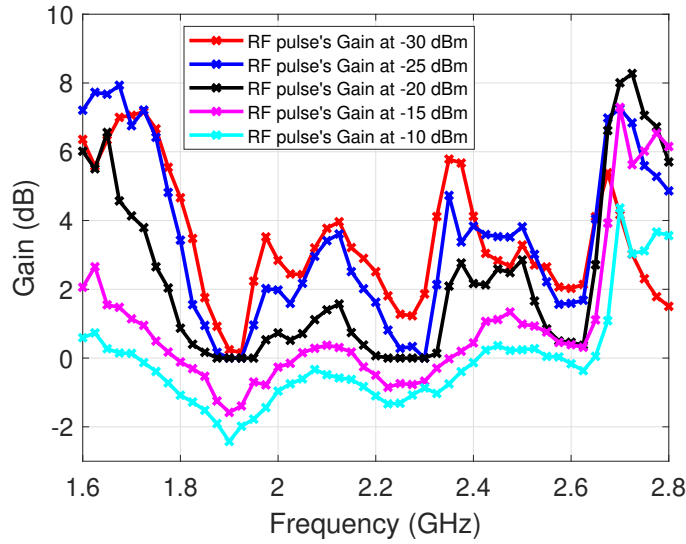


FIGURE 3.42: Voltage/efficiency gain of RF pulse against frequency for different RF power input ( $R_L = 3 \text{ k}\Omega$ ).

The voltage gain is calculated and depicted in figures 3.42 and 3.43 as a function of frequency from 1.6 to 2.8 GHz. Five input power levels are considered from -30 to -10 dBm by a step of 5 dB. In general, the gain is particularly higher for frequencies below 1.8 GHz and above 2.6 GHz.

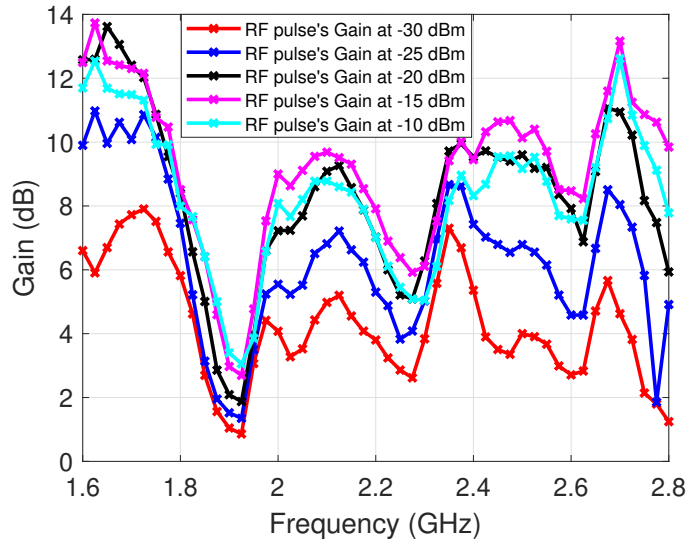


FIGURE 3.43: Voltage/efficiency gain of RF pulse against frequency for different RF power input ( $R_L = 100 \text{ k}\Omega$ ).

In contrast, regardless of the frequency, the gain at  $100 \text{ k}\Omega$  is better than at  $3 \text{ k}\Omega$ . The lowest gain is 0.85 dB at  $100 \text{ k}\Omega$ . The highest gain recorded at  $100 \text{ k}\Omega$  is 13.95 dB at 1.675 GHz and -20 dBm input power, which allows an RF-to-dc conversion efficiency increase from 0.325 to 7.205 %. The improvement in two cases are different. When the resistance load value is  $100 \text{ k}\Omega$ , there is more important gain at higher RF input power (-20 dBm). On the contrary, at the load value of  $3 \text{ k}\Omega$ , the best improvement is found at -30 dBm.

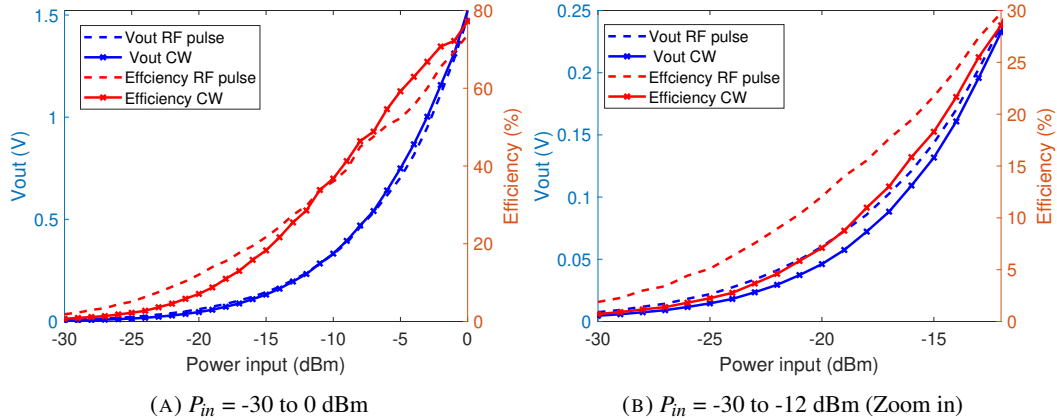


FIGURE 3.44: Output DC voltage and efficiency of RF pulse and CW signals versus input power ( $R_L = 3 \text{ k}\Omega$  and  $f_c = 2.4 \text{ GHz}$ )

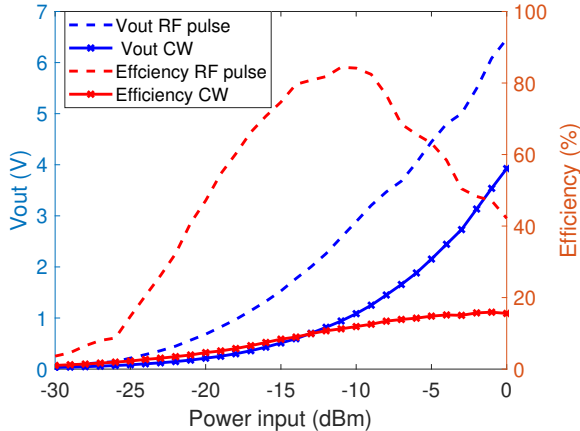


FIGURE 3.45: Output DC voltage and efficiency of RF pulse and CW signals versus input power ( $R_L = 100 \text{ k}\Omega$  and  $f_c = 2.4 \text{ GHz}$ )

DC voltage and efficiency measurements as a function of input power, for two different loads ( $3$  and  $100 \text{ k}\Omega$ ), were carried out. The results are presented in figures 3.44 and 3.45. The carrier frequency is fixed to  $2.4 \text{ GHz}$  and the RF power varies from  $-30$  to  $0 \text{ dBm}$ . For each load value, the voltages and efficiencies obtained for optimized waveform and 1-tone signals are compared and will be discussed. The algorithm presented in Fig.3.39 is also used to characterize the maximum DC output (voltage and efficiency) by optimizing the waveform. For  $3 \text{ k}\Omega$  and small RF power levels from  $-30$  to  $-12 \text{ dBm}$ , the optimized waveform gives more DC voltage compared to 1-tone signal. On the other hand, there is no improvement in the power range from  $-12$  to  $0 \text{ dBm}$ . Meanwhile, for  $100 \text{ k}\Omega$ , the improvement is obtained over the entire power range. The maximum improvement is obtained around  $-15 \text{ dBm}$ . Indeed, the efficiency becomes equal to  $74.7\%$  with the optimized waveform whereas it was only of  $8.3\%$  with the 1-tone signal.

Fig.3.46 shows the voltage/efficiency gain of optimized RF pulse signal compared to CW, for  $3 \text{ k}\Omega$  and  $100 \text{ k}\Omega$ . As can be seen, the gain at  $3 \text{ k}\Omega$  has the maximum value of  $4 \text{ dB}$  at  $-30 \text{ dBm}$ . The gain decreases as the input power increase. From  $-15 \text{ dBm}$ , the gain

is approximately 0 dB, which means there is no improvement between RF pulse signal and CW. For  $100 \text{ k}\Omega$ , the gain is significantly higher with lowest gain of 4 dB at 0 dBm. The gain is 5.7 dB at -30 dBm and it increases to the highest value of 10.4 dB at -20 dBm, then decreases as the input power increases.

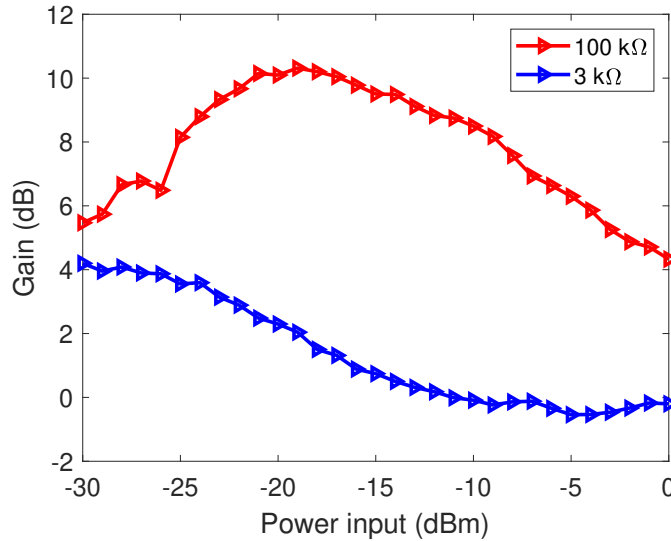


FIGURE 3.46: Voltage gain of RF pulse signal for different input RF powers ( $f_c = 2.4 \text{ GHz}$ ).

Signal	$G_p$ at 1.6 GHz		$G_p$ at 2.2 GHz		$G_p$ at 2.8 GHz	
	-20 dBm	-30 dBm	-20 dBm	-30 dBm	-20 dBm	-30 dBm
CW	1	1	1	1	1	1
2-tone	0.23	-0.01	-0.23	0.07	-0.34	0.04
4-tone	0.41	0.00	0.03	0.22	-0.27	0.00
8-tone	1.02	0.30	0.13	0.45	-0.15	-0.18
RF pulse	6.02	6.36	0.07	2.51	5.70	1.50

TABLE 3.3: RF pulse and multi-sine signal voltage/efficiency gain compared to CW ( $R_L = 3 \text{ k}\Omega$ )

Signal	$G_p$ at 1.6 GHz		$G_p$ at 2.2 GHz		$G_p$ at 2.8 GHz	
	-20 dBm	-30 dBm	-20 dBm	-30 dBm	-20 dBm	-30 dBm
CW	1	1	1	1	1	1
2-tone	0.26	0.05	0.45	0.06	-0.28	-0.02
4-tone	0.53	0.05	0.83	0.24	-0.28	-0.04
8-tone	1.37	0.37	1.41	0.50	-0.16	-0.17
RF pulse	12.49	6.60	7.01	3.80	7.78	1.24

TABLE 3.4: RF pulse and multi-sine signal voltage/efficiency gain compared to CW ( $R_L = 100 \text{ k}\Omega$ )

To sum up, we have the tables 3.2 and 3.3 to show the gain between multi-tone and RF pulse signal compared to 1-tone signal and multi-sine for two load values ( $3\text{ k}\Omega$  and  $100\text{ k}\Omega$ ) and three carrier frequencies (1.6, 2.2 and 2.8 GHz). Obviously from the tables, RF pulse signal gives much better voltage/efficiency gain compared to 1-tone signal and multi-sine signals, especially for the optimum load value of  $3\text{ k}\Omega$ , where the highest gain of 8-tone signal is only 1.02 dB at -20 dBm and 1.6 GHz, meanwhile that value for RF pulse signal is 6.02 dB. The gap is larger in the case of load value of  $100\text{ k}\Omega$ , where the highest gain obtained for RF pulse signal is 12.49 dB while that value for 8-tone signal is 1.37 dB.

### 3.5 Conclusion

This chapter deals with the measurements of broadband rectifier and broadband rectenna.

Firstly, multi-sine signal and RF pulse signal are proposed for WPT with a broadband rectifier. At small input RF powers, the improvement of multi-sine signal compared to a CW waveform in terms of output DC voltage/efficiency is minor and depends on the frequency. Between -20 dBm and -10 dBm, the highest voltage gain of multi-sine signal compared to 1-tone signal is 3.5 dB at 2.8 GHz with 16-tone signal. Then, RF pulse signal is used to perform the measurements on broadband rectifier. The results show the performance improvement of RF pulse compared to 1-tone signal is better than that of multi-sine signal. The output DC voltage is improved at the frequency range of interest despite the variation of load resistance. At -15 dBm and optimum load resistance of  $3\text{ k}\Omega$ , the highest gain recorded is 8 dB at 2.8 GHz with the duty cycle is at 5% and the PAPR of the signal is 16 dB. While varying the load's value, the gain is significantly higher and reach the maximum of 14.25 dB and 12.95 dB at -15 dBm and -5 dBm, respectively. The output DC voltage enhancement also depends on the optimization of the circuit. At central frequencies and smaller load's resistance, the gain is smaller than the two ends frequencies where the voltage output is smaller because the circuit is not well optimized.

For broadband rectenna, two values of resistance load ( $3\text{ k}\Omega$  and  $100\text{ k}\Omega$ ) have been tested at 3 RF powers: -30, -25 and -20 dBm. Multi-sine signals show some minor improvement, while RF pulse signals have a better performance overall. For RF pulse signal, at the resistance load close to the optimum value of  $3\text{ k}\Omega$ , the gain is significantly high at the two ends of the frequency range and smaller at the center of the bandwidth. Regardless of the frequency, the lowest gain is 0 dB for the input power of -20 dBm, -25 dBm and -30 dBm. The highest gain recorded is 8 dB at 1.7 GHz and -25 dBm input RF power and 8.1 dB at 2.7 GHz and -20 dBm of input RF power. Higher gains are found at smaller power input such as -25 dBm and -30 dBm. On the other hand, at  $100\text{ k}\Omega$ , regardless of the frequency, the gains at non-optimized resistance are better than that at optimum resistance in general with the lowest gain is 4 dB at the center of the frequency band. The highest gain recorded is 13.95 dB at 1.675 GHz and -20 dBm input power, which means the efficiency increased from 0.325 % (CW) to 7.205 % (RF pulse).

For both broadband rectifier and broadband rectenna, RF pulse signal with optimum duty cycle improves the output DC significantly compared to 1-tone and multi-sine signals.

In the next chapter, the measurement on cascaded-rectifier rectenna-arrays will be developed and experimental results will be presented.

# Bibliography

- [1] Mahfoudi, Hichem, Mohamed Tellache, and Hakim Takhedmit. *A wideband rectifier array on dual-polarized differential-feed fractal slotted ground antenna for RF energy harvesting.*, International Journal of RF and Microwave Computer-Aided Engineering 29.8 (2019): e21775.
- [2] T. Hirakawa, C. Wang and N. Shinohara *RF-DC conversion efficiency improvement for microwave transmission with pulse modulation*, Wireless Power Transfer, page 1 of 10. Cambridge University Press, 2019
- [3] Ibrahim, Rony, Damien Voyer, Mohamad El Zoghbi, Julien Huillery, Arnaud Bréard, Christian Vollaire, Bruno Allard, and Youssef Zaatar *Novel design for a rectenna to collect pulse waves at 2.4 GHz*, IEEE Transactions on Microwave Theory and Techniques 66, no. 1 (2017): 357-365.



## Chapter 4

# Rectenna arrays experiments : Application to remote supply of a temperature/acceleration wireless sensor

One of the objectives in this chapter is to investigate and show how the optimized waveforms can be used to improve the performances of a wireless power transfer system dedicated to the remote power supply of wireless sensors. The two types of optimized waveforms: multi-sine and RF pulse signals are also deployed to experimentally characterize rectenna arrays of 1x1, 2x2 and 3x3 elements. The measurement setup as well as the measurement results with these rectennas will be presented. Indeed, it will be shown through the different results that it is possible to decrease the minimum or required power density to supply the sensor. This can also result in a reduction in the number of rectenna elements to be used or even in an increase of the maximum distance (or range) between the transmitter and the receiver.

### 4.1 Single rectenna and rectenna arrays description

In this work, we use rectenna arrays, which are designed and optimized to harvest energy from the ISM band at the frequency of 2.45 GHz. In order to obtain a compact and efficient rectenna arrays, the basic cell rectenna is designed as compact as possible and with a high sensitivity at low RF input power levels. The elementary cell consist of 2 parts: the receiving antenna and the rectifying circuit.

The proposed antenna has been developed and presented in [1]. It consists of a third iteration Koch fractal geometry. It allows bandwidth enhancement and size reduction compared to conventional patch antenna design. The size of the antenna is decreased by scratching each side of the square by a Koch curve. Two parameters: IO (iteration order) and IF (iteration factor) are deployed to calculate the fractal curves. IO represents the number of times that the starter shape has been fractalized. IF represents the reduction factor of each iteration. At each iteration, the fractal curves become smaller.

The parameters of fractal shape which based on a square patch are  $L = 26.4$  mm,  $IO = 3$  and  $IF = 0.3$ . It is printed on a low-cost FR-4 substrate, which has a dielectric permittivity of

4.3, a thickness of 1.6 mm and a loss tangent ( $\tan\phi$ ) of 0.02. The proposed fractal antenna has a dimension of  $26.4 \times 26.4 \text{ mm}^2$ . To connect the antenna to the rectifier, a coopered pin via is used. The antenna is designed and optimized with Ansys HFSS software and the configuration can be found in Fig.4.1.

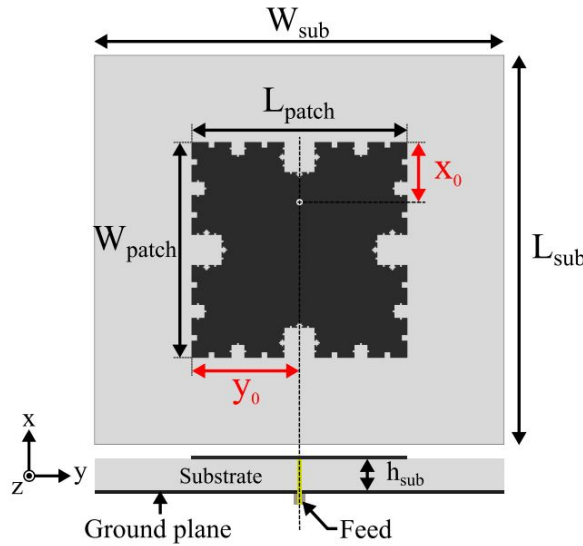


FIGURE 4.1: Configuration of the third iteration Koch fractal antenna. The antenna parameters are:  $W_{sub} = 55 \text{ mm}$ ,  $L_{sub} = 50 \text{ mm}$ ,  $L_{patch} = 26.4 \text{ mm}$ ,  $W_{patch} = 26.4 \text{ mm}$ ,  $X_0 = 8.06 \text{ mm}$ ,  $Y_0 = 13.2 \text{ mm}$ ,  $h_{sub} = 1.6 \text{ mm}$  [1].

The input impedance of the antenna at the operating frequency is  $52-j11 \Omega$ . So, it is well matched with the  $50-\Omega$  impedance. The measurements in anechoic chamber were performed to experimentally determine the antenna gain. The ground plane is placed between the antenna and the rectifier which can limit the backward radiation and allow to place the rectifier close to the antenna without decreasing the gain. The simulated and measured reflection coefficients of the fractal antenna are shown in Fig.4.2. It is well optimized at 2.45 GHz. The measured results shows that the optimized frequency is a few MHz shifted from 2.45 GHz.

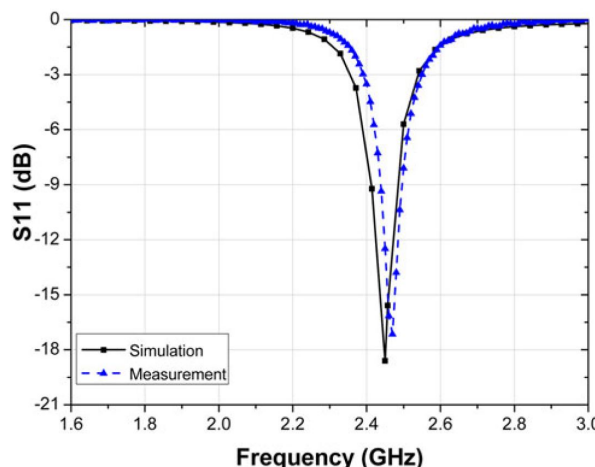


FIGURE 4.2: Simulated and measured reflection coefficients of the fractal antenna, simulation (solid line), and measurement (dashed line) [1].

The rectifier is chosen between several types of rectifier topologies such as series-mounted diode, shunt-mounted diode, voltage doubler rectifier and multiplier circuits. This rectenna is designed to supply power for sensors with a voltage supplied by a high value capacitor. For that reason, the aim is to reach the maximum output DC voltage at low input power levels. The chosen topology is a combination of multiplier circuits and full-wave rectifiers. It consists of cascading two stages of a Dickson voltage multiplier on each branch of a full wave rectifier. The schematic of the rectifier can be found in Fig.4.3.

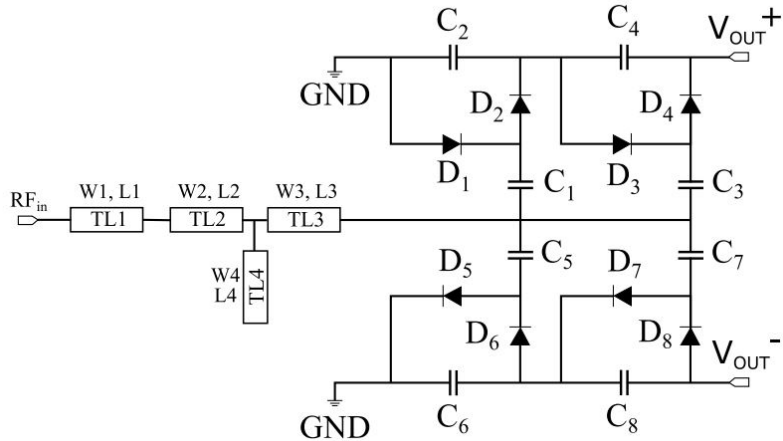


FIGURE 4.3: Topology of the T-junction filter and the dual cascaded Dickson voltage multiplier. The filter parameters are:  $W_1 = 3$  mm,  $L_1 = 3$  mm,  $W_2 = 5$  mm,  $L_2 = 5.33$  mm,  $W_3 = 5$  mm,  $W_4 = 8.66$  mm, and  $L_4 = 2.55$  mm [1].

For the positive branch of Dickson voltage multiplier, the working process is presented as follows: in the negative half cycle of the input RF wave, the capacitors  $C_1$  and  $C_3$  are charged to a voltage equal to the input RF signal across diodes  $D_1$  and  $D_3$ . On the other hand, for the positive half cycle, the capacitors  $C_2$  and  $C_4$  are charged with opposite polarities through forward-biased diodes  $D_2$  and  $D_4$ . The same operating process with a reverse polarity is applied to the negative branch.

Due to the low threshold voltage required for small input signals (a forward voltage of 60 to 120 mV at 0.1 mA and a junction capacitance  $C_{j0} = 0.14$  pF), the Schottky diode SMS 7630-079LF from Skyworks [2] is chosen for the multiplier. A band-pass filter is usually inserted between the antenna and the rectifier. In this case, a 2.45 GHz  $T_{junction}$  filter is placed between the fractal antenna and the multiplier circuit to block the high order harmonics generated by the diode.

The complete RF-to-dc rectifying circuit is optimized using Keysight Advanced Design System (ADS) software. The bottom-side of the antenna is chosen to put the RF-to-dc rectifier so it does not cause any interference with the antenna radiation pattern. The fractal antenna was stacked back-to-back with the rectifying circuit. The antenna and the rectifier are connected by the via holes.

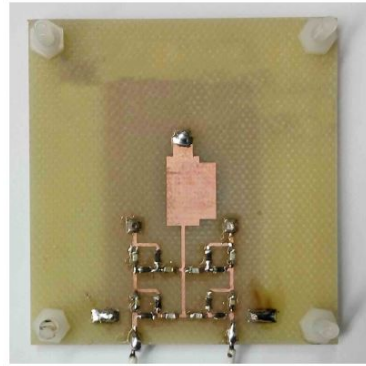


FIGURE 4.4: Photograph of the fabricated rectifier.

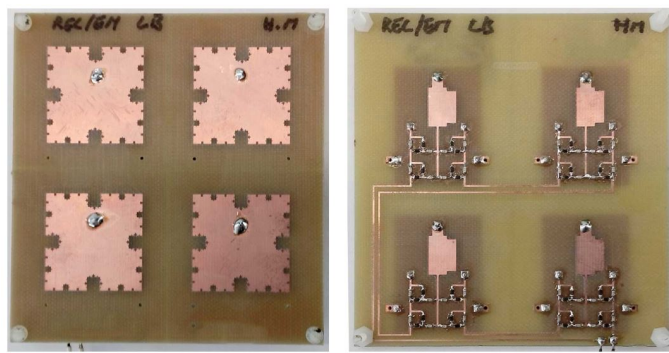


FIGURE 4.5: Top view and bottom view of 2x2 rectenna array.

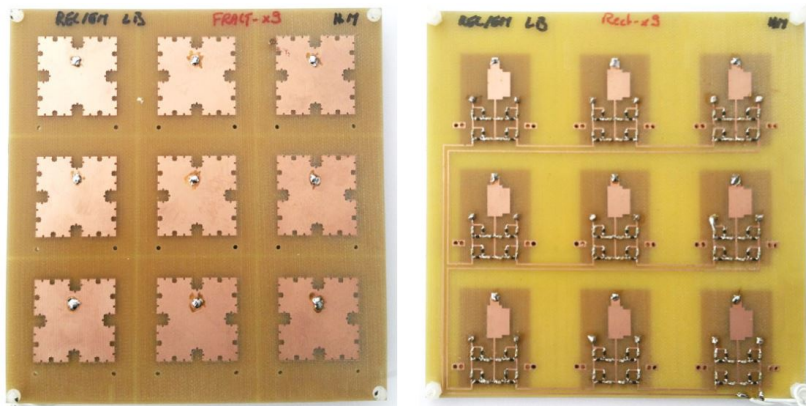


FIGURE 4.6: Top view and bottom view of 3x3 rectenna array.

As mentioned above, the rectenna is designed in order to supply a power to a wireless sensor node. The harvested energy will initially be stored in a capacitor of the sensor node. Then, it is used to power the wireless sensor. Detailed presentation of the sensor will be given in the next section. Normally, with small RF power input, a single rectenna (Fig.4.4) does not deliver enough DC voltage to charge the capacitor and then supply the wireless sensor. For that reason, the use of rectenna arrays is an effective way to increase the captured RF power and to deliver a greater output DC voltage. Four-cells array (Fig.4.5) and 9-cell array (Fig.4.6) rectennas are proposed. They have been developed from the single element

presented above. The DC interconnection scheme of 4-cell and 9-cell rectifying circuits are shown in Fig.4.7. The 4-cell rectenna array has a dimension of  $86 \times 91 \text{ mm}^2$ . The 9-cell rectenna array has a dimension of  $127 \times 131 \text{ mm}^2$ .

Each cell of the rectenna arrays receives the RF power independently then converts it into DC voltage across an output capacitor (DC filter). After that, the DC voltage from each cell will be added to deliver greater DC output compared to a single cell. In the next sections, the combination of the elements of rectenna arrays and power optimized waveforms will be presented to obtain even more output DC voltage/power to supply power to electronic devices and sensors. The measurements also were performed in anechoic chamber with multi-sine signal and RF pulse signal using common measurement setup, which was presented in section 3.2.

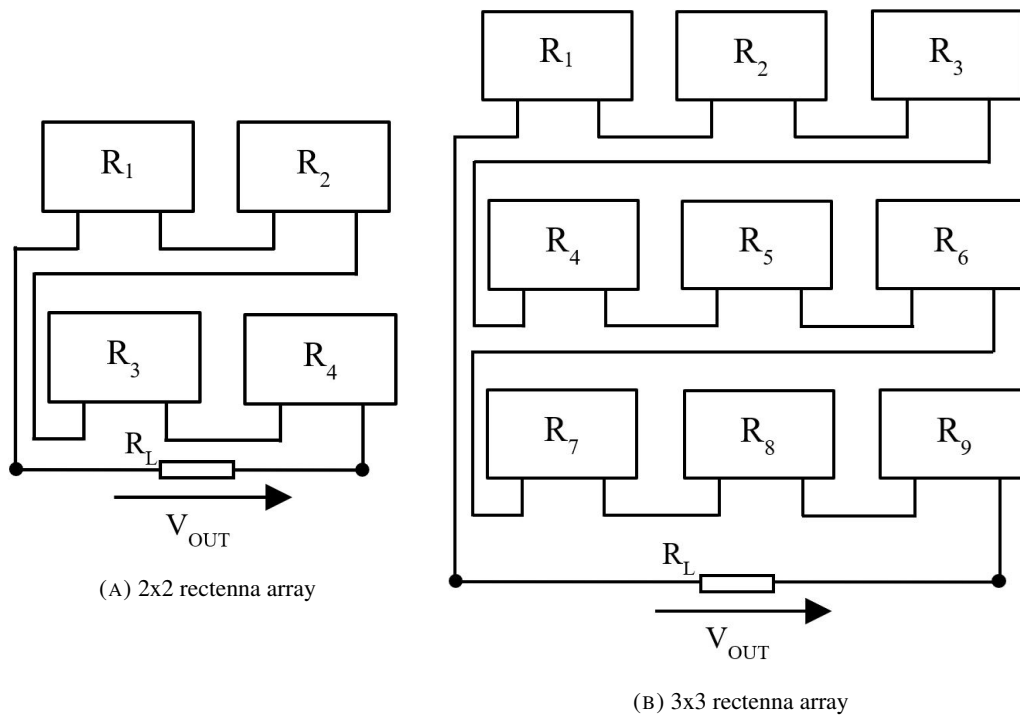


FIGURE 4.7: DC interconnection schemes

## 4.2 Experimental characterization

### 4.2.1 Measurement results with multi-sine signals

The measurements with multi-sine signal have been done with three rectenna arrays: 1x1, 2x2 and 3x3. In the first place, measurements with conventional CW signal are performed at 2 levels of power densities:  $1 \mu\text{W}/\text{cm}^2$  and  $10 \mu\text{W}/\text{cm}^2$  at the receiving antenna, over the frequency band from 2 to 3 GHz. Secondly, multi-sine signals up to 16 tones are applied to perform the measurement at the operating frequency of 2.45 GHz. The frequency bandwidth of multi-sine signal is fixed to 10 MHz. While changing the number of sub-carriers ( $N$ ), the frequency spacing between carrier  $\Delta f$  is equal to  $\frac{10}{N-1}$  (MHz). The frequency bandwidth should keep the frequency spacing between sub-carriers not too small as the number

of sub-carrier can be up to 16 tones. Also, we work with narrow-band rectenna arrays, the frequency bandwidth should not be too high. For that reason, the 10 MHz of frequency bandwidth is suitable for our measurements.

The power density range is considered from 1 to 15  $\mu\text{W}/\text{cm}^2$ . The distance between the horn antenna and the rectenna is 1.5 m. We optimized the output DC voltage of the rectifier, which corresponds to a high load value. For that reason, the output of the rectifier is connected directly to the probes of the multi-meter Agilent 34401A. The output load value in this case is the input load of the multi-meter, which is 10 M $\Omega$ .

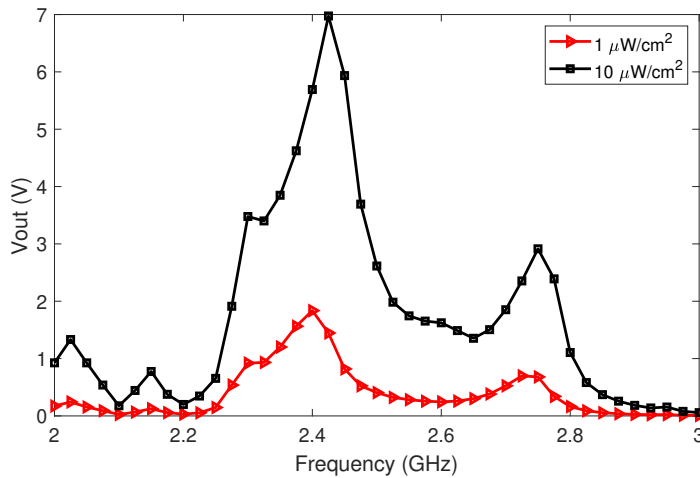


FIGURE 4.8: Measured output DC voltage of CW signal on the 1x1 rectenna versus frequency ( $C_L = 10 \text{ nF}$ ,  $R_L = 10 \text{ M}\Omega$ ).

The output DC voltage of CW over the frequency range from 2 to 3 GHz for 1x1 rectenna array are shown in Fig.4.8. We can see that, despite of the variation of the power density, the output DC voltage is always optimized around 2.45 GHz. The maximum DC voltage are 1.83 V and 6.97 V for the power density of 1  $\mu\text{W}/\text{cm}^2$  and 10  $\mu\text{W}/\text{cm}^2$ , respectively.

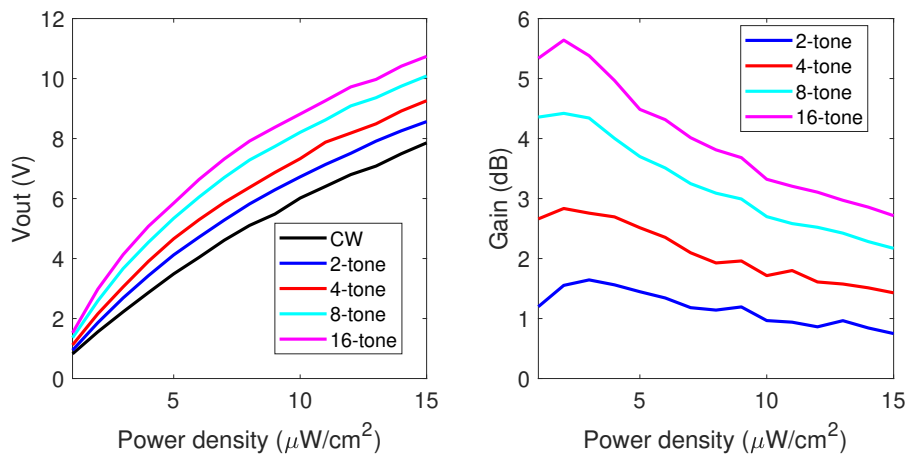


FIGURE 4.9: Measured output DC voltage and voltage gain of multi-sine signal on the 1x1 rectenna versus power density at 2.45 GHz.

Fig.4.9 shows the output DC voltage and the voltage gain of multi-sine signals on the single cell rectenna over the power density range from  $1 \mu\text{W}/\text{cm}^2$  to  $15 \mu\text{W}/\text{cm}^2$ . As can be seen, when the number of sub-carriers increases, the output voltage of the rectenna increases also. As mentioned in previous chapter, as the number of sub-carriers is doubled, the PAPR of multi-sine signal is increased by 3 dB. For single cell rectenna array, multi-sine signal with high PAPR shows a clear advantage compared to CW signal. The 16-tone signal shows the best performance in this case. The highest voltage gain of 16-tone signal is 5.5 dB for the power density of  $2 \mu\text{W}/\text{cm}^2$ . That value at  $15 \mu\text{W}/\text{cm}^2$  is 2.8 dB. From the results, we can see that the highest gain obtained for all multi-sine signals is comprised between 2 and  $3 \mu\text{W}/\text{cm}^2$ . Then, the gain decreases as the power density increases. It means that for the single element rectenna, the multi-sine signal shows the best improvement at low power levels.

The same experimental measurement have been done on 2x2 rectenna array and 3x3 rectenna array.

For 2x2 rectenna array, over the frequency range from 2 to 3 GHz, the output DC voltage of CW also shows the maximum values at the frequency range from 2.4 to 2.45 GHz (Fig.4.10). The highest DC voltages are 3 V and 9.78 V at  $1 \mu\text{W}/\text{cm}^2$  and  $10 \mu\text{W}/\text{cm}^2$ , respectively. Because the optimum frequency is shifted in measurement, the highest output DC voltage obtained is close to 2.4 GHz. The highest output DC voltages are 0.9 V and 7.2 V at  $1 \mu\text{W}/\text{cm}^2$  and  $10 \mu\text{W}/\text{cm}^2$ , respectively. At 2.45 GHz, the RF input power received by the rectenna are -16.23 and -6.23 dBm for  $1 \mu\text{W}/\text{cm}^2$  and  $10 \mu\text{W}/\text{cm}^2$ , respectively.

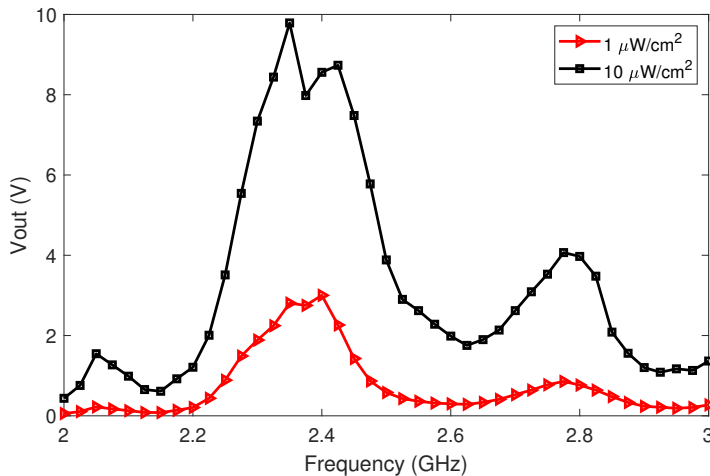


FIGURE 4.10: Measured output DC voltage of CW signal on the 2x2 rectenna array versus frequency ( $C_L = 10 \text{nF}$ ,  $R_L = 10 \text{M}\Omega$ ).

The output DC voltage as well as the voltage gain of multi-sine signal compared to CW signal are shown in Fig.4.11. We can see that there are some improvement when using multi-sine signal. Similar behavior as the case of single cell rectenna can be found here, where multi-sine signal with higher number of sub-carriers shows better performance. But, the improvement (voltage gain) is smaller. The highest gain obtained in this case is only 3.1 dB

at  $2 \mu\text{W}/\text{cm}^2$  of power density for 16-tone signal. Overall, the gains are higher than 0 for multi-sine signals over the power density range of interest.

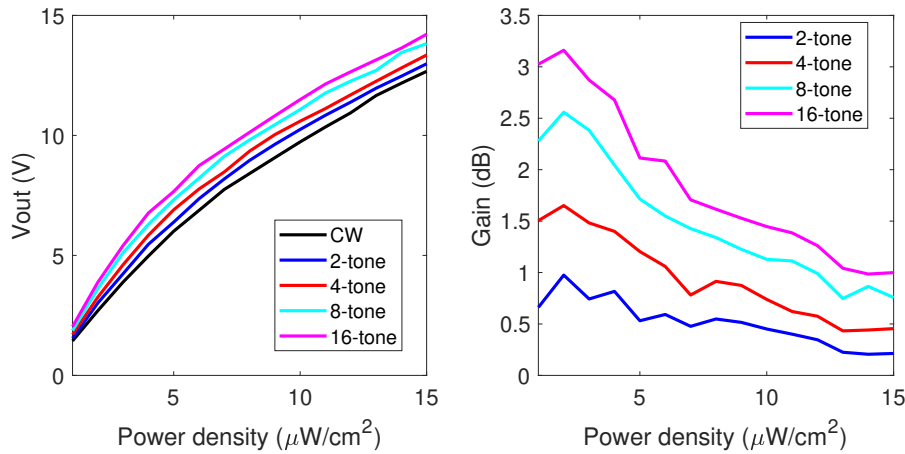


FIGURE 4.11: Measured output DC voltage and voltage gain of multi-sine signal on the 2x2 rectenna versus power density at 2.45 GHz.

For 3x3 rectenna array, the output DC voltages are significantly higher than that of 2x2 and 1x1 rectenna arrays. The highest values of DC voltage are 6.40 V and 26.67 V at 1  $\mu\text{W}/\text{cm}^2$  and 10  $\mu\text{W}/\text{cm}^2$  of power density, respectively (Fig.4.12). That values are obtained at the frequency close to 2.45 GHz.

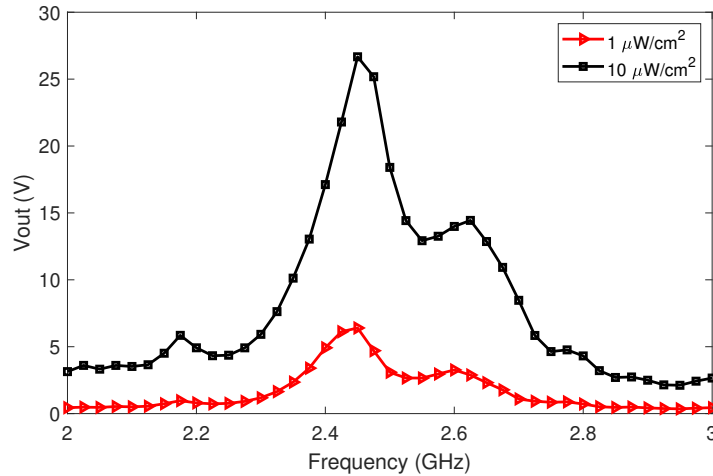


FIGURE 4.12: Measured output DC voltage of CW signal on the 3x3 rectenna versus frequency ( $C_L = 10 \text{ nF}$ ,  $R_L = 10 \text{ M}\Omega$ ).

As can be seen from Fig.4.13, the highest gain obtained is only 1.67 dB for 4-tone signal at  $3 \mu\text{W}/\text{cm}^2$  of power density. Meanwhile, for 8-tone and 16-tone signals, the gain is close to 0 dB at small power densities and increases to approximately 1 dB for  $15 \mu\text{W}/\text{cm}^2$  of power density. The 2-tone and 4-tone signals have better performance than 8-tone and 16-tone signals at small power density.

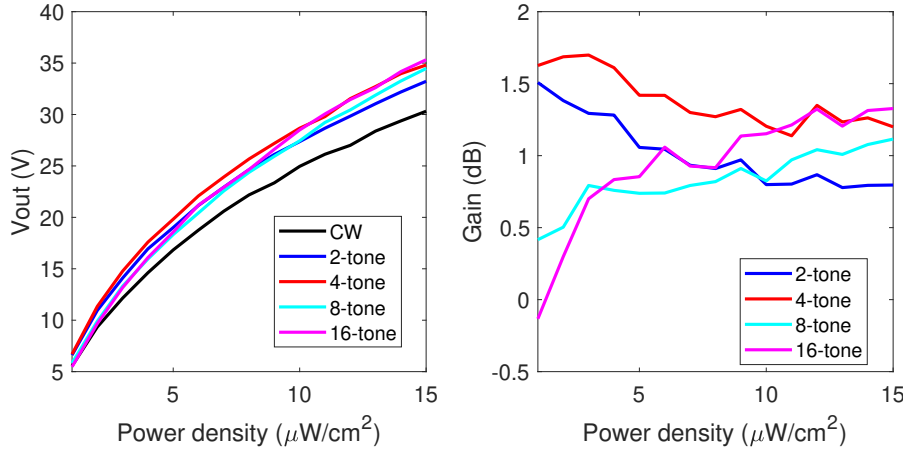


FIGURE 4.13: Measured output DC voltage and voltage gain of multi-sine signal on the 3x3 rectenna versus power density at 2.45 GHz.

Overall, from the results, we can see that for different power densities, the voltage DC output as well as the voltage gain behaviors for 1x1 and 2x2 rectenna arrays are quite similar. With multi-sine signal, the improvement can be observed. The highest gain for 1x1 and 2x2 rectenna arrays are 5.5 dB and 3.1 dB, respectively, for 16-tone signals. In contrast, for 3x3 rectenna array, where the voltage DC output is significantly high for 1-tone signal (6.40 V at  $1 \mu\text{W}/\text{cm}^2$  and 26.67 V at  $10 \mu\text{W}/\text{cm}^2$ ), the improvement is unnoticeable with the highest gain is only 1.67 dB for 4-tone signal. Especially, the voltage of 16-tone signal is degraded and close to the voltage DC output of 1-tone signal at small power density.

The improvement of multi-sine signal in comparison with CW signal is smaller with 2x2 and 3x3 rectenna arrays. For these rectennas, the optimum frequency is shifted from 2.45 GHz to around 2.4 GHz in measurements. Also, the output DC voltage is higher with 2x2 and 3x3 rectenna arrays, there is a smaller margin for improvement. Besides, the coupling between cell elements of 2x2 and 3x3 rectenna arrays can affect the output DC voltage. This coupling does not exist with single cell rectenna.

On the other hand, when increasing the number of cell element, to obtain a proportional output DC voltage, the load value should be increased by the number of elements. In our measurement, when increasing the number of cells, the output load value is unchanged because it is the load value of the multi-meter. The load value is  $10 M\Omega$  for all three rectennas. For that reason, the improvement of multi-sine signal on single cell rectenna is higher than that of 2x2 and 3x3 rectenna arrays. The reverse voltage of the diodes also can cause the degraded performance of 2x2 and 3x3 rectenna arrays.

In the next section, measurement with RF pulse signal on the rectennas will be presented.

#### 4.2.2 Measurement results with RF pulse signal

The measurement with RF pulse signal have been done at the frequency of 2.45 GHz. RF pulse signals with different duty cycle values will be created with the power density varying between 1 to  $15 \mu\text{W}/\text{cm}^2$  for the different rectenna arrays. Also, a capacitor of 10 nF ( $C_L$ ) is connected at the output of the rectenna to eliminate the ripple voltage and to filter the output

DC voltage. As the load resistance is  $10 M\Omega$ , the time constant is 1 second. The equation (2.10) is always correct.

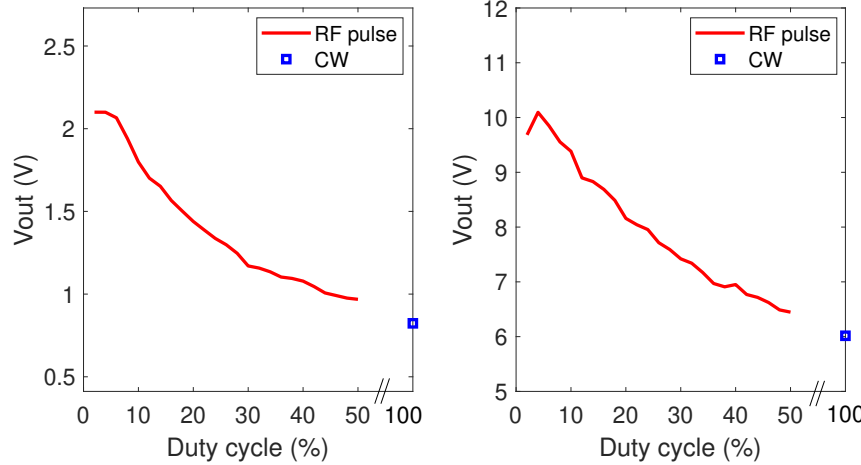


FIGURE 4.14: Measured output DC voltage of the 1x1 rectenna versus duty cycle at  $1 \mu W/cm^2$  (left) and  $10 \mu W/cm^2$  (right).

Firstly, the power density is fixed at 2 levels:  $1 \mu W/cm^2$  (left) and  $10 \mu W/cm^2$  (right). The output DC voltage of RF pulse signal will be compared with 1-tone signal at different values of duty cycle (in Fig.4.14). At  $1 \mu W/cm^2$ , the voltage output of RF pulse signal reaches its highest value of 2.1 V when the duty cycle is 2 % (PAPR of 20 dB), then decreases gradually to the voltage DC output of 1-tone signal as the duty cycle increases. The voltage DC output of 1-tone signal is 0.81 V. For  $10 \mu W/cm^2$  of power density, the same behavior in terms of output DC voltage is found for RF pulse signal. The highest DC voltage for RF pulse signal is 10.1 V for the duty cycle of 2 % while that value of CW signal is 6 V.

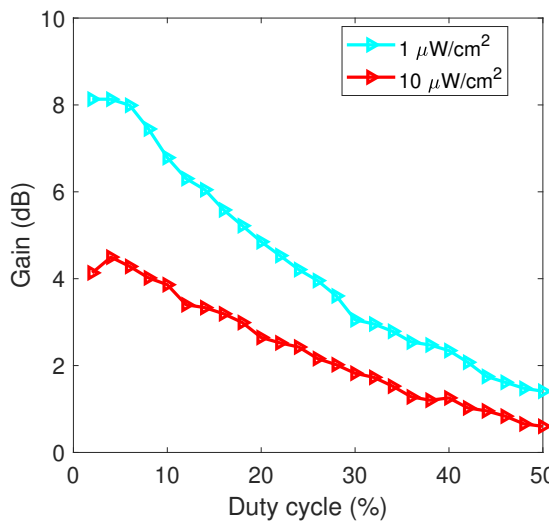


FIGURE 4.15: Measured gain of RF pulse signal on the single cell rectenna versus duty cycle.

In terms of voltage gain, the results are presented in Fig.4.15. It is shown that the voltage

gain of RF pulse signal at  $10 \mu\text{W}/\text{cm}^2$  is smaller than at  $1 \mu\text{W}/\text{cm}^2$  of power density for all the values of duty cycle. The highest gain is 8.15 dB and 4.5 dB for  $1 \mu\text{W}/\text{cm}^2$  and  $10 \mu\text{W}/\text{cm}^2$ , respectively.

The behavior of output DC voltage and voltage gain of RF pulse signal compared to 1-tone signal when the power density varies from 1 to  $15 \mu\text{W}/\text{cm}^2$  are shown in Fig.4.16. For each value of power density, the optimum RF pulse signal with highest DC output is selected and plotted in the figure. RF pulse signal outperforms 1-tone signal. The voltage gain has the highest value of 8.15 dB at  $1 \mu\text{W}/\text{cm}^2$  and then decreases to 3.6 dB at  $15 \mu\text{W}/\text{cm}^2$ . In all cases, the optimum duty cycle of RF pulse signal is below 10 %, which signifies that the PAPR is higher than 13 dB.

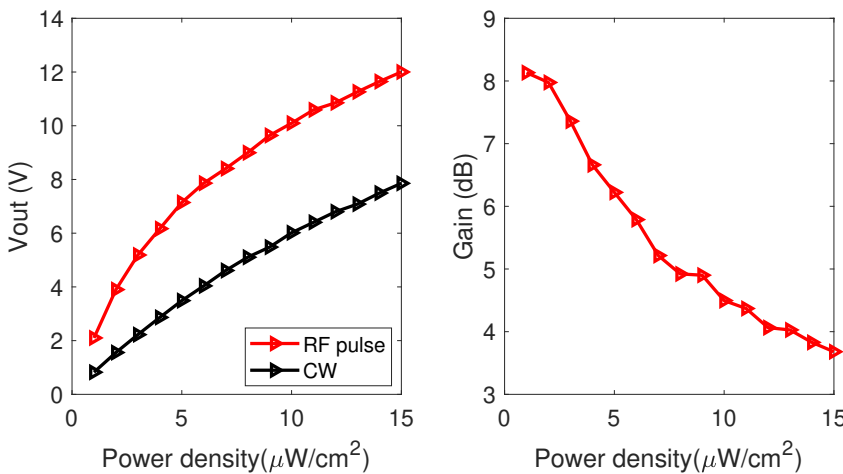


FIGURE 4.16: Measured output DC voltage and voltage gain of RF pulse signal on the single cell rectenna versus power density.

The same measurements of RF pulse signal have been done with  $2\times 2$  and  $3\times 3$  rectenna arrays.

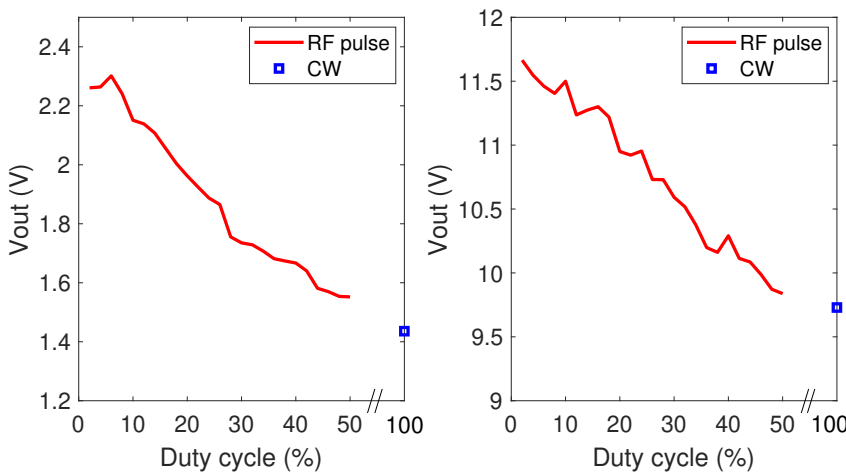


FIGURE 4.17: Measured output DC voltage of the  $2\times 2$  rectenna array versus duty cycle at  $1 \mu\text{W}/\text{cm}^2$  (left) and  $10 \mu\text{W}/\text{cm}^2$  (right).

For the 2x2 rectenna array, Fig.4.17 shows the DC voltage obtained by using RF pulse signal versus the duty cycle. A comparison with 1-tone signal is done. At  $1 \mu\text{W}/\text{cm}^2$ , the maximum DC voltage of RF pulse signal is 2.32 V at the duty cycle of 6 % while the DC voltage of CW signal is only 1.43 V. On the other hand, these values for  $10 \mu\text{W}/\text{cm}^2$  of power density are 11.8 V and 9.8 V, respectively.

The voltage gain of RF pulse signal compared to 1-tone signal are shown in Fig.4.18 over the duty cycle range at 2 levels of power density. Clearly, the gain at  $1 \mu\text{W}/\text{cm}^2$  is much better than the gain at  $10 \mu\text{W}/\text{cm}^2$ . As can be seen, the highest gain values at  $1 \mu\text{W}/\text{cm}^2$  and  $10 \mu\text{W}/\text{cm}^2$  are 4.1 dB and 1.55 dB correspondingly. The gains are smaller than that of the single cell rectifier.

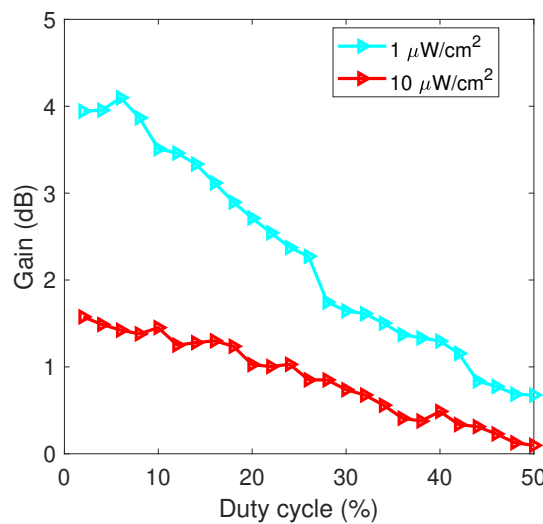


FIGURE 4.18: Measured gain of RF pulse signal on the 2x2 rectenna array versus duty cycle.

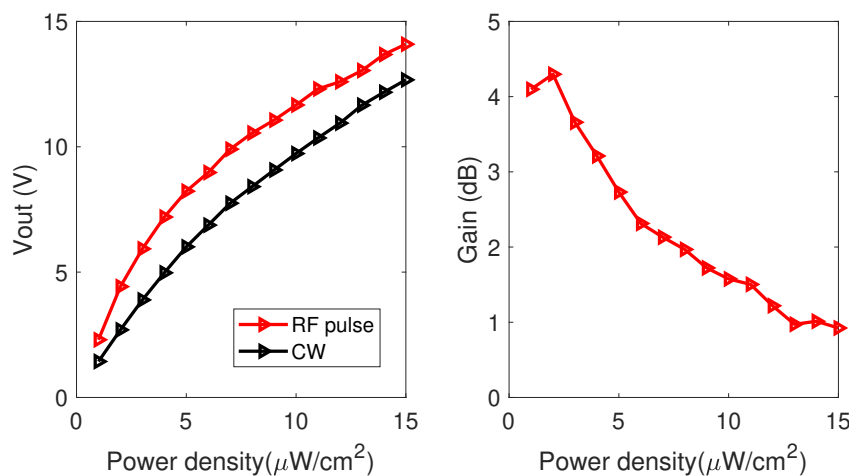


FIGURE 4.19: Measured output DC voltage and voltage gain of RF pulse signal on the 2x2 rectenna array versus power density.

The voltage output and the voltage gain of RF pulse signal compared with 1-tone signal

are presented in Fig.4.19. The improvement of RF pulse signal in terms of output voltage and voltage gain are smaller in comparison with 1x1 rectenna. The gain decreases as the power density increases. The highest gain obtained is 4.3 dB at  $1 \mu\text{W}/\text{cm}^2$  and the lowest gain is 0.9 dB at  $15 \mu\text{W}/\text{cm}^2$ . The optimum duty cycle of RF pulse signal is also below 10 % (PAPR > 13 dB) for all the power density range.

Finally, the measurement results are shown in Fig.4.20 to Fig.4.22 for the 3x3 rectenna array

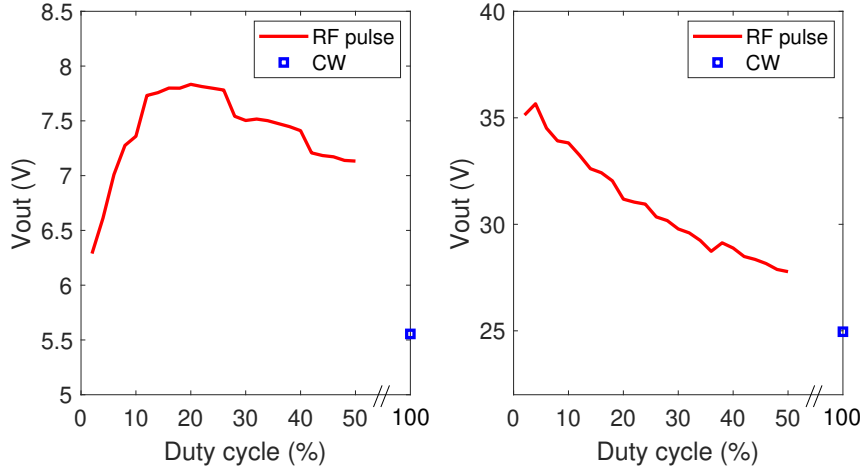


FIGURE 4.20: Measured output DC voltage of the 3x3 rectenna array versus duty cycle at  $1 \mu\text{W}/\text{cm}^2$  (left) and  $10 \mu\text{W}/\text{cm}^2$  (right).

The behavior of output DC voltage and voltage gain of RF pulse signal compared to 1-tone signal in this case is different with 1x1 and 2x2 rectennas. As can be seen, the optimum duty cycle is approximately 20 % (PAPR of 10 dB) for the power density of  $1 \mu\text{W}/\text{cm}^2$ . Meanwhile, for  $10 \mu\text{W}/\text{cm}^2$ , the optimum duty cycle is 4 % (PAPR of 17 dB). In terms of voltage gain (Fig.4.21), the highest gain found by using the two power densities is close to 3 dB. However, these highest gains are obtained at different duty cycles.

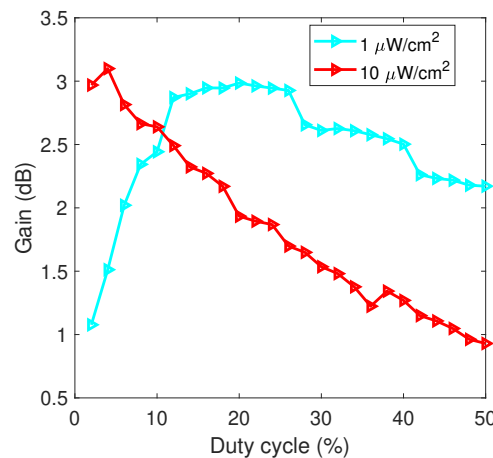


FIGURE 4.21: Measured voltage of RF pulse signal on the 3x3 rectenna array versus duty cycle.

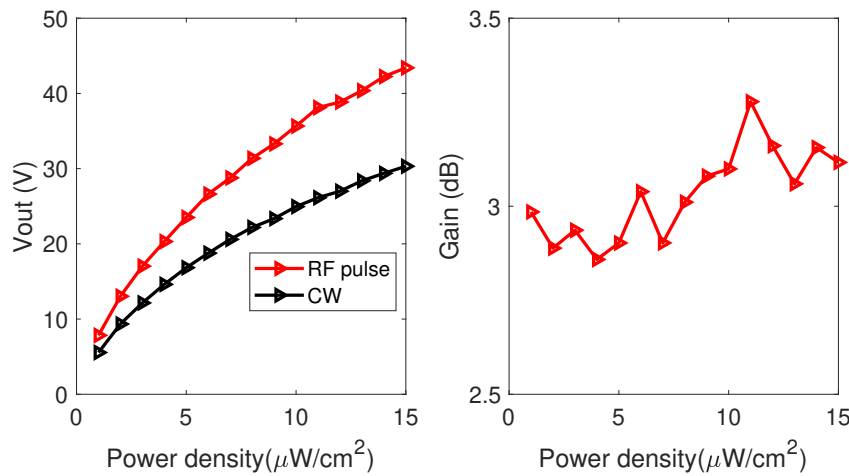


FIGURE 4.22: Measured output DC voltage and voltage gain of RF pulse signal on the 3x3 rectenna array versus power density.

The voltage gain are nearly constant at around 3 dB as shown in Fig.4.22. The DC voltage of RF pulse and 1-tone signal are up to 44 V and 30 V at 15  $\mu\text{W}/\text{cm}^2$  of power density. Compared to 2x2 and 1x1 rectennas, the gain of RF pulse signal on 3x3 rectenna array is unusual. It is more or less 3 dB over the power density range from 1 to 15  $\mu\text{W}/\text{cm}^2$ . The gains at higher power densities are even higher than the gains at smaller power densities. A further study needs to be done to investigate the case of 3x3 rectenna arrays.

Table 4.1 summarizes the results obtained using the different rectenna arrays presented in this chapter. It shows the comparison in terms of voltage gain (dB) between multi-sine signal and RF pulse signal for the three rectenna arrays at two power densities: 1  $\mu\text{W}/\text{cm}^2$  and 10  $\mu\text{W}/\text{cm}^2$ .

Overall, RF pulse signal shows better performance on rectenna arrays than multi-sine signal and CW signals despite of varying the power density. Especially for 3x3 rectenna array, where multi-sine signal's improvement is minor, RF pulse still shows 3 dB of voltage gain at 1  $\mu\text{W}/\text{cm}^2$  and 10  $\mu\text{W}/\text{cm}^2$ .

Waveform type	Single rectenna element		2x2 rectenna array		3x3 rectenna array	
	1 $\mu\text{W}/\text{cm}^2$	10 $\mu\text{W}/\text{cm}^2$	1 $\mu\text{W}/\text{cm}^2$	10 $\mu\text{W}/\text{cm}^2$	1 $\mu\text{W}/\text{cm}^2$	10 $\mu\text{W}/\text{cm}^2$
CW	1	1	1	1	1	1
2-tone	1.19	0.97	0.66	0.45	1.51	0.78
4-tone	2.66	1.71	1.50	0.74	1.63	1.20
8-tone	4.35	2.70	2.28	1.13	0.42	0.82
16-tone	5.33	3.32	3.02	1.45	-0.13	1.15
RF pulse	8.13	4.50	4.01	1.58	2.99	3.01

TABLE 4.1: RF pulse and multi-sine signal voltage gain (dB) compared to CW signal

### 4.3 Application to remote power supply of a temperature/acceleration wireless sensor

The rectenna arrays are used to supply power for a battery-free temperature and acceleration sensor. The measured data will be sent to a smartphone by Bluetooth Low Energy (BLE).

The measurement setup is presented in Fig.4.23. To transmit the RF pulse signal or multi-sine signal to the rectenna, the same measurement setup as in section 3.2 is used. The voltage output of the rectenna will be applied to a  $470 \mu F$  storage capacitor  $C_S$ . As the voltage output is connected directly to the capacitor, the resistance load is consider as infinite. The condition in equation 2.10 is always satisfied. Then, the voltage  $V_S$  across the capacitor  $C_S$  will be controlled by a hysteresis comparator switch in order to supply voltage to a wireless sensor node. When  $V_S$  reaches about 2.5 V, the switch start supplying the voltage to the sensor node. In the mean time, the data is transmitted via Bluetooth Low Energy (BLE) link to a data collection station (smartphone). The capacitor starts to discharge until it reach about 1.9 V. At that moment, the switch is open so the capacitor can recharge to reach 2.5 V again. A new measurement cycle will start to continuously send the data for each period of measurement.

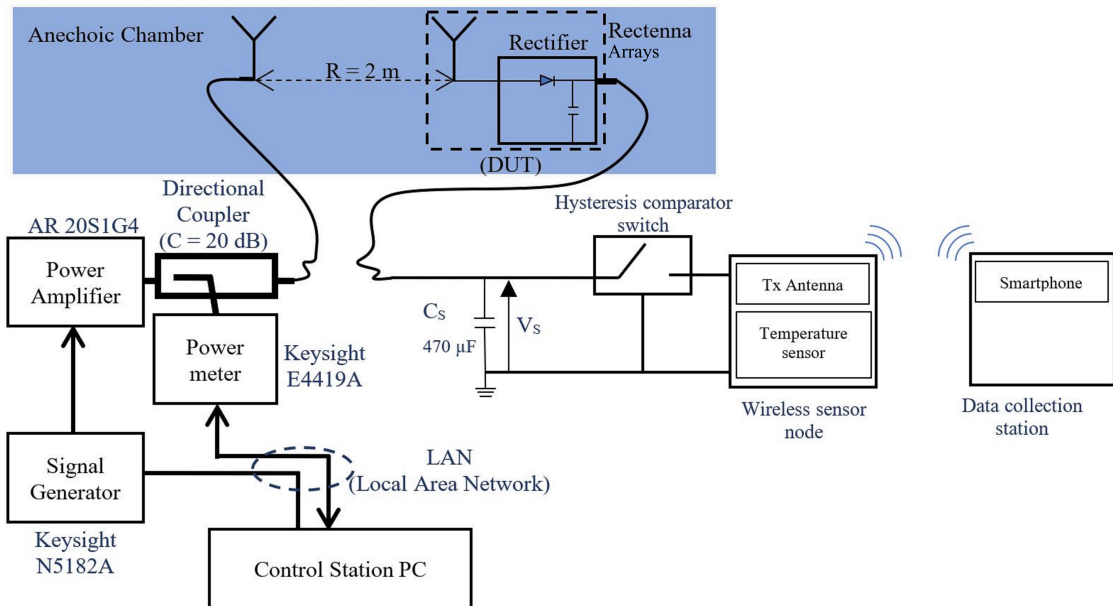


FIGURE 4.23: Measurement setup for rectenna arrays measurement with sensor.

The measurement will be performed to measure the charging time of the capacitor. There are 2 important values: the initial charging time ( $T_1$ ) from 0 to 2.5 V and the second charging time ( $T_2$ ) from 1.9 to 2.5 V. For a faster charging time  $T_1$ , we have smaller period of communication between the sensor node and the data collection station. Therefore, more data will be sent more frequently in a shorter period of time.

Fig.4.24 shows the voltage evolution on  $C_S$  and data display on smartphone. Fig.4.25 demonstrates an example of the evolution of DC voltage on the storage capacitor  $C_S$  in time

domain for 3x3 rectenna array where the input signal is RF pulse signal with the power density of  $1 \mu W/cm^2$  and duty cycle of 30 %. As can be seen, the initial time  $T_1$  is 147 seconds and the recharge time  $T_2$  is 57 seconds. The energy storage in the capacitor is calculated as:

$$W = \frac{1}{2}C.V^2 \quad (4.1)$$

In the phase  $T_1$ , the voltage increases from 0 to 2.5 V, the energy stored in the capacitor  $W_1$  is  $1468.75 \mu J$ . In the phase  $T_2$ , the voltage increases from 1.9 to 2.5 V, the energy consumption for transmitting data  $W_2$  is  $620.4 \mu J$ .

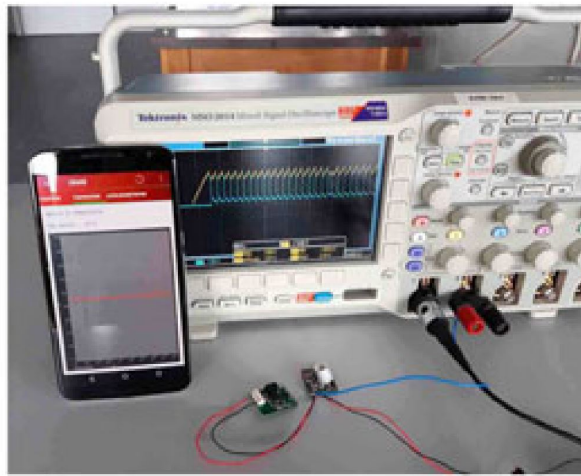


FIGURE 4.24: Temperature/acceleration sensor and data displayed on smartphone and oscilloscope.

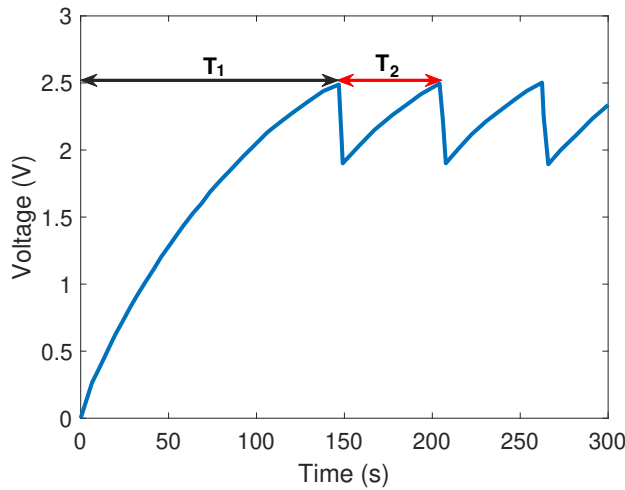


FIGURE 4.25: Measured voltage evolution on  $C_S$  as a function of time.

Overall, for RF pulse signal, in order to charge the capacitor, the optimum duty cycle can not be at small values such as 1 to 4 % as presented in figures 4.14, 4.17, and 4.20. In general, optimum duty cycles are around 10 to 30 %, where the PAPR is from 8.2 to 13 dB.

If the duty cycle is too small, the time where the signal turned on is not sufficient to charge the capacitor.

To compare between CW, multi-sine signal and RF pulse signal, the times  $T_1$  and  $T_2$  are measured for different power densities. For each type of rectenna array and waveform and for a distance between emitter and rectenna fixed at 2 meters, we find a minimum power density possible to operate the sensor and the corresponding times  $T_1$  and  $T_2$ . The results are shown in tables 4.2 and 4.3.

In table 4.2, we can see that the use of multi-sine signal and RF pulse signal can reduce the minimum required power density for 1x1 and 2x2 rectenna arrays. For 1x1 rectenna array, between CW and RF pulse signals, the power density can be decreased from  $4 \mu W/cm^2$  to  $2.75 \mu W/cm^2$  (31 %). For 2x2 rectenna array, it decreases from  $2.5 \mu W/cm^2$  to  $1.85 \mu W/cm^2$  (26 %). The duty cycle of RF pulse signal to obtain that minimum power density varies between 10 to 30 %. Because the output of the circuit is connected to a high-value capacitor of  $470 \mu F$ . For multi-sine signal, as the number of sub-carriers increases, the power density required is also decreased. For 3x3 rectenna array, the minimum power density required does not decrease between the different signals but in terms of charge and recharge times ( $T_1$  and  $T_2$ ), it is noticeably decreased as shown in table 4.3. For CW signal, the time periods  $T_1$  and  $T_2$  for  $0.7 \mu W/cm^2$  of power density are 540 seconds and 330 seconds, respectively. Meanwhile, that values for RF pulse signal are 354 seconds and 140 seconds.

Waveform type	Single rectenna element	2x2 rectenna array	3x3 rectenna array
CW	4	2.5	0.7
2-tone	3.5	2.5	0.7
4-tone	3.25	2.25	0.7
8-tone	2.75	2	0.7
16-tone	2.5	2	0.7
RF pulse	2.75	1.85	0.7

TABLE 4.2: Minimum power density for different input waveforms ( $\mu W/cm^2$ ).

Waveform type	Single rectenna element		2x2 rectenna arrays		3x3 rectenna arrays	
	$T_1$	$T_2$	$T_1$	$T_2$	$T_1$	$T_2$
CW	104	72	490	250	540	330
8-tone	80	44	386	198	580	350
RF pulse	64	34	214	124	354	140

TABLE 4.3: Corresponding  $T_1$  and  $T_2$  (s) for minimum power density of CW, 8-tone and RF pulse waveforms.

In table 4.3, the corresponding time periods  $T_1$  and  $T_2$  for minimum power density given in Table 4.2 of CW, 8-tone and RF pulse are presented.

As mentioned, for 1x1 rectenna, the minimum power density required for CW to operate the sensor node is  $4 \mu W/cm^2$ . At this power density, the time periods  $T_1$  and  $T_2$  for CW, 8-tone and RF pulse signal are: 104 and 72 seconds, 80 and 44 seconds, 64 and 34 seconds, respectively. For the same power density, the time is significantly reduced when using 8-tone or RF pulse signals compared to CW signal.

Besides, for 2x2 rectenna, the minimum power density required for CW is  $2.5 \mu W/cm^2$ . At that power density, the time periods  $T_1$  and  $T_2$  for CW are 490 and 250 seconds. Meanwhile, that values for 8-tone and RF pulse signals are: 386 and 198 seconds, 214 and 124 seconds, respectively.

For 3x3 rectenna, the same power density of  $0.7 \mu W/cm^2$  is required for CW, 8-tone and RF pulse signals. The time periods  $T_1$  and  $T_2$  for these signals are: 540 and 330 seconds, 580 and 350 seconds, 354 and 140 seconds. For this case, 8 tone signal does not show a better performance than CW signal. However, RF pulse signal is always better than CW signal with the time reduced for  $T_1$  is 34 % and the time reduced for  $T_2$  is 58 %. Again, the abnormal performance of 3x3 rectenna arrays needs further investigation to verify the results.

From table 4.3, we have calculated the average energy stored in the capacitor per second (table 4.4). As the charging and recharging time decreases, the average energy storage in the capacitor per second increases.

Waveform type	Single rectenna element		2x2 rectenna arrays		3x3 rectenna arrays	
	$\frac{W_1}{T_1}$	$\frac{W_2}{T_2}$	$\frac{W_1}{T_1}$	$\frac{W_2}{T_2}$	$\frac{W_1}{T_1}$	$\frac{W_2}{T_2}$
CW	14.12	8.62	3.00	2.48	2.71	1.88
8-tone	18.36	14.1	3.80	3.13	2.53	1.77
RF pulse	22.95	18.25	6.86	5.00	4.15	4.43

TABLE 4.4: Stored average power ( $\mu W$ ) in the capacitor for minimum power density of CW, 8-tone and RF pulse waveforms.

From the measurement results displayed in tables 4.2, 4.3 and 4.4, we can see that, for 1x1 and 2x2 rectennas, the multi-sine signal and RF pulse signal reduce the minimum power density required compare to CW signal. Moreover, at the same power density, multi-sine signal and RF pulse signal always give the faster times  $T_1$  and  $T_2$ . For 3x3 rectenna, we have nearly the same minimum power density required for multi-tones and CW signals. However, RF pulse signal gives better performance compared to CW signal.

## 4.4 Conclusion

In this chapter, we have developed a wireless power transfer system to supply a wireless sensor.

Firstly, the measurements have been done in anechoic chamber for single cell rectenna, 4-cell and 9-cell rectenna arrays. With multi-sine signal, similar results are found with single element and 2x2 rectenna arrays. When increasing the number of sub-carriers, the voltage as well as the voltage gain are increased, regardless of the frequency bandwidth. The highest

gain of  $\sim 5.3$  dB is obtained by 16-tone signal at  $1 \mu\text{W}/\text{cm}^2$  for the single rectenna. In contrast, for 3x3 rectenna array, which produces high voltage at small power density for CW signal, the improvement is significantly smaller.

Secondly, for RF pulse signal, the voltage gain decreases as the number of rectenna increases. It means that single cell rectenna has the highest gain, which is 8.13 dB at  $1 \mu\text{W}/\text{cm}^2$ . Meanwhile, the 2x2 rectenna array presents the highest RF pulse signal's voltage gain of 4.3 dB at  $2 \mu\text{W}/\text{cm}^2$ . That value for 3x3 rectenna array is 3.3 dB at  $11 \mu\text{W}/\text{cm}^2$ . RF pulse signal gives better performances than multi-sine signal in all cases.

Measurements using the rectenna in order to supply power to a temperature/acceleration sensor have been done. The pulse signal and multi-sine signal decrease the minimum required power density (for 1x1 and 2x2 rectenna arrays). Moreover, for the same power density, RF pulse signal significantly decreases the charge and recharge times of the capacitor. For 1x1, 2x2 and 3x3 rectenna arrays, we decrease the charge time  $T_1$  between RF pulse and CW by 38, 56 and 34 %. In terms of recharge time  $T_2$ , that values are 53, 50 and 58 %, respectively. However, the abnormal behavior of 3x3 rectenna array needs a further study to verify the results.



# Bibliography

- [1] Mahfoudi, Hichem, Hakim Takhedmit, Mohamed Tellache, and Sebastien Boisseau. *Wireless sensor node remote supply using a compact stacked rectenna arrays with voltage multipliers at 2.45 GHz*, International Journal of Microwave and Wireless Technologies 12, no. 4 (2020): 309-315.
- [2] <https://datasheetspdf.com/pdf/337113/AlphaIndustries/SMS7630-079/1>



# General conclusion

This thesis reports a complete study of multi-sine signal and RF pulse signal applied to the low wireless power transfer systems using high frequency electromagnetic waves.

The statistical study shows that multi-sine signal has its highest PAPR while all the parameters (amplitude, phase, frequency spacing) are identical between sub-carriers. The PAPR of multi-sine signal is increased by 3 dB while the number of sub-carriers is doubled. Meanwhile, the PAPR of RF pulse signal can be adjusted by varying the duty cycle. As the duty cycle decreases from 100 % to 1 %, the PAPR of RF pulse signal increases from 3 to 23 dB.

Different tools of ADS simulation have been presented such as Harmonic Balance, Circuit Envelope, Data Flow, Ptolemy Co-simulation. The process of designing and optimizing three traditional rectifier topologies with and without matching network using ADS are also demonstrated. We have developed an automated measurement setup which allows to perform a large amount of experiments. Measurement results on those rectifiers show that the optimization of the pulse waveform, instead of the conversion circuit, makes it possible to deliver equal or even better performances on three basic rectifier topologies: series-mounted, shunt-mounted and voltage doubler rectifiers. That allows more flexibility in terms of operating frequency and output load. The RF pulse signal has a better performance than multi-sine signal in all cases. At -20 dBm input power, efficiency gains of RF pulse signal compared to 1-tone signal are 58%, 38% and 18% for series, shunt and voltage doubler rectifiers, respectively. Similar results are obtained at other power levels. This work has shown that the optimized RF pulse signals can transform non-optimized rectifiers into wide-band rectifiers in term of frequency and load resistance and with high performances.

On the other hand, RF pulse and multi-sine signals are proposed for WPT with broadband rectifier/rectenna operating in the frequency range from 1.6 to 2.8 GHz. The measurements on broadband rectifier show the performance improvement of multi-sine and RF pulse signals compared to CW signal. Overall, the output voltage is improved at the frequency range of interest despite the variation of load's resistance. While multi-sine signal shows some small improvement, the RF pulse signal has a great advantage compared to CW signal. At optimum load's resistance of  $3 \text{ k}\Omega$ , the highest voltage gain recorded is 8 dB at 2.8 GHz and for a duty cycle of 5% (corresponds to the PAPR of 16 dB). While varying the load's value, the gain is significantly higher at 14.25 dB and 12.95 dB at -15 dBm and -5 dBm, respectively. The output DC voltage enhancement also depends on the optimization of the circuit. At center frequencies and smaller load resistance, the gain is smaller than the two ends of the frequency band, where the voltage output is smaller because the circuit is less optimized.

For broadband rectenna, two values of load resistance ( $3 \text{ k}\Omega$  and  $100 \text{ k}\Omega$ ) have been

tested at three input power levels: -30, -25 and -20 dBm. Similar to broadband rectifier, RF pulse signal is also outperform multi-sine and CW signals. At the resistance load close to the optimum value of  $3\text{ k}\Omega$ , the gain of RF pulse signal is significantly high at the two ends of the frequency range and becomes smaller at the center of the bandwidth. Regardless of the frequency, the lowest gain is 0 dB for the RF power levels from -30 dBm to -20 dBm. The highest gain recorded is 8 dB at 1.7 GHz and -25 dBm input RF power and 8.1 dB at 2.7 GHz and -20 dBm of input RF power. More important gains are found at smaller input power such as -25 dBm and -30 dBm. On the other hand, at  $100\text{ k}\Omega$ , regardless of the frequency, the gain is better than that of optimum resistance ( $3\text{ k}\Omega$ ) in general. The highest gain recorded is 13.95 dB at 1.675 GHz and -20 dBm input power, which means the efficiency increased from 0.325 % (CW) to 7.205 % (RF pulse). The improvement in two cases are different, with more important gains at smaller input power when the load value is  $3\text{ k}\Omega$  and vice versa for the load value of  $100\text{ k}\Omega$ , where the lowest gain recorded is 0.85 dB at 1.925 GHz.

The last chapter focuses on a wireless supply dedicated to a temperature/acceleration sensor. Firstly, multi-sine signal and RF pulse signals are used to perform the measurement with array rectennas in anechoic chamber. Three type of rectenna arrays: 1x1, 2x2 and 3x3 are presented. The measurement results and a comparison between POWs and CW signal on these rectennas have been demonstrated. For multi-sine signal, the same behavior is found for 1x1 and 2x2 rectenna, where the RF-to-dc conversion efficiency is increased with the number of sub-carriers for different power densities. On the other hand, for 3x3 rectenna, the 8-tone and 16-tone do not show better performance in some cases. For RF pulse signal, the improvement is clearer and better than multi-sine signal. The highest gain of 8.3 dB is found at the power density of  $1\text{ }\mu\text{W}/\text{cm}^2$  for the single cell rectenna.

Secondly, in order to supply voltage to the input capacitor of the temperature/acceleration wireless sensor, CW and POWs are applied to measure the charge and recharge time of the capacitor. The measurements show that with POWs, we can reduce the minimum required power density to charge the capacitor for single and 2x2 rectennas. For example with single cell rectenna, the required power density for CW and RF pulse signal are  $4\text{ }\mu\text{W}/\text{cm}^2$  and  $2.75\text{ }\mu\text{W}/\text{cm}^2$ , respectively. Moreover, if we keep the same power density used for CW signal, the charge and recharge time are reduced significantly. For 2x2 rectenna array, applying the signal with a power density of  $2.5\text{ }\mu\text{W}/\text{cm}^2$ , the charge and recharge time of CW are 490 and 250 seconds. Meanwhile, that values for RF pulse signal are 214 and 124 seconds, respectively. For 3x3 rectenna, the minimum power density are unchanged between CW and RF pulse signal but the charge and recharge time are also decreased.

## Perspectives

As the improvement is not clear and the voltage behavior is unusual compared to single cell and 2x2 rectenna arrays, an investigation need to be done for the case of 3x3 rectenna array on the application of supplying power to the wireless sensor.

To develop a simple and fast simulation tool that would allow to estimate the potential of POW signals for energy transfer is necessary. Because ADS simulations were taking a lot of time and does not support a wide range of POW signals.

About POWs, a combination of RF pulse and multi-tone signal to increase the PAPR and therefore further improve the DC output (voltage and efficiency) could be an interesting solution to investigate and validate. .

It is needed to explore other forms of signals, particularly using the digital tool (Matlab).

In view of the limitation of the PAPR (and also the IPV), it is needed to determine the relevance of waveforms for the WPT, explore other parameters that would be better able to estimate more precisely or rather give a preliminary idea with sufficient precision on the relevance of the waveform for the WPT.

Also, Systems for Simultaneous Wireless Information and Power Transfer (SWIPT) is an interesting idea to be embedded in our future work.

## List of Publications

### Journals

1. V. Pham, H. Takhedmit and L. Cirio, *Waveform Optimization using RF Pulse Signal on Broadband Rectenna*, doi: 10.1109/JRFID.2020.3039878  
accepted for publication in IEEE Journal of Radio Frequency Identification.

### International conferences

2. V. Pham, H. Takhedmit and L. Cirio, *Performance Improvement of a 2.4-GHz Multi-stage Rectifier Using Power Optimized Waveforms*, 2018 25th IEEE International Conference on Electronics, Circuits and Systems (ICECS), Bordeaux, France, 2018, pp. 293-296, doi: 10.1109/ICECS.2018.8617904.
3. V. Pham, H. Takhedmit and L. Cirio, *Waveform Optimization For Efficiency Improvement of Traditional RF-to-dc Rectifiers Without Input Matching Network*, 2020 14th European Conference on Antennas and Propagation (EuCAP), Copenhagen, Denmark, 2020, pp. 1-5, doi: 10.23919/EuCAP48036.2020.9135994.
4. V. Pham, H. Takhedmit and L. Cirio, *Impact of Multisine and RF Pulse Signals on The Efficiency of Different Rectifier Topologies for WPT*, 2020 14th European Conference on Antennas and Propagation (EuCAP), Copenhagen, Denmark, 2020, pp. 1-5, doi: 10.23919/EuCAP48036.2020.9135406.

### National conferences

5. V. Pham, H. Takhedmit and L. Cirio, *Amélioration des performances d'un circuit de conversion RF-DC multi-étage à 2,4 GHz par optimisation des formes d'onde*. 21èmes Journées Nationales Micro-ondes (JNM 2019, Caen).
6. V. Pham, H. Takhedmit and L. Cirio, *DC Voltage Improvement of a 2.4-GHz Rectifier using Multisine Signals*. 9th National Days on Energy Harvesting and Storage (JNRSE 2019, Blois).

# Abstract

## **Power optimized waveform for wireless power transmission**

This thesis focuses on POWs (Power Optimized Waveforms) for wireless power transmission. It consists of high PAPR (Peak-to-Average Power Ratio) signals: multi-sine and RF pulse signals. The POWs will be studied to demonstrate their characteristics. As the main part of this thesis, the signal will be used to show the impact on the RF-to-dc conversion efficiency of energy harvesting devices using different rectification topologies.

The traditional rectifier topologies are designed and optimized using ADS software. Then RF pulse and multi-sine signals are applied to those circuits to compare the output DC voltage with that obtained by using CW signal. The experimental results shows that with RF pulse signal, the non-optimized rectifiers can obtain a comparable or even better performance than the optimized rectifiers in a wide frequency range.

Also, RF pulse and multi-sine signals are applied to a broadband rectifier/rectenna operating at the frequency range from 1.6 to 2.8 GHz. Both signals give a better performance than CW signal on the broadband rectenna/rectifier. RF pulse signal show a clear improvement in all the frequency range of interest and in a wide range of output-load values.

Finally, RF pulse and multi-sine signals help the rectenna arrays reach a higher output DC voltage at small power densities. For that reason, it allows to reduce the charge and recharge time of the input capacitor for remote power supply of a temperature/acceleration wireless sensor à 2.45 GHz. Moreover, using RF pulse signal, the minimum power densities required to charge the capacitor for single cell and 2x2 rectennas are reduced by 31 % and 26 %, respectively, compared to CW signal.

**Keywords :** *Power optimized waveforms, rectifier, rectenna, PAPR, Wireless power transmission, RF pulse, multi-sine, broadband rectenna, wireless sensor, remote power supply.*

## **Optimisation de formes d'onde pour la transmission d'énergie sans fil**

Cette thèse porte sur l'optimisation des formes d'onde (POW pour Power Optimized Waveforms) d'entrée pour la transmission d'énergie sans fil. Il s'agit de signaux à PAPR (Peak-to-Average Power Ratio) élevés. Les signaux multi-porteuses et impulsion modulée ont été utilisés. Les POWs seront étudiés afin de démontrer leurs caractéristiques mais aussi leur potentiel. En tant que partie principale de cette thèse, le signal sera utilisé pour montrer l'impact sur l'efficacité de la conversion RF-DC des dispositifs de collecte d'énergie tels que les circuits de conversion RF-DC et les rectennas.

Des topologies de redresseurs traditionnelles sont été conçues et optimisées à l'aide du logiciel ADS. Ensuite, les signaux considérés dans cette thèse sont appliqués à ces circuits pour comparer la tension continue de sortie avec celle obtenue par le signal CW. Les résultats expérimentaux montrent qu'avec une impulsion modulée, le redresseur non optimisé peut fournir des performances comparables voire meilleures que celles d'un redresseur optimisé dans une large gamme de fréquences mais aussi de résistance de charge.

En outre, ces signaux sont également appliqués à un redresseur/rectenna à large bande fonctionnant dans la gamme de fréquences de 1,6 à 2,8 GHz. Les deux signaux donnent de meilleures performances que le signal CW. Le signal impulsionnel montre une nette amélioration sur toute la gamme de fréquences concernée et dans une large gamme de valeurs de charge.

Enfin, ces signaux ont permis d'améliorer considérablement la tension de sortie de réseaux de rectennas basés sur un redresseur multi-étage et ce à des densités de puissance faibles. Cela a permis donc de réduire les temps de charge et de recharge du condensateur d'entrée dans une application d'alimentation à distance et sans fil d'un capteur de température et d'accélération à la fréquence de 2.45 GHz. De plus, en utilisant le signal impulsion modulée, les densités de puissance minimales requises pour charger le condensateur pour la cellule unitaire (réseau 1x1) et le réseau 2x2 ont pu être réduites de 31 % et 26 %, respectivement, par rapport au signal CW.

**Keywords :** *Transmission d'énergie sans fil, formes d'onde optimisées, circuit de conversion RF-DC, rectenna, large bande, impulsion modulée, multi-porteuses.*